INTERNATIONAL ATOMIC ENERGY AGENCY
UNITED NATIONS EDUCATIONAL, SCIENTIFIC AND CULTURAL ORGANIZATION
INTERNATIONAL CENTRE FOR THEORETICAL PHYSICS
I.C.T.P., P.O. BOX 586, 34100 TRIESTE, ITALY, CABLE CENTRATOM TRIESTE

UNITED NATIONS INDUSTRIAL DEVELOPMENT ORGANIZATION

INTERNATIONAL CENTRE FOR SCIENCE AND HIGH TECHNOLOGY

SMR.550 - 2

SPRING COLLEGE IN MATERIALS SCIENCE ON

"NUCLEATION, GROWTH AND SEGREGATION IN MATERIALS SCIENCE AND ENGINEERING"

(6 May - 7 June 1991)

BACKGROUND MATERIAL - II

for lectures on

"GEOMETRY AND ENERGY OF INTERFACES"

A.A. CHERNOV
Institute of Crystallography
Academy of Sciences of the USSR
Leninsky prospekt 59
Moscow 117333
U.S.S.R.

Chapter 3

GROWTH SHAPES AND THEIR STABILITY AT ANISOTROPIC INTERFACE KINETICS: THEORETICAL ASPECTS FOR SOLUTION GROWTH

A. A. CHERNOV and T. NISHINAGA

A_1, A_2	proportionality constant in Eq. (7)
A', A''	integration constants
a_0	interatomic distance
a	$\beta(C_\infty - C_0)(D+\beta d)^{-1}$
a_s	length of macrostep riser
$B(p)$	kinetic coefficient for R
B', B''	integration constants
B^*	$B(p_0)(1 - \Omega(2C_\infty - C_0))$
b	$(C_\infty D + C_\infty \beta_\infty d)(D+\beta_\infty d)^{-1}$
$b(p)$	$B(p)\sin\alpha$
C	concentration of solute
C^*	concentration of solute at the growth interface
$C(z)$	concentration distribution for unperturbed interface
$\tilde{C}(p, z)$	change of concentration with perturbation
δC	net increase or decrease of concentration at the tip of perturbed interface
C_0	concentration at solution boundary for planar crystal growth
C_∞	concentration at an infinite point
C_e	equilibrium concentration at solid-liquid interface
$C_{e\infty}$	equilibrium concentration for planar interface
C_s	number of growth unit per unit volume of the growing material
C^*_{st}	concentration of the growth unit in the vicinity of step
D	volume diffusion constant of solute
D_s	surface diffusion constant
E_{des}	heat of desolvation
E_{dis}	heat of dissolution
e	unit vector along the constant slope trajectory
$f(\omega)$	δ'/δ
f_0	area per one growth unit along a step
h	macrostep height
I	flux of growth unit per elementary surface site
K	curvature
k_B	Boltzmann constant
L	total length of macrostep
L_c	critical size of crystal above which growth become unstable
L_s	size of crystal or boundary layer thickness
l	length of macrostep riser projected on a horizontal plane
n	normal unit vector at an arbitrary point on the growing surface
n_{s0}	equilibrium surface concentration of growth unit
p	local slope
p_0	slope of unperturbed hillock (Section 5) or surface (Section 6)
$\bar{p}$	average slope of macrostep riser
$\tilde{p}$	increment of slope by perturbation
p^*	slope at which $B(p)$ becomes maximum
q	concentration gradient for unperturbed interface
R	growth rate normal to a singular plane
R_g	gas constant
r	radial coordinate and radius of curvature (Section 4)
r_0	radius of cylindrical or spherical crystal
r_1	radius of outer boundary for cylindrical or spherical crystal growth

r_P	AP in Fig. 29a
S	$(1+x_P)/(1-x_P)$
s	distance between two points on the growing surface
s_d	degeneracy of screw dislocation
T	temperature
t	time
t	tangential unit vector at an arbitrary point on the growing surface
V	growth rate normal to the interface
V_c	growth velocity in the direction of constant slope trajectory
V_n	normal growth velocity of macrostep riser (Fig. 36)
V_y	growth velocity of macrostep terrace in y direction
V_z	local growth velocity in z direction
$\bar{V}_z$	spatially average of V_z
v	horizontal growth velocity
v_s	horizontal velocity of macrostep
v_{st}	step velocity
v_x	growth velocity of macrostep riser in x direction after subtraction of V (Fig. 37)
w_+, w_-	number of growth unit entering (+) and leaving (−) a kink per elementary surface site per unit time
x_P	x coordinate of P′ (Fig. 29b)
α	angle between terrace and riser of a macrostep
β	kinetic coefficient
β_A	$b_{iA}(1+p_0^2)^{1/2}$
β_∞	$\beta(p_\infty)$
Γ	capillary constant
γ	interfacial free energy
γ'	step free energy
γ_1	q_1/q_2
$\delta(t)$	amplitude of perturbation
δ_0	amplitude of perturbation at $t=0$
$\dot{\delta}$	time derivative of δ
$\hat{a}(\chi)$	Fourier transformation of $\tilde{z}(p)$
σ_m	$\beta_\infty(b-C_{e\infty})/b\omega$
$\zeta_0(t)$	increment of hillock height after perturbation
ζ	$(1+(D_s\tau_s/a_l\lambda_s)\tanh(\lambda_s/2\lambda_s))^{-1}$
Φ	$(\beta_s h/D)\sqrt{1+p^2}(2/(\pi-\tan^{-1}\bar{p})-\bar{p})$
η	angle defined in Fig. 9
$\eta(x)$	$\tilde{y}(x)/h$, $\tilde{y}$ being the position of macrostep surface
ϑ	slope of the local plane measured from a singular plane
θ	anisotropy coefficient
ρ	$(x^2+y^2)^{1/2}$
σ	supersaturation
τ_s	average time from adsorption to desorption of the growth unit
τ_s	relaxation time of entering growth unit at a kink
φ	crystallographic angle measured from some standard orientation
φ_P	$\tan^{-1}(V_z/V_P)$
Ψ	$\pi/2 - \pi/n$ (n the number of edges of polygon)
ψ	angle defined in Fig. 9
ψ_s	angle between the macrostep riser trajectory and y axis
Ω	precipitate volume per mol of growing species
ω	angle frequency of perturbation

ω_0	at which $f(\omega)$ changes sign
ω_{max}	ω at which $f(\omega)$ takes maximum
Λ	horizontal size of perturbation
Λ_c	critical horizontal size of perturbation above which unstable growth occurs
λ	wavelength of perturbation
λ_s	interstep distance
λ_k	interkink distance
λ_c	$\sqrt{D_s \tau_s}$
μ	$B^* \Lambda / D$
μ_c	$(C_e - b)(1 + \beta_c / D\alpha)$
μ_0	proportionality constant appeared in Schwartz-Christoffer transformation
ν	R / B^*
ν_+, ν_-	frequencies with which a building unit enters (+) or leaves (−) a kink
ν_m	$a\Gamma_s(D\alpha + \beta_s)(D\alpha - \beta_s)^{-1} + \beta_s(a - C_{eq}\Gamma_{kink}\alpha^2)$

Morphology of Crystals, edited by I. Sunagawa, pp. 207–267.

Chapter 3

GROWTH SHAPES AND THEIR STABILITY AT ANISOTROPIC INTERFACE KINETICS: THEORETICAL ASPECTS FOR SOLUTION GROWTH

A. A. CHERNOV* and T. NISHINAGA**

**Institute of Crystallography, Academy of Sciences of The USSR, Leninsky Prospect 59, Moscow 117333, USSR*
***Department of Electronic Engineering, Faculty of Engineering, The University of Tokyo, 7-3-1 Hongo, Bunkyoku, Tokyo 113, Japan*

1. Introduction

The study of growth forms is very important for both pure and applied crystallography. From the point of view of industry, flat or specially shaped as-grown surfaces are often required. For instance, a very flat epitaxial silicon layer is important for integrated circuit fabrication and special as-grown structures are needed for high efficiency laser diodes. To control as-grown surfaces, one has to understand the mechanism that forms the surface during growth. The scientific interest is based upon the fact that the growth shape is an overall result of the growth process, and the growth form contains a great deal of information to assist understanding of growth phenomena. A careful investigation of the grown surface provides various kinds of evidence for or against a certain growth model.

One of the most important features of the growth form is its stability against a certain morphological perturbation (reviewed by CHERNOV, 1972, and SEKERKA, 1973). If the perturbation disappears, we define the surface as being stable, while if the perturbation is amplified during growth, the surface is defined as unstable. There are competing forces to make the surface stable or unstable. Solute or heat diffusion often act to cause instability. One of the well known examples of this type is the formation of a cell structure during the growth from a melt possessing impurity in high concentration. This has been explained in terms of constitutional supercooling (reviewed, for instance, by HURLE, 1973). There are many forces which stabilize the perturbed surface. These are growth kinetics (CHERNOV, 1972), surface free energy (MULLINS and SEKERKA, 1963; VORONKOV, 1965), convection currents in the solution or melt, surface diffusion etc. (reviewed by SEKERKA, 1973). If the stabilizing

forces dominate, the perturbation may disappear and the growth surface will finally become plane. On the other hand, if the stabilizing forces are weak as compared with destabilizing diffusion phenomena, some surface perturbations are amplified and the final complex interface shape is governed by nonlinear effects. If these competing forces equilibrate each other, a certain structure persists on the growing surface. Macrosteps are studied in detail later as one of the examples.

In the present chapter of the book, we take solution growth as an example to study the growth form. In the case of typical solution growth, one can assume the growing interface to be isothermal, thus neglecting thermal effects. This greatly simplifies the treatment while, still keeping the main features governing the growth shape.

In the following, we define first the growth velocity of a face in terms of step kinetics and express this velocity as a function of the face slope measured from a singular orientation. Then, we shall see how the growth kinetics determine the growth velocity and the supersaturation. The next section is devoted to deriving a differential equation with which one finds the quasi-steady state growth shape, when the growth rate depends both on the crystallographic orientation and on the supersaturation, the latter being a function of position on the interface. In the last two sections, we describe various examples of growth forms, especially from the viewpoint of stability. In Section 5, we shall see how the growth kinetics stabilize the growing interface. The main features of stability analysis for non-singular surfaces are also described for the sake of comparison. Finally, in Section 6, we shall study how macrosteps behave during growth.

2. *Definition of Growth Rates and Their Anisotropies*

An interface between a crystal and mother medium – melt, solution or gas – may be either stepped or atomically rough, depending on the phase transition entropy. The growing stepped surface becomes finally flat since the steps reach the face boundary. The atomically flat surface is called singular. If one plots the surface free energy as a function of crystallographic surface orientation, the energy reaches singular minima for such surfaces. On the other hand, a kinetically or thermodynamically rough interface appears when one employs a high supersaturation or grows a crystal above the temperature of the thermodynamic roughening transition respectively. At high supersaturations, there appear many $2d$ or $3d$ nuclei covering the whole growing surface, which results in the kinetic roughening of the surface (reviewed by CHERNOV *et al.*, 1983). The thermodynamic roughening occurs as a $2d$ phase transition above a definite ratio of temperature to the excess bond energy per one atomic interface site. At low temperatures, this excess of bond energy associated with the interface exceeds the configurational entropy of surface

atoms. As the temperature increases, the entropy term in the free interface energy becomes more important than the binding energy term and above a certain temperature (the roughening transition temperature) the flat interface can not withstand the thermal fluctuation any more, the thermodynamically stable rough surface being the result. The step free energy vanishes at the roughening temperature. The roughening transition is described in more detail elsewhere in this book (Bennema and Van der Eerden, Chap. 1).

The stability analysis for the singular and rough interfaces are very different. The former has been studied by the group of one of the present authors (CHERNOV, 1974), while the latter has been extensively studied by Mullins and Sekerka and their successors (reviewed by SEKERKA, 1973).

The singular surface grows layer by layer. If one denotes λ_0 and a_1 to be the interkink and interatomic distances respectively, as shown in Fig. 1. Let us assume that λ_0 is much smaller than the thickness of the diffusion boundary layer. Then one obtains the following numbers of atomic species entering (+) and leaving (−) a kink per elementary surface site per unit time:

$$w_+ = \nu_+ C^*_{s1} a_1^4 / \lambda_0 \tag{1}$$

and

$$w_- = \nu_- (1 - C^*_{s1} a_1^3) a_1 / \lambda_0. \tag{2}$$

Here ν_+, ν_- are the frequencies with which a building unit enters or leaves a kink, C^*_{s1} being the concentration of the units in the vicinity of the step. Hence, the net flux of crystallizing species per elementary surface site

$$\begin{aligned} j &= w_+ - w_- = (\nu_+ C^*_{s1} a_1^4 / \lambda_0) - \nu_- (1 - C^*_{s1} a_1^3) a_1 / \lambda_0 \\ &= a_1^2 C_s \nu_{st}, \end{aligned} \tag{3}$$

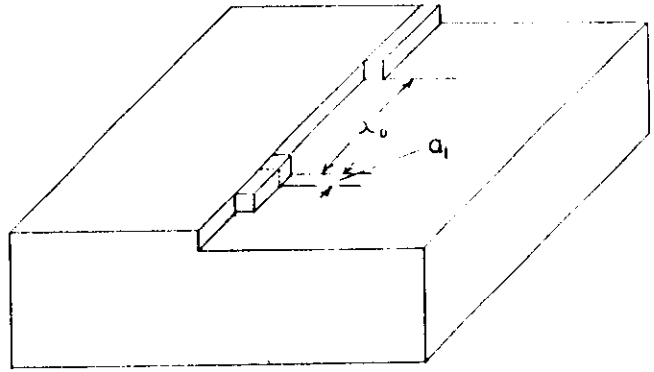

FIG. 1. Step and kinks on growth surface.

where C and v_{st} are the concentration of the species in the crystal and the step velocity respectively. In equilibrium, j should be zero and hence one gets

$$C_e = \nu_+ / (\nu_+ + \nu_-) a_1^3. \tag{4}$$

Here, C_e is the concentration in equilibrium, which is uniform in the ambient mother liquid. Equations (3) and (4) give the following expression for the step velocity,

$$C_e v_{st} = \frac{(\nu_+ + \nu_-) a_1^2}{\lambda_0} (C^*_{st} - C_e)$$

$$= \beta_{st}(C^*_{st} - C_e) \tag{5}$$

where

$$\beta_{st} = (\nu_+ + \nu_-)\, a_1^2/\lambda_0$$
$$= \nu_- / C_e a_0 \lambda_0. \tag{6}$$

In the case of solution growth, ν_+ and ν_-, respectively, could be written in the form:

$$\left.\begin{aligned} \nu_+ &= A_+ \exp(-E_{des}/kT) \\ \nu_- &= A_- \exp(-E_{dis}/kT) \end{aligned}\right\} \tag{7}$$

where the potential barriers E_{des} and E_{dis} include heats of desolvation and dissolution respectively.

There may be two paths of building units from solution to a crystal. The first path is direct diffusion from the bulk solution to the steps and the second consists of two stages; 1) diffusion from the solution to the atomically flat surface and 2) diffusion along the surface to the steps. It is still a subject of discussion at the moment which path is predominant in actual solution growth. Although BENNEMA and GILMER (1973) insist on the surface diffusion model, based on their detailed interpretation of experiments, there is experimental evidence in electrocrystallization that the direct incorporation from the bulk solution to the step makes the main contribution to the growth rate (BOSTANOV *et al.*, 1977).

Let z' and x' be the axes normal and parallel to the stepped surface respectively, the origin being located on the step line as shown in Fig. 2. Then, the concentration distribution of the crystallizing species in the solution $C(x', z')$ according to the bulk diffusion model (CHERNOV, 1974) is:

$$C(x', z') = A' \ln\left[\sin^2 \frac{\pi x'}{\lambda_{st}} + \sinh^2 \frac{\pi z'}{\lambda_{st}}\right]^{1/2} + B' \tag{8}$$

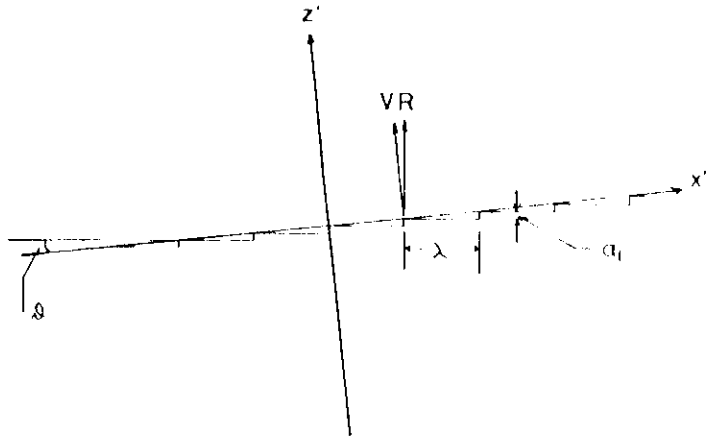

FIG. 2. Definition of x' and z' axis on stepped interface.

where A' and B' are integration constants and λ_{st} is the interstep distance. This equation includes the interaction between the steps via bulk diffusion. Far from the interface, where $z' \gg \lambda_{st}$, Eq. (8) can be approximated as follows:

$$C(x', z') \simeq C(z') = \frac{A' \pi z'}{\lambda_{st}} + B'. \tag{9}$$

On the other hand, at a point far from the interface, the concentration should satisfy the one dimensional Laplace equation from which one gets

$$C(z') = A'' z' + B''. \tag{10}$$

Defining V as the normal growth velocity to the interface, one gets the boundary condition in the form,

$$D \frac{\partial C}{\partial z'} = (C_e - C^*)V, \tag{11}$$

where C^* and C_e are the concentrations at $z'=0$ and in the crystal. If the step density on the growing interface is so high that the normal growth rate V depends linearly on supersaturation, the following relation, analogous to Eq. (5) may be written:

$$C_e V = \beta(C^* - C_e) = \beta C_e \sigma \tag{12}$$

where the supersaturation at the growing interface is expressed as,

$$\sigma = \frac{C^* - C_e}{C_e}. \tag{13}$$

Equations (10), (11) and (12) give the following one-dimensional concentration distribution:

$$C(z') = \frac{(C_s - C^*)}{D} Vz' + \frac{(C_s - C^*)}{\beta} V + C_s. \tag{14}$$

In the limit of small x' and z', Eq. (8) reduces to:

$$C(r) = A' \ln\left(\frac{\pi r}{\lambda_{st}}\right) + B' \tag{15}$$

where $r = \sqrt{z'^2 + x'^2}$. At $r = a/\pi$, the concentration given by Eq. (15) should satisfy Eq. (5) which may be rewritten in the form of

$$D \left.\frac{\partial C}{\partial r}\right|_{r=\frac{a}{\pi}} = \beta_{st}\left\{C\left(\frac{a_1}{\pi}\right) - C_e\right\}$$
$$= C_s \nu_{st}. \tag{16}$$

This gives A' and B' in Eq. (8) after comparing Eqs. (9) and (14):

$$\left.\begin{aligned} A' &= \frac{(C_s - C^*)}{D\pi} V\lambda_{st} \\ B' &= \frac{(C_s - C^*)}{\pi D} V\lambda_{st}\left\{\ln\left(\frac{\pi}{a}\right) + \frac{D\pi}{\beta_{st}a_1}\right\} + C_e \\ &= \frac{(C_s - C^*)V}{\beta} + C_e. \end{aligned}\right\} \tag{17}$$

Hence, β can be expressed via β_{st} in the following manner:

$$\beta = \frac{\beta_{st}(a_1/\lambda_{st})}{1 - \frac{\beta_{st}a_1}{D\pi}\ln\left(\frac{a_1}{\lambda_{st}}\right)}. \tag{18}$$

Here, a_1/λ_{st} is the slope of the stepped surface with respect to the nearest singular plane. We denote it by p:

$$p = \frac{a_1}{\lambda_{st}} = \tan\vartheta, \tag{19}$$

where ϑ is defined in Fig. 2. The quantity p can be positive or negative. With p thus defined, Eq. (18) takes the form:

$$\beta = \frac{\beta_{st}|p|}{1 - \frac{\beta_{st}a_1}{D\pi}\ln|p|}. \tag{18'}$$

The second term in the denominator gives the effect of interstep interaction. If $(\beta_{st}a_1/D\pi)\ln|p| \ll 1$,

$$\beta \simeq \beta_{st}|p|. \tag{20}$$

Analogously,

$$\nu_{st} = \frac{\sigma}{C_s} C_e \beta_{st}\left[\frac{\beta\lambda_{st}}{D\pi}\ln\left(\frac{a_1}{\lambda_{st}}\right) + 1\right], \tag{21}$$

where σ is the supersaturation given by Eq. (13).

From Eqs. (8) and (17), one gets

$$C^* = C\left(\frac{\lambda_{st}}{2}, 0\right). \tag{22}$$

This means that the concentration at the growing interface in the one-dimensional model is a maximum rather than an average surface concentration as in the two-dimensional model shown in Fig. 3. The average surface concentration

$$\bar{C}(0) = \frac{1}{\lambda_{st}}\int_{-\lambda_{st}/2}^{\lambda_{st}/2} C(x', 0)\,dx'$$
$$= B' - A'\ln 2. \tag{23}$$

Hence, if

$$\frac{C^* - \bar{C}(0)}{C^*} \simeq \frac{A'\ln 2}{B' - C_e} \simeq \frac{\beta_{st}a_1}{D} \ll 1$$

C^* approaches the average surface concentration value. The above requirement is fulfilled for typical solution growth with β_{st} in the range of 1 to 10^{-1} cm/sec.

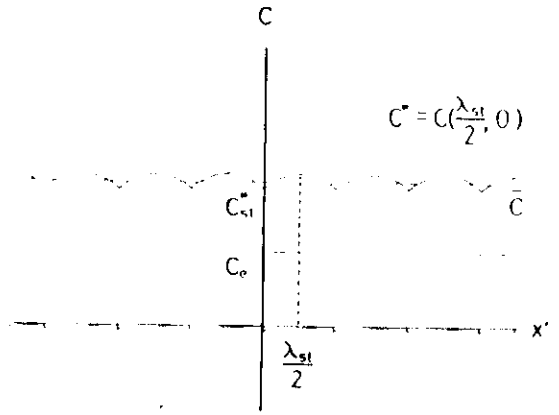

FIG. 3. Change of surface concentration and the position of atomic steps.

If surface diffusion gives an essential contribution to the growth rate, the velocity of a straight step (reviewed e.g. in; CHERNOV, 1961, BENNEMA and GILMER, 1973, and CHERNOV *et al.*, 1983) is given by

$$v_{st} = 2\frac{D_s n_{s0} f_0 \zeta \sigma}{\lambda_s} \tanh\frac{\lambda_{st}}{2\lambda_s} \tag{24}$$

where

D_s the surface diffusivity,

n_{s0} the equilibrium surface concentration of building units,

$f_0 = a^2$ the area per building unit along the step,

$$\zeta = \left[1 + \frac{D_s \tau_k}{a_0 \lambda_s} \tanh\frac{\lambda_{st}}{2\lambda_s}\right]^{-1}$$

τ_k the relaxation time of entering atoms at the kink, in other words, $\tau_k = a_0/\beta_{kink}$,

and

$\lambda_s (= \sqrt{D_s \tau_s})$ the mean distance of growing species covering the surface during τ_s, the time from adsorption to desorption.

Equation (24) includes the effect of inter-step interaction via surface diffusion, which is reflected in the hyperbolic tangent term.

Let us now define the growth rate, R, along the normal to the singular plane, as shown in Fig. 2. It is evident, that

$$R = \frac{a_0}{\lambda_{st}} v_{st} = p v_{st} . \tag{25}$$

When the steps are supplied by a screw dislocation from an s_0-fold spiral, the interstep distance, λ_{st}, is given by the well-known formula,

$$\lambda_{st} = \frac{19}{s_0} \frac{\gamma'}{k_B T} \frac{a_0}{\sigma} \tag{26}$$

where γ' is the step free energy. Basing on the surface diffusion model, one gets from Eqs. (25) and (26),

$$R = \frac{2 s_0 k_B T \sigma^2 D_s n_{s0} f_0 \zeta}{19 \gamma' \lambda_s^2} \tanh\frac{\lambda_{st}}{2\lambda_s} = \frac{\zeta D_s n_{s0} \Omega}{\lambda_s^2} \frac{\sigma^2}{\sigma_1} \tanh\frac{\sigma_1}{\sigma} \tag{27}$$

where

$$\sigma_1 = \frac{9.5\,\gamma' a_0}{s_0 k_B T \lambda_s} , \qquad \Omega = f_0 a_0 . \tag{28}$$

Equation (24) leads to

$$R = p v_{st} = \left(\frac{2 D_s n_{s0} f_0 \zeta}{\lambda_s} p \tanh\frac{a_0}{2\lambda_s p}\right)\sigma . \tag{29}$$

Analoglous to Eq. (12), one can define the kinetic coefficient for R by

$$C_e R = B(p)(C^* - C_e) = B(p) C_e \sigma . \tag{29'}$$

In the case of the bulk diffusion model, R is described in the form,

$$R = \frac{p C_e}{C_s} \beta_{st} \left[\frac{a_0}{D\pi|p|\left(1 - \frac{\beta_{st} a_0}{D\pi} \ln|p|\right)} + 1\right]\sigma$$

$$= \frac{p\beta_{st}}{C_s} \left[\frac{a_0}{D\pi|p|\left(1 - \frac{\beta_{st} a_0}{D\pi} \ln|p|\right)} + 1\right](C^* - C_e). \tag{30}$$

Both models give R in the form of $(C^* - C_e)$ multiplied by a function of the slope p. If the steps are supplied from a dislocation, p itself becomes a function of supersaturation as we have seen in Eq. (26).

One can define horizontal growth velocity, v, by simple geometrical consideration as shown in Fig. 4;

$$\left.\begin{aligned} v &= \frac{R}{p} - \frac{\sqrt{1+p^2}}{p} V \\ &= v_{st}. \end{aligned}\right\} \tag{31}$$

Using Eqs. (12) and (31), one gets

$$\left.\begin{aligned} C_s R &= \beta(p)\sqrt{1+p^2}\,(C^* - C_e) \\ &= B(p)\,(C^* - C_e) \end{aligned}\right\} \tag{32}$$

and

$$\left.\begin{aligned} C_s v &= \frac{\beta(p)}{p}\sqrt{1+p^2}\,(C^* - C_e) \\ &= b(p)\,(C^* - C_e)\,. \end{aligned}\right\} \tag{33}$$

The factors $\beta(p)$, $B(p)$ and $b(p)$ are all called kinetic coefficients for corresponding growth rates. They are measured in units of velocity, say, cm/sec. If those kinetic coefficients are large with respect to typical bulk diffusion, the concentration on the growing surface, C^*, is close to the equilibrium concentration, C_e. The relation between C^*, C_e and C is shown in Fig. 5 for the case the simplest planar interface.

In the case of the surface diffusion model, if the step density is low enough to neglect interstep interaction, $\tanh(a_l/2\lambda_s p)$ in Eq. (29) tends to unity and R is directly proportional to p as shown in Fig. 6 by lines, a–o and a′–o. This gives V being proportional to $\sin\vartheta$. If the step density increases and the steps

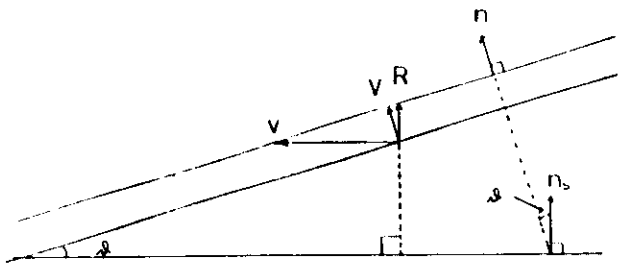

Fig. 4. Relationship between R, V and v with respect to a singular plane.

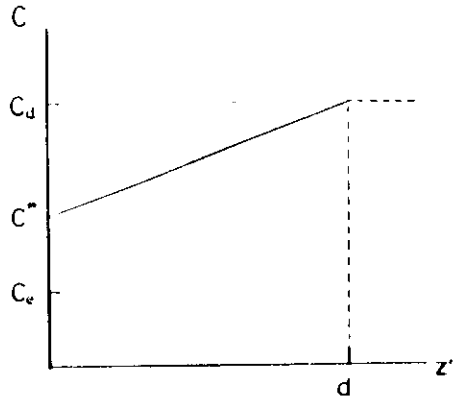

Fig. 5. Concentration distribution of solute for planar interface.

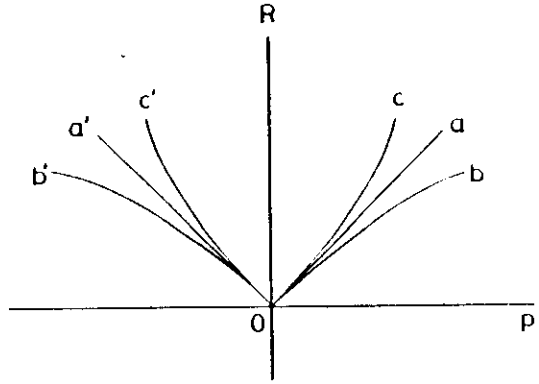

Fig. 6. Various R-p relationships. a–0–a′: no interstep interaction, b–0–b′: the smaller λ_s gives the lower v_{st} and c–0–c′: the smaller λ_s gives the higher growth rate due to, for instance, impurity effect.

interact one with another, the diffusion fields around the steps overlap. Then, the step velocity falls with the increasing slope and R does not increase linearly with the slope any more (Fig. 6, curve b–o–b′).

If an impurity which decelerates the step movement is added, diminishing the step distance gives rise to an increase in the growth velocity and hence the R-p relation becomes superlinear (Fig. 6, curve c–o–c′).

3. *Effect of Interface Kinetics on Growth Rate*

We saw in the previous section that if the kinetic coefficient, $\beta(p)$, $B(p)$ or $b(p)$, is very large as compared with the typical transport rate, the surface concentration C^* takes almost exactly its equilibrium value and the overall growth rate is governed by material transport to the growing surface. On the other hand, if the kinetic coefficient is small, one finds at the growing surface nearly the same supersaturation as in the bulk and the growth rate is now controlled by the interface kinetics. Under isotropic transport control the growth rate is isotropic. In contrast, the growth becomes anisotropic under kinetics control since the kinetics coefficient usually exhibits pronounced anisotropy. Here, for the convenience of the reader, we shall repeat the well-known consideration of the interplay between isotropic surface growth kinetics and bulk diffusion which determine the growth rate. The expression for planar, cylindrical and spherical growing interfaces will be given.

Choosing the z-axis normal to the growing surface, as shown in Fig. 7, one obtains a diffusion equation for the growing atoms in the form of Laplace's equation for a stationary state:

$$D \frac{d^2 C(z)}{dz^2} = 0 . \tag{34}$$

With the boundary conditions:

$$\left.\begin{aligned} C(d) &= C_\infty \\ C(0) &= C^* \end{aligned}\right\}$$

and

$$D \frac{dC(z)}{dz} = \beta(C^* - C_e) = C_e V \tag{35}$$

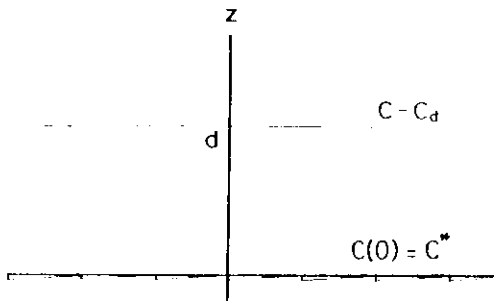

FIG. 7. Axis and boundary conditions for planar growth.

one gets

$$C(z) = az + b , \tag{36}$$

where d is the position of the boundary,

$$a = \frac{\beta(C_\infty - C_e)}{D(1 + \beta d/D)} \tag{37}$$

and

$$b = C^* = \frac{C_\infty + C_e \beta d/D}{1 + \beta d/D} . \tag{38}$$

The normal growth velocity, V is given by

$$V = \frac{\beta}{C_e} \frac{C_\infty - C_e}{1 + \beta d/D} \tag{39}$$

from Eq. (35).

If one takes into account the relative movement of the growing interface against the diffusion field, one should solve

$$D \frac{d^2 C(z)}{dz^2} + V \frac{dC(z)}{dz} = 0 \tag{40}$$

with the same boundary conditions as before. Now, the concentration is given by

$$C = C_\infty - (C_\infty - C_e) \frac{\exp\left(-\frac{V}{D} z\right) - \exp\left(-\frac{V}{D} d\right)}{1 - \exp\left(-\frac{V}{D} d\right) + \frac{V}{\beta}} \tag{41}$$

in the approximation of $(C_\infty - C_e)/C_e \ll 1$, which is established for usual solution growth.

If one puts the substrate into a solution with a certain supersaturation, there is no steady state any more and one has to solve a time dependent diffusion equation with similar boundary conditions as before. GHEZ and GIESS (1974) obtained the normal growth velocity $V(t)$ and the position of the growth front $Z(t)$ in the form

$$V(t) = \frac{C_\infty}{C_s}\frac{C_\infty}{C_s}\sqrt{\frac{D}{\pi t}} \quad \frac{C_\infty}{C_s}\frac{C_\infty}{C_s} D\left[\frac{1}{\sqrt{\pi D t}}\right.$$

$$\left. - \frac{\beta}{D} e^{\frac{\beta^2}{D}t} \operatorname{erfc}(\beta\sqrt{t/D})\right] \tag{42}$$

and

$$Z(t) = \frac{2(C_\infty - C_e)}{C_s}\sqrt{\frac{Dt}{\pi}} - \frac{C_\infty - C_e}{C_s}\frac{D}{\beta}$$

$$\left[1 - e^{\frac{\beta^2}{D}t} \operatorname{erfc}(\beta\sqrt{t/D})\right], \tag{43}$$

where C_∞ is the concentration at infinity.

Similar analysis for cylindrical and spherical growths gives the concentrations and the normal growth velocities:

(a) growth of a cylinder:

$$C = C_{r_1} + \frac{\beta r_0}{D}(C_{r_1} - C_e)\frac{\ln(r/r_1)}{1 + (\beta r_0/D)\ln(r_1/r_0)} \tag{44}$$

and

$$V = \frac{\beta}{C_s}\frac{C_{r_1} - C_e}{1 + (\beta r_0/D)\ln(r_1/r_0)} \tag{45}$$

(b) growth of a sphere:

$$C = C_\infty - (C_\infty - C_e)\frac{\beta r_0/D}{1 + \beta r_0/D}\frac{r_0}{r} \tag{46}$$

and

$$V = \frac{\beta(C_\infty - C_e)}{C_s(1 + \beta r_0/D)} \tag{47}$$

where r_0 denotes the radius of the growing cylinder or sphere, r_1 the radius of the outer boundary for cylindrical growth, and C_{r_1} is the concentration at the outer boundary.

4. *Diffusion Kinematic Wave*

Here we try to describe an evaluation of a growing interface possessing an arbitray shape (Nishinaga and Chernov, unpublished), following the approach

developed by CHERNOV (1963). Let us consider an arbitrary growth front AB shifting to the position A′B′ in the time dt (Fig. 8). The point C under consideration is located on AB at the moment t. The intersection of the normal to AB at the point C with the new position A′B′ gives us the point C′. At the point C″, the slope of A′B′ is the same as the slope AB at C. The vectors $\boldsymbol{n}$ and $\boldsymbol{n}'$ are the normals to AB and A′B′ at C and C′ respectively. $\boldsymbol{t}$ is the unit vector parallel to $\boldsymbol{n}$ $\boldsymbol{n}'$. CC″ is a trajectory of constant local slope and we denote the unit vector along this trajectory by $\boldsymbol{e}$. The length of CC″ is $V_e dt$, where V_e is the velocity of the growth in the direction of $\boldsymbol{e}$. Then we draw A″B″ translating AB parallel to itself along vector $\boldsymbol{n}$. The intersection of A″B″ and OC″ is denoted by C‴ (Fig. 8a). If we denote the length of the segment C′C″ by δs, C″C‴ is given by $(dV/ds)\delta s dt$. The angle $d\varphi$ between $\boldsymbol{n}'$ and $\boldsymbol{n}$ equals[1]

$$d\varphi = \left(\frac{dV}{ds}\right)\delta s dt/\delta s = \left(\frac{dV}{ds}\right)dt\,. \tag{48}$$

Hence, we get

$$\delta\boldsymbol{n} = \boldsymbol{n}' - \boldsymbol{n} = \frac{dV}{ds}\,dt\boldsymbol{t}. \tag{49}$$

On the other hand,

$$\delta\boldsymbol{n} = \frac{d\boldsymbol{n}}{ds}\delta s\,. \tag{50}$$

Equations (49) and (50) give

$$\frac{ds}{dt} = \frac{dV}{d\boldsymbol{n}}\boldsymbol{t} = \frac{dV}{d\varphi} \tag{51}$$

and consequently

$$\delta s = \frac{dV}{d\varphi}\,dt\,. \tag{52}$$

The growth velocity along the constant slope trajectory, V_e, is now given by the expression

[1] We have used here φ to denote the local orientation of the growth surface. This is the same as ϑ (Fig. 4) if one chooses the y-axis perpendicular to a singular plane.

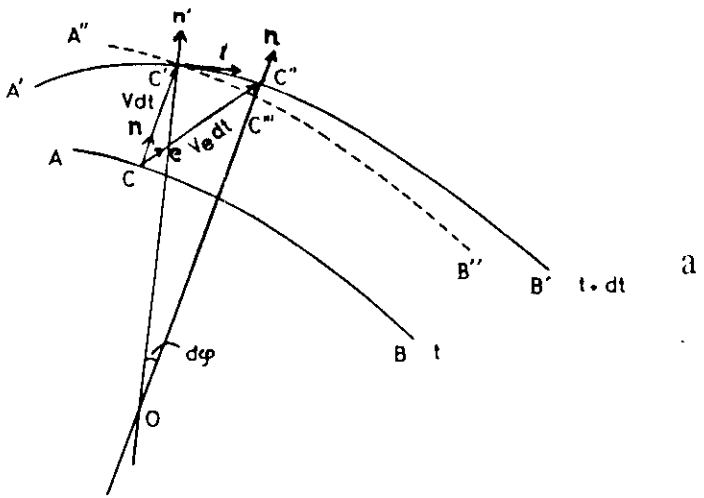

FIG. 8. Definition of various vectors and growth rates for arbitrary growth interface.

$$\boldsymbol{e}V_e = V\boldsymbol{n} + \frac{\mathrm{d}V}{\mathrm{d}\varphi}\,\boldsymbol{t} \tag{53}$$

or

$$V_e = \sqrt{V^2 + \left(\frac{\mathrm{d}V}{\mathrm{d}\varphi}\right)^2}. \tag{54}$$

To find V_e, we have to know the normal growth velocity as a function of crystallographic orientation i.e. of the slope p defined by Eq. (19). If we move from C''' to C' along A'B', we find not only the change in orientation of the front but also the change in the supersaturation, because the latter, generally

speaking, is a function of spatial coordinates. Hence, both terms contribute to $\mathrm{d}V/\mathrm{d}\varphi$, namely,

$$\frac{\mathrm{d}V}{\mathrm{d}\varphi} = \left(\frac{\partial V}{\partial \varphi}\right)_\sigma + \left(\frac{\partial V}{\partial \sigma}\right)_\varphi \frac{\mathrm{d}\sigma}{\mathrm{d}\varphi}. \tag{55}$$

First we assume that the supersaturation is uniform all over the growing interface. In this case

$$\frac{\mathrm{d}V}{\mathrm{d}\varphi} = \left(\frac{\partial V}{\partial \varphi}\right)_\sigma. \tag{56}$$

For simplicity, we write

$$\left(\frac{\partial V}{\partial \varphi}\right)_\sigma \equiv \frac{\partial V}{\partial \varphi}.$$

Then, we get

$$\boldsymbol{e}V_e = V\boldsymbol{n} + \frac{\partial V}{\partial \varphi}\,\boldsymbol{t}. \tag{57}$$

For uniform supersaturation, FRANK (1958) showed that the trajectory of constant slope is a straight line with the slope $p = R/(\partial R/\partial p)_\sigma$. This statement may be proved in our language, making use of Fig. 9, where an arbitrary coordinate axis ox is introduced. The axis may be parallel to a singular plane. The unit time interval is taken to elapse between AB and A'B', for the sake of convenience. Using Eqs. (31) and (57), one gets for the angle ψ defined in Fig. 9:

$$\tan\psi = \frac{V}{(\partial V/\partial\varphi)} = \frac{R}{(1+p^2)(\partial R/\partial p) - Rp}. \tag{58}$$

On the other hand, since $p = \tan\varphi$, we get from Eq. (58) and Fig. 9 the relationship

$$\begin{aligned}\tan\eta &= \tan(\psi - \varphi)\\ &= \frac{\tan\psi - \tan\varphi}{1 + \tan\psi\tan\varphi}\\ &= \frac{R}{\left(\frac{\partial R}{\partial p}\right)} - p\end{aligned} \tag{59}$$

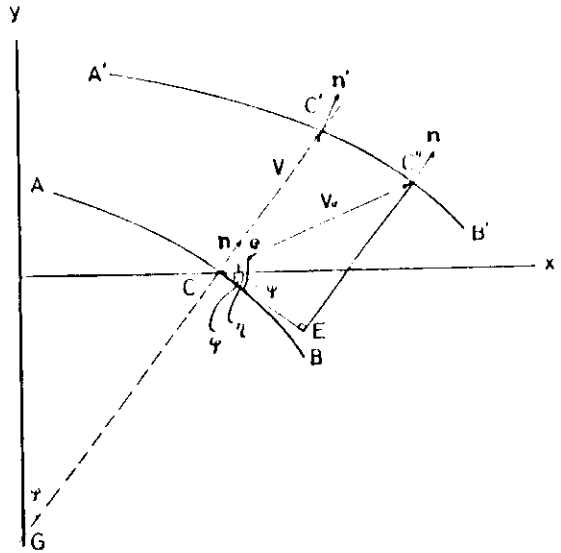

FIG. 9. Growth interface and growth rates with respect to a singular plane (0 A).

which coincides with Frank's result. The straightness of the trajectory is maintained by the constancy of V and $\partial V/\partial\varphi$ at constant φ along the trajectory, as is seen from Eqs. (58) or (59). If the function $V = V(\varphi)$ is known, the location of the growth front at any time is uniquely determined by its initial position.

For the shape preserving growth,

$$\frac{\partial e V_c}{\partial \varphi} = \left(V + \frac{\partial^2 V}{\partial \varphi^2} \right) \frac{\partial n}{\partial \varphi} \tag{60}$$

should be constant. If R is a linear function of p, η in Fig. 9 becomes zero and not a function of the local slope. Then, AB simply shifts in the horizontal direction with absolutely the same shape. In this case, V is proportional to $\sin\varphi$. In other words,

$$V + \frac{\partial^2 V}{\partial \varphi^2} = 0 \tag{61}$$

and

$$\frac{\partial e V_c}{\partial \varphi} = 0 \tag{62}$$

are established. Equation (61) stands for the case where there is no interstep interaction. Hence, if the supersaturation is uniform and the steps are too far apart to interact with each other, the growth shape is absolutely preserved.

For three dimensions, one can extend the previous discussion and obtain

$$e\boldsymbol{V}_c = V\boldsymbol{n} + \frac{\mathrm{d}V}{\mathrm{d}\varphi_1}\boldsymbol{t}_1 + \frac{\mathrm{d}V}{\mathrm{d}\varphi_2}\boldsymbol{t}_2 \tag{63}$$

and

$$V_c = \sqrt{V^2 + \left(\frac{\mathrm{d}V}{\mathrm{d}\varphi_1}\right)^2 + \left(\frac{\mathrm{d}V}{\mathrm{d}\varphi_2}\right)^2} \tag{64}$$

where $\boldsymbol{t}_1$, $\boldsymbol{t}_2$, $\mathrm{d}\varphi_1$ and $\mathrm{d}\varphi_2$ are unit vectors and changes of angle shown in Fig. 10.

If the supersaturation varies along the interface, both terms in the right side of Eq. (55) should be evaluated. For simplicity, we drop again the notations of σ and φ out of the parentheses. Equations (53) and (54) can be now rewritten in the form

$$e\boldsymbol{V}_c = V\boldsymbol{n} + \left(\frac{\partial V}{\partial \varphi} + r\frac{\partial V}{\partial \sigma}\frac{\mathrm{d}\sigma}{\mathrm{d}s} \right) \boldsymbol{t} \tag{65}$$

and

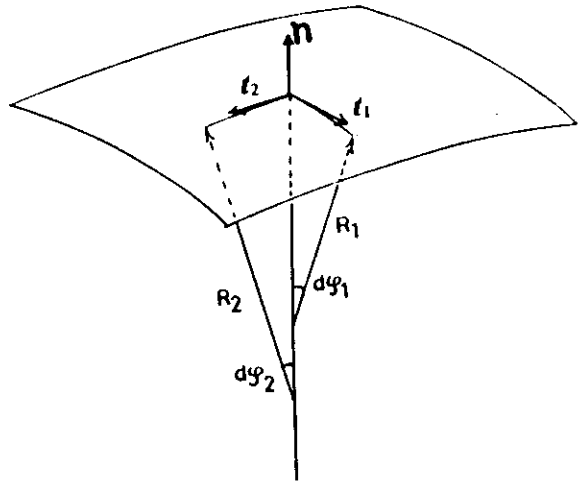

FIG. 10. Definition of three dimensional tangential unit vector and radius of curvature.

$$V_c = \sqrt{V^2 + \left(\frac{\partial V}{\partial \varphi} + r \frac{\partial V}{\partial \sigma} \frac{d\sigma}{ds} \right)^2} \tag{66}$$

where the radius of the interface curvature

$$r = \frac{ds}{d\varphi} . \tag{67}$$

Under these conditions the trajectory of constant slope is not a straight line any more. Again, for shape-preserving growth,

$$\frac{d(eV_c)}{d\varphi} = \left\{ V + \frac{d}{d\varphi} \left(\frac{\partial V}{\partial \varphi} + r \frac{\partial V}{\partial \sigma} \frac{d\sigma}{ds} \right) \right\} \frac{dn}{d\varphi} \tag{68}$$

should be constant. Putting Eq. (68) zero, one gets the condition for absolute shape-preserving growth in the form of

$$V + \frac{\partial^2 V}{\partial \varphi^2} + 2r \frac{\partial^2 V}{\partial \varphi \partial \sigma} \frac{d\sigma}{ds} + \frac{\partial V}{\partial \sigma} \left[r \frac{dr}{ds} \frac{d\sigma}{ds} + r^2 \frac{d^2\sigma}{ds^2} \right] + r^2 \frac{\partial^2 V}{\partial \sigma^2} \left(\frac{d\sigma}{ds} \right)^2 = 0 . \tag{69}$$

This equation is the same as $SV=0$, where the operator S is given by Eq. (2.12a) in Chapter 11 (van Suchtelen) of this book.

5. *Stability of Growing Interface: Fast and Slow, Isotropic and Anisotropic Growth Kinetics*

5.1 *Stability of rough surfaces*

If a growth surface is highly misoriented with respect to a singular plane or if the growth is performed under high supersaturation, the growth surface might be covered by tremendous numbers of steps and kinks. This means that the surface becomes rough. In this case, the growth kinetic coefficient is high enough to keep the concentration of growth species at the surface almost identical with the equilibrium concentration. Under these conditions the transport processes are the rate determining factor rather than the interface kinetics. Namely, the overall growth rate is governed by the diffusion of the solute and solvent. The stability problem for rough interfaces has been extensively studied in the last twenty years. Here, two simple examples will be described.

MULLINS and SEKERKA (1963) applied a general perturbation technique. They put a shape perturbation on a growing interface and investigated how this perturbation behaves by solving the equation of diffusion around this perturbed growth surface. A full and good tutorial presentation is made in the standard text book for crystal growth (SEKERKA, 1973). Thus, only a brief analysis of rough interface stability is given here to compare it with the stability of a singular interface.

For simplicity, we consider a two-dimensional isothermal solution growth as an example. Let us imagine a planar piece of a growth front (Fig. 11) moving to the right with velocity V which is much smaller than the typical diffusion velocity, D/l, in the system, l, being size of the crystal, or thickness of the boundary layer. In other words, the concentration may be described by the two-dimensional Laplace equation;

$$D \left(\frac{\partial^2 C}{\partial x^2} + \frac{\partial^2 C}{\partial z^2} \right) = 0 . \tag{70}$$

Then, we put a shape perturbation on the planar interface. In principle, one can choose any shape for the perturbation. Since however, an arbitrary shape can be expanded in a Fourier series, it is sufficient to consider the sinusoidal perturbation as depicted in Fig. 12. Let us suppose the shape of the perturbed interface to be

$$z_0 = \delta(t) \sin \omega x \tag{71}$$

where ω is $2\pi/\lambda$, δ being a weak function of time.

The boundary conditions are expressed as,

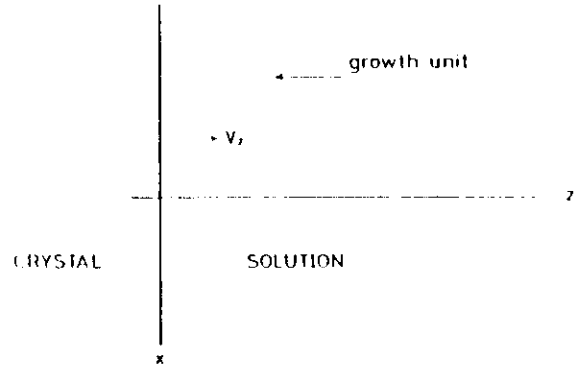

FIG. 11. Definition of coordinates.

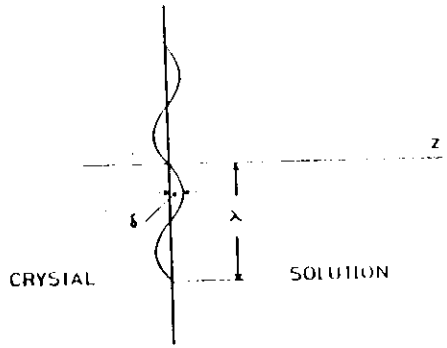

FIG. 12. Planar interface with perturbation.

$$\left.\begin{aligned} C(0) &= C_{\infty} \\ C(d) &= C_{\mathrm{d}} \\ C(z_0) &= C_{\infty}(1 + \Gamma_{\mathrm{D}} K) \end{aligned}\right\} \tag{72}$$

and

$$D\frac{\partial C}{\partial z}\bigg|_{z_0} = V_z(C_{\mathrm{s}} - C(z_0)) , \tag{73}$$

where d, Γ_{D}, K, C_{∞}, V_z and C_{s} are respectively the distance between the growth surface and solution boundary, the capillary constant ($\gamma\Omega/R_{\mathrm{g}}T$, γ being the interfacial free energy, Ω the precipitate volume per mol of growing species, R_{g} the gas constant), the curvature, the equilibrium concentration for planar interfaces, the local growth velocity in the z direction with the perturbation and the concentration of growth species in the crystal. The last equation of (72) denotes the change of equilibrium concentration with curvature due to the Gibbs-Thomson effect. The local growth velocity V_z can be written as

$$V_z = \bar{V}_z + \dot{\delta} \sin \omega x \tag{74}$$

where $\dot{\delta}$ is time derivative of δ and $\bar{V}_z$ is now the macroscopic (spatially averaged) growth velocity.

Since the one-dimensional solution for Eq. (70) is given as

$$C = C_{\infty} + \left(\frac{C_{\mathrm{d}} - C_{\infty}}{d}\right) z , \tag{75}$$

we can find the solution for the two-dimensional case in the form of

$$C = C_{\infty} + \left(\frac{C_{\mathrm{d}} - C_{\infty}}{d}\right) z + Ae^{\omega z} \sin \omega x . \tag{76}$$

Substituting Eq. (76) into (73) and using the boundary conditions (72), we get

$$f(\omega) = \frac{\dot{\delta}}{\delta} = \frac{D\omega}{(C_{\mathrm{s}} - C_{\infty})}\left\{\frac{(C_{\mathrm{d}} - C_{\infty})}{d} - C_{\infty}\Gamma_{\mathrm{D}}\omega^2\left(1 - \frac{V_z}{\omega D}\right)\right\} , \tag{77}$$

where we have picked up the terms of the first order in the perturbation. If V_z is small enough to assume $V_z/\omega D \ll 1$, one gets

$$f(\omega) = \frac{D\omega}{(C_{\mathrm{s}} - C_{\infty})}\left\{\frac{(C_{\mathrm{d}} - C_{\infty})}{d} - C_{\infty}\Gamma_0\omega^2\right\} . \tag{78}$$

From the definition of $f(\omega)$ given in Eq. (77), one finds

$$\delta = \delta_0 \exp(f(\omega)\, t) \tag{79}$$

where δ_0 is the initial amplitude of the perturbation. If $f(\omega)$ is positive, δ increases with time and the perturbation is amplified. In this case, the growth surface becomes unstable. On the other hand, if $f(\omega)$ is negative, the perturbation disappears and the surface becomes stable. $f(\omega)$ given by Eq. (78) is shown schematically in Fig. 13. ω_0 in the figure is given by

$$\omega_0 = \sqrt{\frac{C_{\mathrm{d}} - C_{\infty}}{C_{\infty}\Gamma_{\mathrm{D}}d}} . \tag{80}$$

For $\omega < \omega_0$, $f(\omega)$ is positive and the growth is unstable while for $\omega > \omega_0$, it becomes stable. The Fourier component with $\omega = \omega_{\max}$ is amplified most rapidly and hence finally the growth surface may be covered with those waves. $\omega_{\max}$ is given by

$$\omega_{\max} = \sqrt{\frac{C_{\mathrm{d}} - C_{\infty}}{3C_{\infty}\Gamma_{\mathrm{D}}d}} = \frac{\omega_0}{\sqrt{3}} \tag{81}$$

$f(\omega)$ is composed of two terms. The first term is positive (for growth) and proportional to ω and the macroscopic concentration gradient. This term acts to force the system to be unstable due to the flux inhomogeneity over the sinusoidally perturbed interface. In Fig. 14, contours of constant concentration are schematically shown for the case where the Gibbs-Thomson effect is neglected. As shown in the figure, the flux of growing species is concentrating

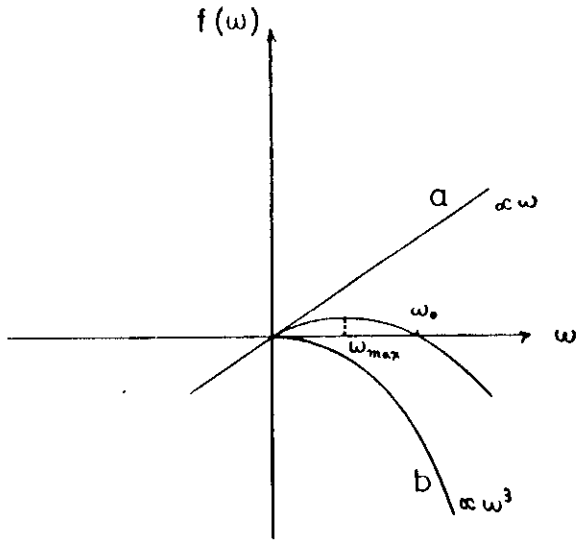

FIG. 13. Schematic illustration of $f(\omega)$. Curves a and b show the contributions of destabilizing diffusion and the stabilizing surface energy terms respectively.

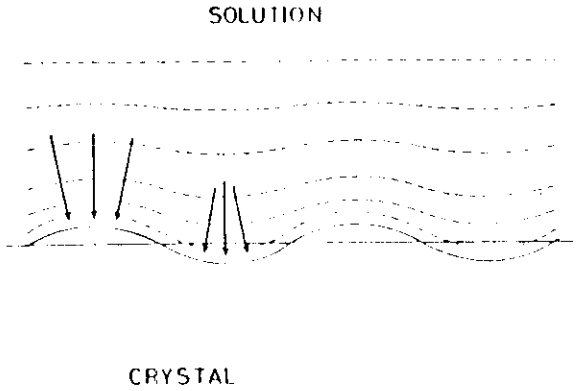

FIG. 14. Concentrating and diverging flux of solute entering the perturbed interface. Broken line shows the contour of constant concentration (schematic) without Gibbs-Thomson effect.

at the top of the sinusoidal surface while it is dispersing at the bottom. This means that the growth rate at the top is larger than that at the bottom resulting in the amplification of the sinusoidal perturbation. On the other hand, the second term of Eq. (78) stabilizes the system. This is due to the fact that to minimize the surface energy the growth at the top of the sinusoidal perturbation tends to be depressed while the growth at the bottom is accelerated. This has been done through the difference of equilibrium concentration over the sinusoidal surface. The contributions of these two terms to $f(\omega)$ are shown in Fig. 13. There are other stabilizing factors such as surface diffusion, solution stirring and so on. Growth kinetics also stabilize the surface and we shall see this in the following.

In the case of dissolution, the sign of the first term in Eq. (78) is changed and now the term contributes to stabilize the surface. However, this depends on the structure of the phase diagram and an unstable dissolution interface actually does exist (CHEN and JACKSON, 1971).

5.2 *Stability of a singular plane*

To maintain growth, sources of steps, screw dislocation or two-dimensional nuclei are required. However, the latter appear in macroscopically random positions on the interface and they can not be the centers of shape perturbation unless the generation of nucleation repeats continuously at the same place. Each of the screw dislocations, however, gives rise to a growth hillock whose slope p_0 is determined by the supersaturation. An occasional perturbation of the slope from p_0 to $p_0+\tilde{p}$ may cause steeper hillocks (if $\tilde{p}<0$) and lead to instability. The growing interface with unperturbed hillocks may be approximated by a plane whereas the perturbations of the hillocks may be considered as hillocks on this plane. Unlike the former case, the concentration above the singular face does not reach equilibrium and there exists a supersaturation. The surfaces of constant concentration (lines in two-dimension) now cross the crystal surface even independintly of the Gibbs-Thomson effect. This is illustrated in Fig. 15 a and b. As shown in the figure, the top of a hillock is exposed to a higher supersaturation than the bottom. As we saw in the previous section, diffusion effects stimulate the apex to grow faster than the residual plane part of the interface. However, if the slope of the hillock is made up of numerous steps whose density increases together with the slope, these steps consume the growth species and hence the steeper is the slope the lower should be the supersaturation at the apex. This decelerates the step generation at the apex and stabilizes the perturbed interface. Again, there are competing forces to make the growing interface stable or unstable. This kind of problem has been studied by one of the present authors. We will review in the following some of the results obtained (CHERNOV, 1972, 1974 and 1979).

Let us assume the perturbation in the form:

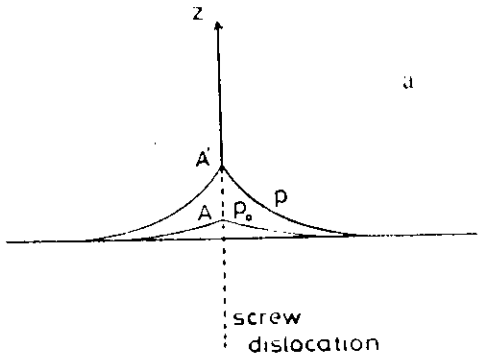

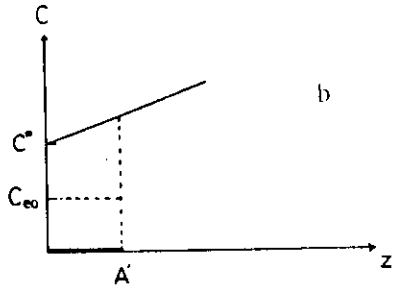

FIG. 15. Flux of solute entering the apex(a) and unperturbed concentration distribution(b). p_o denotes the slope of unperturbed hillock, which is shown here in exaggerated manner and is actually indistinguishable from plane.

$$\tilde{z} = \zeta_0 \exp(-\rho/\Lambda), \qquad \rho = (x^2 + y^2)^{1/2}. \tag{82}$$

Defining p_0 as the local slope of unperturbed hillocks existing on the growing singular interface (Fig. 15a), one gets from Eq. (32),

$$B(p_0)(C^* - C_e) = D\frac{\partial C}{\partial z} = Dq = C_3 R \tag{83}$$

and hence,

$$C^* = C_e + \frac{Dq}{B(p_0)}, \tag{84}$$

where

$$q = \frac{\partial C}{\partial z}. \tag{85}$$

For the unperturbed interface, the concentration is given as

$$C(z) = C^* + \frac{\partial C}{\partial z} z. \tag{86}$$

Substituting Eq. (84), one gets

$$C(z) = C_e + qz + Dq/B(p_0). \tag{87}$$

The concentration above the perturbed surfce may be presented in the form:

$$C(\rho, z) = \bar{C}(z) + \tilde{C}(\rho, z). \tag{88}$$

Keeping the terms proportional to the first power of the slope perturbation, $\tilde{p}$, one can write:

$$\begin{aligned} B(p) &= B(p_0 + \tilde{p}) \\ &\simeq B(p_0)(1 + \theta\tilde{p}), \end{aligned} \tag{89}$$

where θ is given by

$$\theta = \frac{1}{B}\frac{\partial B}{\partial p}\bigg|_{p = p_0}. \tag{90}$$

Since $\tilde{p}$ is written approximately as

$$\tilde{p} = \tilde{z}/\Lambda \tag{91}$$

one gets

$$B(p) = B(p_0)(1 + \theta\tilde{z}/\Lambda). \tag{92}$$

Choosing the z coordinate perpendicular to the average orientation of the growing interface (Figs. 15a, 16) and moving the coordinate together with the interface at the rate R, one has in the steady state approximation:

$$D\nabla^2 C + R\frac{\partial C}{\partial z} = 0. \tag{93}$$

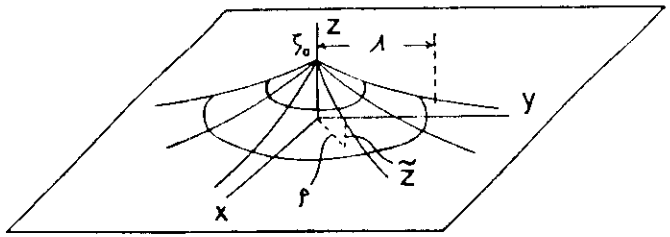

FIG. 16. Form of perturbed hillock.

At the interface,

$$C(\rho, \tilde{z}) = \bar{C}(0) + \left.\frac{d\bar{C}}{dz}\right|_0 \tilde{z} + \tilde{C}(\rho, 0) \tag{94}$$

$$\left.\frac{\partial C}{\partial z}\right|_{\tilde{z}} = \left.\frac{d\bar{C}}{dz}\right|_0 + \left.\frac{d^2\bar{C}}{dz^2}\right|_0 \tilde{z} + \left.\frac{\partial \tilde{C}}{\partial z}\right|_0 \tag{95}$$

and

$$D\left.\frac{\partial C}{\partial z}\right|_{\tilde{z}} = B(\rho)(1 - \Omega C(\rho, \tilde{z}))(C(\rho, \tilde{z}) - C_e), \tag{96}$$

where Ω is the volume of the growth unit. Subscript 0 means the value on the unperturbed interface.

Substituting Eqs. (94) and (95) into Eq. (96) and picking up the terms of the first order in the approximation, one gets

$$D\left.\frac{\partial \tilde{C}}{\partial z}\right|_0 = B^*\tilde{C}(\rho, 0) + (B^* + R + D\theta/\Lambda)q\tilde{z}, \tag{97}$$

where

$$B^* = B(\rho_0)\{1 - \Omega(2C_0 - C_e)\}. \tag{98}$$

To derive Eq. (97), we have used similar equations for the unperturbed solution $\bar{C}(z)$ satisfying (93) and (96).

$\tilde{C}(\rho, z)$ can be expressed in Fourier series,

$$\tilde{C}(\rho, z) = \frac{1}{2\pi}\int\int_{\chi} e^{\chi z - i\chi\rho} A(\chi)d\chi, \tag{99}$$

where $\boldsymbol{\rho}$ and $\boldsymbol{\chi}$ are two-dimensional vectors with the components (x, y) and (χ_x, χ_y) respectively, $\chi = |\boldsymbol{\chi}|$,

$$\chi_+ = \frac{R}{2D} + \frac{R}{2D}\sqrt{1 + \frac{4D\chi^2}{R^2}} \tag{100}$$

and

$$A(\chi) = -q\varepsilon(\chi)\frac{B^* + R + D\theta/\Lambda}{B^* + D\chi_+}. \tag{101}$$

The expression (101) for $A(\chi)$ follows from Eqs. (97), (99) and (78). $\varepsilon(\chi)$ in Eq. (101) is the Fourier transform of the perturbation:

$$\varepsilon(\chi) = \frac{1}{2\pi}\iint_{\infty}^{\infty}\tilde{z}(\rho')\, e^{i\chi\rho'}d\boldsymbol{\rho}'$$

$$= \frac{\zeta_0\Lambda^2}{(1 + \chi^2\Lambda^2)^{3/2}}. \tag{102}$$

If the tip of the perturbed hillock penetrates deeper into the solution than the unperturbed one, as shown in Fig. 17, and is at the point $z = \zeta_0$, it

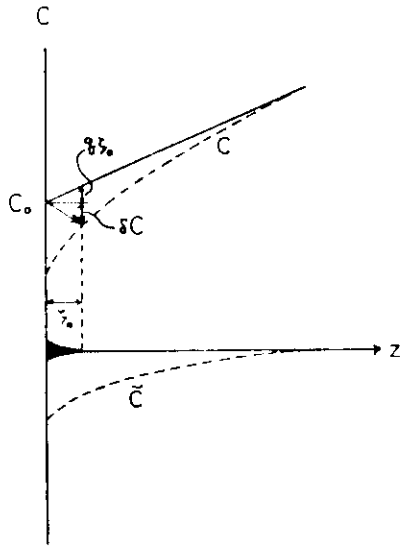

FIG. 17. Concentration distribution of solute with and without the perturbation.

experiences the concentration $\bar{C}(0) + q\zeta_0$, whereas the unperturbed hillock tip is at the concentration $\bar{C}(0)$. On the other hand the solute consumption effect lowers the concentration by the amount of $\bar{C}(0,0)$ at the center of the perturbation. Hence, making use of Eq. (94), one gets the net change of the concentration at the tip,

$$\begin{aligned}\delta C &= \bar{C}(0, \bar{z}) - \bar{C}(0) \\ &= \left.\frac{d\bar{C}}{dz}\right|_0 \bar{z} + \bar{C}(0, 0) \\ &= -q\zeta_0 + \bar{C}(0, 0) \, . \end{aligned} \tag{103}$$

For the stable case, δC is shown schematically in Fig. 17. If δC is negative as shown in this figure, the perturbed tip is in contact with a lower supersaturation than the unperturbed one and hence the surface remains planar on average. For $\delta C > 0$, the surface becomes unstable.

Substituting Eqs. (100), (101) and (102) into Eq. (99), we get the following equations after some calculation,

$$\frac{\delta C}{q\zeta_0} = 1 - \left(1 + \nu + \frac{\theta}{\mu}\right) \int_0^\infty \frac{\chi \, d\chi}{(1 + \chi^2\Lambda^2)^{1/2}(1 + D\chi_z / B^*)}$$

$$= 1 - \frac{\theta + \mu(1+\nu)}{1 + \mu^2(1+\nu)} \left\{ 1 + \mu \frac{\mu\left(1 + \frac{\nu}{2}\right)}{(1 + \mu^2(1+\nu))^{1/2}} \ln \left(\frac{\frac{1}{2}\mu^2\nu(1+\nu) - 1 - \sqrt{1 + \mu^2(1+\nu)}}{\mu(1+\nu)\left[\mu\left(-1 + \frac{\nu}{2}\right) - \sqrt{1 + \mu^2(1+\nu)}\right]} \right) \right\}, \tag{104}$$

where

$$\left.\begin{aligned} \mu &= B^*\Lambda / D \\ \nu &= R/D = \frac{\Omega(\bar{C}_0 - C_e)}{1 - \Omega(2\bar{C}_0 - C_e)} \, . \end{aligned}\right\} \tag{105}$$

$\delta C / q\zeta_0$ is shown as a function of μ in Figs. 18 and 19 for $\theta = 2$ and 5 respectively. ν, which means normalized growth rate, is taken as a parameter. The interface rapidly becomes stable as the horizontal size of the apex, Λ

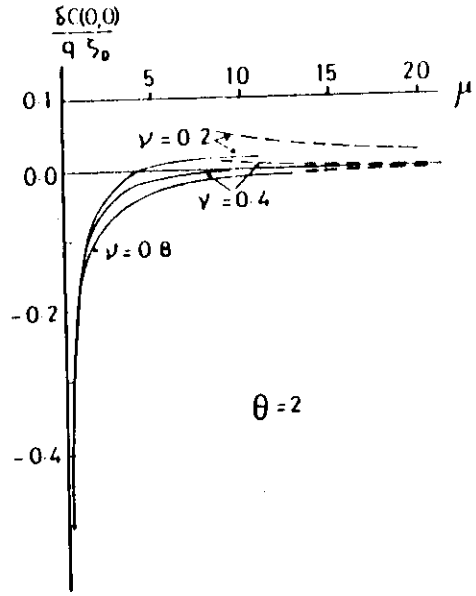

FIG. 18. $\delta C / q\zeta_0$ as a function of normalized size of the perturbation(μ), taking normalized growth rate(ν) as a parameter for $\theta = 2$. Broken line shows the approximation give by Eq. (107).

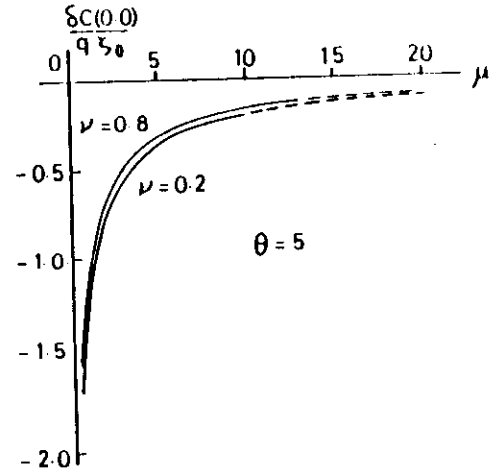

FIG. 19. The same relation as Fig. 18 for $\theta = 5$.

decreases. This is because the smaller is Λ, the higher is the absorbtive ability of the perturbation slope (the solute consumption effect), and the lower is the supersaturation at the tip. Larger values of θ, i.e. higher anisotropy of the growth rate, make the interface more stable, again due to the more pronounced solute consumption effect. Equation (104) is approximated by

$$\frac{\delta C}{q\zeta_0} = 1 - \theta \tag{106}$$

for $\mu \leq 1$ and by

$$\frac{\delta C}{q\zeta_0} = \frac{1}{\mu}\left(\frac{\theta}{1+\nu} + 1 - \ln\frac{4}{\nu}\right) \tag{107}$$

for $\mu \gg 1$. $\delta C/q\zeta_0$ given by Eq. (107) is shown by the broken line in Figs. 18 and 19.

The two-dimensional apex or ledge, depicted in Fig. 20, can be similarly analyzed as follows. Expressing the perturbation in the form of

$$\zeta = \zeta_0 \exp(-|x|/\Lambda) \tag{108}$$

one gets

$$\frac{\delta C}{q\zeta_0} = 1 - \frac{\mu(1+\nu)+\theta}{\mu^2(1+\nu)+1}\left[\mu\left(1+\frac{\nu}{2}\right) + \frac{1}{\pi}\sqrt{1-\frac{\mu^2\nu^2}{4}}\right.$$

$$\left. + \ln\frac{1+\sqrt{1-\mu^2\nu^2/4}}{1-\sqrt{1-\mu^2\nu^2/4}} + \frac{1+\frac{\nu}{2}}{\sqrt{1+\nu}}\ln\frac{\sqrt{1+\nu}-1}{\sqrt{1+\nu}+1}\right]. \tag{109}$$

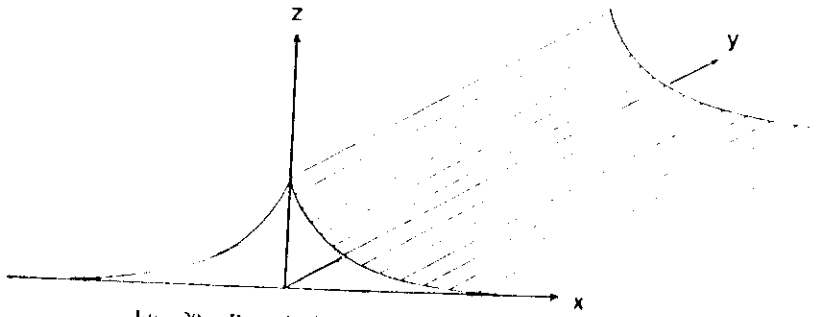

FIG. 20. Perturbation in the form of two dimensional apex

For $\mu \gg 1$ and $\nu \ll 0.1$, Eq. (109) is approximated by

$$\frac{\delta C}{q\zeta_0} = 1 - \frac{\mu+\theta}{\mu^2+1}\left(\mu - \frac{2}{\pi}\ln\mu\right). \tag{110}$$

5.3 Stability of polyhedra

It has often been observed that small polyhedra grow preserving their shape. We shall consider the reason for this phenomenon very briefly, taking the growth of a cube as an example. Detailed analysis is given by CHERNOV (1972, 1974), KURODA *et al.* (1977) and OOKAWA (1977).

Let us assume that a cubic crystal is growing in a solution. This shape will be maintained stably during the growth if the normal growth rate, R, is uniform everywhere along each face. On the other hand, if steady state growth is established, the concentration around the crystal obeys the Laplace equation with the boundary condition of constant concentration gradient over the growing surface. The concentration distribution can be found by making use of a conformal transformation (SEEGER, 1953) or numerically by computer (KURODA *et al.*, 1977). The results showed that the surfaces of constant concentration are almost spherical and concentric irrespective of the cubic shape. This is schematically shown in Fig. 21a. If the equilibrium concentration, C_e, is uniform all over the growth surface, the supersaturation over the growth surface changes like the concentration and is schematically illustrated in Fig. 21b. The growth rate can be uniform under the condition of non-uniform supersaturation, if this nonuniformity is compensated by such a variation of local slope p, and thus the kinetic coefficient $B(p)$, that the normal growth rate R is constant:

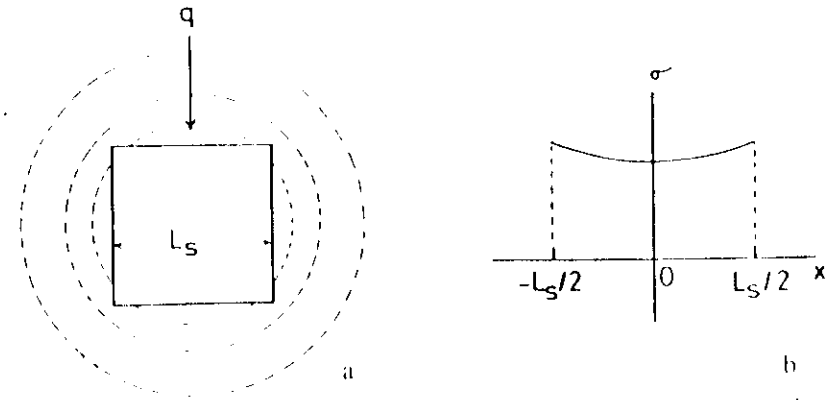

FIG. 21. Contour of constant concentration for the growth of square (a) and concentration distribution along one of the side (b).

$$R \quad \frac{B(p^*(x))}{C_e} (C^*(x) \quad C_e) - \text{constant.} \tag{111}$$

At first sight, it seems contradicory to assme a change of local slope together with the flat surface of the cube. However, because of high growth rate anisotropy, very small changes less than 1° in the slope can compensate for a super saturation difference as large as 20%. The change of the slope by 1° can be assumed not to affect the flatness of the cube surfaces in the sense of macroscopic growth and the associated diffusion field.

There are two possible slope distributions to compensate the supersaturation inhomogeneity. They are illustrated in an exaggerated manner in Fig. 22a and b. On the true scale, however, the shape distortion is very small and each face can not be distinguished from a flat surface. Figure 22a shows the case where steps are supplied from the cube corners. This can be done by two-dimensional nucleation at the corners where the supersaturation is highest. Figure 22b shows the opposite kind of distribution, at which screw dislocations supply steps. The former case is typical of a high overall supersaturation while the latter case is realized when the supersaturation is not sufficient for two-dimensional nucleation. When the cube grows larger, the supersaturation difference between the corner and the center increases in proportional to BL_s/D and finally becomes too large to be compensated by the change of slope. This is because $B(p)$, in general, saturates with increasing p. Once it happens, the corner in the case of Fig. 22a grows more rapidly than the center and shape-preserving growth is not possible any more. The same kind of instability happens when one increases the overall supersaturation instead of increasing the crystal size.

The critical size, L_s above which the shape preserving-growth is not possible, can be determined as the size above which an avalanche-like increase of face slope begins. This happens when the local slope exceeds a value p^* of

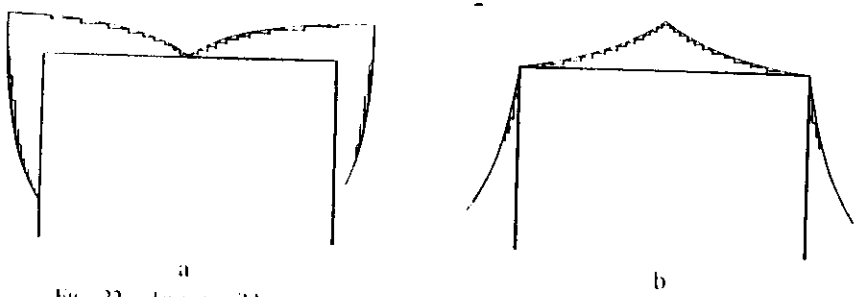

a b

Fig. 22. Two possible arrangements of steps to realize uniform growth over the square.

the order of 10^{-2} 10^{-1}, at which the fast increase of $B(p)$ with p is altered to the vicinity of a smooth maximum. The condition for the size may be written in the form:

$$R_{\text{corner}} = B_{\max} (C^*(0) - C_e) \tag{112}$$

where R_{corner} is the growth rate at the corner, $B_{\max} = B(p^*)$ and $C^*(0)$ is the concentration on the growing surface at the center depending on the critical size L_s. R_{corner} depends on the nucleation rae there and is also a function of $C^*(L_s/2)$. The explicit expression for L_s is given by CHERNOV (1974).

If the mode of growth is that shown in Fig. 22b, shape-preserving growth is maintained continuously. However, as the crystal size is increasing, the supersaturation in the middle of the face approaches zero, and either the growth mode changes to the former one or the growth rate continuously tends to zero. If one increases the overall supersaturation, as in the case of Fig. 22b, the instability shown in 5.2 or the mode change may occur, depending on the degree of supersaturation.

The criterion given by Eq. (112) is not enough to guarantee complete stability. Instability may occur by some perturbation in the shape, even if the crystal size is below the critical one. To study this kind of instability, we take a square as an example and see how the growth shape changes after perturbation of the ledges as shown in Fig. 23. We assume here a perturbation in the form of

$$\tilde{y}' = \zeta_0 \exp(-|x'|/\Lambda) \tag{113}$$

where the origin of the coodinates (x', y') shown in Fig. 23 coincides with the corner of the unperturbed square. Assuming that OA is a singular surface with $p=0$, one gets the slope of the perturbed surface ($x' \leq 0$) in the form of

$$p = \frac{(\zeta_0/\Lambda)\sin^2\Psi \exp\left[-\frac{1}{2}(L_s - 2x)\sin\Psi\right]}{1 + (\zeta_0/\Lambda)\sin\Psi\cos\Psi \exp\left[-\frac{1}{2}(L_s - 2x)\sin^2\Psi\right]} \tag{114}$$

where $\Psi = \pi/2 - \pi/n$ and n is the number of edges of the polygon. For a square, n is 4.

The change of concentration, $\tilde{C}$, due to the perturbation can be calculated by using a similar technique to the one we have used in 5.2. The boundary condition analogous to Eq. (97) is:

$$D\frac{\partial \tilde{C}}{\partial y}\bigg|_0 = B\tilde{C}\bigg|_0 + Bq\tilde{y} - D\frac{\partial^2 C}{\partial y^2}\bigg|_0 \tilde{y} + Dq(0)\tilde{y}, \tag{115}$$

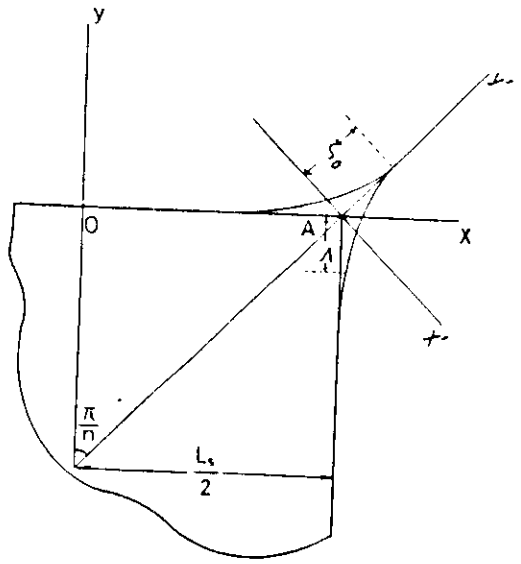

FIG. 23. New coordinate to express apex appeared at the corner of polygon.

where 0 denotes the values at $y=0$ and B is the kinetic coefficient of the unperturbed interface. Equation (115) can be approximated by

$$D\frac{\partial \tilde{C}}{\partial y}\bigg|_0 = Dq\theta\tilde{\rho} \tag{116}$$

because the first to the third terms in the right hand side of Eq. (115) are of the order of Λ/L_s with respect to the last one. Denoting the unperturbed concentration by $C(x, y)$, one can present the concentration gain at the tip of the perturbation in the form:

$$\frac{\partial \tilde{C}}{\partial y'}\zeta_0 = \frac{\partial C}{\partial y}\frac{\partial y}{\partial y'}\zeta_0$$

$$\frac{q\zeta_0}{\cos(\pi/n)} \tag{117}$$

where $q = \partial C/\partial y$. With the approximation, $|\tilde{\rho}| = \zeta_0/\Lambda$, one gets

$$\frac{\delta C}{q\zeta_0} = \frac{1}{\cos(\pi/n)} + \theta \ln\frac{\Lambda}{L_s}. \tag{118}$$

Instability occurs if $\delta C<0$. Hence, if the base of the perturbation exceeds a critical value Λ_c, the corner of the polygon must grow much faster than the faces. Λ_c is given as

$$\frac{\Lambda_c}{L_s} = \exp\left[-\frac{1}{\theta\cos(\pi/n)}\right]. \tag{119}$$

A more rigorous criterion has been obtained by making use of a conformal transformation to calculate the concentration field. The corresponding version for Eq. (118) is:

$$\frac{\delta C}{q\zeta_0} = 2^{1/2} + \frac{2^{3/2}}{3\pi}\left[\frac{2\Lambda}{\zeta_0}\ln\left(1+\frac{\zeta_0}{\Lambda}\right)\ln\left(\frac{\Lambda}{L_s}+1.6\right) + \int_0^\infty \frac{\ln z\, dz}{\exp(z)+\frac{1}{2}\zeta_0}\right]. \tag{120}$$

For such a gentle slope that $\zeta_0/2\Lambda \ll 1$, one obtains

$$\frac{\delta C}{q\zeta_0} = 2^{1/2} - 0.58 + 0.3\,\theta\left(\ln\frac{\Lambda}{L_s}+1.6\right). \tag{121}$$

The critical length, Λ_c, follows from this equation under the condition $\delta C=0$:

$$\frac{\Lambda_c}{L_s} = 0.2\exp(-2.8/\theta). \tag{122}$$

If a perturbation for which $\Lambda>\Lambda_c$ is introduced at the corner by a certain fluctuation of the supersaturation, this perturbation grows giving rise to the instability. On the other hand, the perturbation with $\Lambda<\Lambda_c$ disappears because the perturbation slope intensively consumes the solute making δC negative. In the case of instability, there are two possible growth shapes. The first is a dendrite with a sharp tip. The second is associated with the generation of macrosteps at the corner and the resulting shape is called "box-like". It is speculated that the formation mechanism of this shape may be as follows. If the perturbation begins to grow, at some stage of sharpening the slope and its consuming ability becomes large enough to change the sign of δC, which becomes negative. Then the tip ceases to grow and lateral growth starts to cover the slope as shown in Fig. 24a. The macrosteps thus introduced propagate from the corner to the face center. Once the macrostep has moved far from the corner, the latter is again subjected to high supersaturation and a

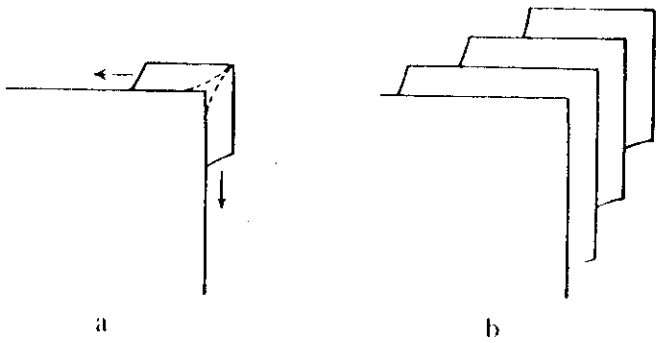

FIG. 24. Speculated mechanism for "box like" growth.

new perturbation may be formed at the corner. Thus initiation of a new apex occurs periodically, giving a "box-like" shape as shown Fig. 24b.

6. *Macrosteps*

We often observe macrosteps on crystal surfaces grown or growing from the vapor, solution or melt. The steps possess heights of the order of tens of angstroms up to several tens of microns. Microfacets may also be considered as special kinds of macrosteps. So far, there is no unified theory describing the behaviour of these macrosteps. In the following, we summarise the existing theories, which are restricted to solution growth.

Once a macrostep has been formed on a growing interface, the typical equiconcentration lines and the flux of the growth species may be schematically represented, as in Fig. 25, by dashed lines and arrows respectively. Over the top corner (edge) of the macrostep, the higher supersaturation and corresponding focusing of the stream lines enhance the growth rate there. The opposite phenomenon occurs in the vicinity of the bottom reentrant corner, namely, the depression of the growth rate due to the lower supersaturation and diverging flux lines. Macrosteps are thus developed until they reach a steady state. On the other hand, interface growth kinetics and surface free energy both oppose the development of the macrostep. Thus, the problem of macrostep formation is close by related to the stability analysis which we studied in a previous section. As we have seen in Section 3, the relationship

$$\beta h / D \simeq 1$$

should be established to find a significant concentration difference between the top and the bottom corners of the macrostep, where β, h and D are the

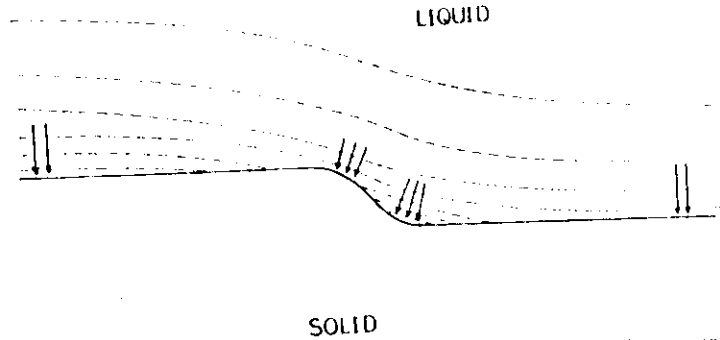

FIG. 25. Schematic illustration of contours of constant concentration around a macrostep.

kinetic coefficient, macrostep height and diffusion coefficient in the solution respectively. If h and D are of the order of 1 μm and 10^{-4} cm^2/sec correspondingly $\beta = 1$ cm/sec should be sufficient to provide inhomogeneity in feeding the top and the bottom of the macrostep.

6.1 *Macrostep undulations*

Let us imagine the growing interface with a sinusoidally varying step density which forms what we call macrostep undulations. One side of the sinusoidal wave is flattened by the kinetic effect as shown in Fig. 25, thus giving rise to a macrostep called a real macrostep or terraced macrostep. By real macrostep we also understand one whose lateral interface (stepriser) is formed by a crystallographic plane. This kind of macrostep preserves its shape in the course of growth, contray to the disappearing shock waves (FRANK, 1958; CHERNOV, 1961). We shall study real macrosteps in the next section.

In the following, the stability of macrostep undulations is studied, based on the perturbational approach (NISHINAGA *et al.*, 1978), and taking into account anisotropic growth kinetics (Nishinaga and Chernov, unpublished).

Let us assume that a stepped interface (vicinal surface) is perturbed with a sinusoidal wave of small amplitude, as shown in Fig. 26. As an example, we use the simplest solution growth model which we have studied in Section 3. The concentration of solute upon the unperturbed interface is given by Eqs. (36) (38) in the form:

$$C = \frac{\beta(C_0 - C_{e\infty})}{D\left(1 + \frac{\beta d}{D}\right)} z + \frac{1}{1 + \frac{\beta d}{D}} \left\{ C_0 + C_{e\infty} \frac{\beta d}{D} \right\}$$

$$= az + b. \qquad (123)$$

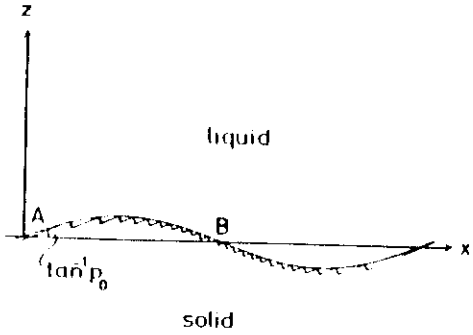

FIG. 26. x-z axis and macrostep undulation.

Now, we express the sinusoidal perturbation as

$$\begin{aligned} \tilde{z} &= \delta\sin(\omega x + \phi) \\ &= \delta_1\sin\omega x + \delta_2\cos\omega x, \end{aligned} \tag{124}$$

where

$$\left.\begin{aligned} \delta &= \sqrt{\delta_1^2 + \delta_2^2}\,, \\ \phi &= \tan^{-1}\left(\frac{\delta_2}{\delta_1}\right). \end{aligned}\right\} \tag{125}$$

Due to the difference in kinetic coefficients on both sides, A and B, of the sinusoidal perturbation shown in Fig. 26, the perturbation moves not only in a vertical direction but also in a horizontal direction, in contrast to the case studied in Section 5, where the perturbation moved only in a vertical direction. The horizontal movement of the sinusoidal perturbation is called phase shift and is expressed by ϕ in Eq. (124), $\phi = \phi(t)$, t being the time. Let us choose the concentration above the perturbed interface in the form:

$$C = az + b + e^{-\omega z}(A\sin\omega x + B\cos\omega x) \tag{126}$$

satisfying the two-dimensional Laplace equation:

$$D\left(\frac{\partial^2 C}{\partial x^2} + \frac{\partial^2 C}{\partial z^2}\right) = 0. \tag{127}$$

The boundary conditions at the perturbed growing interface $z = \tilde{z}(x)$ are now expressed as

$$D\left.\frac{\partial C}{\partial z}\right|_{\tilde{z}} = \beta(p)\,(C^*(\tilde{z}) - C_e(\tilde{z})), \tag{128}$$

$$= (\bar{V}_z + \dot{\delta}_1\sin\omega x + \dot{\delta}_2\cos\omega x)[C_s - C^*(\tilde{z})] \tag{129}$$

$$C_e(\tilde{z}) = C_{e0}\{1 + \Gamma_D\omega^2(\delta_1\sin\omega x + \delta_2\cos\omega x)\}. \tag{130}$$

As for the kinetic coefficient, we use the following approximation,

$$\begin{aligned} \beta(p) &= \beta(p_0)(1 - \theta\tilde{p}) \\ &= \beta_0\{1 + \theta(\delta_2\omega\sin\omega x - \delta_1\omega\cos\omega x)\} \end{aligned} \tag{131}$$

where $\theta = (1/\beta)(\partial\beta/\partial p)_{p_0}$. Here, p_0 and β_0 are the average slope of the unperturbed stepped interface and $\beta(p_0)$ respectively. Substituting Eq. (126) into Eqs. (128) to (130) and neglecting the terms of the second or higher order in δ_1 and δ_2, one gets a set of two differential equations as follows:

$$\left.\begin{aligned} \mu_m\dot{\delta}_1 &= \nu_m\delta_1 + \varepsilon_m\delta_2 \\ \mu_m\dot{\delta}_2 &= \nu_m\delta_1 - \varepsilon_m\delta_2 \end{aligned}\right\} \tag{132}$$

where $\dot{\delta}_i$ is the time derivative of of δ_i and μ_m, ν_m and ε_m are introduced as follows:

$$\left.\begin{aligned} \mu_m &= (C_s - b)(D\omega + \beta_0)(D\omega - \beta_0)^{-1} \\ \nu_m &= aV_z(D\omega + \beta_0)(D\omega - \beta_0)^{-1} + \beta_0(a - C_{e0}\Gamma_D\omega^2) \\ \varepsilon_m &= \beta_0(b - C_{e0})\theta\omega\,. \end{aligned}\right\} \tag{133}$$

The solution of Eq. (132) is:

$$\left.\begin{aligned} \delta_1 &= \delta_0\, e^{\frac{\nu_m}{\mu_m}t}\cos\left(\frac{\varepsilon_m}{\mu_m}t + \phi_0\right) \\ \delta_2 &= -\delta_0\, e^{\frac{\nu_m}{\mu_m}t}\sin\left(\frac{\varepsilon_m}{\mu_m}t + \phi_0\right) \end{aligned}\right\} \tag{134}$$

where δ_0 and ϕ_0 are the amplitude and the phase of the perturbation at $t = 0$ respectively. Hence, after the perturbation, the sinusoidal wave change its form according to

$$\tilde{z} = \delta_0\, e^{\frac{\nu_m}{\mu_m}t}\sin\left\{\omega x - \frac{\varepsilon_m}{\mu_m}t - \phi_0\right\} \tag{135}$$

We define

$$f(\omega) = \frac{v_m}{\mu_m}$$

in an analogous way to Section 5. Then, we get

$$f(\omega) = \frac{1}{\left(1 + \frac{\beta_0}{D\omega}\right)(C_s - b)}\left\{a(V_s + \beta_0) - \left(1 - \frac{\beta_0}{D\omega}\right)\beta_0 C_{e0}\Gamma_D\omega^2\right\} \quad (136)$$

If

$$\beta_0 \gg V_s \qquad \text{and} \qquad C_s \gg b,\ C_d,\ C_{e0} \quad (137)$$

one gets

$$f(\omega) = \frac{\beta_0}{C_s}\left\{\frac{\beta_0(C_d - C_{e0})}{D\left(1 + \frac{\beta_0 d}{D}\right)} - C_{e0}\Gamma_D\omega^2\right\}\frac{1}{\left(1 + \frac{\beta_0}{\omega D}\right)}. \quad (138)$$

This function is schematically presented in Fig. 27. The overall feature of the curve is quite similar to the previous rough surface case (Section 5): namely, $f(\omega)$ is positive for smaller ω and negative for larger ω. The critical value of ω at which $f(\omega) = 0$ is given by

$$\omega_0 = \sqrt{\frac{\beta_0(C_d - C_{e0})}{C_{e0}\Gamma_D(D + \beta_0 d)}}. \quad (139)$$

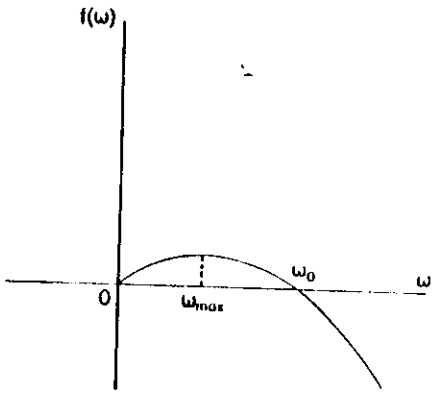

FIG. 27 Schematic illustration of $f(\omega)$ for macrostep undulation.

As the interface becomes rough, β_0 tends to infinity*, so that

$$\beta_0 d \gg D$$

and

$$\omega_0 = \sqrt{\frac{C_d - C_{e0}}{C_{e0}\Gamma_D d}}, \quad (140)$$

which is identical to Eq. (80) in Section 5.

The phase shift per unit time or phase velocity V_p can be given as

$$V_p = \frac{\varepsilon_m}{\omega\,\mu_m} = \frac{(C_d - C_{e0})\,\beta_0\theta}{\left(1 + \frac{\beta_0}{D\omega}\right)\left(1 + \frac{\beta_0 d}{D}\right)C_s} \quad (141)$$

$$\simeq \frac{\bar{V}_z\,\theta}{1 + \frac{\beta_0}{D\omega}}. \quad (142)$$

To get Eq. (142), we have used inequalities (137).

As we have mentioned, the macrostep undulation moves in both vertical and horizontal directions. The trajectory of the inflection point has and angle φ_p which is given by

$$\varphi_p = \tan^{-1}(\bar{V}_z/V_p) = \tan^{-1}\left\{\frac{1}{\theta}\left(1 + \frac{\beta_0}{D\omega}\right)\right\}. \quad (143)$$

For a rough surface, β_0 (see foot note below) and θ become infinitely large and zero respectively and we get $\varphi_p = \pi/2$. This means that the macrostep undulation moves only in a vertical direction for a rough interface, being consistent with the result obtained in the previous section

A similar analysis has been made by CAHN (1977), who expressed growth velocity and solid composition as functions of undercooling, supersaturation, local slope and curvature. By expanding them around an unperturbed state, he obtained the expressions for amplitude and phase shift when a sinusoidal

*In solution, β_0 may be finite even for a rough surface, because of the high potential barriers for desolvation and incorporation of growth units into the growing lattice (CHERNOV and TEMKIN 1977).

perturbation is introduced. However, to employ his expression one has to know the partial derivatives of the functions with all variables determined either experimentally or theoretically. These derivatives are usually not obtained and hence this restricts the applicability of the method.

6.2 *Real macrosteps*

6.2.1 *Concentration distribution around a real macrostep*

In contrast to the macrostep undulation, a real macrostep (Fig. 28) is composed of a shape-preserving step riser, which is surrounded by two flat terraces whose linear size is large as compared with that of the riser. Hereafter, we shall call the real macrostep simply macrostep. The macrostep riser is not necessarily plane but is often composed of curved surfaces. The concentration profile of the solute around the macrostep can be calculated by solving the diffusion equation. Its solution should take into account two main circumstances which are, generally speaking, independent: i) the kinetic coefficient is not constant along the interface, ii) the interface is not flat; the larger is the step height h, and thus the parameter $\beta h/D$, the more pronounced is this purely geometrical effect. The simplest way to take both these factors into account is to accept that the step riser is flat, as depicted in Fig. 29a. The analysis which takes into account only the inconstancy of the kinetic coefficient has recently been made by VORONKOV (1980). Steady-state growth displacement of the shape-preserving macrostep requires uniform growth rates along each direction and hence requires constancy of the corresponding concentration gradient at any point of the interface (NISHINAGA *et al.*, 1985). The boundary condition is now given:

$$\begin{aligned} \mathrm{d}C/\mathrm{d}n &= q_1 \qquad \text{at the step riser} \\ &= q_2 \qquad \text{at the terrace} . \end{aligned}$$

To solve the present problem, it is convenient to employ a conformal transformation (SEEGER, 1953). As shown in Fig. 29, the part above the macrostep EABF in the w-plane is mapped into the upper half of the z-plane.

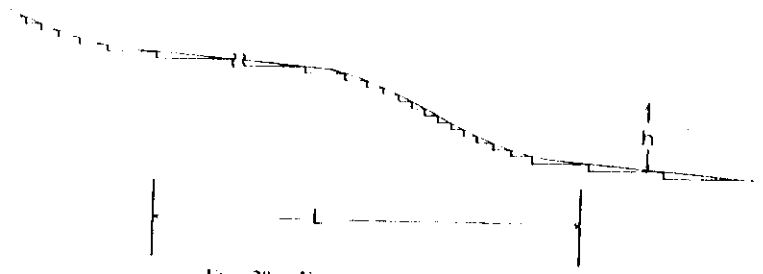

FIG. 28. Form of "true" macrostep

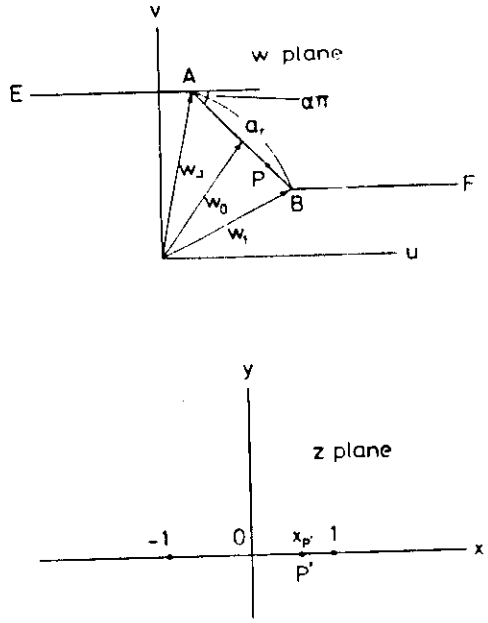

FIG. 29. Macrostep dipicted in w plane(a) and its conformal transformation into z plane(b)

This can be done by Schwarz-Christoffel transformation:

$$w = \mu_0 \int_0^t (t+1)^{\alpha}(t-1)^{\alpha} \mathrm{d}t + w_0, \tag{144}$$

where w_0 is the vector (complex number) to a middle point of the riser as shown in Fig. 29a. w_1, the vector from A to B, is given by

$$w_1 = w_J - w_{-1} = a_r e^{i(2-\alpha)\pi}$$

$$= \mu_0 \int_{-1}^{1} \left(\frac{t+1}{t-1}\right)^{\alpha} \mathrm{d}t \tag{145}$$

where w_J and w_{-1} are vectors shown in Fig. 29a and a_r is the length between A and B. From (145), we get

$$a_r = \mu_0 \int_0^{\infty} \frac{2x^{\alpha}}{(1+x)^2} \mathrm{d}x$$

$$= \frac{2\mu_0 \alpha\pi}{\sin\alpha\pi} , \tag{146}$$

hence, μ_0 is given by

$$\mu_0 = \frac{a_1 \sin\alpha\pi}{2\alpha\pi} . \tag{147}$$

An arbitrary position P on the riser is transformed into P' on the x-axis of the z-plane. The relation between r_p ($=AP$) and $x_{p'}$ (x' coordinate of P') is not linear and is given by

$$r_p = \mu_0 \int_{-1}^{x_{p'}} \left(\frac{1+t}{1-t} \right)^{\alpha} dt$$

$$= 2\mu_0 S \frac{1}{\alpha+1} {}_2F_1(2, \alpha+1, \alpha+2; -S), \tag{148}$$

where $S = (1+x_{p'})/(1-x_{p'})$ and $F(\alpha, \beta, \gamma; z)$ is the appropriate hypergeometric function. As mentioned before, the concentration gradient of solute in steady-state growth should be uniform over the terrace and the riser. Then the concentration distribution in the z-plane is given as:

$$C(z) = Re \frac{q_2\mu_0}{\pi} \int_{-\infty}^{-1} \ln|z-\xi| \left(\frac{\xi+1}{\xi-1} \right)^{\alpha} d\xi$$

$$+ Re \frac{q_1\mu_0}{\pi} \int_{-1}^{1} \ln|z-\xi| \left(\frac{1+\xi}{1-\xi} \right)^{\alpha} d\xi$$

$$+ Re \frac{q_2\mu_0}{\pi} \int_{1}^{\infty} \ln|z-\xi| \left(\frac{\xi+1}{\xi-1} \right)^{\alpha} d\xi . \tag{149}$$

It is much more convenient for the calculation to use the concentration gradient along the x-axis rather than the concentration itself. This graident is written as:

$$G(x_{p'}) = \left. \frac{\partial C^*}{\partial x} \right|_{x_{p'}} = \frac{q_2\mu_0}{\pi} \int_{-\infty}^{-1} \frac{1}{x_{p'}-\xi} \left(\frac{\xi+1}{\xi-1} \right)^{\alpha} d\xi$$

$$+ \frac{q_1\mu_0}{\pi} \int_{-1}^{1} \frac{1}{x_{p'}-\xi} \left(\frac{1+\xi}{1-\xi} \right)^{\alpha} d\xi$$

$$+ \frac{q_2\mu_0}{\pi} \int_{1}^{\infty} \frac{1}{x_{p'}-\xi} \left(\frac{\xi+1}{\xi-1} \right)^{\alpha} d\xi . \tag{150}$$

After integration, one gets

$$\left.\begin{aligned} G(x_{p'}) &= \frac{a_1 q_2}{2\alpha\pi} \{(-S)^{\alpha} - 1\}(\gamma_r - \cos\alpha\pi) \quad \text{or} \quad x_{p'} < -1 \\ &= \frac{a_1 q_2}{2\alpha\pi} \{\cos\alpha\pi - \gamma_r - S^{\alpha}(1-\gamma_r\cos\alpha\pi)\}, \quad -1 < x_{p'} < 1 \end{aligned}\right\} \tag{151}$$

where $\gamma_r = q_1/q_2$.

The solute concentration along the x-axis is now given by

$$\left.\begin{aligned} C^*(x_{p'}) &= \frac{a_1 q_2}{2\alpha\pi} (\gamma_r - \cos\alpha\pi) \left[1 - x_{p'} + 2 \frac{(-S)^{\alpha}}{\alpha+1} {}_2F_1(2, \alpha+1, \alpha+2; -S) \right] \\ &\quad + C^*(1) \qquad x_{p'} > 1 \\ &= \frac{a_1 q_2}{2\alpha\pi} (1-\gamma_r\cos\alpha\pi) \left[\frac{\cos\alpha\pi - \gamma_r}{1-\gamma_r\cos\alpha\pi} (x_{p'}+1) - 2\frac{S^{\alpha}}{\alpha+1} \right. \\ &\quad \left. \times {}_2F_1(2, \alpha+1, \alpha+2; -S) \right] + C^*(-1) \qquad 1 > x_{p'} > -1 \\ &= \frac{a_1 q_2}{2\alpha\pi} (\gamma_r - \cos\alpha\pi) \left[-x_{p'} - 1 - 2\frac{(-S)^{\alpha}}{\alpha+1} \right. \\ &\quad \left. \times {}_2F_1(2, \alpha+1, \alpha+2; S) \right] + C^*(-1) \qquad x_{p'} < -1 . \end{aligned}\right\} \tag{152}$$

The concentration difference ΔC^* between the top and the bottom corners (edges) of the macrostep can be given as

$$\Delta C^* = C^*(-1) - C^*(1)$$

$$= -\int_{-1}^{1} G(x_{p'}) dx_{p'}$$

$$= -\frac{a_1 q_2}{2\alpha\pi} (1-\gamma_r\cos\alpha\pi) \left[\frac{2(\cos\alpha\pi - \gamma_r)}{1-\gamma_r\cos\alpha\pi} - \frac{2\alpha\pi}{\sin\alpha\pi} \right] . \tag{153}$$

The gross feature of the profile is shown in Fig. 30 for $q_1 > q_2$. The singularities correspond to the corners (edges). The concentration minimum at the step riser reflects the enhanced absorption ability of the step riser as compard with that of the terrace ($q_1 > q_2$), while asymmetry in the $C^*(x_p)$ distribution reflects the geometrical non-equivalence of the top and the bottom corners of the step (NISHINAGA *et al.*, 1986).

6.2.2 *Macrostep under interface kinetics control*

For simplicity, we assume $q_2 = 0$. This corresponds to the case when the velocity of the riser in the lateral direction is much larger than the normal velocity of the terrace. Denoting the lateral velocity of the riser by v_1, one has from Eq. (29):

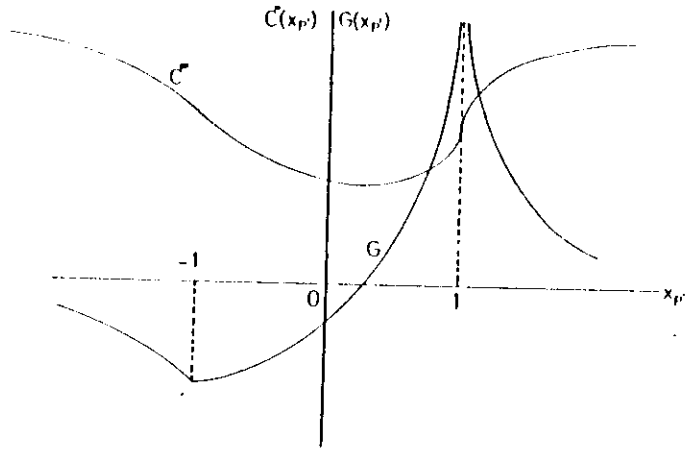

FIG. 30. C^* and G as a function of position in z plane(schematic).

$$v_l = \sin\alpha\pi \cdot R$$
$$= \frac{\sin\alpha\pi}{C_s} B(p)(C^* - C_\infty)$$
$$\equiv \frac{b_l(p)}{C_s}(C^* - C_\infty)\,. \qquad (154)$$

Here, we choose R as shown in Fig. 31. C^* is given by Eq. (152) in which x_P should be replaced by r_p using Eq. (148). However, we use the approximation $r_p/a_s \simeq (1+x_P)/2$, namely, we employ the direct correspondence of AB to the segment $-1 \le x_P \le 1$ on the x-axis of the z-plane.

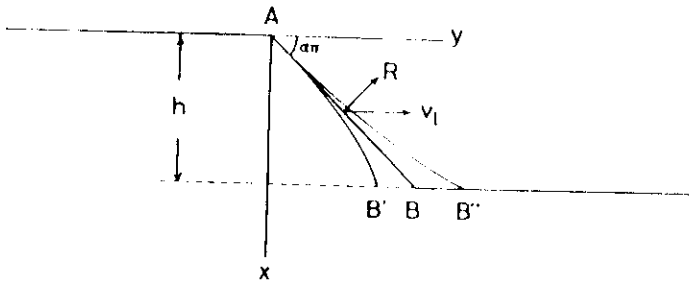

FIG. 31. Two possible end faces of macrostep to maintain uniform growth.

For the shape-preserving step, v_l should be uniform over the riser surface. If AB is approximated by a plane along which the normal flux of crystallizing species is constant, the concentration at the plane, $C^*(x)$ is given by Eq. (152) with $q \to 0$. In this case, $C^*(x)$ decreases from A to B and $b_l(p)$ should correspondingly increase to keep v_l constant. If the riser plane inclines very much from a singular plane, the changes in $b_l(p)$ may no longer be able to compensate for the concentration difference along the plane. We shall consider here the situation in which the riser is close to a singular plane whose orientation corresponds to p_A in Fig. 32. In order to keep v_l=constant along the riser, its slope should be close to p_A in the vicinity of the upper edge A. There are two possible ways to realize v_l constant as shown in Fig. 31: namely, the riser shape is either convex (AB′) or concave (AB″). A schematic illustration of $b_l(p)$ is shown in Fig. 32 as a function of slope p. In this figure, $p_{A'}$ and $p_{A''}$ are respectively the slopes of the top corner for the convex and the concave risers. If as shown in Fig. 32, there is another minimum in $b_l(p)$ on the way from A to B in Fig. 31, a new riser plane with a slope p_0 appears at C as shown in Fig. 33. Returning to Fig. 31, we examine the stability of the macrostep. Since v_l is also the velocity along the constant slope trajectory, V_c, which is given by Eq. (57); constant v_l along the riser guarantees the satisfaction of Eq. (69). The condition v_l=constant is insufficient for the stability of the macrostep. To analyze the stability, we have to examine the behaviour of the macrostep by applying a certain perturbation to its shape. Imagine that some concentration fluctuation over the concave riser pushes B″ to the right (Fig. 31). The solute concentration near B″ is then increasing due to the increase of average slope (referes to the x-axis) of the riser. Since $b_l(p)$

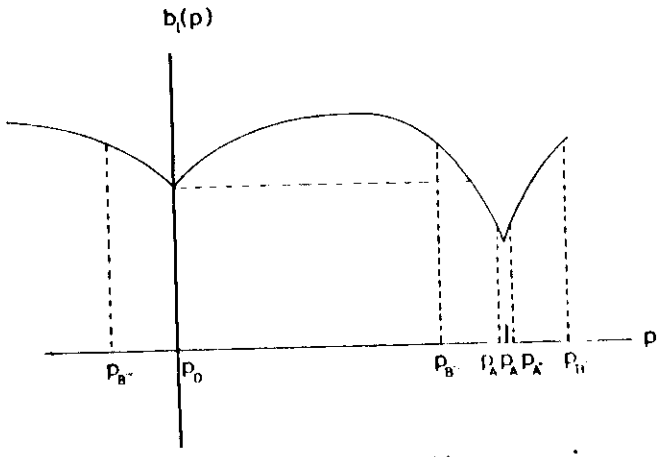

FIG. 32. The typical form of $b_l(p)$.

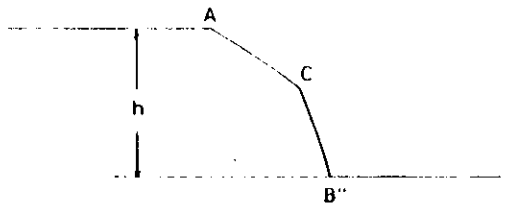

FIG. 33. Macrostep composed of two end faces of nearly singular plane.

near B″ also increases with p (Fig. 32), the growth rate near B″ is accelerated and pushes B″ further to the right, until the macrostep disappears. On the other hand, the convex riser is stable with respect to the perturbation as can be easily shown by repeating a similar argument. Hence, hereafter we shall study the behaviour of the convex macrostep when its height is increasing.

Since ΔC^* given by Eq. (153) increase as the step height h increases, $b_i(p)$ should also increase at the bottom to keep the growth velocity there constant. However, $b_i(p)$ saturates or has a maximum as shown in Fig. 32. This means that the compensation of inhomogeneity of supersaturation at the riser becomes impossible and that the macrostep cannot propagate preserving its shape. In this sense, the macrostep becomes unstable when its height reaches a certain value, above which the base of the riser advances more slowly, resulting in an overhang, as shown in Fig. 34.

In the following, we shall study this type of stable-to-unstable transition (CHERNOV and BUDUROV, 1965). For simplicity, linear approximations for $C(x)$ and $b_i(p)$ will be used:

$$C^*(x) = C_A^* + (C_B^* - C_A^*)x/h \tag{155}$$

$$b_i(p) = b_{iA} + b'_{iA}(p - p_A) \tag{156}$$

with the axes shown in Fig. 31. Here, C_A^*, C_B^*, b_{iA} and p_A are the values at the position denoted by the indices and $b'_{iA} = \partial b_i/\partial p$ at $p = p_A$. Now, the horizontal velocity v_i at the position A ($x=0$) is given from Eq. (154) in the form

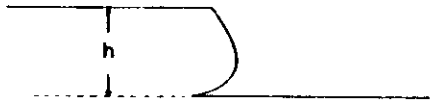

FIG. 34. Break down of stable growth for larger h to start the formation of inclusion.

$$v_{iA} = \frac{b_{iA}}{C_s}(C_A^* - C_{eo}). \tag{157}$$

At an arbitrary position on the riser, the horizontal velocity is

$$v_i(x) = \frac{b_i(p)}{C_s}(C^*(x) - C_{eo}). \tag{158}$$

For steady-state growth, this must always be equal to v_{iA}. This gives us

$$p = \frac{b_{iA}}{b'_{iA}} + p_A + \frac{b_{iA}}{b'_{iA}}\left\{1 - \frac{\Phi x}{h}\right\}^{-1}, \tag{159}$$

$$= \frac{dy}{dx}$$

where Φ may be found making use of Eqs. (153) and (157) and is given as

$$\Phi(p) = \frac{C_A^* - C_B^*}{C_A^* - C_{eo}}$$

$$= \frac{\beta_A h}{D}\sqrt{1 + p^2}\left(\frac{2}{\pi - \tan^{-1}p} - p\right) \tag{160}$$

where

$$\beta_A \equiv b_{iA}(1 + p_A^2)^{1/2}. \tag{161}$$

Integration of Eq. (159) gives

$$y = \left\{p_A - \frac{b_{iA}}{b'_{iA}}\left[1 + \frac{h}{\Phi x}\ln\left(1 - \frac{\Phi x}{h}\right)\right]\right\}x. \tag{162}$$

With average slope

$$\bar{p} \equiv y(h)/h, \tag{163}$$

one gets from Eq. (162)

$$\bar{p} = p_A - \frac{b_{iA}}{b'_{iA}}\left[1 + \frac{1}{\Phi}\ln(1 - \Phi)\right]. \tag{164}$$

In the first approximation, we take $\bar{p} \approx p_A$. This means that the riser is almost plane, for instance because the anisotropy of $b_i(p)$ is very strong and/or the step height is small enough. In this case $\bar{p}$ can be replaced by p_A in Eq. (160). If

h becomes so large that Φ exceeds unity, the stable growth breaks down at the point $x = h/\Phi$ as is seen in Eq. (162). Hence, the condition for stable growth is given by

$$\Phi = \frac{\beta_A h}{D}\sqrt{1+p_A^2}\left(\frac{2}{\pi-\tan^{-1}p_A}-p_A\right)<1. \tag{165}$$

This gives the critical condition in the form

$$\left(\frac{\beta_A h}{D}\right)_c = \frac{1}{\sqrt{1+p_A^2}}\left(\frac{2}{\pi-\tan^{-1}p_A}-p_A\right)^{-1}.$$

In general, when the riser is curved, one has to solve Eqs. (160) and (164) simultaneously to find p and Φ. This can be done graphically as shown in Fig. 35, where we take p_A as origin. For $b_{1A}/b'_{1A}>0$, one has positive $\bar{p}$, which means the riser is concave and unstable. On the other hand, for $b_{1A}/b'_{1A}<0$, we have two solutions for small $\beta_A h/D$ and no solution for $\beta_A h/D>(\beta_A h/D)_c$. Namely, for large $\beta_A h/D$, we have no stable solution. Among the two solutions the one near or the origin has meaning. As h is increased, the surface near B should be more curved to the left in Fig. 31, resulting in a more negative value of p. A detailed analysis is given in an article (CHERNOV and BUDUROV, 1964) for the stability of a riser composed of two planes such as is shown in Fig. 33.

6.2.3 Macrostep with a riser having an infinite interface kinetics coefficient

If a macrostep riser is highly misoriented from a singular plane, the distance between elementary steps becomes very small and the riser now

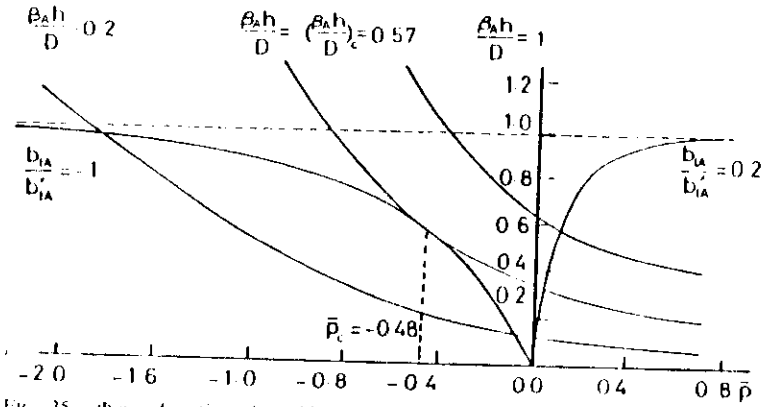

FIG. 35. Φ as a function of p taking p_A as the origine. $p>0$ and $p<0$ correspond to concave and convex end face to the solution respectively.

becomes rough in the sense discussed in 5.1. In this case, $C^*(x)$ approaches C_∞ and an equilibrium shape of the riser is determined by diffusion of the solute and the surface free energy. We shall present an analysis of this case after VORONKOV (1980).

As shown in Fig. 36, B_0A_1, B_1A_2 etc. are terraces which are close to a singular plane while A_1B_1, A_2B_2 etc. are step risers that are composed of highly misoriented surfaces. We define l, L and h respectively as shown in the same figure. The angle ϑ_0 between the average surface orientation and the terrace is assumed to be amaller than the angle $\tilde{\vartheta}$ between this average orientation and the riser. Next, velocities V_y, $v_\perp$ and V_n are defined as shown in Fig. 37, $V_\perp$ being

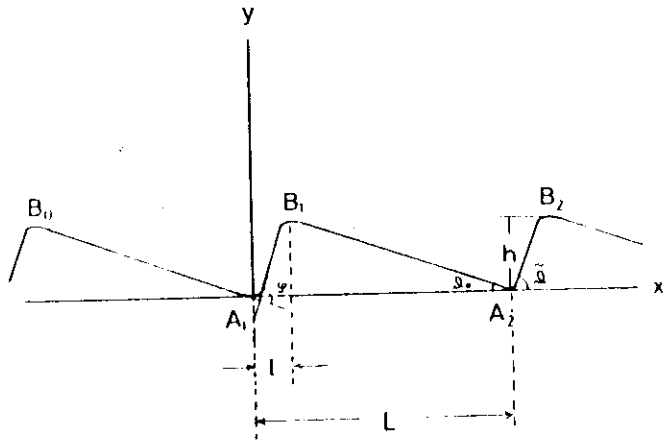

FIG. 36. Definition of variables used in Voronkov model.

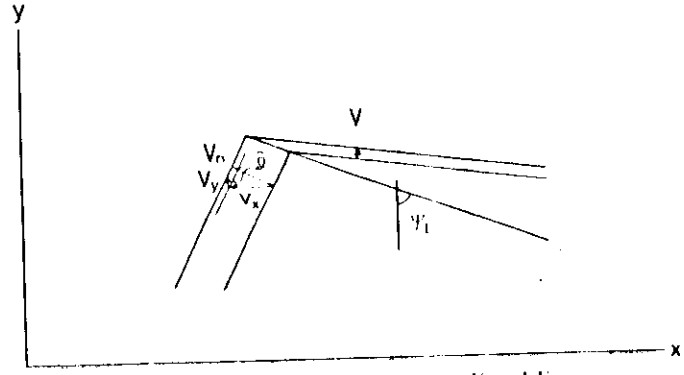

FIG. 37. Relationship between $v_\perp$, $V_\perp$ and V_n.

the velocity of the whole surface along the y-axis normal to the average orientation, v_x being the additional rate of the riser along ($-x$)-axis and V_n is the total velocity normal to the riser. The trace of the riser moved during growth is shown by the hatched area in Fig. 37. The line dividing the sections grown by the riser and terrace makes an angle ψ_t with the y-axis:

$$\psi_t = \tan^{-1}(v_x/v_y). \tag{166}$$

Expressing the shape of the macrostep by $\tilde{y}(x)$, one gets the local slope of the interface:

$$\tilde{\vartheta} = \mathrm{d}\tilde{y}(x)/\mathrm{d}x. \tag{167}$$

This can be assumed to be much smaller than unity ($\tilde{\vartheta} \ll 1$) for a small perturbation, while it is large compared with ϑ_0 in the region of the step riser. Thus, the following approximation is thought to be reasonable.

$$\tilde{\vartheta} = h/l \gg \vartheta_0$$

$$l \gg l$$

$$h = l\,\vartheta_0.$$

The normal growth velocity

$$v_n = v_y\cos\tilde{\vartheta} + v_x\sin\tilde{\vartheta}$$

$$\simeq v_y + v_x\frac{\mathrm{d}\tilde{y}}{\mathrm{d}x}. \tag{168}$$

The solute concentration, $C(x,y)$, above the perturbed (i.e. stepped) interface can be expressed as

$$C(x, y) = C_0(y) + \tilde{C}(x, y) \tag{169}$$

where $C_0(y)$ is the concentration above the flat unperturbed interface and $\tilde{C}(x,y)$ is the additional concentration due to the perturbation. In the approximation of a dilute solution, the normal growth velocity V_n obeys the relationship:

$$D\frac{\partial C}{\partial n} = C_s V_n. \tag{170}$$

Thus, from Eq. (168) one gets:

$$\frac{\partial\tilde{C}}{\partial y} = \frac{C_s v_x}{D}\frac{\mathrm{d}\tilde{y}}{\mathrm{d}x}, \tag{171}$$

where $\partial C/\partial n$ means the concentration gradient normal to the growing riser. For small $\tilde{\vartheta}$ and ϑ_0, $\tilde{C}(x,y)$ can be approximately given by

$$\tilde{C}(x, y) = \frac{C_s v_x}{\pi D}\int \left.\frac{\mathrm{d}\tilde{y}}{\mathrm{d}x}\right|_{x'} \ln r\,\mathrm{d}x' + \text{constant}, \tag{172}$$

where $r = \sqrt{(x-x')^2 + y^2}$. Since $\mathrm{d}\tilde{y}/\mathrm{d}x$ is small for the terraced region, the integral can be performed with sufficient accuracy for $0 < x' < 1$.

On the riser surface, where the kinetic coefficient is supposed to be very large, the concentration approaches its equilibrium value. The equilibrium concentration changes, however, according to the Gibbs-Thomson effect as was given by Eq. (72), namely

$$C_e = C_{e0}(1 + \Gamma_D K) \tag{173}$$

the curvature K being given by

$$K = -\frac{\mathrm{d}^2\tilde{y}}{\mathrm{d}x^2}. \tag{174}$$

The concentration $C(x,y)$ should be equal to C_e everywhere on the riser surface and hence we get

$$\frac{\mathrm{d}^2\tilde{y}}{\mathrm{d}x^2} + \frac{C - C_{e0}}{\Gamma_D C_{e0}} = 0. \tag{175}$$

At the origin where the terrace meets the riser (Fig. 36), $C(x,y)$ must be equal to C_{e0} because the curvature vanishes there. Hence, on the step riser, the solute concentration can be expressed in the form:

$$C(x, y) - C_{e0} = [C_0(\tilde{y}) - C_0(0)] + [\tilde{C}(x, 0) - \tilde{C}(0, 0)]. \tag{176}$$

On the other hand, the first bracket on the right hand side is approximated by

$$[C_0(\tilde{y}) - C_0(0)] \simeq \frac{C_s\tilde{y}}{D}. \tag{177}$$

Substituting Eq. (176) into (175) with Eq. (172), one gets:

$$\frac{d^2\eta(\xi)}{d\xi^2} + \lambda_1\eta(\xi) + \lambda_2 \int_0^1 \frac{d\eta}{d\xi} \ln\left(\frac{|\xi - \xi'|}{\xi'}\right) d\xi' = 0 \qquad (178)$$

where $\xi = x/l$, $\eta = \tilde{y}/h$, $\lambda_1 = C_s V_x \hat{l}/\Gamma_D D C_e$, $\lambda_2 = \lambda_1 v_x/\pi V_y$. By expanding η in polynomial of ξ and making use of subsequent iterations, Voronkov obtained the eigenvalues $\lambda_1 = 16.37$ and $\lambda_2 = 5.37$ for which there exists a solution of Eq. (178). From these eigenvalues it follows

$$v_x/V_y = 1.1$$

and

$$l = 4.05(DC_{e0}\Gamma_D/C_s V_y)^{1/2}.$$

Hence, in this approximation, ψ_1 is uniquely determined as 48°. It is also suggested that l is inversely proportional to V_y which shows the same dependence as $1/\omega$ given in 5.1.

This work was done in large part as a joint research in the Institute of Crystallography, Academy of Sciences of the USSR. The author (T. N.) thanks the Japan Society for Promotion of Science for making him possible to stay 10 months in Moscow and to carry out the present work.

REFERENCES

Bennema, P. and Gilmer, G. H. (1973): Kinetics of crystal growth, in *Crystal Growth*, Ed. P. Hartman, North-Holland, pp. 263–327.

Bostanov, V., Resinova, R. and Budevski, E. (1977): Monoatomic layer propagation rate and the electrolytic deposition mechanism for silver, in *Growth of Crystals*, Vol. 11, Ed. A. A. Chernov, Consultant Bureau, (English translation).

Cahn, J. W. (1977): Theoretical aspects of the formation of cells and dendrites, Record of Japan-U.S. Joint Seminar on Solidification of Metals and Alloys.

Chen, H. S. and Jackson, K. A. (1971): Stability of a melting interface, *J. Crystal Growth*, **8**, 184–190.

Chernov, A. A. (1961): The spiral growth of crystal, *Sov. Phys. Uspekhi*, **4**, 116–148, (English translation).

Chernov, A. A. (1963): The kinetics of growth form of crystals, *Sov. Phys. Crystallography*, **7**, 728, (English translation).

Chernov, A. A. and Budurov, S. I. (1964): Growth forms of macroscopic steps, development of faces on the end of steps, *Sov. Phys. Crystallography*, **9**, 309–314, (English translation).

Chernov, A. A. and Budurov, S. I. (1965): Growth forms of macroscopic steps, smooth curvature of the end faces and the formation of inclusions, *Crystallography*, **9**, 388–392, (English translation).

Chernov, A. A. (1972): Theory of the stability of face forms of crystals, *Sov. Phys. Crystallography*, **16**, 734–753, (English translation).

Chernov, A. A. (1974): Stability of faceted shapes, *J. Crystal Growth*, **24/25**, 11–31.

Chernov, A. A. (1979): Stability of planar growth front for anisotropic surface kinetics, in *Growth of Crystals*, Vol. 11, Ed. A. A. Chernov, Consultants Bureau, New York, (English translation).

Chernov, A. A., Givargisov, E. I., Bagdasarov, Kh. S., Kuznetsov, V. A., Demyanets, L. N. and Lobachev, A. N. (1983): *Modern Crystallography III, Crystal Growth*, Springer.

Frank, F. C. (1958): On the kinetic theory of crystal growth and dissolution processes, in *Growth and Perfection of Crystals*, Eds. R. H. Doremus, B. W. Roberts and D. Turnbull, John Wiley, New York, pp. 411–419.

Gilz, R. and Giess, E. A. (1974): The temperature dependence of garnet liquid phase epitaxy growth kinetics, *J. Crystal Growth*, **7**, 221.

Hurle, D. T. J. (1973): Melt growth, in *Crystal Growth*, Ed. P. Hartman, North Holland, pp. 210–247.

Kuroda, T., Irisawa, T. and Ookawa, A. (1977): Growth of a polyhedral growth from solution and its morphological stability, *J. Crystal Growth*, **42**, 41–46.

Mullins, W. W. and Sekerka, R. F. (1963): Morphological stability of a particle growing by diffusion or heat flow, *J. Appl. Phys.*, **34**, 323–329.

Nishinaga, T., Pak, K. and Uchiyama, S. (1978): Studies of LPE ripple based on morphological stability theory, *J. Crystal Growth*, **43**, 85–92.

Nishinaga, T., Sasaoka, C. and Chernov, A. A.: A numerical analysis for the supersaturation distribution around LPE macrostep, *Proc. OJI Int. Seminar on Morphology and Growth Unit of Crystals*, Zao Hot Spring, Aug. 1985 to be published.

Nishinaga, T., Tsukamoto, K., Komatsu, H., Sasaoka, C. and Mochizuki, K. (1986): Shape of atomic steps and interface supersaturation between LPE macrosteps, *J. Crystal Growth*, **79**, 806–810.

Ookawa, A. (1977): *Crystal growth*, Syokabo, Tokyo, pp. 212–224, (in Japanese).

Seeger, A. (1953): Diffusion problems associated with the growth of crystals from dilute solution, *Phil. Mag.*, **44**, 1–13.

Sekerka, R. F. (1973): Morphological stability, in *Crystal Growth*, Ed. P. Hartman, North-Holland, pp. 403–443.

Voronkov, V. V. (1965): Conditions for formation of mosaic structure on a crystallization front, *Sov. Phys. Solid State*, **6**, 2378–2381, (English translation).

Voronkov, V. V. (1980): The movement of gently sloping macrostep, in *Growth of Crystals*, Vol. 13, Nauka, Moscow, pp. 112–120, (in Russian).

Journal of Crystal Growth 97 (1989) 765–769
North-Holland, Amsterdam

GROWTH OF DIPYRAMIDAL FACE OF DISLOCATION-FREE ADP CRYSTALS: FREE ENERGY OF STEPS

A.I. MALKIN, A.A. CHERNOV and I.V. ALEXEEV

Institute of Crystallography, Academy of Sciences of the USSR, 59 Leninskii Prospekt, Moscow 117333, USSR

Received 19 December 1988; manuscript received in final form 3 April 1989

The kinetics of dislocation-free growth of the dipyramidal face of ADP crystals have been studied by laser interferometry and X-ray topography in the supersaturation range $1.5\% < \sigma < 6.4\%$. The reproducible growth of dislocation-free crystals ($R > 3 \times 10^{-8}$ cm/s) started at supersaturations $\sigma_c = 1.5$–3% in the form of spontaneous nucleation. The two-dimensional character of nucleation is confirmed by the linear character of the $\ln(R/\sigma^{5/6})$ versus $1/\sigma$ dependence. It was also revealed that the $R(\sigma)$ curve consists of two linear portions intersecting at $\sigma = 4.5\%$. It is assumed that at $\sigma > 4.5\%$ the process of nucleation is homogeneous and occurs at atomically smooth terraces, whereas at $\sigma < 4.5\%$ it proceeds at sites more active than regular, e.g., at impurity particles. The results obtained give the effective surface energy of the step end as $\alpha_1 = 11.8$ erg/cm^2 for $\sigma > 4.5\%$ and $\alpha_2 = 4.2$ erg/cm^2 for $1.5 < \sigma < 4.5\%$. Similar treatment yields the concentration of active centers on the surface: $n_s^* = 1.3 \times 10^3$ cm^{-2}.

1. Introduction

At present there are almost no reliable and moreover directly measured data of the kinetics of two-dimensional nucleation in growth from condenced media. The only exception is data on the electrocrystallization of silver [1]. There are no direct experimental, quantitative data on the effect of impurities and other growth conditions on the nucleation parameters, surface energy, kinetic coefficient of steps, and the characteristics of the preferential nucleation centers. An important step in such studies was the implementation of controlled dislocation-free growth from solutions [2] and the discovery of growth rate scatter of several orders of magnitude.

The present paper is devoted to the study of two-dimensional nucleation on dislocation-free crystals by precision laser interferometry.

2. Experimental

Growth rates of 10^{-8} cm/s and higher were measured continuously and automatically at random points in the central region of the face by a laser interferometer with an accuracy of ~ 5% [3]. The laser probe diameter on the face under study was ~ 0.7 mm. The sensitivity limit of laser interferometry used in our experiments for measuring the normal growth rate was 3×10^{-9} cm/s. The solution was prepared from twice distilled water and the corresponding "supra pure" trademark salt. The necessary solution acidity, pH = 5.0, was attained by addition of a certain amount of NH_4OH of the same purity. Dislocation free crystals were chosen with the aid of X-ray topography. Plane-parallel seeds $3 \times 3 \times 1$ mm^3 in size were cut out from these crystals and the dislocation-free structure of specimens checked up by ex situ X-ray topographs.

3. Dislocation-free growth

The most important part of the experiment is need regeneration which was performed under relative supersaturation $\sigma = 0.02$–0.03% for 40–70 h. The supersaturation is defined as $\sigma = (c - c_e)/c_e$, c and c_e being the actual and equilibrium solution concentrations. This provided either minimum presence or even complete absence of

0022-0248/89/$03.50

liquid inclusions (i.e., dislocation sources) in crystals. Despite special precautionary measures taken during seed regeneration and improved hydrodynamic conditions in the growth chamber, the regenerated seeds had no dislocations only in 10–15% of experiments. If dislocation sources were formed on seeds, the face started growing at a rate of $R \simeq 10^{-6}$ cm/s at supersaturations as low as $\sigma \simeq 0.05\%$. This is in accordance with the data obtained earlier [3,4]. Such a relatively "high" rate indicated the appearance of dislocations.

In cases where no dislocations were observed during regeneration, supersaturation was gradually increased by decreasing temperature. A nongrowing crystal was kept for some time at each new supersaturation: within 2–3 h at $\sigma \simeq 0.1\%$ and up to several tens of minutes at $\sigma > 1\%$. The noticeable growth of dislocation-free crystal began if the supersaturation exceeds a definite value, which we denotes as σ_n. Typically, $\sigma_n \simeq 1.5$–3%. The minimum supersaturation for dislocation-free growth observed in ref. [2] was $\sigma_n \simeq 2.7\%$. For $\sigma < \sigma_n$ growth proceeded, if at all, with a noncontrollable rate of about $R < 3 \times 10^{-9}$ cm/s. The attainment of the critical supersaturation, σ_n, does not necessarily trigger the face growth. Thus in one experiment face growth started only 15 min after the attainment of supersaturation $\sigma \simeq 3\%$, then for more than 30 min growth proceeded at a nonsteady rate, and only then reached steady-state growth at a rate of $R \simeq 11.5 \times 10^{-5}$ cm/s. In other experiments growth due to two-dimensional nucleation began at $\sigma \simeq 1.5\%$ at a rate of $R \simeq 10^{-6}$ cm/s. Fig. 1 shows the data obtained for dislocation growth of the dipyramidal face from solution with pH = 5.0. For $\sigma = 1.5\%$ and $\sigma = 3\%$ the dislocation growth proceeded at rates $R = 3 \times 10^{-6}$ cm/s and $R = 2 \times 10^{-5}$ cm/s, respectively. Upon the beginning of growth at $\sigma > \sigma_n$, supersaturation in some experiments were decreased by several tenths of percent down to values $\sigma < \sigma_n$. As a result, growth ceased and did not start again for several hours. If supersaturation was set again to be higher than σ_n, growth restarted at high rates corresponding to the dislocation kinetics.

A similar result was also obtained in one experiment upon the transition from $\sigma \simeq 5.4\%$ to $\sigma \simeq 0.1\%$. A nongrowing crystal was kept for about 10 h at $\sigma \simeq 0.1\%$ and then σ was increased (by decreasing the solution temperature).

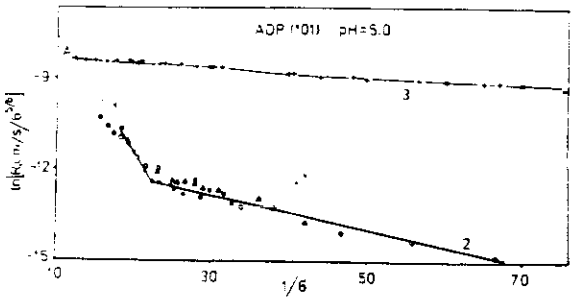

Fig. 1. Normal rate of dislocation-free growth, R, versus supersaturation σ. The slope of curve 1 yields the value of the effective linear energy of the step end ($\alpha_1 \simeq 11.8$ erg/cm); the slope of curve 2 yields $\alpha_2 \simeq 4.2$ erg/cm. Curve 3 relates to dislocation growth. Saturation temperature is 41.5°C. The supercooling of 1 K corresponds to $\sigma = 1.5 \times 10^{-2}$.

Ex situ X-ray topographs confirmed the above described picture of dislocation formation and growth of (101) face of dislocation free crystals. Growth proceeds due to two-dimensional nucleation since no layers from the neighbouring prismatic faces appear on the (101) face: no dislocations are observed on the (100) faces.

3.1. Nonregular growth due to two-dimensional nucleation under high supersaturations

Fig. 2 shows the dependence of the normal growth rate (R) of the (101) face on supersaturation ($1.5 < \sigma < 6.4\%$) for five dislocation-free crystals (the data for different crystals are denoted by different figures).

For $1.5\% < \sigma < 5\%$, growth is regular for all the studied crystals, i.e., fluctuations in R are small under constant supersaturation, being, as a rule, $\delta \equiv |R_{max}|/R < 15\%$.

For $\sigma > 5\%$ the data for two crystals were recorded. For the first crystal, fluctuations in R did not exceed $\delta \simeq 20\%$ under the above indicated supersaturations (open circles in figs. 1 and 2) *.

* At $\sigma \simeq 5.4\%$, a parasitic crystal was formed in the growth chamber. Its appearance decreased the supersaturation above the growing crystal. Therefore the R-values for $\sigma > 5.4\%$ denoted by half-filled circles are shown in figs. 1 and 2 are in fact somewhat underestimated.

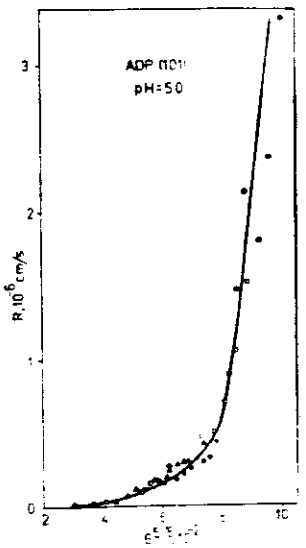

Fig. 2. Normal growth rate due to two-dimensional nucleation, R, versus solution supersaturation σ. Experimental data are denoted by different symbols different crystals. Saturation temperature is 41.5°C. The supercooling of 1 K corresponds to $\sigma = 1.5 \times 10^{-2}$.

For the second crystal (filled circles in figs. 1 and 2), fluctuations in R become substantial. $\delta > 25\%$ already at $\sigma \simeq 5\%$, and then increase for higher σ. For $\sigma \simeq 5.4\%$, growth is strongly nonregular; 1–2 min acceleration periods alternate with 1–2 deceleration periods.

4. Discussion

4.1. Multiple nucleation and basic relationships

As is well known [5], the normal growth rate R (cm/s) of a face having area S due to formation on it of two-dimensional nuclei at a rate of J ($\mathrm{cm^{-2}s^{-1}}$) is

$$R = hSJ \quad \text{if} \quad S^{1/2} < (v/J)^{1/3}, \tag{1}$$

$$R = h(v^2 J)^{1/3} \quad \text{if} \quad S^{1/2} > (v/J)^{1/3}, \tag{2}$$

where

$$v = \omega c_e \beta_l \sigma \tag{3}$$

is the velocity of nucleated steps and h is their height. We take on the (110) face $h = 5.3 \times 10^{-8}$ cm. For ADP crystals the specific molecular volume is $\omega = 1.07 \times 10^{-22}$ cm^3, the equilibrium volume concentration of the dissolved substance is $c_e = 2.12 \times 10^{21}$ $\mathrm{cm^{-3}}$ (at $t = 35°C$), and the kinetic coefficient for the (110) face averaged over azimuth is $\beta_l = 0.3$ cm/s [3,4]. Therefore at $\sigma = 1.5 \times 10^{-2}$, we arrive at $v = 9 \times 10^{-4}$ cm/s. The surfaces studies in our experiments had an area of $S = 0.1$ cm^2. Using the above values of $R = 10^{-5}$ cm/s, S, and v, we obtain $J_1 = 2.1$ $\mathrm{cm^{-2}s^{-1}}$ and $J_2 = 10^4$ $\mathrm{cm^{-2}s^{-1}}$ from eqs. (1) and (2), respectively. The obtained values of J, S and v indicate the validity of inequality (2) or, in other words, confirm that growth proceeds by multiple nucleus formation at several points on one growing face, the so-called multiple nucleation mode.

The rate of two-dimensional nucleus formation J [5] is

$$J = B \exp(-\delta\phi_c/kT). \tag{4}$$

Here the work of the formation of a nucleus in the shape of a flat disk is

$$\delta\phi_c = \pi\omega\alpha^2 h/kT\sigma. \tag{5}$$

where α is the effective surface energy of the step end taking into account center activity.

The factor B is

$$B = \mathscr{L} a h Z n_s c_e \nu \exp(-\epsilon/kT). \tag{6}$$

The Zel'dovich factor Z [5,6] is

$$Z = kT\sigma^{3/2}/2\gamma, \tag{7}$$

where n_s is the surface density of admolecules of the dissolved substance (each admolecule may play the role of a nucleation center). $\mathscr{L} = 2\pi\gamma a/kT\sigma$ is the nucleus perimeter, $\gamma = \alpha a h$, $a \simeq 10.7 \times 10^{-8}$ cm is the distance between the neighbouring atoms in the ⟨110⟩ direction, ϵ is the activation energy of the attachment of new atoms (ions) to the nucleus, and $\nu \simeq 10^{13}$ $\mathrm{s^{-1}}$.

The kinetic coefficient of steps [6] is

$$\beta_l = a\nu \exp(-\epsilon/kT); \tag{8}$$

therefore

$$B = Z n_s \mathscr{L} h c_e \beta_l. \tag{9}$$

Substituting expressions (3)–(7) into (2) and taking the logarithm, we arrive at

$$\ln\left(\frac{R}{\sigma^{5/6}}\right) = \ln\left\{hc_e\beta_l\left[\omega^2 h a n_s\right]^{1/3}\right\} - \frac{\pi\omega\alpha^2 h}{3(kT)^2}\frac{1}{\sigma}. \tag{10}$$

In eq. (10), ω, c_e, β_l, T and h are known, and therefore, representing the experimental data of fig. 2 in the $\ln(R/\sigma^{5/6})$, $1/\sigma$ coordinates (fig. 1), it is possible to calculate the unknowns α and n_s by measuring the slope of the line and the intersept cut by its continuation on the ordinate axis. The number of nucleation centers on the face may be represented as

$$n_s = hc_e \exp(-\epsilon_{ad}/kT). \tag{11}$$

If n_s is determined, it is possible to evaluate the energy ϵ_{ad} of admolecule adsorption on the surface.

4.2. Two-dimensional nucleation; elementary parameters

The most interesting result seems to be the kink in the curves shown in fig. 1. The slopes of curves 1 and 2 (fig. 1) give the surface energy of the step ends, $\alpha_1 \approx 11.8$ erg/cm^2 and $\alpha_2 \approx 4.2$ erg/cm^2. These values correspond to $\alpha_{l_1} \approx 6.3 \times 10^{-7}$ erg/cm and $\alpha_{l_2} \approx 2.2 \times 10^{-7}$ erg/cm, respectively.

It is of interest to compare the surface energies obtained above with the ones following from growth rates on dislocations. For that measurements we have used the same solution as for the dislocation-free growth. The growth rates on dislocations are indicated by crosses (+) in fig. 1 and are described by the expression:

$$R = \frac{mh^2\omega c_e\beta_l kT\sigma^2}{19\omega\alpha_l + 2Lhk T\sigma}, \tag{12}$$

where mh is the Burgers vector of a dislocation or a group of dislocations providing growth, $2L$ is the perimeter of the region of dislocation outcrops. The above expression is valid for the following parameters:

$$\beta_l \approx 8.4 \times 10^4 L \text{ (cm)/cm} \cdot \text{S}^{-1},$$
$$\alpha_l = 3.7 \times 10^{-2} L \text{ (cm) erg/cm}^2. \tag{13}$$

The β_l and α_l parameters were obtained by linearizing the functions $R(\sigma)$ [3,4]. If we use the values of ω, c_e, h, k and T indicated in section 4.1, and the values of α_l and β_l obtained from (13), eq. (12) acquires the form

$$\ln\left(\frac{R}{\sigma^{5/6}}\right) = \ln\frac{4.3 \times 10^{-4}(1/\sigma)^{-1/6}}{1 + 1.6 \times 10^{-2}(1/\sigma)}. \tag{14}$$

This dependence is depicted in fig. 1 by the dashed line 3.

The surface energy of the step ends on the (101) surface were determined earlier from the kinetics of dislocation growth [3,4] and also from independent direct measurements of R and the slope P of the vicinal hillock [7]. They yield the following values: $\alpha \approx 15$–16 erg/cm^2 and $\alpha \approx 16$ erg/cm^2, respectively.

The underestimated value of α_2 may be caused, e.g., by the fact that in the range $\sigma \approx 1.5$–4.5% (straight line 2, fig. 1) nucleation may be facilitated because it occurs not homogeneously on adsorbed impurity particles. This assumption is favoured by the fact that in this supersaturation range an increase in σ results in almost linear and not exponential increase in R (fig. 2). In some instances, an increase in σ resulted even in a decrease of the normal growth rate. The above described phenomena seem to be explained by two competing processes. On the one hand, with an increase in σ the barrier for the formation of nuclei decreases, and R should increase. On the other hand, with an increase in supersaturation and step velocity the "lifetime" $t_1 = h/R$ of each atomically smooth terrace in the solution decreases. For smaller t_1, a smaller number of particles accelerating nucleation are adsorbed on the surface. Therefore the growth rate may increase with supersaturation slower than for the constant center density.

In accordance with experimental data and eq. (10), we obtain $n_s \approx 1.6 \times 10^{14}$ cm^{-2}.

If nucleation occurs not around "native" admolecules but at active impurity particles, n_s^* in (9) should be substituted by n_s, the concentration of active particles on the surface. The length of the intersept out by the continuation of line 2 on the ordinate axis (fig. 2) yields, in accordance with (9)

and (10). $n_2^* \simeq 1.3 \times 10^3$ cm^{-2}. In accordance with (11), we obtain quite a sound value: $\epsilon_{ad} \simeq 2.6$ kcal/mol. Earlier we observed two types of stoppers in growth of the ADP dipyramid [8]. The adsorption fluxes of such stoppers are:

$j_{+1} \approx 2.4 \times 10^6$ cm^{-2} s^{-1},

$j_{+2} \approx 8 \times 10^4$ cm^{-2} s^{-1}.

The mean time t_1 of the existence of the atomically smooth terrace between the neighbouring elementary steps of height h is $t_1 \simeq h/R \simeq 0.25$ s (in the range $\sigma \simeq 2.5$–4%, $R \simeq 2 \times 10^{-7}$ cm/s). Thus 6×10^5 cm^{-2} and 2×10^4 cm^{-2} stoppers of the first and second type are adsorbed for time t_1. These values (in particular, the latter one) are close to the above obtained value of n_2^*. Note also that such a comparison is not quite justified, since the experiments in ref. [8] were carried out from solutions with lower pH (pH = 3.6) therefore the state of impurities and their adsorption on the growing surface should should differ from those observed in the present experiment.

Concluding this section, we should like to note that the fluctuation in R for $\sigma > 5\%$ described in section 3.1 seem to be due to macrostep formation. Indeed, if a macrostep passes through the spot illuminated by the light probe, the growth rate should drastically increase. But the phenomenon of fluctuations should be studied separately and will not be discussed here.

5. Conclusions

The above described experiments lead to the following conclusions.

(1) Slow regeneration of dislocation-free seeds allows one to avoid dislocation formation and provides the growth process caused by two-dimensional nucleation on the (011) face. In the range $1.5 < \sigma < 5\%$ (pH = 5.0) the scatter in the growth rates does not exceed 15% whereas fluctuations in the rate of dislocation-free reach up to two orders of magnitude (pH = 4.4) [2]. Such a difference may be explained by the effect of the solution acidity and different ADP salts used in the experiments. The above described scatter in the local growth rates (exceeding 25% for $\sigma > 5\%$) seems to be associated with the formation of macro steps.

(2) Dislocations free growth with reproducible rates occurs in the mode of multiple nucleation on the face. Two qualitatively different portions are observed on the $R(\sigma)$ dependence. One of the portions ($1.5 < \sigma < 4.5\%$) is described by the effective linear energy of the end of a nucleated step, $\alpha_2 \simeq 4.2$ erg/cm^2. The other portion, ($\sigma < 4.5\%$) yields $\alpha_1 = 11.8$ erg/cm^2. The latter value is comparable with the value $\alpha = 16$ erg/cm^2 obtained from the spiral growth kinetics [4,7]. The low value of α_2 ($\alpha_2 \simeq 4.2$ erg/cm^2) can be ascribed to facilitated two-dimensional nucleation on adsorbed impurity particles or surface defects.

(3) For supersaturations $\sigma \gtrsim 10\%$ (point A in fig. 1) the growth rate due to two-dimensional nucleation should be higher than the rate of dislocation growth.

Acknowledgement

The authors express their deep gratitude to Yu.G. Kuznetsov for his valuable advice in implementation of controllable dislocation free growth.

References

[1] R. Kaischew and E. Budevski, Contemp. Phys. 8 (1967) 489.
[2] Yu.G. Kuznetsov, I.L. Smol'skii, A.A. Chernov and V.N. Rozhanskii, Dokl. Akad. Nauk SSSR 260 (1981) 864.
[3] I.L. Smol'skii, A.I. Malkin and A.A. Chernov, Kristallografiya 31 (1986) 769.
[4] A.A. Chernov, A.I. Malkin and I.L. Smol'skii, Kristallografiya 32 (1987) 1508.
[5] A.A. Chernov, Crystallization Processes, in: Modern Crystallography, III. Crystal Growth (Springer, Berlin, 1984).
[6] Nai-ben Ming, K. Tsukamoto, I. Sunagava and A.A. Chernov, J. Crystal Growth 91 (1988) 11.
[7] Yu.G. Kuznetsov, A.A. Chernov, P.G. Vekilov and I.L. Smol'skii, Kristallografiya 32 (1987) 994.
[8] A.A. Chernov and A.I. Malkin, J. Crystal Growth 92 (1988) 432.

Contemporary Physics, 1989, volume 30, number 4, pages 251–276

Formation of crystals in solutions

A. A. CHERNOV

Growth of high quality crystals has played an important role in sophisticated, modern-day technologies and in recent advances in physics. It has also provided examples in the study of self-organizing dissipative structures. This paper reviews the science of crystal growth and discusses recent data, particularly with regard to kinetics of growth and defects in crystal lattices.

Preface

It is relatively easy to crystallize many solutions or melts and to obtain crystals of poor quality. However, the lack of availability of crystals with strictly controlled composition and defect structure is still an obstacle to understanding of high-T_c superconductivity. Analogous problems have arisen and have partly been solved in preparation of semiconductor crystals and structures such as, e.g., the quantum well structures. High-quality tens-of-centimetre size frequency-doubling crystals from aqueous solutions can now be grown within a couple of weeks instead of 12 months that was needed several years ago. This provides a strong support for laser-fusion programmes.

People are developing technologies to produce desired and efficient laser crystals and others for the optical, magnetic and energy storage devices. Crystallography of proteins is based on the growth of protein crystals.

Still, the art of growing crystals remains an important feature, although a scientific understanding now prevails in some of the most sophisticated technologies.

As a fundamental problem of physics, growth of crystals has provided examples of self-organized dissipative structures such as dendrites, fractals or macrosteps (see section 4.2 below).

Kinetic phase transitions, numerous examples of which are now known from synergetics, were first found and named in the study of the crystallization of binary alloys (Chernov 1967, 1970, 1973).

Surface melting, discovered by M. Faraday in 1859, has become became nowadays a popular subject (Chernov, 1988).

Author's address: Institute of Crystallography, U.S.S.R. Academy of Sciences, 117333 Moscow, Leninski prospekt, 59, U.S.S.R.

The present paper is devoted to the science of crystal growth. The main topic is the kinetics of crystal growth which proceeds by the subsequent deposition of atomic layers on crystal faces. This mode is the most typical for solution and vapour growth and for molecular beam epitaxy. We discuss recent data on how the new layers arise, propagate and (briefly) how they produce macro defects in crystal lattices.

1. Introduction

1.1. A FEW WORDS OF HISTORY

In 1944 in cold, hungry, war-time Moscow at the Institute of Crystallography, my teacher Professor George L. Lemmlein was scrutinizing the surface of an artificially grown silicon carbide (SiC) crystal under a microscope. He was tired and without taking his eye away from the microscope sighed deeply: 'Oof...'. Immediately the visually flat surface of the crystal was covered with a great number of droplets, arranged into lines. The droplets were the dew produced by his exhalation. Lemmlein breathed at the surface again, this time intentionally. The pattern was repeated. It became clear that the droplets did not condensed uniformly along the surface, but instead only at the most favourable sites, 'decorating' them. The 'dew technique' was thus discovered, revealing the fine relief of a crystal surface, which was invisible under normal conditions (Lemmlein 1945, 1947). The water droplets dried up rapidly, and later Lemmlein and Gliki (1954) replaced liquid dew with a solid—they started precipitating ammonium chloride (NH_4Cl) crystallites from vapour. Then Basset (1958) reported on his technique of decorating the surfaces of NaCl crystals with gold, before they were studied in an electron microscope. Decoration techniques became very popular (Distler *et al.* 1976).

0010-7514/89 $3.00 © 1989 Taylor & Francis Ltd

What was it that Lemmlein saw? He saw a pattern of the type shown in figure 1, although a less clear one. Figure 1(*a*) is an undecorated SiC surface, and figure 1(*b*) is a surface decorated with NH_4Cl crystallites. The thick lines on both photographs are steps with a height of tenths of a micron. The thin lines in figure 1(*b*) are steps with a 14·6 Å height. These steps constitute the edges of unfinished atomic planes on the crystal surface. A staircase of steps, approximately parallel to each other and separated by smooth terraces, is a typical relief of the growing surface of a crystal. But the most interesting are the spirals seen in a great number in figure 1(*b*). Lemmlein (1945) found spirals to be also present on hematite, barite, apatite. He noted both the wide-spread occurrence of this phenomenon and its importance in the growth process. Soon Lemmlein guessed that a spiral 'turns around' its centre, and, therefore, a step on the surface never disappears. Lemmlein showed this process in an animated cartoon film which he drew in 1946. The fragments of this film have been published recently by Treivus in his review (1987). Lemmlein, however, did not understand that the centre of an elementary spiral is the point D where the screw dislocation line DD emerges on the surface (figure 2(*a*)). Atoms and molecules from a supersaturated vapour or solution, or from a supercooled melt, attach to the step. As a result, the atomic plane ending in a step (hatched in figure 2(*a*) is continuously being built up, and the step moves. The step inevitably ends on an immobile dislocation DD and, therefore, the

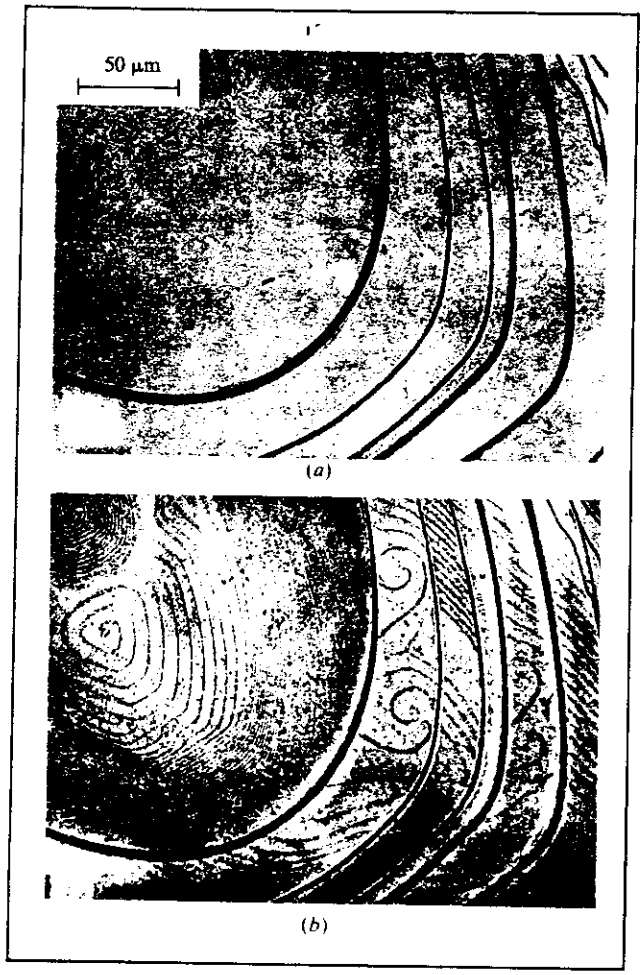

Figure 1. Basal face (0001) of SiC crystal: (*a*) before, (*b*) after the decoration with NH_4Cl crystallites precipitated from vapours. The crystallites, precipitating along the steps, make them visible. Spiral steps are seen around the points where dislocations outcrop on the surface (Lemmlein and Gliki 1954).

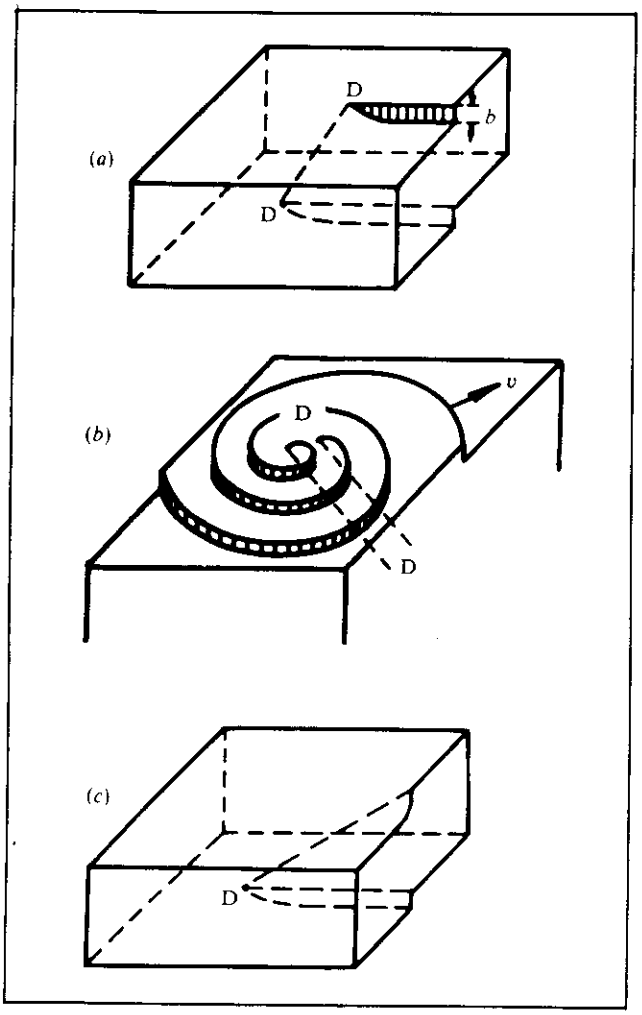

Figure 2. Generation of steps by screw dislocations: (*a*) the screw dislocation DD produces steps on the upper and the lower crystal faces, (*b*) a double spiral around the points of the outcrop of two dislocations, the arrow shows the rate of step movement during the crystal growth, (*c*) if the point where the dislocation outcrops reaches the edge the step disappears. The sloping dashed lines with D at each end symbolize dislocations.

end of the step at the point D must also be immobile. During the growth process, the step cannot rotate around the centre D and still remain straight: for that, the step displacement velocity, v (like the one shown by an arrow in figure 2(*b*), at any particular point of the step, must increase linearly with the distance of this point to D. This increase is impossible since the linear step velocity v is determined fully by the supersaturation and molecular processes. Thus the periphery of the initially straight step (hatched in figure 2(*a*)) will rotate with a lower angular rate than its central part and the step will finally curve into a spiral as seen in figure 2(*b*). If two dislocations in the vicinity of each other outcrop on the surface, a double spiral is formed (figure 2(*b*)). From figure 2(*b*) it is clear that the spirals form a conical hillock. Its apex is the region of the outcropping of the dislocations. Rotating constantly around the points of the outcropping of the dislocations, the steps do not disappear, and the growth can continue endlessly. This most beautiful idea was formulated in 1949 by F. C. Frank and gave rise to a 'spiral rush'. Very soon spirals were revealed on the surfaces of numerous crystals that had grown from vapour, solution or melt. It turned out that Heck (1937) had seen spirals on paraffin as early as 1936, but had not attached any importance to them. It became clear that the dislocational mechanism of growth is by no means anything exotic, as previously thought.

1.2. NUCLEI AND DISLOCATIONS

Interest in spiral growth was, however, roused by deeper considerations as well. The point is that the idea of growth on dislocations removed the discrepancy between the expected rate of the formation of two-dimensional nuclei and the experimental value (Burton *et al.* 1951). It might be useful to recall here what is the essence of this problem of new phase nucleation.

Let an atomically smooth (see section 2) face of a crystal be in contact with the supercooled mother phase—vapour, solution and melt. Atoms, molecules or ions of the substance forming the crystal and situated in the mother medium—vapour, solution or melt—can be reversibly adsorbed on the surface of a crystal, passing from site B to site A as shown in figure 3(*a*). Adsorption, however, is not yet attachment to the lattice, since, as distinct from the crystal particles, the adsorbed particles are almost devoid of 'regular' neighbours, or have no neighbours whatsoever, in the face plane. Therefore, the potential binding energy of the adsorbed particles, with respect to each other and to the lattice, their kinetic vibration energy, configuration and vibration entropy are different from those in the crystal. Their chemical potentials are different as well. Therefore, in the absence of steps, a layer of adsorbed particles can be in thermodynamic equilibrium with the supercooled mother medium surrounding the crystal, but not with the crystal itself. Only the attachment of the particle to the kink on a step (figure 3(*a*)) makes it a 'member' of the crystal lattice. Indeed, attachment of any new particle to the kink only continues the development of the not yet complete row along the step, but does not change the number of unsaturated interatomic bonds on the surface. Thus, for a crystal to grow it is required that there should be kinks on its surface. In the case under consideration, of an atomically smooth face, the kinks can only exist on steps.

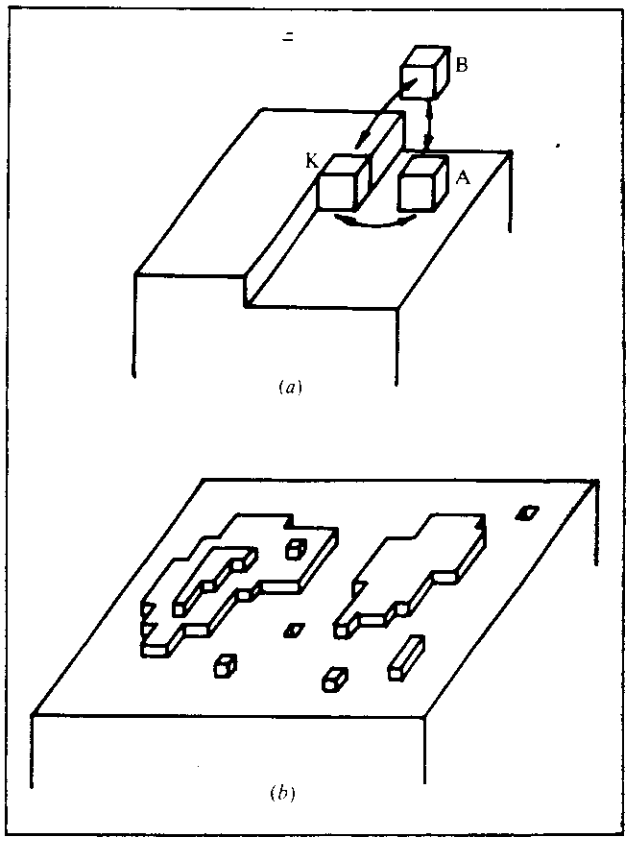

Figure 3. Step, kink and two-dimensional nuclei: (*a*) a particle in the kink K on a step can exchange places with the particles of the adsorption layer (position A) or the mother phase (position B); (*b*) nuclei of a new atomic plane can arise both on the face already developed and over the growing islets.

What is it then that hinders the atoms, molecules or ions from merging into islets of new crystal planes bordered by steps with kinks (figure 3(*b*))? This is what should happen because the solution (for definiteness, we shall speak of only this kind of mother phase) is supersaturated and this means that the crystalline phase is thermodynamically more favourable.

The problem is the same for the supersaturated bulk solution. The dissolved molecules (or ions) are prevented

from forming large sections of crystal planes by their chaotic arrangement and motion. It is only the trial and error pathway that remains for the molecules or ions to combine and decompose into small aggregates of the crystalline phase. Combining into a crystalline aggregate would seem to be more favourable, since a section of a more favourable phase is being formed. But at the same time a boundary to the aggregate inevitably arises, with its own free energy. Even if one regards the 'inside' of a small aggregate to be as favourable as a macrocrystal, still the fraction of surface molecules relative to the internal ones is so large that the loss associated with this surface energy proves to be greater than the gain. And only if it so happens that the aggregate has a chance to grow to a sufficiently large, critical, size, will it become 'profitable'. A large aggregate can arise only from a small one. That is why for a nucleus of critical size to be formed the system has to climb by fluctuations to the top of the potential barrier, and this event is rather rare. It is for this reason that a supersaturated solution can remain for years without giving rise to crystals.

The same reasoning holds true for a 'two-dimensional' nucleus—an islet of a new atomic plane on the macroscopic face of a crystal. The islet boundary is a step, the edge of an unfinished plane. The formation barrier of such nuclei, and, correspondingly, the frequency of their appearance on the face, is determined by the specific free energy of the steps α_1 (erg cm^{-1}). A very gross estimate of this is $\alpha_1 = \alpha h$, where α is the surface energy of the step riser and h is the height of the step. For elementary steps, h coincides with the lattice parameter or, much less often, equals 1/2 of it.

Having once arisen as a two-dimensional nucleus (figure 3(*b*)), the new atomic plane is rapidly built up and occupies a whole face, and a new nucleus then becomes necessary for the crystal to grow further. Estimates of the rate of formation of two-dimensional nuclei on a unit surface of the face per unit of time show that the face can grow at the observed rate only when the motive force of crystallization—supersaturation,

$$\sigma \equiv \frac{C - C_e}{C_e}, \qquad (1)$$

exceeds scores of percents. (Here C and C_e are the actual and the equilibrium concentrations of the solution, respectively). In fact, however, the crystals grow quite noticeably (at a rate of $\simeq 10^{-6}$ cm s^{-1}) with $\sigma = 10^{-3}$–10^{-2}, i.e., $\sigma = 0{\cdot}1$–1%. Dislocation theory has explained this contradiction: simply the mechanism of two-dimensional nucleation acts on crystals only if there are no dislocations. At the same time, crystals produced without special precautions always contain dislocations.

From the aforesaid it becomes clear that the layer-by-layer growth of crystals includes two processes: generation of steps by two-dimensional nuclei or dislocations and their movement, i.e. attachment of atoms of molecules or ions to step risers. These very processes are discussed below (sections 3, 4).

The layer-by-layer growth of a crystal is not the only possible one. The other, normal, mechanism is characteristic of atomically rough surfaces of crystals, discussed in section 2.

Finally, some new data on the so-called secondary nucleation of crystals in solutions will be discussed briefly in section 5. Ripening in an ensemble of crystals is discussed in section 6.

2. The structure of steps and surfaces

The surface of a crystal on an atomic scale can be either smooth (figure 4(*a*)) or rough (figure 4(*b*)). In the former case the terraces between steps (there are two of them in figure 4(*a*)), or a whole face (if there are no steps on it), constitute regular and almost completely packed atomic planes. The number of holes in such planes, or the number of atoms, molecules or ions adsorbed on the surface, is much smaller than that of regular sites. The steps, however, are rectilinear only on average; on an atomic scale they are blurred by thermal fluctuations, as happens with any one-dimensional object at non-zero

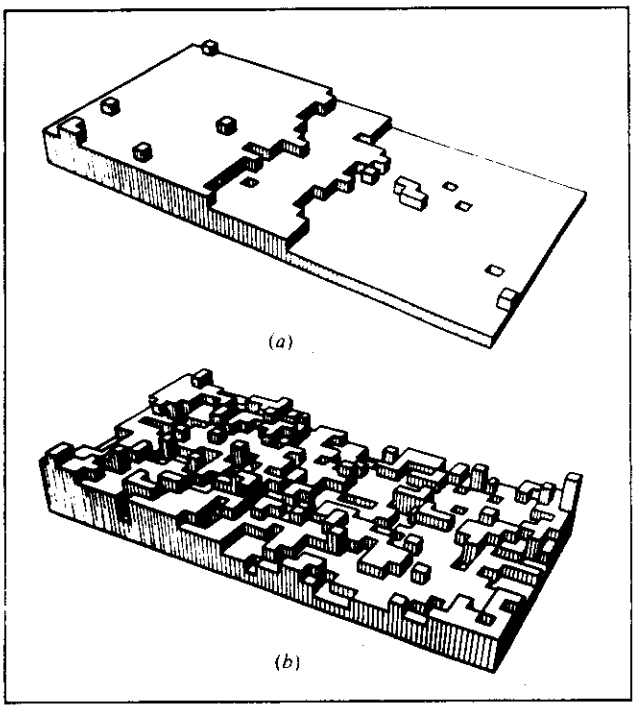

Figure 4. Computer modelling of the surface structure by the Monte Carlo method (Gilmer and Weeks 1978). Surface (001) of a simple cubic crystal with two steps: (*a*) in an atomically smooth state, (*b*) in an atomically rough state.

temperature $T > 0$. In other words, at $T > 0$ a step is zig-zagged with kinks (figures 3(*a*), 4(*a*)). The free energy of a step per one atomic site on its riser is given by

$$\alpha_1 a = \varepsilon - Ts. \tag{2}$$

Here ε is the energy needed to create one new atomic site (on the step riser), i.e. for a step to be elongated by a (we regard an atomic site as having the size a along the step); s is the entropy of one-dimensional solution of two types of kinks facing the opposite sides on the step. With an increase in the ratio T/ε the density of kinks on the step and their configuration entropy on the step, s, increase. Correspondingly, the free energy of the step, α_1, drops and, at a certain value of T/ε, can be reduced to zero. A further increase in T/ε would lead to a negative free energy α_1. The latter occurrence is obviously tantamount to the decomposition of an atomic plane limited by the step into a multitude of individual adsorbed atoms and their small groups (figure 4(*b*)). A macroscopically extended step ceases to exist, as happens with the gas–liquid interface at the critical point. The decomposition of a step, described above, also means the disappearance of atomically smooth terraces and their transformation into an atomically rough surface (figure 4(*b*)). The 'roughening' temperature is denoted by T_R.

Fluctuations of the surface can also be regarded as some kind of capillary waves on it, i.e. without resorting to the notion of a step. Analysis of such waves with the help of the renormalization group technique (Chui and Weeks 1978; Nozières and Gallet 1986) gave

$$T_R = \frac{2}{\pi}\alpha d^2. \tag{3}$$

Here α (erg cm^2) is the specific energy of the step riser per unit surface of the riser, d is the distance between the atomic planes parallel to the surface in question, i.e. $\alpha d^2 \simeq \varepsilon$. As we shall see below, for crystals of ADP ($NH_4H_2PO_4$) and KDP (KH_2PO_4) types, $\alpha \simeq 20$ erg cm^{-2}. For these crystals the lattice parameter in different directions is given by $d \simeq 7$–10 Å. Taking $d = 8$ Å, from equation (3) it is easy to get $T_R \simeq 600$ K. Thus, at $T \lesssim 600$ K the surface in solution must be atomically smooth and, therefore, grow by successive deposition of layers, which actually happens in reality. An absolute majority of other crystals grow from solutions by layers as well. This fact is in qualitative agreement with empirical data (figure 5) on the surface energies of numerous

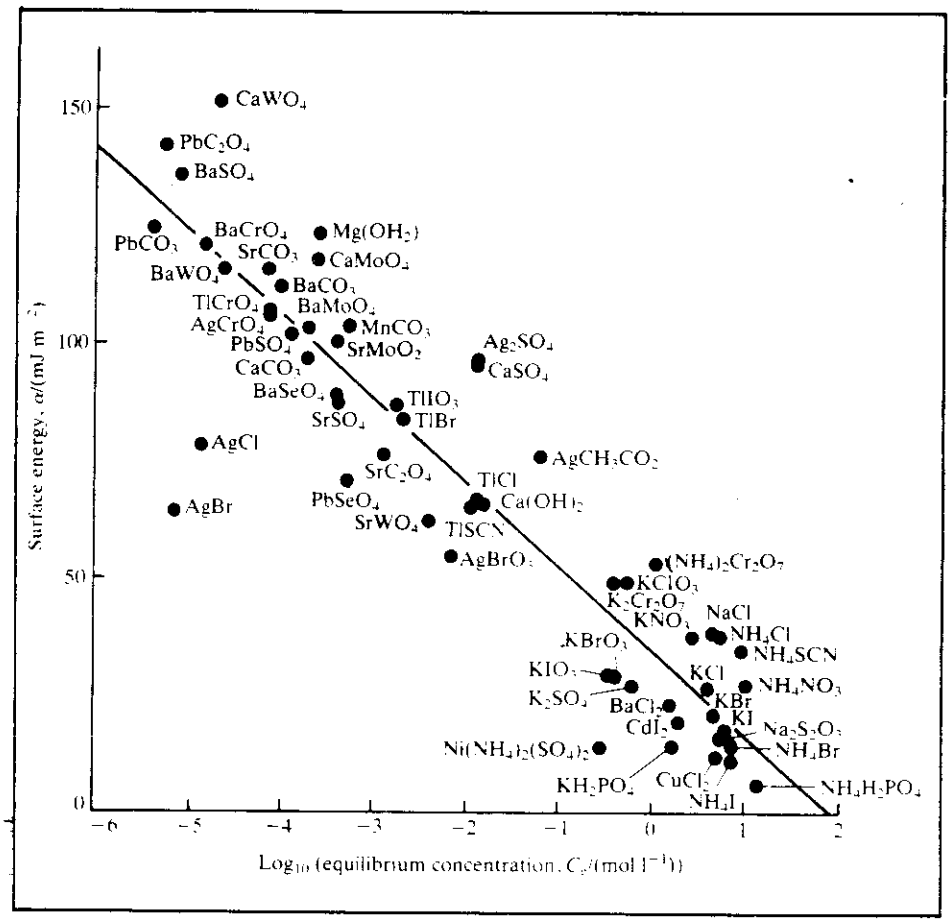

Figure 5. Surface energy α of the crystal–solution interface as a function of the concentrations C_e of saturated solutions (Söhnel 1982).

poorly soluble salts in aqueous solutions. Despite the great scatter of the data in figure 5, it should be useful to cite the empirical expression for the specific free surface energy of ionic crystals of electrolytes in aqueous solutions (Söhnel 1982, 1983):

$$\alpha(\text{mJ m}^{-2} = \text{erg cm}^{-2}) = -18{\cdot}3 \ln C_e + 34{\cdot}5, \quad (4)$$

where the concentration C_e of a saturated solution in equilibrium with the crystal is expressed in mol l^{-1}. This formula is very crude. It does not take into account, among other things, the anisotropy of surface energy and, which is most important, the empirical constants in the equation were found from the data on the nucleation of crystals in solutions. This nucleation, despite all the possible precautions, in most cases seems to have been heterogeneous. The latter fact means that nuclei arise not in the bulk of an ideally pure solution, but on extraneous particles, walls of vessels, etc., which facilitates the surmounting of the potential barrier. A decrease in the barrier is qualitatively equivalent to a decrease in the surface energy of the crystal–solution interface. That is why the values of α in figure 5, summarised by expression (4), are most probably underestimated (primarily because of the constant term in expression (4)). The large scatter of data is also associated with heterogeneous nucleation. This makes even more necessary the independent measurements of surface energy at the crystal–solution interface.

As already mentioned, a kink is the only gate for a particle to enter the crystal lattice. Therefore, the density of kinks on the surface determines the absolute value and the anisotropy of crystal growth rate. The fact that kinks on smooth faces are only present on steps makes the growth of such faces impossible without the generation of steps by dislocations or two-dimensional nuclei. The density of kinks in these cases does not exceed 10^{-2}–10^{-6} out of all the atomic sites on the surface. On an atomically rough surface the kinks occupy tens of percents of all the sites. Correspondingly, the faces growing by layers move much more slowly than the rough ones and remain flat. On rough surfaces the particles are incorporated into the lattice so fast that the rate of growth is limited only by the arrival of new 'construction units' at the surface, which more or less coincides with the isotherm or isoconcentrate, where the temperature or concentration reaches close to equilibrium values. Diffusion and thermal conductivity are isotropic in liquids, and in crystals they are characterized by a comparatively small, and, at any rate, nonsingular, anisotropy. That is why the isoconcentrates and isotherms, and together with them the growing rough surfaces, are rounded. The shape of the growing crystal thus serves as the simplest indicator of the atomic growth mechanism.

Most crystals growing from solutions are polyhedrons. However, NH_4Cl and NH_4Br crystals in solution are rounded. The normal mechanism of growth (or a mechanism closely resembling it) is also characteristic of the pinacoid face (0001) of the quartz crystal in hydrothermal solutions ($T \simeq 650$ K, pressure—hundreds of atmospheres), which affects the morphology of this surface and the defects in the material formed with such a growth.

3. Kinetics of the layerwise growth

3.1. ACTIVITY OF DISLOCATIONS AND THE INTERNAL STRUCTURE OF THE DISLOCATION SOURCES OF STEPS

Let us return to figure 2(*a*) where the dislocation DD is shown. The component of its Burgers vector, **b**, normal to the surface differs from zero, and so this dislocation gives rise to a spiral (figure 2(*b*)). In recent years, however, it has been reported (Bauser and Strunk 1981; Keller, 1986) that the layers of growth, i.e. the steps, are generated not only by screw but also by edge dislocations with $|\mathbf{b}| = 0$. (N.B. **b** is the *normal* component of the Burgers vector). Indeed, NaCl deposition from molecular beams at high supersaturations has shown the spiral steps of growth on the surface to be replaced after a certain time by the concentric ones (Chernov and Kopylova, 1977). From data obtained indirectly, it was possible to conclude with sufficient confidence that such concentres originate at points where edge dislocations are outcrops on the surface (Keller 1986). Nucleation seems to be facilitated by electric charges on dislocations in ionic crystals. The charged point of the outcrop of the dislocation acts as does a charge in a Wilson cloud chamber (Trusov and Chernov 1979). It is, however, difficult to apply this explanation to GaAs crystals growing from solution in gallium melt. Nevertheless, according to Bauser and Strunk (1981), growth hillocks on dislocations with $|\mathbf{b}| = 0$ were revealed on the faces (111) of such crystals by means of the surface decoration and X-ray topography.

We performed experiments on the growth of $NH_4H_2PO_4$ (ADP) crystals from aqueous solutions with X-ray topographic control *in situ* (Chernov *et al.* 1980). X-ray topography is known to allow direct viewing of the lines of dislocations in crystals. It uses the disturbances of the Bragg reflection condition on the curved portions of atomic planes near the dislocation lines. In this way one can observe simultaneously the growth of the crystals and the dislocations, as well as other defects of the crystal lattice. Edge dislocations proved to be inactive: the edge of the dipyramid, intersected by such dislocations in a solution with supersaturation given by $\sigma = 2$–3%, did not grow (at least with an observed rate of >

10^{-8} cm s^{-1}) (Kuznetsov *et al.* 1986). On the contrary, screw dislocations gave an easily observed growth. When screw dislocations no longer intersect the face its growth practically stops (figure 6).

Another interesting peculiarity was revealed. Let the dislocation D_1 (figure 7(*a*)) come out on the surface of dipyramid (011) at the moment of time answering to the profile 1 of the crystal. The face (011) grows noticeably faster than the face of the prism (010). So, after some time D_1 reaches edge E on profile 2. This is simply the result of the (011) face displacement, since the dislocation is immobile with respect to the lattice. If D_1 is the sole dislocation providing for the growth of the face (011), then, as soon as D_1 comes out on the edge of the face, the growth of this face must stop. Indeed, a dislocation coming out on the edge does not give rise to a step on the face, as distinct from a dislocation that comes out on the face (figure 2(*c*)). Approach of a dislocation to a distance x from the edge, comparable with the radius of curvature of the two-dimensional nucleus (figure 7(*b*)), reduces the power of a dislocation as a generator of steps to a small value, depending on x because of the Gibbs–Thomson effect (the effect of curvature on vapour pressure or chemical potential). If, therefore, the face of the prism (010) (figure 7(*a*)) continues to grow, e.g. owing to the activity of dislocation D_2, the face (011) will continue its growth at such a rate that dislocation D_1 stays all the time near edge E, as is shown on profiles 2 and 3 in figure 7(*a*). The rate of growth for the dipyramid face will thus be wholly determined not by its own properties, but by

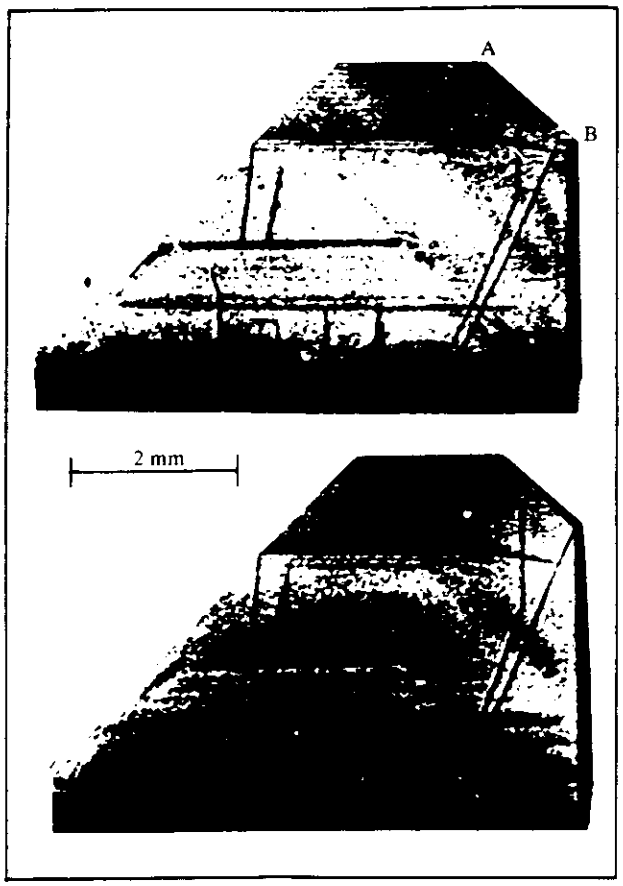

Figure 6. Sequential X-ray topograms from a growing $NH_4H_2PO_4$ crystal. Seen on the right are two dislocation lines, the lower one reaching the edge of dipyramid AB. After the point of the outcrop of this dislocation reaches the edge B the growth of the AB face practically stops. Only the growth by the formation of two-dimensional nuclei is possible; it proceeds at a rate as a minimum by two orders of magnitude slower even at supersaturation $\sigma = 7\%$. In this experiment supersaturation $\sigma = 1\%$; X-ray reflection 022.

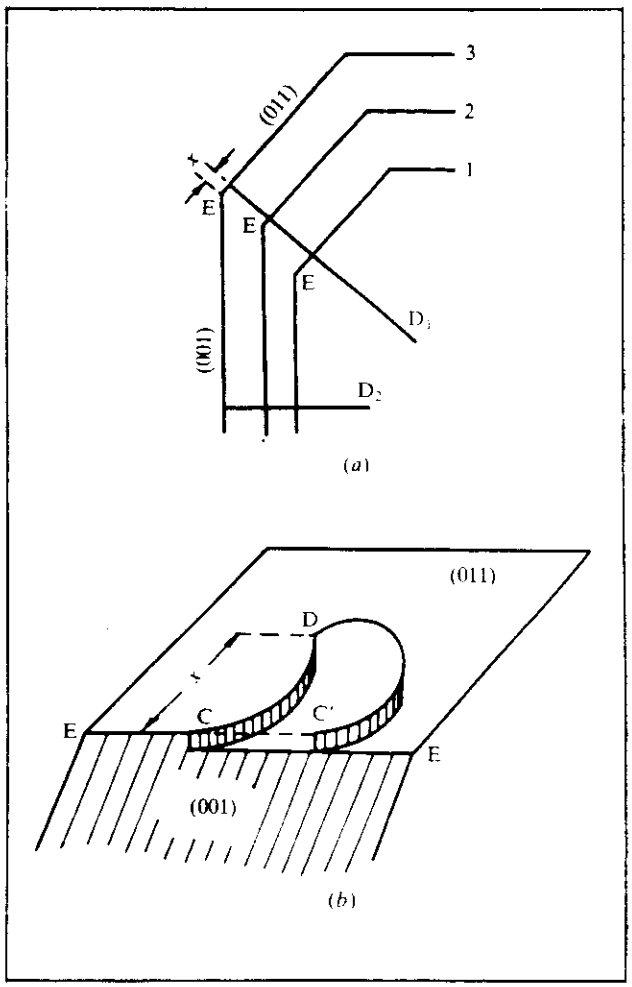

Figure 7. Interdependent growth of the neighbouring (001) and (011) faces and the mechanism controlling the activity of dislocation D_1: (*a*) sequential profiles of the crystal with time, (*b*) geometry of the surface in the case when the distance x from the point D, where the dislocation outcrops, to the edge EE is comparable with the critical radius of the nucleus, ρ_c, shown in figure 12.

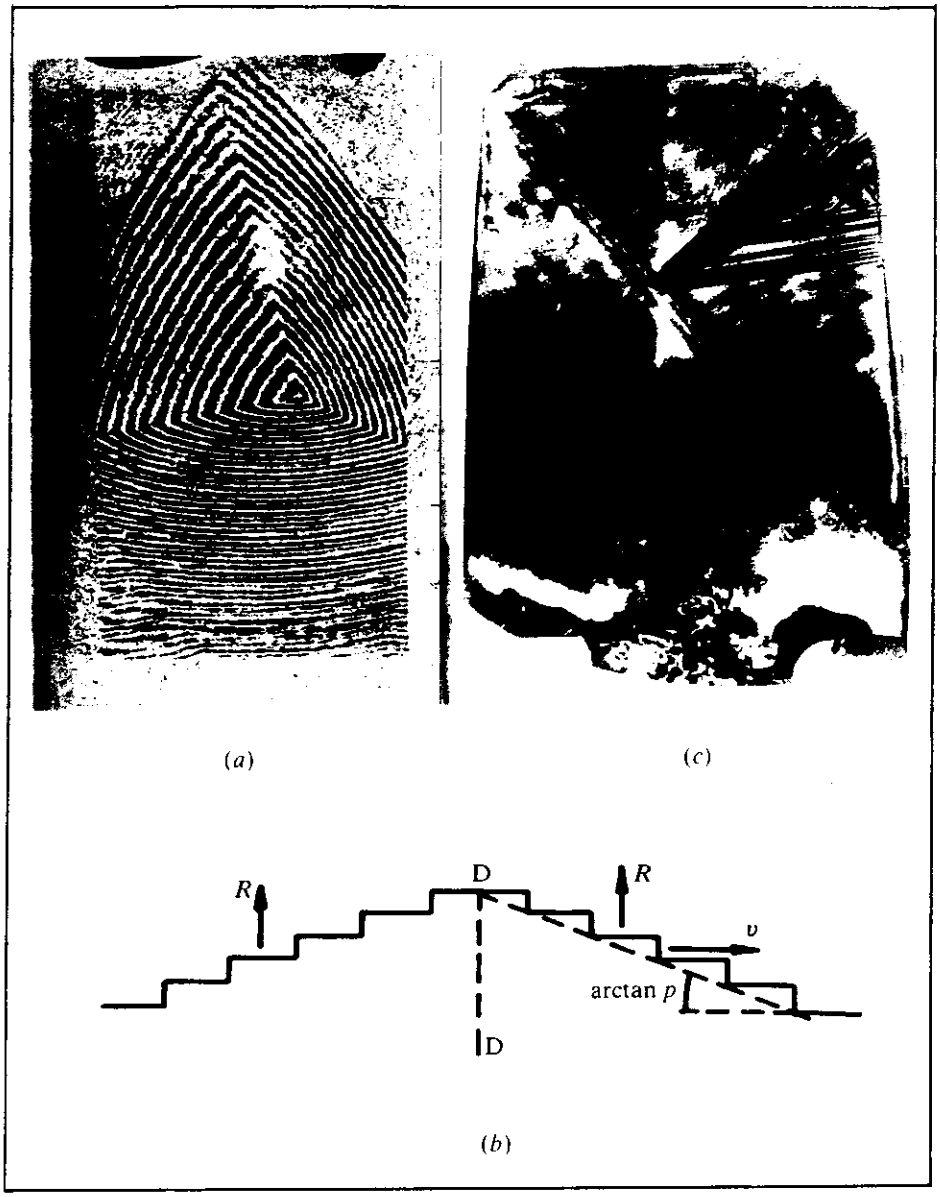

Figure 8. Relief of the surface of growth and the dislocations generating it: (*a*) Interferogram of the growing face of the $NH_4H_2PO_4$ crystal dipyramid. Concentric fringes are the topographic equiheight lines on the growth hillock surface. The difference in heights between the adjacent bands is 0·314 μm. (*b*) Profile of vicinal hillock generated by the dislocation DD. The normal rate R of the face growth is the same in all points of the hillock. (*c*) In situ X-ray topogram taken in profile from the growing crystal whose face is shown in (*a*). An inclusion is seen, giving rise to a powerful bunch of dislocations. Although there are many of them and they cross the dipyramid face on a large area, the centre of the hillock of growth in (*a*) is localized on the dislocation cluster with the maximum activity.

the rate of the prismatic (010) face adjacent to it, the angle between the faces and the orientation of the 'binding' dislocation D_1. The fact that such growth is observed explains the mutual dependence of the growth rates of adjacent faces.

The Burgers vector of a dislocation that forms a step source is comparatively rarely equal to one lattice parameter. More often one observes larger values, and X-ray topography reveals sometimes one line of dislocation and sometimes several such lines.

The influence of the structure of a dislocation source on its activity as a generator of steps was studied by us with the help of *in situ* laser interferometry and X-ray topography, as well as by using these two techniques simultaneously, also *in situ* (Smol'sky *et al.* 1985). Figure 8 shows an example of combining the two techniques.

Figure 8(*a*) is a Michelson interferogram of the growing dipyramidal face of an ADP crystal. The crystal together with the cell with a supersaturated solution flowing through it was placed in one of the arms of a Michelson interferometer. The pattern in figure 8(*a*) consists of concentric curved triangles. Each triangle is the section of a cone—a very gently sloping hillock—by a plane. The centre of the rings—the hillock apex—is the site where the dislocational source of the steps comes out on the surface. The distance between the interference fringes corresponds to the difference in heights, equal to half the wavelength ($\lambda/2$) of the light used ($\lambda =$

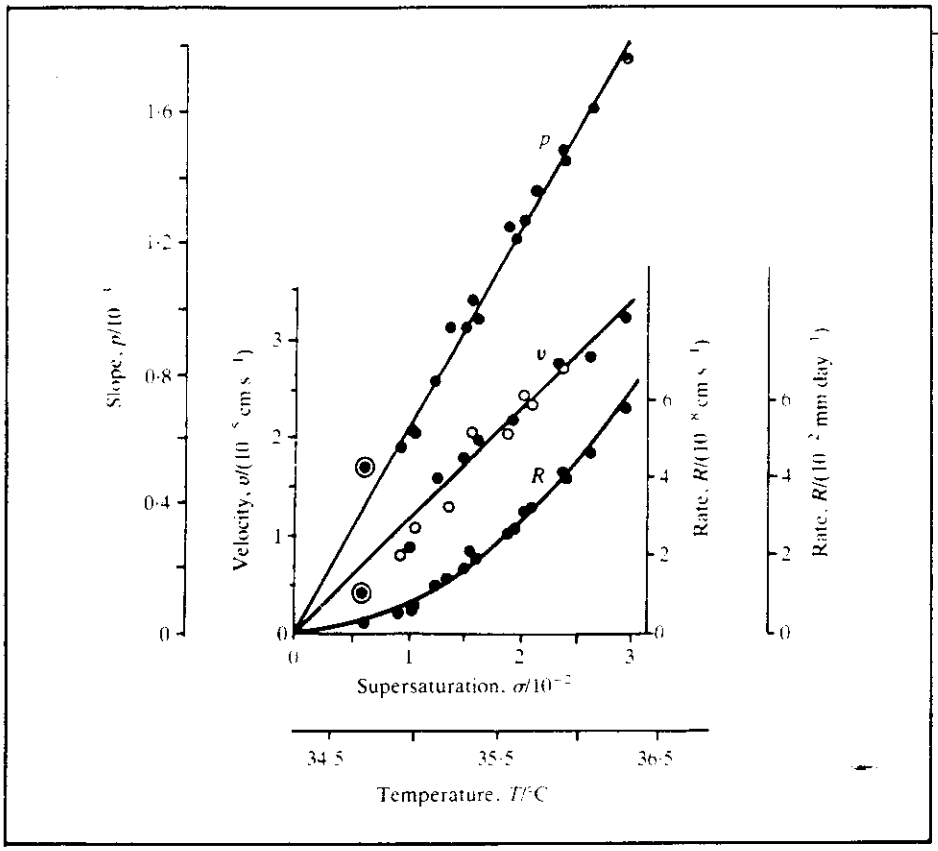

Figure 9. Dependence of tangential velocity v of the steps, slope p of the vicinal dislocation hillock of growth and rate R of the face growth on this hillock. The value of $R = pv$. Elementary dislocation source. The face of $NH_4H_2PO_4$ prism.

0·6328 μm). That is of course why the elementary spiral steps are not seen. By measuring the distance between the fringes one can easily find the slopes of the vicinal hillock†, p (figure 8(*b*), with respect to the particular orientation (the terraces). The number of new fringes appearing in the centre of a hillock per unit of time gives the normal face movement rate

$$R = pv. \tag{5}$$

Knowing R and p one can easily find the average effective velocity of the steps $v = R/p$. The velocity v can also be measured directly by the rate of the fringe motion.

Figure 8(*c*) is an X-ray topogram where the face of the dipyramid, photographed from the front in figure 8(*a*), is perpendicular to the plane of the photograph. One of the positions of the plane proved to be decorated with inclusions that arose after the face had stopped. The largest inclusion gave rise to a whole bunch of dislocations having different directions. It was the dislocations of such a bunch that produced a hillock in figure 8(*a*). Comparing these photographs one easily concludes that not all the dislocations, but only some of the most powerful of them, actually work as the sources of steps. A difference in the power of the dislocation sources of steps is seen from comparing the growth rates R of the prism faces as a function of the relative supersaturation σ in figures 9 and 10. Both the investigated faces of the prism have grown from the same solution at the same temperature, acidity and supersaturation. Nevertheless, e.g. at $\sigma = 3\%$, the normal growth rate of the one prism face (figure 10) is almost four times greater than that of the other (figure 9). In figures 9 and 10 are also shown the supersaturation dependences of the tangential velocities v of the steps on these faces and the slopes p of the vicinal spiral hillocks of growth formed around the dislocations on the faces. These very hillocks of growth ensure the growth of the face with the rate of R. Presented in figure 10 are the data on the growth on two hillocks, whose interferogrammes are shown in figure 11 and marked by the same crosses and circles as the corresponding data in figure 10.

† A 'staircase' of steps separated by atomically flat terraces, i.e. by pieces of the particular faces, form, on average, a face slightly inclined away from this particular orientation. Such a face is called 'vicinal' (from the Latin vicinalis—neighboring). A vicinal hillock is a hillock whose slopes are slightly inclined away from the particular face orientation.

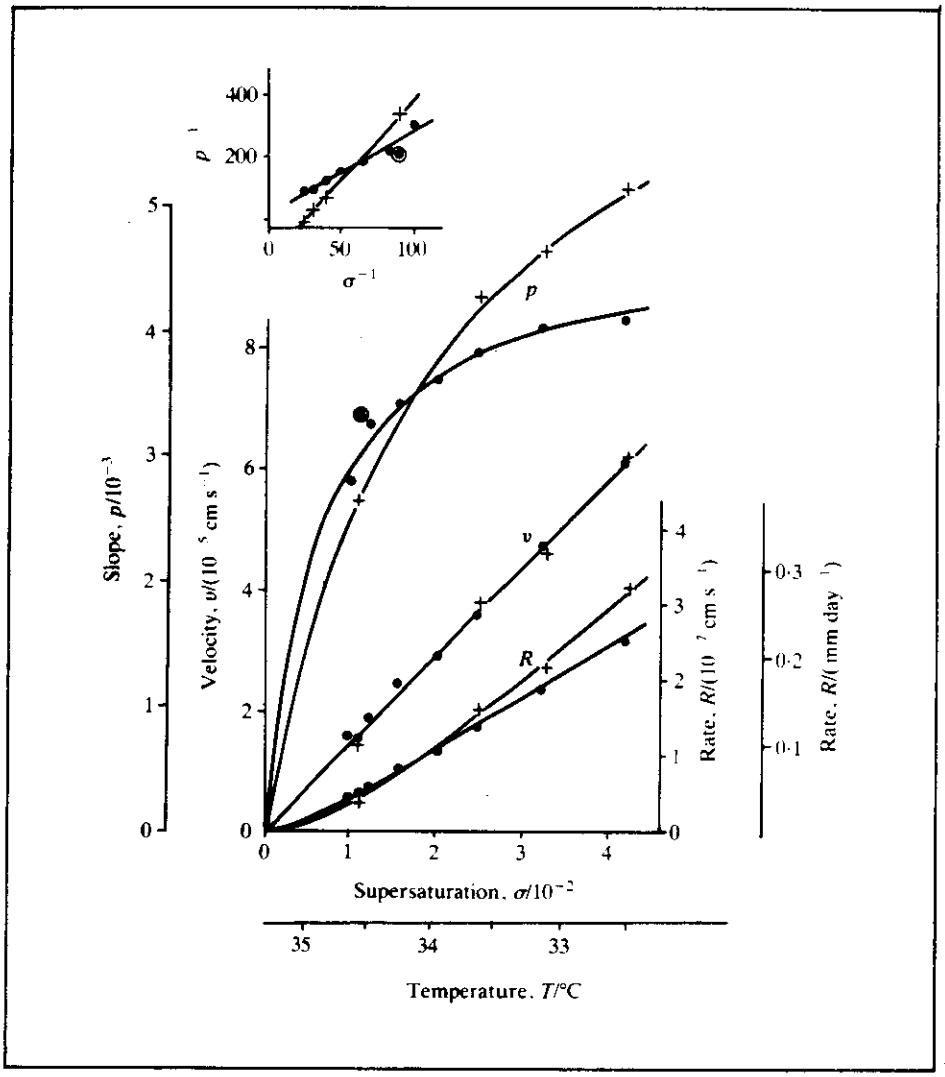

Figure 10. Same as in figure 9, but for two complex dislocation sources. The interferogram of the face with these two sources is shown in figure 11. The sources and the p, v, R values for them are indicated by the symbols • and +.

Figure 9 refers to the growth on a dislocation with a unit Burgers vector†. For it, according to the theory of Burton *et al.* (1951).

$$p = \frac{hkT\sigma}{19\omega\alpha}, \tag{6}$$

where h is the height of the step (e.g. equal to the lattice parameter), T is the temperature, ω is the specific molecular volume of the crystal, α is the specific free energy of the step riser. Agreement of equation (6) with the experimental $p(\sigma)$ dependence of figure 9 makes it possible to estimate $\alpha = 20\,\mathrm{erg\,cm^{-2}}$ (we do not consider here the more subtle question of the anisotropy of α_1).

† This was proved by I. L. Smol'sky who applied section topography to this particular sample.

Generally speaking, a nonelementary dislocation or a group of dislocations (figure 12(*b*)) has the net component $b = mh$ of the Burgers vector along the normal to the surface differing from the lattice parameter h. The sign of m may be either positive or negative providing spirals of opposite signs but it hardly influences the activity of the dislocation group, thus only $|m|$ being of much importance. A complex dislocation source, i.e. a group of dislocations is charterized by its perimeter $2L$ which may be noticeably larger than the interatomic distance. In the case of two dislocations, L is simply the distance between them. For $|m| \gg 1$, it is natural to expect larger L values for larger $|m|$ values, typical of the group including many dislocations. However, generally speaking, the m and L values are independent of each other, both characterizing the complex step source. For instance, $|m| = 1$ may characterize a bunch of several

mutually compensating dislocations whose outcrops, though occupying rather extended territory on the growing face, possess only the elementary total Burgers vector. Even $|m| = 0$ does not mean that at any supersaturation the group of dislocation is inactive; if at least some distances between dislocations exceed $2\rho_c$, the diameter of 2-dimensional critical nuclei ($\rho_c = \omega\alpha/kT\sigma$), some pairs of dislocations and the whole group will generate closed dislocation loops. The picture given above, first developed by Burton *et al.* (1951), results in the following expression for the slope of a hillock provided by a complex step source:

$$p = \frac{|m|hkT\sigma}{19\omega\alpha + 2LkT}. \qquad (7)$$

From (7) follows a linear p^{-1} *vs.* σ^{-1} dependence, satisfied in reality, as seen from the upper insert in figure 10. The two straight lines in this insert refer to the two dislocation hillocks of growth, shown in figure 11. From the slopes and the positions of the above two straight lines there follow the values of $|m_0| = 12$ and $|m_+| = 6$, with $L_0 = 0{\cdot}92\ \mu$m, $L_+ = 0{\cdot}31\ \mu$m (Chernov *et al.* 1986).

It is thus seen that not only the presence but also the internal structure of a dislocation source with a cross-section as small as $\simeq 1\ \mu$m can cause a several-fold change in the growth rate of the macroscopic face of a crystal.

The reason is that the power of a dislocation source as a generator of steps is fully determined by its centre. In the simplest case of a single dislocation (figure 12(*a*)) the radius of curvature of a step in the central point D must be equal to the radius of the critical nucleus $\rho_c = \omega\alpha/kT\sigma$, related to the supersaturation σ of the solution

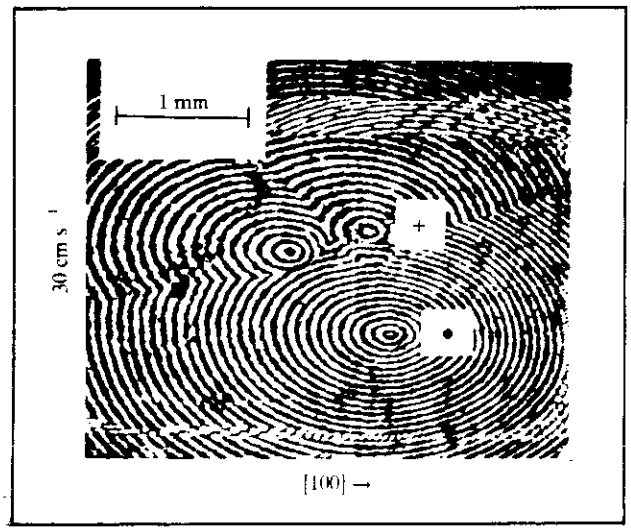

Figure 11. Interferogram of a portion of the face with two dislocation sources, the kinetics of the growth on which is presented in figure 10.

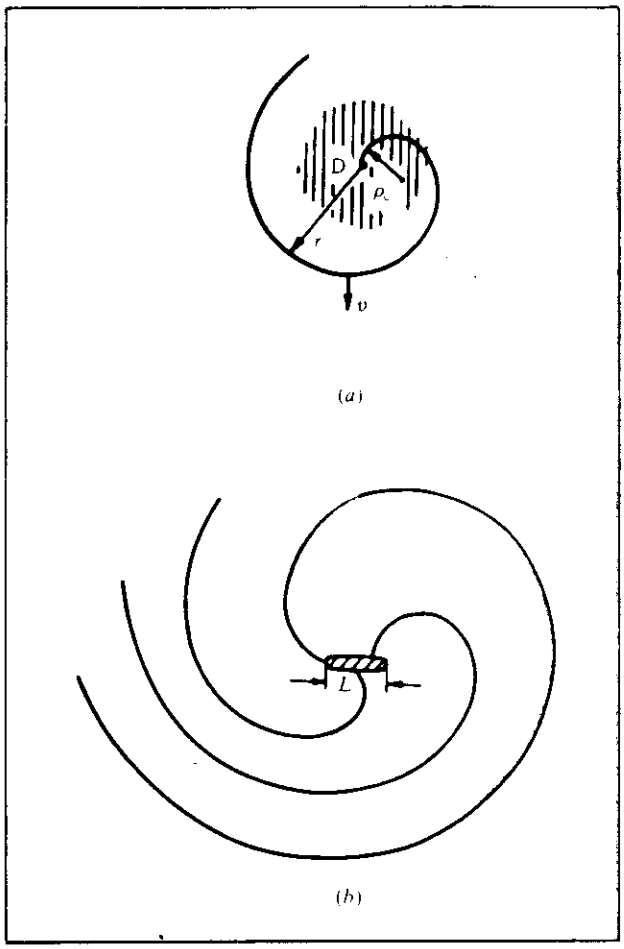

Figure 12. Spiral steps: (*a*) Single spiral; near the point D, where the dislocation comes out on the surface, the radius of curvature of the step is equal to the radius of the critical nucleus, ρ_c. r indicates an arbitrary point on the spiral step. The cross-hatched region is that of the existence of internal stresses in the crystal, generated by the dislocation and reducing the movement rate of the growth step. This region becomes wider the lower the supersaturation. (*b*) Triple spiral—cross-hatched area is the internal region of the dislocation source, around which the steps must move during growth and dissolution.

over this centre. Indeed, the rate of a step at the point where a dislocation outcrops on the surface must equal zero, because the centre is immobile. That is why the pitch of the spiral is proportional to the only linear dimension of the problem, ρ_c, i.e. $r = \text{const.} \times \rho_c$ (figure 12(*a*)). To be more precise, the distance between the loops is equal to $19\rho_c$ (Cabrera and Levine 1956), and the average slope of a vicinal hillock $p = h/19\rho_c$ is therefore given by formula (5). The time of one revolution of the spiral around the centre is $19\rho_c/v$, where v is the rate of motion of the step.

Let us now look at how a complex dislocation source, shown in figure 12(*b*), works. It has $b = 3h$ and a core in

the form of a cavity cross-hatched in figure 12(*b*). Firstly, since the magnitude of the total Burgers vector of this source equals $3h$, this source generates a triple spiral, and not a double one as in figure 12(*b*). Secondly, added to the time it takes for each step to revolve around the centre, $19\rho_c/v$, is the time $2L/v$ needed for the step to turn around the core of the source. As a result, the period of revolution increases to $(19\rho_c + 2L)/v$, and the distance between the loops of each individual spiral (one of the three in figure 12(*b*))—to $19\rho_c + 2L$. Delocalization of the source core thus decreases the capacity of the source to generate steps. At the same time, an m-fold increase in the Burgers vector (in figure 12(*b*) $m = 3$) increases the density of all the steps, and, correspondingly, the power of the source m-fold. Allowance for both these effects leads to the formula (7).

The influence of the centre of a dislocation source on the rate of generation of layers by it and, therefore, on the face growth rate also results in the asymmetry of growth and dissolution on the dislocation source (see section 3.3).

3.2. WHAT LIMITS THE RATE OF GROWTH?

Figures 9 and 10 help in solving another problem, discussed for many years now: is surface diffusion important in the growth of crystals from solutions?

When a crystal grows from vapour, molecular beams and (to a smaller extent) from the gas phase with the participation of chemical reactions, surface diffusion is highly significant. The point is that the density of the crystallized substance in the gas phase is much ($\sim 10^6$ times) lower than that of the same substance in the state of adsorption on atomically smooth terraces between the steps. If the temperature is not very low the adsorbed molecules (atoms) can diffuse sufficiently fast on the surface. This two-dimensional diffusion flux provides a considerably more intensive input of the crystallized matter to the steps than the one achieved by direct attachment from the gas phase.

Every step is rather strongly incised with fluctuations, i.e. carries a great number of kinks (figure 4(*a*)). For this reason the particles are attached to the kinks independently of each other, and the rate of the step must grow linearly with the supersaturation that exists in the direct vicinity of the step. At the same time, each step constitutes a linear sink for the crystallized matter, and so it is surrounded by a diffusion field. If the decisive role in the feeding of a step belongs to diffusion in the bulk of the mother solution, then the symmetry of diffusive concentration distribution near the step is cylindrical. If diffusion proceeds only on the surface of terraces between the rectilinear steps, the diffusion field is one-dimensional and depends only on the coordinate along the normal to the steps. Overlapping of the diffusion fields of the neighbouring (and more distant) steps serves as the measure of the competition between the steps for the crystallizing matter. The more complete the overlapping the lower the supersaturation in the direct vicinity of each step and the lower its velocity v at the same supersaturation in the bulk of solution. In the experiments illustrated by figures 9, 10 an increase in supersaturation is accompanied by an increase in the slope p of the dislocation hillocks, i.e. the steps come nearer to each other. That is why, if the overlapping of the diffusion fields of steps is actually taking place, the velocity v of the steps forming a vicinal hillock must, with the growing σ, grow more slowly than if it adhered to a linear law. In actual fact, according to figures 9 and 10, the $v(\sigma)$ dependence is a linear function of supersaturation. Therefore, the steps do not compete for the feeding, and supersaturation over each step is the same as in the bulk of solution. From this it follows that the observed rate of the steps, and with it the growth rate of the face as well, are wholly determined by the process whereby the ions are being built into the lattice directly onto the steps. (The growth rate of the face is of course also strongly dependent on the rate of step generation.)

The building-in process on the steps is characterized by a kinetic coefficient β_1 of the proportionality between the growth rate of the step and the supersaturation σ over it

$$v = \omega C_e \beta_1 \sigma. \tag{8}$$

The kinetic coefficient β_1 is anisotropic. On the face of the prism it is smaller along the optical axis, $\beta_1 \simeq 4 \times 10^{-3}$ cm s^{-1} (Chernov *et al.* 1986), and approximately 1·5 times larger in the perpendicular direction. On the face of the dipyramid β_1 is markedly higher, and for the three different orientations of steps in the plane of this face amounts to 0·8, 0·6 and 0·4 cm s^{-1}. The linear energy of steps for the faces of the prism and the dipyramid, found in our experiments, proved to be practically the same, the surface energy of a step riser being 15 and 20 erg cm^{-2}. A large difference in the rates of the ADP prism and dipyramid faces (observed at low supersaturations) is thus wholly determined by the kinetics of step movement, i.e. by the acts of the particles being built into the lattice on the kinks.

It may be useful to note that the kinetic coefficients of the growth rates of garnet faces, found by a quite different method, are equal to 3×10^{-3}–3×10^{-4} cm s^{-1} (Görnert and Voigt 1984).

The kinetics characterizing the incorporation of the molecules of ions into the lattice on steps determine not only the growth rate and the morphology of the face, but also the trapping of impurities, the density of point defects in the crystal, the morphological stability of the face and the trapping of impurities by it.

3.3. ASYMMETRY OF GROWTH AND DISSOLUTION

It has been known for a long time that the rate of crystal dissolution is several times greater than the rate of its growth. Moreover, a crystal, acquiring the shape of a perfectly faceted polyhedron in the course of its growth, becomes close to a sphere when dissolved for a sufficiently long time (Heimann 1975). The reason for these kinetic and morphological differences lies in the fact that crystal edges serve as powerful sources of layers as the crystal dissolves, but are absolutely passive when it grows. Even a very slight dissolution causes, already in its early stages, the round of edges and apexes, as a result of their giving rise to numerous steps that spread to the face centre.

And are the growth and dissolution kinetics symmetrical on the steps themselves? In other words, will the rates of step movement be equal in their absolute value when the atomic plane is being built ($v > 0$) and when it decomposes ($v < 0$), under the condition that the absolute values of supersaturation ($\sigma > 0$) and undersaturation ($\sigma < 0$) are the same? A positive answer is given by the symmetry of the right and the left parts in figure 13, where the absolute values of v are laid off along the vertical and the supersaturation and undersaturation† along the horizontal axis. With a sufficiently high degree of accuracy figure 13 yields $v(-\sigma) = -v(\sigma)$. However, as seen from figure 14, the normal growth rate modulus, $|R|$, is not invariant to the $\sigma \to -\sigma$ substitution. Namely, $-R(-\sigma) > R(\sigma)$, and for $\sigma \simeq 0{\cdot}25\%$ $|R(-\sigma)| \simeq 3|R(\sigma)|$, i.e. the asymmetry is considerable.

The rates of steps are thus symmetrical during the growth and the dissolution, while the rates of faces are asymmetrical. Therefore, the cause of asymmetry lies in the generation of steps by dislocations. Indeed, the dislocation core is surrounded by an elastically stressed region with the energy density $\varepsilon_{el} \simeq Gb^2/8\pi^2r^2$ (Hirth and Lothe 1982), where G is the shear modulus, b is the modulus of the Burgers vector, r is the distance to the point of observation. If $G \simeq 10^{11}$ erg cm^{-3}, $b = 5h$, $r = 50h \simeq 250$ Å, the specific molecular volume $\omega = 10^{-22}$ cm^3,

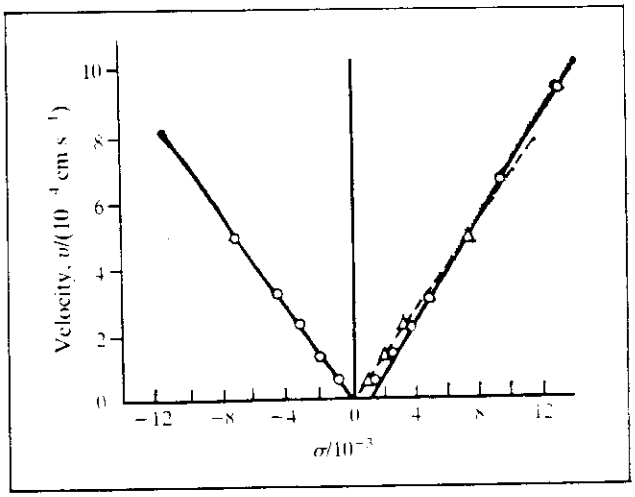

Figure 13. Average speed of steps, v, as a function of supersaturation ($\sigma > 0$) and undersaturation ($\sigma < 0$) of solution. For the dissolution rate the $-v$ value is plotted on the vertical axis. The growth and the dissolution processes are symmetrical (in the sense of $v(\sigma) = -v(-\sigma)$). The face of $NH_4H_2PO_4$ crystal dipyramid, pH = 5·6, kinetic regime of growth.

then the elastic energy in terms of one molecule $\omega\varepsilon_{el} \simeq 10^{-15}$ erg. This is comparable with the difference $\Delta\mu = kT\sigma$ of the chemical potentials of the crystal, μ_k, and the solution, μ_{sol}, at $\sigma = 2{\cdot}5\%$. Likewise the radius of the critical nucleus $\rho_c = \omega\alpha/kT\sigma = \omega\alpha/\omega\varepsilon_{el} = 20$ erg cm$^{-2}/(10^7$ erg cm$^{-3}) = 2 \times 10^{-6}$ cm is compar-

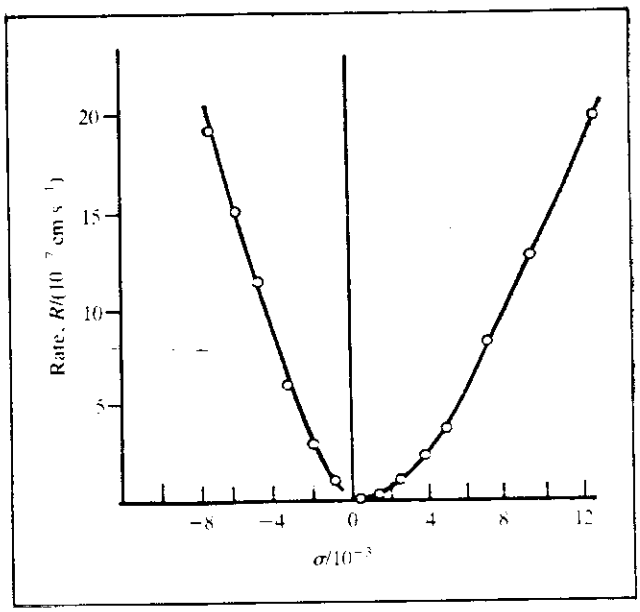

Figure 14. Normal rate R of the same $NH_4H_2PO_4$ dipyramid face as the one shown in figure 13. For dissolution, the $-R$ value is plotted on the vertical axis. Growth and dissolution are not symmetrical: $R(\sigma) < -R(-\sigma)$. The influence of steps emitted during dissolution by the crystal apexes and edges is excluded.

† The values of R were measured with the help of local laser interferometry as follows. A laser beam is focussed on the surface of the growing face, producing a spot $\simeq 0{\cdot}7$ mm in diameter. The beams reflected from the investigated face of a crystal plate and the second face parallel to it interfere, producing lines of an equal slope on a translucent mirror. The intensity was measured in one of the fringes occupying practically the whole spot. The rate of face dissolution was measured during comparatively short periods of time after long periods of steady-state growth. This procedure of measurements in the non-steady state mode excludes the influence of steps emitted by the apexes and edges of samples during dissolution. The slope p was found from the kinetics of the shock waves of steps (Chernov *et al.* 1987). From the known values of R and p, $v = R/p$ was calculated.

able with the value taken for $r = 50h \simeq 250$ Å. Thus, there is enough elastic energy around the dislocation for the crystal chemical potential to be raised noticeably at distances of the order of the critical nucleus radius for supersaturations $\sigma_{el} \equiv \varepsilon_{el}\omega/kT$. This region is schematically shown in figure 12(*a*) by cross-hatching. The lower the supersaturation σ assigned from without the greater the role of elastic stresses. At $\sigma < \sigma_{el}$ favourable conditions arise for a hollow channel to be formed around the dislocation (Frank 1951; Sunagawa 1984).

The overall scheme of the levels of chemical potentials in growth and dissolution is shown in figure 15. The motive forces $\pm\Delta\mu$ of crystallization and dissolution, those assigned from without and really measured by the supersaturation or undersaturation in solution, are taken to be the same. However, the chemical potential of a crystal near the dislocation is higher (by $\omega\varepsilon_{el}$). Therefore, the absolute value of supersaturation acting in reality upon the central part of the spiral during the growth is higher than the absolute value of undersaturation during the dissolution. In short, the elastic energy hinders the growth of steps and helps their dissolution.

As already noted in section 3.1, the rate of generation of layers is wholly determined by the region with a radius of $\simeq \rho_c$ around the spiral centre. The difference in the absolute values of supersaturation and undersaturation, $\Delta\mu_+$ and $\Delta\mu_-$, in this region clearly observed from figure 15 is what determines the asymmetry of the curves in figure 14, emphasizing the role of elastic stresses in the vicinity of dislocations. A detailed numerical analysis of the development of a spiral, with elastic stresses taken into account, has been given in the works of Van der Hoek *et al.* (1982, 1983).

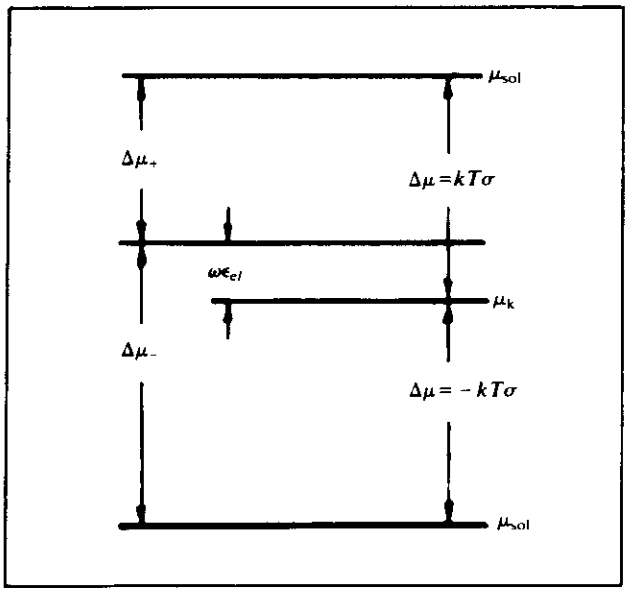

Figure 15. Chemical potentials of unstressed crystal (μ_k) and of dissolved matter in solution (μ_{sol}) in the growth ($\mu_{sol} > \mu_k$) and the dissolution ($\mu_{sol} < \mu_k$). In a stressed crystal, e.g. around a dislocation, the chemical potential is by $\omega\varepsilon_{el}$ higher. Correspondingly, at the same average supersaturation of solution, σ, the deviation from equilibrium, really moving the step at the centre of the spiral (figure 12(*a*)) during the growth ($\Delta\mu_+$), is lower than in dissolution ($\Delta\mu_-$).

3.4. NON-CLASSICAL KINETICS OF LAYER-SPIRAL GROWTH

Dependences of the $p(\sigma)$, $v(\sigma)$, $R(\sigma)$ types in figures 9 and 10 are in good agreement with the classical theory of dislocational growth put forward by Burton *et al.* (1951). This cannot be said, however, of the dependences in figures 16–18 (Chernov and Rashkovich, 1987). Here the kinetic coefficient of the steps of growth sharply increases when supersaturation exceeds a certain critical value $\sigma = \sigma_*$, equal in figures 16–18 to 3–5%, and the slope of the dislocation hillock of growth $p(\sigma)$ proves to be altogether nonmonotonic. The corresponding growth rate of a face as a whole sharply increases at $\sigma > \sigma_*$.

A strongly nonlinear $v(\sigma)$ dependence seems to be caused by the impurities firmly adsorbed on the growing face, but poorly entering into the crystal. A change in σ_* resulting from the addition of an impurity of trivalent chromium, well-known for its influence on the growth of the crystals of KDP group, is clear from figure 17(*a*,*b*). Neither can we exclude the effect of organic impurities that are poorly detectable. They may be responsible for the existence of a threshold supersaturation σ_* in the absence of detectable (< 1 ppm) ions of trivalent metals (Cr^{3+}, Fe^{3+}, Al^{3+}).

The molecules (ions, complexes) of the above types of impurities, together with the solvate shells surrounding them, act as the stoppers for the movement of steps. If the distance between the stoppers, $C_{Si}^{-1/2}$, is less than the diameter $2\omega\alpha/\Delta\mu$ of the two-dimensional critical nucleus at a given supersaturation, the steps cannot overcome the 'fence' of impurities, and their movement stops completely (Cabrera and Vermilyea 1958). Here the surface concentration of stoppers C_{Si} (cm^{-2}) is related to the concentration of impurities in the bulk by the conventional formulae of adsorption. Every given surface concentration C_{Si} thus has a corresponding threshold supersaturation $\sigma_* = 2\omega\alpha C_{Si}^{1/2}/kT$, below which the face does not grow. Our $v(\sigma)$ and $R(\sigma)$ dependences in figures 14–16 bear a resemblance to those with a threshold, but the face growth does not completely stop at $\sigma < \sigma_*$. The stoppers do not seem to have an infinitely long but instead a finite lifetime in the state of adsorption. Undergoing desorption they make it possible for the steps to move at sufficiently small supersaturations as well. The rate of such movement will be determined both by the

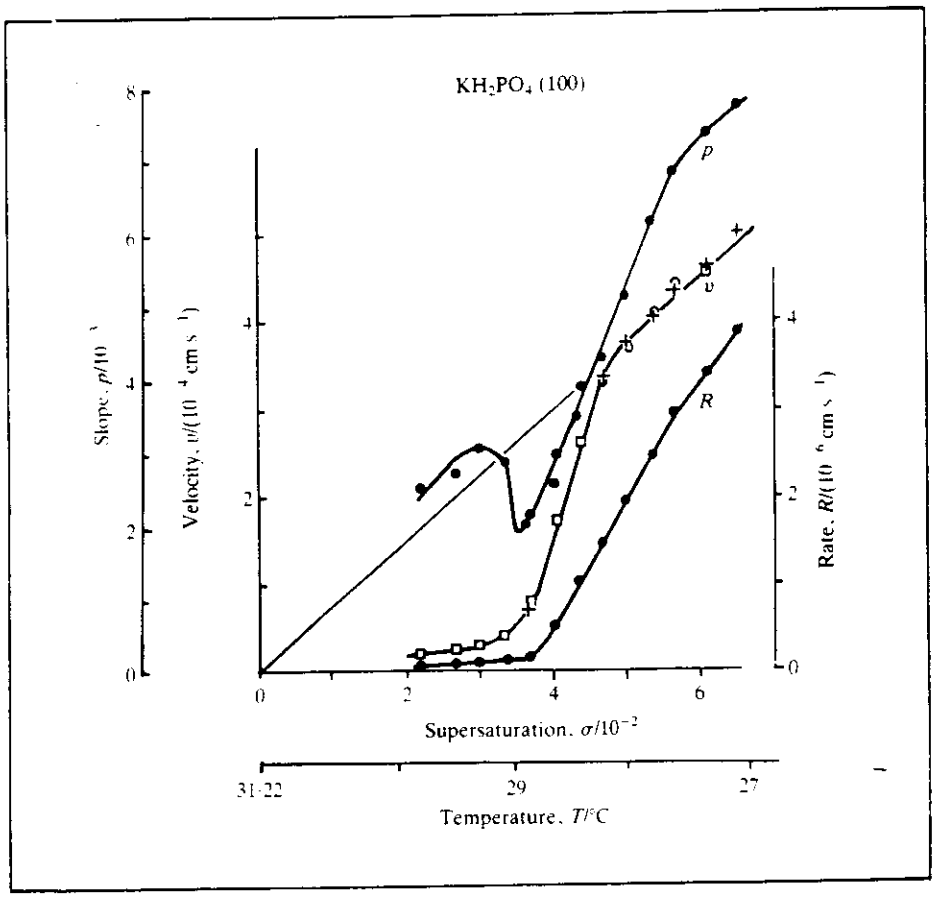

Figure 16. Effective speed v of steps, slope p of vicinal hillock and normal growth rate of face, R, determined by the hillock, as functions of supersaturation σ. A sharp increase in v in the region of $\sigma \simeq 3{\cdot}5\%$ occurs when impurity stoppers can no longer restrain the movement of steps. The nonmonotonic nature of $p(\sigma)$ is a consequence of a sharp increase in $v(\sigma)$. KH_2PO_4 crystal, prism face. Different symbols on v graph are related to different hillocks.

supersaturation and by the lifetime of stoppers. The situation is similar to the one observed during the movement of dislocations in a crystal with impurities. Analytical solutions of such problems are not known.

If the rate of steps varies nonlinearly with supersaturation the classical layer-spiral growth theory is inapplicable, since it is based on the relationship (8). An adequate analytical theory for the piecewise linear $v(\sigma)$ dependence (v curve in figure 19), describing approximately the $v(\sigma)$ nonlinear curve in figures 16–18, has been recently developed by Chernov and Rashkovich (1987). Mikhailov *et al.* (1989) have performed numerical calculations for arbitrary $v(\sigma)$. The principal effect of the nonmonotonic $p(\sigma)$ dependence within the framework of the ideology of Chernov and Rashkovich (1987) is explained in the following way.

Let us consider a step ending at point D, where a screw dislocation comes out on the surface (figure 20). We shall assume the $v(\sigma)$ dependence to be a piecewise linear one (figure 17) and try to establish the nature of the $p(\sigma)$ dependence.

As in the case of linear kinetics, the step at the centre D is stationary, and the radius of curvature of the step at this centre must be exactly equal to that of the critical two-dimensional nucleus. Consider a point C on the step. The further C is from the centre D of the spiral (figure 20), the smaller the curvature of the step at this point and the closer the supersaturation that really moves the step (the Gibbs–Thomson effect) to its value in the bulk of solution. Therefore, there exists such a portion DC of the step near D, where the active supersaturation is lower than the threshold one, σ_*. Here the growth of the step is determined by slow kinetics. At distances from the centre that are greater than DC the movement and the shape of the step are determined by fast kinetics ($\sigma/\sigma_* > 1$, figure 19). Under steady-state conditions the flow of steps and, therefore, the growth rate of the face are the same at any point of the face, since $R = pv = \text{const.}$ (figure 8(*b*)). On the peripheral portion of the step the kinetic coefficient β_1 and, therefore, the velocity v too are approximately an order of magnitude higher than at the centre of the spiral, where the active supersaturation is lower than the threshold one, σ_*. Correspondingly, the slope p on the periphery is approximately an order of magnitude lower. If supersaturation in the bulk of solution is lower than its threshold value, $\sigma < \sigma_*$, the whole spiral, from the centre to the periphery, is characterized by slow and, roughly speaking, linear kinetics (figures 9 and 10). With linear

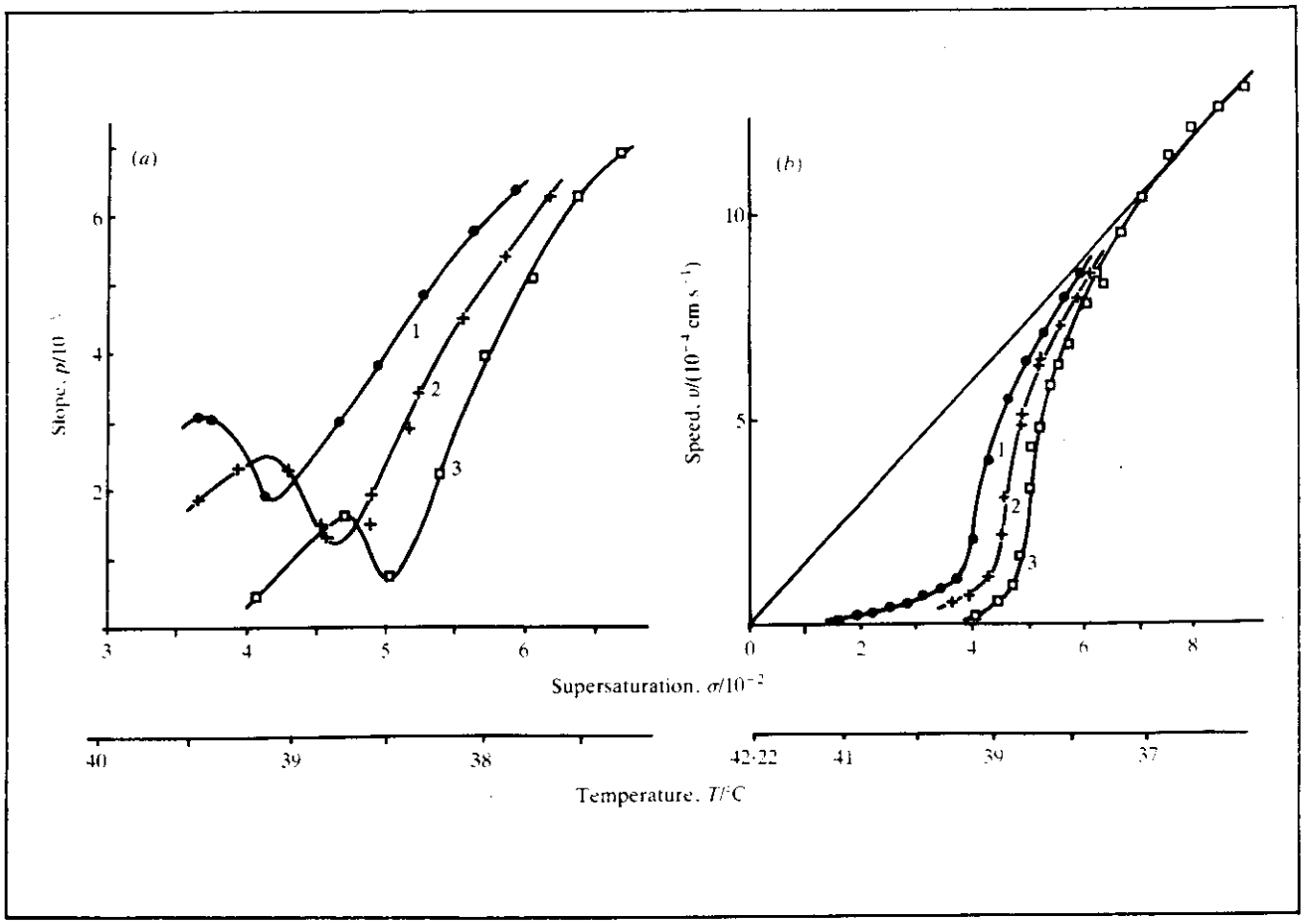

Figure 17. Influence of chromium impurity upon (*a*) the steepness (*a*) and the tangential speed of steps (*b*) on a dislocation hillock of growth on the face of a KDP crystal prism: 1 (filled circles)—nominally pure solution, 2 (crosses)—$2 \cdot 7 \cdot 10^{-6}$ and 3 (empty squares)—$5 \cdot 10^{-6}$ mole Cr^{3+}/mole KDP.

kinetics the slope p obeys expressions (6) or (7) and does not depend on the kinetic coefficient of the steps. That is why the $p(\sigma)$ dependence at $\sigma/\sigma_* < 1$ must be linear (figure 19). If supersaturation, while increasing, passes through the value of σ_* the slope of the actually observed peripheral portion drops as many times as the coefficient of fast kinetics exceeds that of the slow kinetics. This jump at $\sigma/\sigma_* = 1$ is seen in the p curve, figure 19. With a further increase in supersaturation the central, slowly growing, region of the spiral decreases, and the slope of the hillock p again approaches the value determined by (8). This dependence is represented in figure 19 by the $p(\sigma)$ curve for $\sigma/\sigma_* \gtrsim 3$.

The normal rate $R(\sigma)$ in the model described (figure 19) does indeed have the shape of the experimental curve in figure 16: it is very small at $\sigma/\sigma_* < 1$ and begins to increase linearly at $\sigma \gtrsim \sigma_*$. It is clear from the aforesaid that the steep linear rise of $R(\sigma)$ in figure 16 at $\sigma > \sigma_*$ has nothing in common with the normal growth and the high density of steps on the surface; likewise the threshold supersaturation itself has nothing in common with the critical value for the formation of two-dimensional nuclei. Both these peculiarities are associated with impurities.

3.5. GROWTH BY TWO-DIMENSIONAL NUCLEATION

Dislocations easily appear in crystals, especially in the initial stages of their growth. That is why two-dimensional nucleation is difficult to realize. Only a few groups have studied this mechanism. In particular, Sears (1956) has studied local evaporation of dislocation-free platelets, Ovsienko and Alfintsev (1967) the growth of gallium platelets from its melt, Hayashi and Shichiri (1974) the growth of NaCl wiskers. In most detail, the electrocrystallisation of dislocation-free silver crystals growing into a capillary $\sim 100\,\mu m$ in diameter has been investigated

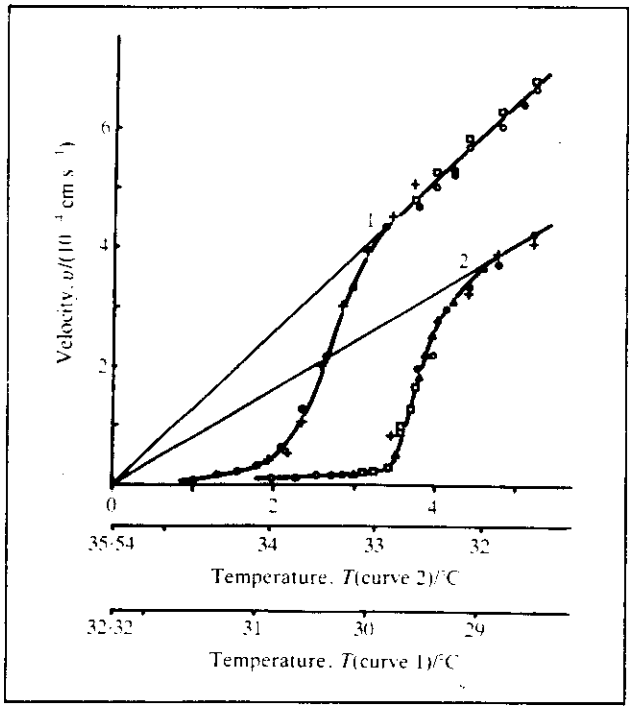

Figure 18. Dependence of the average speed of steps, v, upon supersaturation σ on DKDP prism face before (1) and after (2) adding 100 g of H_2O to 1300 g of solution in D_2O. Degree of crystal deuteration: 1—92 %, 2—85 %. Different designation of experimental values refer to different hillocks of growth.

by the Bulgarian school (Kaishev and Budevsky 1967; Budevsky *et al.* 1980). Absence of dislocations was registered in KDP crystals grown from aqueous solution (Fishman 1972); however, the kinetics of such growth have not been studied. The first successful intentional realization of dislocation-free growth from aqueous solution on a dislocation-free seed (Kuznetsov *et al.* 1981) opened the way to the systematic study of growth by two-dimensional nucleation (Malkin *et al.* 1989). In the latter experiments, the $3 \times 3 \times 1$ mm^3 seed platelet parallel to the (101) face was cut out of a dislocation-free part of an ADP crystal. After preparation, the seed was analyzed by ex situ X-ray topography to prove that there are no dislocations in it. Then the seed was fixed in a special growth cell through which supersaturated solution (pH = 5·0) flows at a velocity ($\gtrsim 25$ cm s^{-1}) sufficient to achieve the seed growth rate limited only by interface kinetics. During and after growth, in situ X-ray topography control was also used. The growth rates at various supersaturations were measured by automated laser interferometry. The results are given in figure 21 in coordinates $\ln(R/\sigma^{5/6})$ *vs.* σ^{-1} following from the model of multiple two-dimensional nucleation. According to this model, the two-dimensional nuclei appear independently at various points of a sufficiently large face and, reaching each other, complete the next lattice layer on this face. Neglecting the mutual influence of steps via their diffusion fields, one obtains the face growth rate (Chernov 1984):

$$R = h(v^2 J)^{1/3} = \text{const.} \times \sigma^{5/6} \exp(-\pi\omega\alpha^2 h/kT\sigma), \quad (9)$$

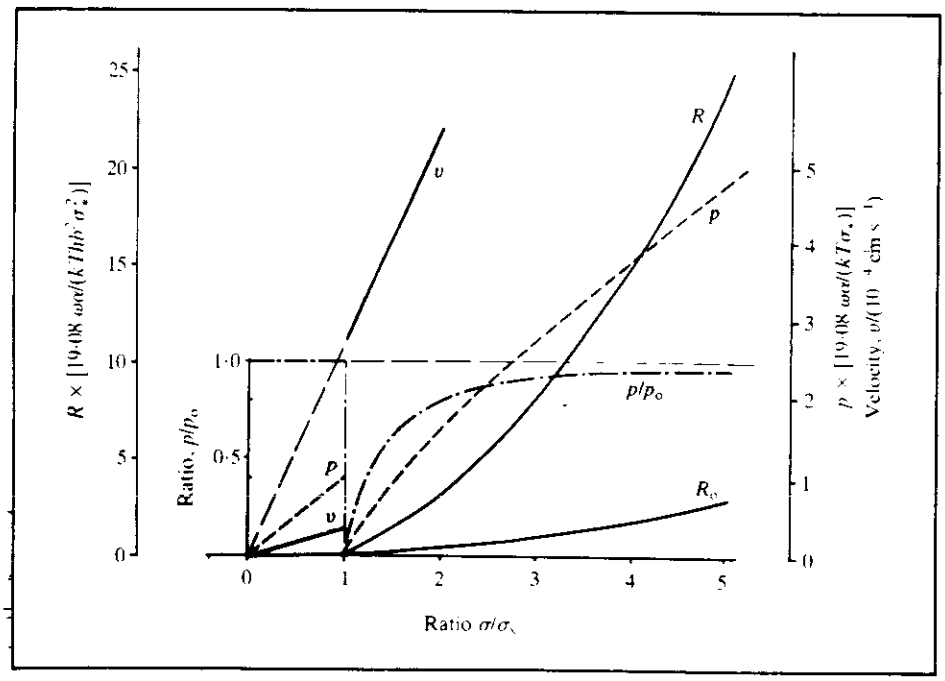

Figure 19. Piecewise linear $v(\sigma)$ dependence (approximating the $v(\sigma)$ dependences of the type presented in figure 16, 17(*b*) and 18) and the $p(\sigma)$ and $R(\sigma)$ dependences theoretically following from it. The $p(\sigma)$ $p_0(\sigma)$ curve shows the ratio of the hillock slope $p(\sigma)$ for the piecewise linear $v(\sigma)$ to the slope $p_0(\sigma)$ in the case of wholly linear $v(\sigma)$ dependence. The $R_0 \sim \sigma^2$ parabola corresponds to the wholly linear $v(\sigma)$ kinetics with the kinetic coefficient equal to the lower slope ($at\ \sigma/\sigma_* < 1$) of the piecewise linear $v(\sigma)$.

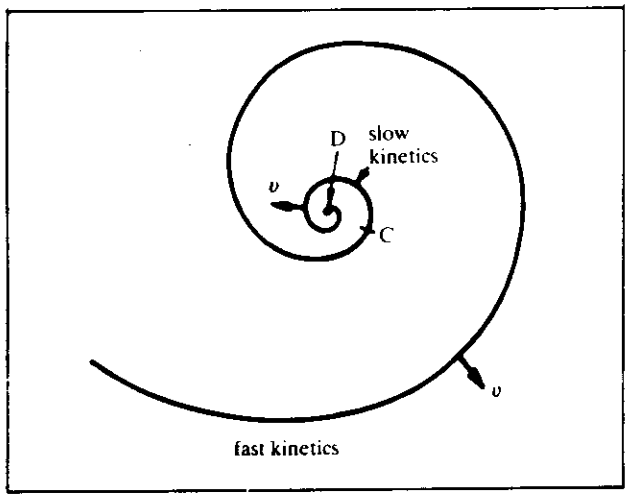

Figure 20. Dislocation spiral in the case of nonlinear kinetics of steps, expressed by the $v(\sigma)$ dependences of the type shown in figures 16, 17(*b*), 18. On the inner part of the spiral, DC, the acting supersaturation is small because of the Gibbs-Thomson effect. For this reason the growth kinetics is slow, and the loops are more frequent. On the outer part of the spiral the kinetic coefficient is much higher, the steps move faster, and the loops are rarer.

where J stands for the rate of two-dimensional nucleation (nuclei $cm^{-2} s^{-1}$).

If diffusion fields of growing steps overlap, equation (9) should be replaced by $R = \text{const.} \times \sigma \exp(-\pi\omega\alpha^2 h/kT\sigma)$ with a slightly different constant. For the range of supersaturations used, $10^{-3} < \sigma < 10^{-1}$, the value $\sigma^{1/6}$ varies slightly causing renormalization of the constant only. Therefore equation (9) was used to describe our experiments.

The constant in equation (9) includes the step kinetic coefficients and the surface density at the places where the nuclei may appear.

The lower curve in figure 21 presents the $R(\sigma)$ dependence for dislocation-free crystals; the upper curve was obtained for crystals with dislocations. Both curves were obtained under precisely the same conditions, often even for the same crystals—if dislocations appear spontaneously in these crystals during growth. The comparison of the upper and lower curves demonstrates a dramatic difference in growth rates provided by two-dimensional nucleation or by dislocations. It is clear from equation (9) that if the growth proceeds by two-dimensional nucleation, the slope of the $\ln R/\sigma^{5/6}$ *vs.* σ^{-1} straight line gives the effective surface energy of the step riser. In figure 21, the longer straight line 2 corresponding to lower supersaturations gives $\alpha = 4{\cdot}2\ \text{erg cm}^{-2}$, the shorter, steeper, segment 1 gives $\alpha = 11{\cdot}8\ \text{erg cm}^{-2}$. The latter value is not too far from $15\ \text{erg cm}^{-2}$ obtained from dislocation growth kinetics (Kuznetsov *et al.* 1987). The lower value, $4{\cdot}2\ \text{erg cm}^{-2}$, probably means that two-dimensional nucleation occurs not on every surface site but on specific surface centres, e.g. adsorbed impurities, which lower the nucleation barrier and are thus effectively described by a lower step energy. Estimating the constant in equation (9), we obtained reasonable densities of nucleation centres: $1{\cdot}6 \times 10^{14}\ \text{cm}^{-2}$ for homogeneous nucleation or regular lattice sites (line 1) and $1{\cdot}3 \times 10^{3}\ \text{cm}^{-2}$ for heterogeneous nucleation on, say, foreign impurities; this density should be lower than the density of regular sites. The nature of the nucleation centres is not yet known.

4. Hydrodynamics and dissipative surface structures

4.1. HYDRODYNAMICS OF SOLUTIONS

All the experiments described above were conducted in the so-called kinetic regime of growth: the solution was

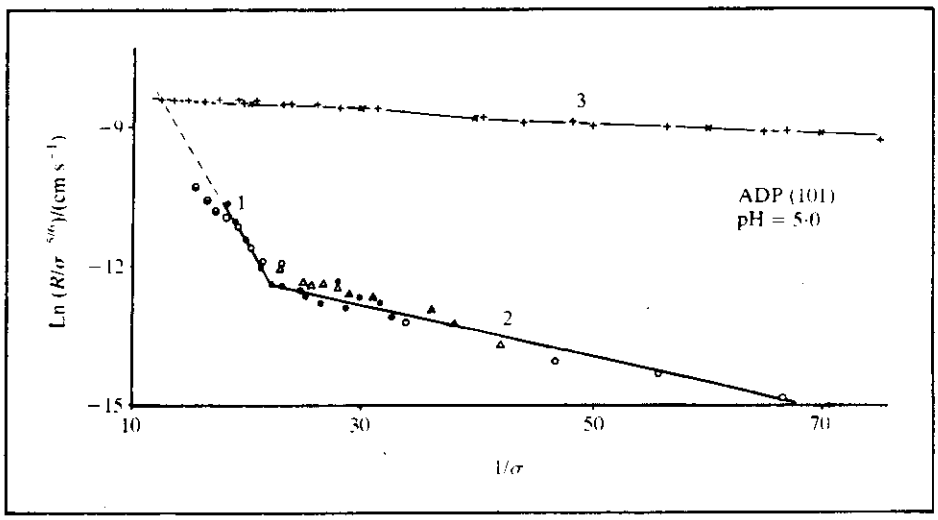

Figure 21. Dependence of the growth rate R on relative supersaturation σ for the (101) ADP face. Curves 1 and 2—growth rates of dislocation-free crystals, curve 3—growth rates of the same face under the same conditions as curves 1 and 2, but for the crystals with dislocations. Various kinds of experimental points are related to various samples. Three upper half-filled circles left from the dashed line 1 were obtained for the run in which a parasitic crystal spontaneously appeared in solution flow tract, thus slightly decreasing actual supersaturation at which the crystal under investigation grew.

stirred so intensively that diffusive resistance of the boundary layer to the supply of crystallized matter to the surface was much lower than resistance to crystallization directly on the surface. For the kinetic regime to be reached it was in practice sufficient to raise the rate of solution flow around the investigated face to $\simeq 30\,\mathrm{cm\,s^{-1}}$. The corresponding thinning of the boundary diffusion layer is seen from the series of interferogrammes in figure 22(*a-c*) obtained by L. N. Rashkovich and B. A. Shekunov. The solution moved from right to left in a cuvette of rectilinear cross-section. The cuvette was placed in the interferometer in such a way that the beam was directed perpendicular to the direction of solution flow and parallel to the face limiting the crystal in figure 22 from the top. Correspondingly, the interference fringes seen in figure 22 are lines of equal slope. In a homogeneous solution of constant concentration they would be rectilinear. The curving of these lines near the surface of the growing crystal is the measure of how the solution is depleted with respect to the crystallizing matter. Comparison of figure 22(*a-c*) with each other shows how the boundary layer is becoming thinner with increasing solution flow rate. At the flow rate of $15\,\mathrm{cm\,s^{-1}}$ (figure 22(*c*)) the boundary layer is no longer discernible. The boundary layer thickness is also seen (figure 22(*a,b*)) to be strongly dependent on the orientation of the face relative to the flow. On the upper horizontal face the boundary layer thickness is maximal at the centre of the face, and does not increase monotonically along the flow. These peculiarities are caused by the complex nature of the flow around a crystal having the form of a cylinder with a square cross-section.

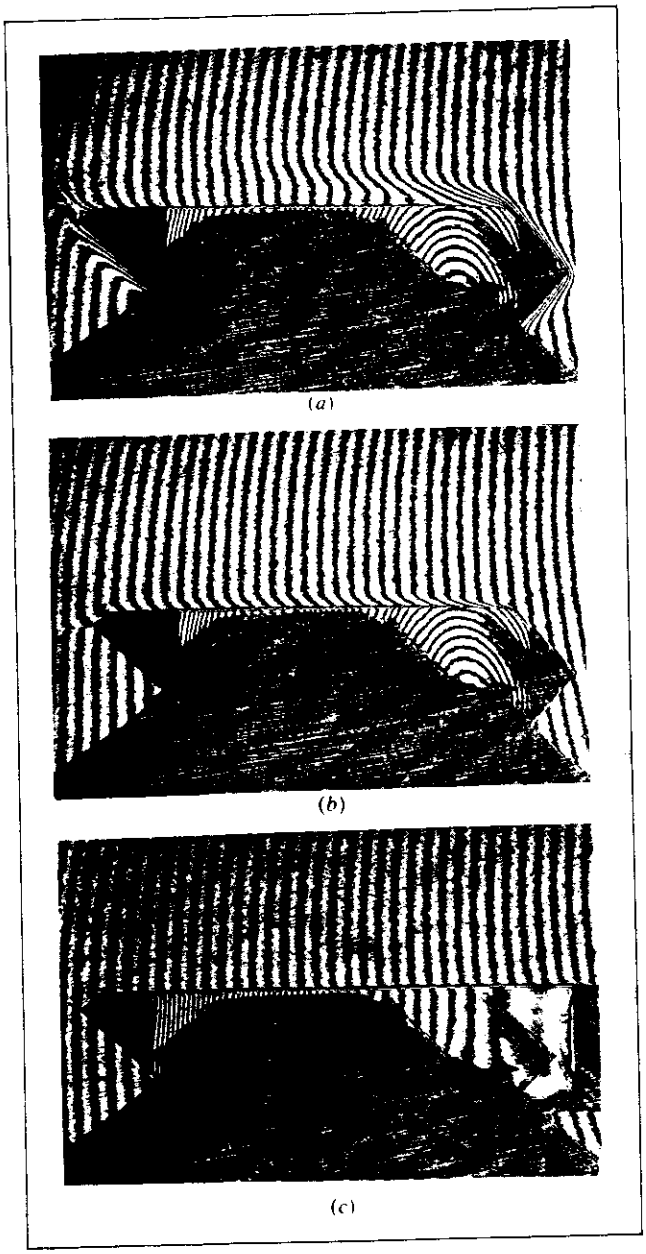

Figure 22. KH_2PO_4 crystal in supersaturated solution flow moving from right to left. Interference bands in solution represent equiconcentration lines. The bending of lines near the surface corresponds to the solution depletion by the growing crystal. Solution flow rate: (*a*) 0·4, (*b*) 4, (*c*) 15 cm s^{-1}. (L. N. Rashkovich and B. A. Shekunov).

Because the diffusive resistance of the boundary layer depends on its thickness, the supersaturation actually recurring on the face is highest near that edge of the face which first meets the approaching flow. In figure 23(*a,b*) the same face of an ADP crystal prism has been photographed with solution flowing along it in two opposite directions. In the left-hand upper corner of figure 23(*a*) the black arrow indicates a powerful dislocation source the steps from which propagate over the whole face. A few minutes after the solution flow inversion the echelon of steps seen in figure 23(*a*) disappears, and another source is seen, indicated by the black arrow in figure 23(*b*). This second source is situated at the centre of the face. It can therefore compete with the source prevalent in figure 23(*a*) only if solution flows upward. In this case supersaturation over the second source is somewhat higher than over the first one, and the second source now prevails. Notice, however, that the difference in supersaturations on the surface, associated with the variable boundary layer thickness, is not large. For instance, an approximately two-fold change in solution flow rate does not lead (within an accuracy of 5–10%) to any measurable changes in the rate of face growth.

The replacement of the leading dislocation source of steps upon the change in solution flow direction is also observed on the face of an ADP dipyramid (Chernov *et al.* 1986). The growth rate dependence on the position of the dislocation source was also discussed by Bredikhin *et al.* (1987).

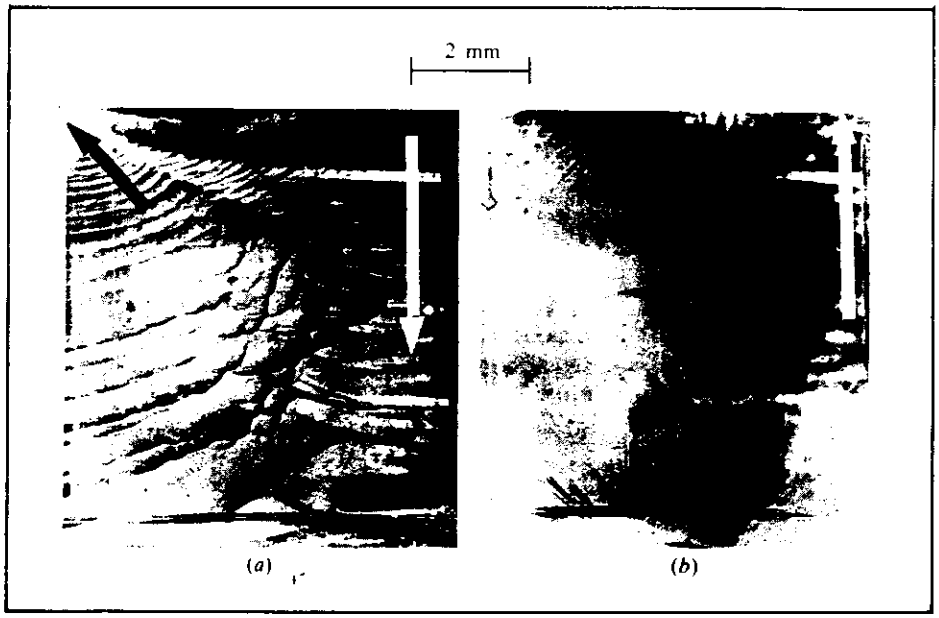

Figure 23. Influence of solution flow direction (indicated by the white arrows) upon the competition of two dislocation sources of growth layers (indicated by the black arrows): (*a*) being best fed the source near the upper edge prevails, (*b*) being better fed than the upper source the one at the face centre 'overcomes' it.

4.2. HYDRODYNAMIC-MORPHOLOGICAL INSTABILITY OF VICINAL FACES

It is well known that atomically rough surfaces growing from a supercooled melt or a supersaturated solution are always morphologically unstable. This means that the growing surface, initially flat, spontaneously breaks up with time into narrow and long parallel 'ridges' and 'domes' separated by more or less deep grooves. Correspondingly, the grown single crystal becomes made up of parallel plates and at later stages of instability transforms into a tight bundle of hexahedral pencils (see Chernov 1984, 1988). The layer-wise growing vicinal faces, forming the slopes of dislocation hillocks of growth, are morphologically unstable, too. The steps on such vicinals are no longer equidistant, they combine into groups, forming macroscopic bunches—macrosteps (Chernov and Nishinaga, 1987). This is how it comes about (Chernov, Kuznetsov *et al.* 1986).

Let us examine a part of a vicinal face, e.g. the slope of a vicinal hillock made up of equidistant steps. We shall place it in a horizontal position, as shown in figure 24(*a*). Now let a perturbation be superimposed on the equidistant distribution of steps, transforming it into a wavy surface of the type shown in figure 24 (*b*). Above this surface is a supersaturated solution, and the steps move from left to right (and slightly upward, along the particular face). The supersaturation in solution increases with the distance from the growing surface. Because of this the steps on the protrusions 2, 6 and the like move faster than in the valleys of the type 4. The accelerated movement in the region 2-3, as compared with the region 3-4, can lead to an increase in the density of steps over the whole region 2-4, and a bunch of elementary steps, i.e. a macrostep M, will arise. Such macrosteps are shown in figure 24(*e*). Counteracting the above instability is the surface energy, which, owing to the Gibbs-Thomson effect, tends to level off the perturbation as it arises. The levelling-off is the stronger the smaller the wavelength and, therefore, the larger the local curvatures of the surface. Both the factors described act on the atomically smooth as well as the atomically rough surfaces.

The specificity of a perturbed vicinal face which is growing layer by layer consists in the periodic change in the density of steps and, therefore, in the 'absorbing capacity' of the face. The measure of this capacity is the kinetic coefficient of the surface, $\beta_1 p$, where β_1 is the kinetic coefficient of steps (see equation (8)) and p is the local slope of the surface relative to singular orientation, i.e. the density of steps. The $\beta_1 p$ dependence on the coordinate x along the perturbed vicinal is given in figure 24(*c*). The higher the value of $\beta_1 p$ the lower the supersaturation on the surface, σ_s (figure 24(*d*)). This means that the highest supersaturations will be observed over the protruding portions of the 1-2, 5-6 types, where the density of steps is low, and the lowest one—over the portions of the 3-4 type. Such a distribution leads even faster to the formation of macrosteps, i.e. to morphological instability. A consistent theory has been given by Cahn (1977), Yuferev (1983, 1989) and Chernov and Nishinaga (1987).

The pattern changes if one takes into account the movement of solution near the surface inside the boundary layer. Let the solution move towards the right in figure 24 (at the rate of u). Then the most supersaturated

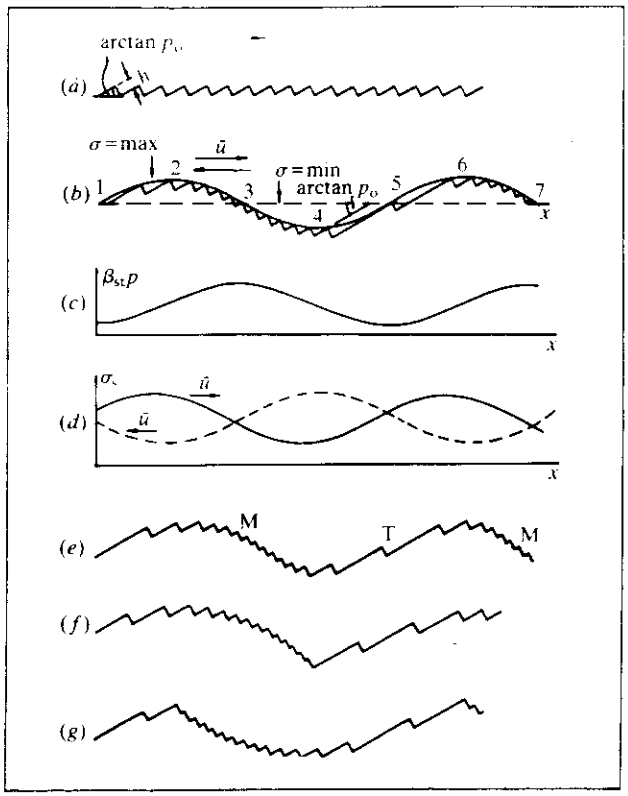

Figure 24. Instability development on vicinal face. (*a*) unperturbed vicinal surface with elementary steps; (*b*) periodic perturbation of the vicinal leads to periodic bunching (2–4) and rarefying (4–6) of steps; (*c*) kinetic coefficient of the surface, $\beta_1 p$, follows the density of steps; (*d*) distribution of the supersaturation σ_s directly above the surface in the case of two solution flow rates u in the opposite direction; (*e*) instability development consists in a further increase in the density of elementary steps at the regions of type 2–4 in (*a*) and, independently, of macrosteps M separated by the terraces T; (*f*) shock wave of the density of steps with the edge (a jump in the density of steps) in front; (*g*) shock wave with the edge behind in the direction of step movement.

portion of solution, from the regions 1–2, 5–6, etc., will be carried to the slopes of the 2–4 type. Here the density of steps is the highest, and the solution is depleted most of all of the crystallized matter. This depleted solution moves further into the region of the 4–6 type, where the density of steps is the lowest, and is again enriched there. Thus, the enriched solution from the regions of minimum density of steps arrives at the protrusions (2–3), and the depleted solution from the regions where the density of steps is maximal—at the valleys (3–4). In other words, the supersaturation on the surface, σ_s, will vary as shown in figure 24(*d*) by the solid line. This means that, again, the protruding regions 2–3 exist in conditions of highest supersaturation and the valleys 3–4 in conditions of lowest supersaturation. Therefore, the periodic perturbation that has occurred in a random fashion will grow with time, i.e. the surface is unstable.

Let now the solution move towards the left in figure 24. Then the enriched solution from the regions with the minimum density of steps (type 6–4) will first penetrate into the hollows (type 4–3) and only after that, having become depleted, onto the protrusions of type 3–2. Because of this the valleys must grow at a higher rate than the protrusions—the periodic perturbation ends, i.e. the surface is stable.

The aforesaid explains a new type of morphological instability, revealed on ADP crystals, and differing from that previously known by the substantial role of solution hydrodynamics.

Figure 25 shows the morphology of a hillock of growth around a dislocation for which the point of outcropping is indicated by the black arrows. The white arrows indicate the direction of the flow of mother solution along the face. The 'surface wrinkles'—the macrosteps—are seen to be always formed on the slope of the hillock of growth where the elementary steps while growing move in the same direction as the mother solution. The smoothing-out of macrosteps on one slope of the hillock and their formation on the opposite side after the change-over in direction of solution flow (transition from figure 25(*a*) to figure 25(*b*)) takes a time of about 1–2 minutes. The instability just described is observed in a purely kinetic regime of growth, when the solution flow rate ($\simeq 30\,\mathrm{cm\,s^{-1}}$) is so high that its further increase no longer influences the growth rate.

Macrosteps exist permanently on a layer-wise growing face and constitute a certain kind of dissipative structure. Having once arisen they can change their shape. In particular, kinematic shock waves of steps can arise on them, i.e. jumps in the density of their distribution along the face. These jumps are obviously equivalent to edges. An edge can be formed both on the forward (figure 24(*f*)) and on the rear (figure 24(*g*)) front of the macrostep. The theory of the shock waves of steps was developed long ago (Frank 1958, Cabrera and Vermilyea 1958, Chernov 1961) and is also based on the mutual diffusive influence of elementary steps. This influence is noticeable only for a high density of steps, when $\beta_1 p/D$ exceeds at least 0·1, which would answer to 10% of the diffusive regime of growth for a part of the surface with slope p. If the boundary layer thickness $\delta \simeq 10^{-3}$ cm, $\beta_1 \simeq 4 \times 10^{-3}\,\mathrm{cm\,s^{-1}}$, diffusion coefficient in solution $D \simeq 10^{-5}\,\mathrm{cm^2\,s^{-1}}$, then the condition is satisfied at $p \gtrsim 4 \times 10^{-2}$. This is appreciably higher than the average slope of vicinal hillocks (see figures 9, 10, 16, 17(*a*)), but is quite possible on macrostep slopes.

There also exists another mechanism of instability in the echelon of steps (Frank 1958, Van der Eerden and Müller-Krumbhaar 1986). The gist of it is that on the

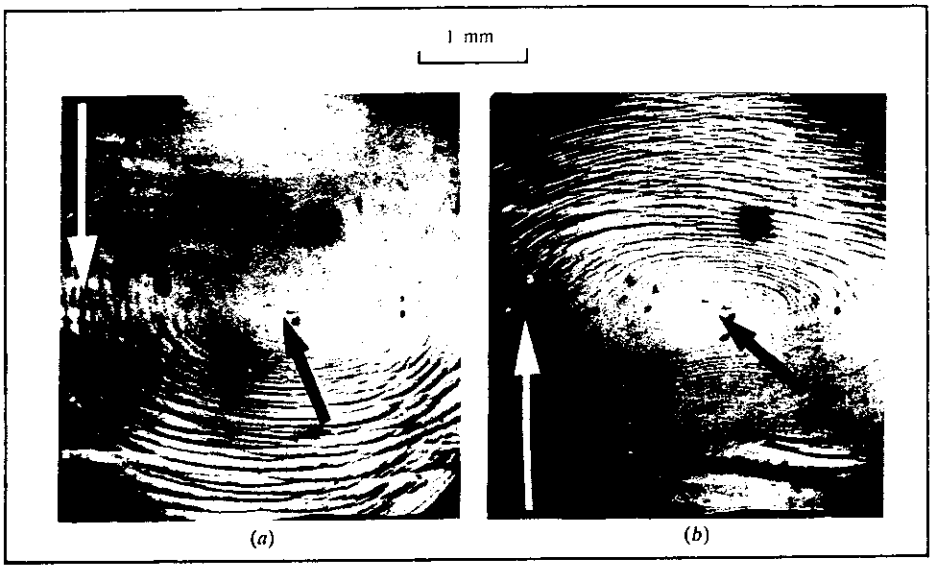

Figure 25. Morphology of vicinal hillock around dislocation source (indicated by the black arrow) on $NH_4H_2PO_4$ crystal prism face. (*a*) When solution flows downward (white arrow) the lower slope of the hillock loses its stability and is covered with macrosteps. (*b*) After the reversal of flow macrosteps on the lower slope of the hillock disappear and form on its upper slope, where the directions of the movement of steps and solution coincide. As the distance from the centre increases the steps are seen to become gradually larger. The morphology replacement process takes ≃ 2 min after the solution flow has been reversed.

terraces between elementary steps an impurity can be adsorbed, inhibiting the movement of these steps. The shorter the terrace the smaller the amount of impurity that can be adsorbed on it and the weaker the inhibition. As a result, the randomly arising clusters of steps must move faster than the rare steps, which will entail an even greater increase in the density of steps in the clusters with time. In the 'diffusion ideology', vice versa, the clusters move more slowly than the more isolated steps (Chernov 1961). It has been reliably established that the rate of macrosteps decreases with their growing height (Chernov 1984), but the structure of step risers has not been properly studied yet. For this reason the contribution of the diffusive and the impurity mechanisms to the instability is not yet clear.

An important feature in the behaviour of macrosteps is their coalescence and enlargement in the course of movement. This process can also be described in terms of a partially diffusive regime of step movement: thin steps, having a higher growth rate, catch up with the thick ones and coalesce with them (Chernov 1961). The interpretation of enlargement in the 'impurity ideology' (Van der Eerden and Müller-Krumbhaar 1986) presupposes an increase in the density of elementary steps on the riser of the macroscopic ones.

4.3. INCLUSIONS

The risers of macrosteps of sufficient height may lose stability themselves. This results in the inclusions of mother medium being formed in the body of the crystal. The latter is extremely dangerous, e.g. in the crystals used for doubling the frequency of powerful laser radiation, such inclusions cause the cracking of the operating crystals. The stresses near the microinclusions, or those resulting from nonuniform distribution of the trapped impurities, seem to be responsible for the anomalous birefringence. That is why everything possible is done to prevent the formation of macrosteps, primarily by means of a thorough stirring of solutions. The inconstancy of the boundary layer along the face and the dependence of instability on the direction of solution flow, described in section 4.2, dictate that the mother solution be stirred so that the direction of solution flow over each portion of the surface changes with sufficient frequency.

Exclusion from solutions of impurities that actively inhibit growth is also necessary to obtain crystals free of inclusions.

5. Secondary nucleation and defects

Secondary nucleation consists in the spontaneous appearance of new crystals in solution (or melt) where growing crystals already exist. What is called the primary nucleation, or simply nucleation, is the spontaneous appearance of nuclei in supersaturated solutions without any crystals in them.

Secondary nucleation is especially important in mass crystallization, when a solution with a great number of crystals suspended in it is stirred in a crystallizer. Secondary nucleation in this case exerts a strong influence on the total number of crystals and, therefore, on their average size, as well as on the distribution of crystals in size. The latter parameter, as well as the average size, constitutes an important characteristic of the final product.

Numerous studies have been devoted to ascertaining the nature of secondary nucleation (Nyvlt *et al.* 1985). As a result, among other things, it has been established (Garside *et al.* 1979) that even a slight touch to the surface of a growing crystal leads to the appearances of

very small (5–25 μm) fragments with each one becoming the 'nucleus' of a new crystal. Naturally, the crystals suspended in the crystallizer collide with the stirrer, the vessel wall and with each other, and thus 'reproduce' themselves.

Experiments (Belyustin *et al.* 1966, Sung *et al.* 1973) have been described, however, in which secondary nuclei appeared without any contact between the main crystal and a foreign solid body except of crystal holder or vessel bottom. These experiments were conducted with an individual crystal, so that the collision of crystals with each other was also excluded. Sung *et al.* observed secondary nucleation in a two-chamber crystallizer. In the upper chamber at a lower supersaturation one crystal was growing freely. The supersaturated solution flowing around it went into the lower chamber, where the supersaturation was higher, but still not so high as would be necessary for primary nucleation. The nuclei that originated in the upper chamber rapidly grew in the lower one to visible dimensions and in this way 'developed themselves'. In a check experiment, a 'dummy' was placed in the first chamber—an organic glass body whose size and shape were the same as those of the growing crystal. At a not too high supersaturation, the nuclei proved to appear in the lower chamber only in the presence of a real crystal in the upper one.

Experiments similar to the one described above led to the 'fluid shear' hypothesis (Nyvlt 1985). It assumes that the solution flowing around the crystal carries away from the surface the clusters arising near it under the action of the crystal molecular field. Subsequently, the clusters —molecular aggregates of the crystallizing matter —reach their critical size in supersaturated solution and grow to visible dimensions. This hypothesis is, however, difficult to believe. Firstly, supersaturation near the growing crystal face is much lower than that needed for homogeneous primary nucleation, and the probability of nucleation undergoes an extremely sharp drop with a drop in supersaturation. Secondly, it is difficult to imagine that the crystal molecular field concentrates the dissolved matter particles into clusters. At the same time, secondary nucleation, even in the absence of stirring, is a firmly established fact, which calls for an explanation. In my opinion, it is caused by the small fragments that separate from the growing crystal during the formation of inclusions and cracks in it. In fact it is well known (figure 8(*c*)) that inclusions of the mother solution in a crystal often constitute the source of dislocation bunches so that the overall Burgers vector in every bunch is equal to zero). The scheme of the formation of dislocations is especially simple for flat inclusions parallel to the growing face. This is shown in figure 26. Let two macrosteps move toward each other as shown in figure 26(*a*). The feeding of the protruding edge E of the higher left step is

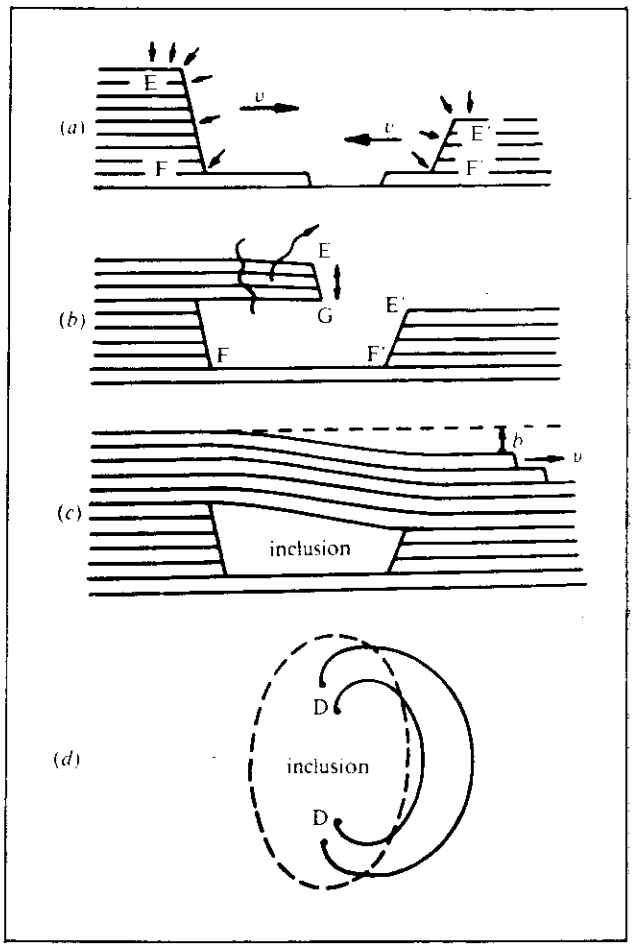

Figure 26. Scheme of the formation of inclusions and dislocations, demonstrating a possibility of the overhanging layer deformation and breakaway: (*a*) two macrosteps and two elementary steps moving towards each other, the protruding edge E is fed better than the re-entrant edge F (shown by short arrows); (*b*) better feeding of the step riser near E leads to the formation of the overhanging layer EG, its end can break away (shown symbolically by the arrow and the wavy line) under the action of pressure fluctuations in the liquid on both sides of the layer, the breakaway is also possible from the contact with the front of the step E′F′: (*c*) a flat inclusion sealed when atomic planes on the step risers EGF and E′F′ in (*b*) do not exactly coincide; (*d*) view from the top of a sealed flat inclusion with two dislocation sources DD of steps (each source is made up of two dislocations).

better than that of the edge F of the re-entrant angle. This results in an overhanging surface layer growing out from the upper part of a high step (figure 26(*b*)). Under the action of hydrodynamic pressure and temperature fluctuations the overhanging layer, generally speaking, is bent and can also undergo vibrations. Because of this at the moment when the macrostep EG meets the approaching macrostep E′F′ horizontal atomic planes may not exactly coincide. A discrepancy arises—the Burgers

vector **b** (figure 26(*c*)). This discrepancy can only take place within a limited portion DD of the line along which the EGF and E'F' steps meet (figure 26(*d*)). Then the ends of the DD portion will be the sites where the screw dislocations with the Burgers vectors **b** and $-\mathbf{b}$ come out on the surface. The inner surface of the inclusion sealed as a result of the macrosteps meeting each other will also contain the outcrops of these dislocations (Chernov 1973). Formation of dislocations on inclusions is the commonest way of forming them during growth from solutions and is illustrated by figure 8(*c*). The overhanging layer EG, merging with the step E'F' upon the sealing of the inclusion (figure 25(*b*)), can be deformed (statically or dynamically). Also possible therefore is the breakaway of this layer, especially after meeting with another step†. A fragment or fragments can serve as secondary nuclei. A sealed inclusion and the strong dislocation bunches emanating from it can yield internal stresses in the crystal sufficient for its cracking even in the course of growth. Fragments, rather frequently produced by any cracking, will become secondary nuclei.

At least two another sources may cause internal stress:

(1) Difference in lattice parameters between the already grown crystal (for example, a seed) and the new deposited layers. The relative lattice mismatch ε may be due to a difference in impurity concentration trapped at different growth rates. For low growth rates ($\simeq 10^{-6}$ cm s^{-1}), X-ray topography suggests $\varepsilon \simeq 10^{-5}$. For elevated rates, ($\simeq 3 \times 10^{-5}$ cm s^{-1}), $\varepsilon \simeq 10^{-4}$. In the latter case, the homogeneous stress in an overgrown layer, $G\varepsilon \simeq 10^{-8}$ dyne cm$^{-2} \simeq 1$ kg mm^{-2}.

(2) Crystallization pressure†, $kT\sigma/\omega$, is developed if two steps (or crystals) growing in opposite directions meet one another such that the gap between the encountering bodies is filled by substance, e.g. an impurity, which allows the crystallising material to reach the encountering growing surfaces and, at the same time, the substance does not become squeezed out of the gap. At $kT \simeq 4 \times 10^{-14}$ erg, $\omega \simeq 10^{-22}$ cm^3, $\sigma = 0{\cdot}1$ (i.e. 10%), one has $kT\sigma/\omega \simeq 0{\cdot}4$ kg mm^{-2}.

The tensile strength of ADP is 9 kg mm^{-2}. Thus both stress sources per se seem to be insufficient to cause cracking, especially at low supersaturations. Nevertheless, concentration of stress around inclusions and (or) close to lines where three different growth sectors meet together might be sufficient to cause cracking and thus fragmentation.

There is evidence that the appearence of secondary nuclei is correlated with the appearence of cracks and inclusions. On the other hand, N. P. Zaitseva has observed sealing of macroscopic inclusions when secondary nuclei do not appear. Anyhow, the concept of secondary nucleation as a result of defect formation needs further experimental analysis. If this concept is correct secondary nucleation can be avoided under conditions that prevent the formation of macroscopic defects in the growing crystal, i.e. the problem of the quality of crystals and that of reaching high supersaturations in solution are interrelated. The latter is necessary to grow crystals at unconventionally high rates (Bespalov *et al.* 1982, 1986, Bespalov and Katsman 1984, Amandosov *et al.* 1983, Rashkovich 1984, Zundelevich 1986).

† Crystallization pressure (see Chernov 1984) is defined as the pressure which, being applied normally to the crystal surface, brings the crystal into thermodynamic equilibrium with the supersaturated solution in contact with this surface.

6. Kinetic (non-Ostwaldian) ripening

The multitude of small ($<1\,\mu$m) crystals existing in solution at a constant equilibrium temperature are actually not in absolute equilibrium. The smaller crystals dissolve, and the larger ones grow at their expense (Chernov 1984). Such ripening, studied by W. Ostwald, is taking place because the system tends to decrease its surface energy. It is known, however, that particles with a size reaching several milimetres also grow at the expense of small ones (Bazhal 1971). The ripening rates observed in this case are orders of magnitude higher than would be expected if a decrease in the surface energy of such coarsely dispersed systems were the motive force of ripening. Responsible for this non-Ostwaldian ripening is the kinetics—the asymmetry between growth and dissolution under the conditions of inconstant, fluctuating temperature and supersaturation.

The mechanism of this kinetic ripening with a periodic change in temperature can be schematically presented as follows. Let us consider a large and a small crystal (figure 27(*a,b*)). During the halfperiod of dissolution both of them are being rounded, as the edges and apexes serve as more powerful sources of layers than the dislocations and other defects. On a large crystal the layers emitted by the apexes do not reach the face centre if the period τ of temperature fluctuations is not too long for a given crystal ($\tau < L/v$, figure 27(*a*)). On a small crystal, if $\tau > l/v$ (figure 27(*b*)), the layers annihilate at the face centre, providing a much higher rate of dissolution, R, then dislocations and other defects. That is why, during the halfperiod of dissolution, small crystals (under the influence of temperature variations of suitable period and amplitude) lose a relatively greater part of their volume than the larger ones. During the halfperiods of growth, both the smaller and the larger crystals are being faceted and grow in the same way in accordance with the dislocation mechanism. As a result of the inequivalence of dissolution of large and small crystals the latter will dissolve more intensively than the former, and will finally

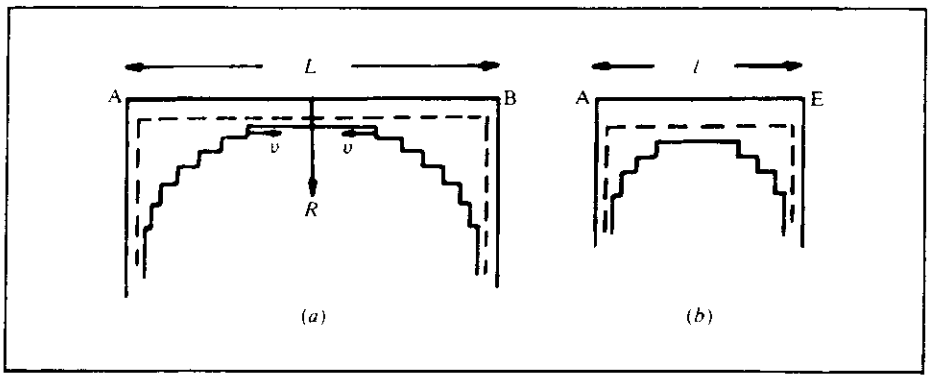

Figure 27. Large (*a*) and small (*b*) crystals after halfperiod of dissolution (solid stepwise profile) and growth (dashed line profile). Steps emitted by edges A and B have time to reach each other on the small crystal but do not on the large one. Therefore, the small crystal dissolves relatively faster than the large one.

disappear. In solution, however, a certain small supersaturation, created mainly by the small crystals and absorbed mainly by the large ones, will be automatically established and maintained throughout the whole ripening process.

In a similar way we can understand the experiments in which spheres, artificially prepared and submerged in solution, are transformed into polyhedrons as the temperature fluctuates periodically about its equilibrium value (Shubnikov 1935, 1947). In this case a crystal having the size of ~ 1 cm or more is also being faceted under the action of kinetic factors, and not of the surface energy. It is the stepped, nonsingular surfaces that grow faster than the singular ones and thus disappear from the surface and turned into edges and apexes. Correspondingly, the final polyhedron by no means provides a minimum of surface energy, but constitutes a form of growth.

7. Conclusions

The use of modern *in situ* methods of investigating the processes of crystallization from solutions, primarily laser interferometry and X-ray topography, has made possible advances in the quantitative understanding of crystal growth from solutions. In particular, it has became possible to find the fundamental parameters of crystallization: the linear energy of steps and their kinetic coefficient. Impurities make the kinetics of step movement essentially nonlinear and the conventional spiral growth theory of Burton *et al.* inapplicable. A new nonlinear theory has therefore been developed.

The fields of elastic stresses around dislocations, shifting the value of the chemical potential of the crystal, create the asymmetry of growth and dissolution. At the same time, the growth and dissolution kinetics on the elementary steps, or those similar to them, are practically symmetrical.

Moreover, the morphological instability of vicinal faces, in particular of the slopes of the vicinal hillocks of growth, proved to depend substantially on the direction of solution flow: the flow promotes instability when the directions of solution and step movement coincide, and promote stability when the directions are antiparallel. Accounting for these effects is essential in making possible the fast growth of perfect large crystals for nonlinear optics, laser thermonuclear fusion, and other applications.

The next stage will be the investigation of defective structures on the atomic and subatomic levels.

Acknowledgements

I am very grateful to L. N. Rashkovich, Yu. G. Kuznetsov, I. L. Smol'sky, V. F. Parvov, A. I. Malkin, N. P. Zaitseva and I. V. Alkseev, who cooperated in obtaining most of the original results described above.

References

Amandosov, A. T., Pashina, Z. S., and Rashkovich, L. N., 1983, *Kvantovaya electronika*. **10**, 469 (*Soviet quant. Electron.*).
Bassett, G. A., 1958, Phil. Mag., **3**, 1042.
Bauser, E., and Strunk, H., 1981, *J. Cryst. Growth*, **51**, 362.
Bazhal, I. G., 1970, *Soviet Phys. Crystallogr.*, **14**, 127.
Belyustin, A. V., and Rogacheva, E. C., 1966, *Growth of Crystals*, vol. 6, edited by N. N. Sheftal, (Moscow: Nauka) p. 3.
Bespalov, V. I., Bredikhin, V. I. Ershov, V. P., Katsman, V. I., Kiseleva, N. V., and Kuznetsov, S. P., 1982, *Kvantovaya electronika*, **9**, 234. (*Soviet quant. Electron.*).
Bespalov, I. V., and Katsman, V. I., 1984, *Vestnik Akad. Nauk USSSR*, **N9**, 11.
Bespalov, V. I., Bredikhin, V. I., Katsman, V. I., Ershov, V. P., and Lavrov, L. A., 1987, *J. Cryst. Growth*, **82**, 776.
Bespalov, V. I., Bredishin, V. I., Ershov, V. I., Katsman, V. I., and Lavrov, L. A., 1986, *International Conference on Crystal Growth, York*, abstract PA1-418.
Bredikhin, V. I., Ershov, V. P., Korolikhin, V. V., Lizyakina, V. N., Potapenko, S. Yu., and Khlylunev, N. V., 1987, *J. Cryst. Growth*, **84**, 509.
Budevski, E., Bostanov, V., and Staikov, G. 1980, *Annual Review of Material Science*, vol. 10 (Palo Alto: Annual Reviews Inc.), p. 85.
Burton, W. K., Cabrera, N., and Frank, F. C., 1951, *Phil. Trans. R. Soc., Lond.*, **A243**, 299.
Cabrera, N., and Levine, M. M., 1956, *Phil. Mag.*, **1**, 450.

Cabrera, N., and Vermilyea, D. A., 1958, *Growth and Perfection of Crystals*, edited by R. H. Doremus, B. W. Roberts, and D. Turnbull (London: Chapman and Hall), p. 393.
Cahn, J. W., 1977, *Japan–US Joint Seminar of Solidification of Metals and Alloys*.
Chernov, A. A., Malkin, A. I., and Smol'sky, I. L., 1987, *Kristallografiya*, **32**, 1508.
Chernov, A. A., and Malkin, A. I., 1988, *J. Cryst. Growth*, **92**, 432.
Chernov, A. A., Kuznetsov, Yu. G., Smol'sky, I. L., and Rozhansky, V. N., 1986, *Kristallografiya*, **31**, 1193. (*Soviet Phys. Crystallogr.*, **31**, 705).
Chernov, A. A., Rashkovich, L. N., Smol'sky, I. L., Kuznetsov, Yu. G, Mkrtchan, A. A., and Malkin, A. I., 1986, *Rost Kristallov (Crystal Growth)*, vol. 15, edited by E. I. Givargizov (Moscow: Nauka), p. 43.
Chernov, A. A., 1984, *Modern Crystallography III: Crystal Growth* (Berlin: Springer-Verlag).
Chernov, A. A., 1988, *Z. Phys. Chem.* Leipzig, **269**, 941.
Chernov, A. A., 1961, *Soviet Phys. Uspekhi*, **4**, 116.
Chernov, A. A., and Nishinaga, T., 1987, *Morphology of Crystals* (Tokyo: Terra Scientific Publishing Co.), p. 207.
Chernov, A. A., 1973, *Annal Review of Material Science*, vol. 3, (Palo Alto: Annual Reviews Inc.) p. 397.
Chernov, A. A., and Kopylova, G. F., 1977, *Sov. Phys. Crystallogr.* **22**, 709.
Chernov, A. A., Smol'sky, I. L., Parvov, V. F., Kuznetsov, Yu. G., and Rozhansky, V. N., 1980, *Kristallografiya*, **25**, 821 (*Soviet Phys. Crystallogr.* **25**, 469).
Chernov, A. A., Rashkovich, L. N., and Mkrtchan, A. A., 1987, *Kristallografiya*, **32**, 737.
Chernov, A. A., and Rashkovich, L. N., 1987, *J. Cryst. Growth*, **84**, 389.
Chernov, A. A., Rashkovich, L. N., and Mkrtchan, A. A., 1986, *J. Cryst. Growth*, **74**, 101.
Chui, S. T., and Weeks, J. D., 1978, *Phys. Rev. Lett.* **40**, 733.
Distler, G. I., Vlasov, V. P., Gerassimov, Yu. M., Kobzareva, C. A., Kortukova, E. I., Lebedeva, V. H., Moskvin, V. V., and Shenyavskaya, L. A., 1976, *Dekorirovaniye poverchnosti tverdykh tel (Decoration of Solid Surface)* (Moscow: Nauka).
Fishman, Yu. M., 1972, *Soviet Phys. Crystallogr.*, **17**, 524.
Frank, F. C., 1951, *Acta crystallogr.*, **4**, 497.
Frank, F. C., 1958, *Growth and Perfection of Crystals*, edited by R. H. Doremus, B. W. Roberts, and D. Tunbull (London: Chapman and Hall), p. 411.
Frank, F. C., 1949, *Discuss Faraday Soc.*, **5**, 48.
Frank, F. C., 1981, *J. Cryst. Growth*, **51**, 361.
Garside, J., Rusli, I. I., and Larson, M. A., 1979, *Am. Inst. Chem. Eng.*, **25**, 57.
Gilmer, G. H., and Weeks, J., 1978, *J. chem. Phys.*, **68**, 950.
Gordeeva, N. V., and Shubnikov, A. V., 1967, *Soviet Phys. Crystallogr.* **12**, 154.
Görnert, P., and Voigt, F., 1984, *Current Topics in Materials Science*, Vol. 11, edited by E. Kaldis (New York: Elsevier) p. 1.
Hayashi, M., and Shishiri, T., 1974, *J. Cryst. Growth*, **21**, 254.
Heck, C. M., 1937, *Phys. Rev.*, **51**, 686, 690.
Hirth, J. P., and Lothe, J., 1982, *Theory of Dislocations*, (New York: McGraw-Hill).
Heimann, R. B., 1975, *Auflösung von Kristallen* (Berlin: Springer-Verlag).
Kaishev, R. A., and Budevski, E., 1967, *Contemp. Phys.*, **8**, 489.
Keller, K. W., 1986, *J. Cryst. Growth*, **74**, 161, 469.
Kossel, W., 1930, *Quantentheorie und Chemie* (Leipzig: Falkenhagen), p. 901.
Kuznetsov, Yu. G., Chernov, A. A., Vekilov, P. G., Smol'sky, I. L., 1987, *Kristallografiya*, **32**, 994 (*Soviet Phys. Crystallogr.* **32**, 584).
Kuznetsov, Yu. G., Chernov, A. A., and Zakhazov, N. D., 1986, *Kristallografiya*, **31**, 1201 (*Soviet Phys. Crystallogr.*)
Kuznetsov, Yu. G., Smol'sky, I. L., Chernov, A. A. and Rozhansky, V. N., 1981, *Dokl. Akad. Nauk SSSR*, **260**, 864 (Sov. Phys. Doklady).
Lemmlein, G. G., 1947, *Dokl. Akad. Nauk SSSR*, **58**, 1939.
Lemmlein, G. G. and Gliki, N. V., 1954, *Dokl. Akad. Nauk SSSR*, **94**, 473.
Lemmlein, G. G., 1945, *Vestnik Akad. Nauk SSSR*, **N4**, 119.
Malkin, A. I., Chernov, A. A. and Alekseev, I. V., 1989, *J. Cryst. Growth* (submitted for publication).
Mikhailov, A. A., Rashkovich, L. N., Rzevsky, V. V. and Chernov, A. A., 1989, *Kristallografiya*, **34**, 439.
Nozières, P. and Gallet, F., 1987, *J. Phys., Paris*, **48**, 353.
Nyvlt, J., Söhnel, O., Matuchova, M., and Broul., M., 1985, *The Kinetics of Industrial Crystallization* (Prague: Academia), p. 105.
Ovsienko, D. E. and Alfintsev, G. A., 1967, *Crystal Growth, Proceedings of the International Conference on Crystal Growth*, Boston, 20–24, 1966, edited by H. S. Peiser (Oxford: Pergamon Press), p. 757.
Parvov, V. F., 1965, *Kristallografiya*, **10**, 263.
Parvov, V. F., 1967, *Kristallografiya*, **12**, 532.
Rashkovich, L. N., 1984, *Vestnik Akad. Nauk SSSR*, **N9**, 11.
Sears, G. W. 1956, *J. chem. Phys.*, **24**, 868.
Shubnikov, A. V., 1947, *Obrasovaniye kristallov (Crystallization)* (Moscow: Akademii Nauk SSSR).
Shubnikov, A. V., 1935, *Kak rastut kristally (How do the Crystals Grow)* (Moscow: Akademii Nauk SSSR).
Smol'sky, I. L., Malkin, A. I., Kuznetsov, Yu. G., Chernov, A. A., Gussak, Ya. D., Kogan, A. Ya., and Rozhansky, V. N., 1985, *Kristallografiya*, **30**, 570.
Stranski, I. N., 1928, *Z. phys. Chem.*, **136**, 259.
Stranski, I. N., Kaishev, R., 1931, *Z. Kristallogr*, **78**, 373.
Söhnel, O., 1982, *J. Cryst. Growth*, **57**, 101.
Söhnel, O., 1983, *J. Cryst. Growth*, **83**, 174.
Sung, C. Y., Estrin, J., Youngquist, G. R., 1973, *Am. Inst. Chem., Eng.*, **19**, 957.
Tsukamoto, K., Ohba, H., and Sunagawa, I., 1983, *J. Cryst. Growth*, **63**, 18.
Treivus, E. B., 1987, *Kristallografiya*, **32**
Trusov, L. I. and Chernov, A. A. 1979, *Kristallografiya*, **24**, 11.
Van der Eerden, J. P. Müller-Krumbhaar, H., 1986, *Phys. Rev. Lett.*
Van der Hoek, B., Van der Eerden, J. P., and Bennema, P. 1982, *J. Cryst. Growth*, **58**, 365; **56**, 621.
Yuferev, 1983, *Poverkhnost' (Surface)*, N7, 29
Yuferev, 1989, *Kristallografiya*, **34**, 16.
Zundelevich, Y. Cooper, J. F., and Singleton, M. F., 1986, *8th International Conference on Crystal Growth, York*, collected abstr. PA1 415.

A. A. Chernov, Professor, Corresponding Member of the U.S.S.R. Academy of Sciences is head of the Department of Crystallization Physics and Real Crystal Structure at the Institute of Crystallography, U.S.S.R. Academy of Sciences. Born 5 October, 1931 in Moscow, he graduated from Department of Physics, Moscow State University, in 1954. Since then he has been associated with the Institute of Crystallography working on crystal growth and surface sciences, which attracted him by the variety of phenomena that resulted in exciting pictures, beautiful both in a direct physical and in an intellectual sense.

Journal of Crystal Growth 91 (1988) 11–19
North-Holland, Amsterdam

STACKING FAULTS AS SELF-PERPETUATING STEP SOURCES

Nai-ben MING *, K. TSUKAMOTO and I. SUNAGAWA

Institute of Mineralogy, Petrology and Economic Geology, Faculty of Science, Tohoku University, Aoba, Sendai 980, Japan

and

A.A. CHERNOV

Institute of Crystallography, Academy of Sciences of the USSR, Leninskii Prospekt 59, Moscow 117333, USSR

Received 20 August 1987; manuscript received in final form 18 April 1988

Atomic configurations of sub-steps created on a (111) growth surface of an fcc crystal by stacking faults with fault vectors $\frac{1}{6}\langle 112\rangle$ and $\frac{1}{3}\langle 111\rangle$ show that they can act as self-perpetuating step sources. Growth kinetics provided by such sub-steps have been analyzed, and it has been shown that the 2D heterogeneous nucleation barrier at the sub-steps is always smaller than that of conventional 2D nucleation. It has also been shown that the 2D heterogeneous mono-nuclear and birth-and-spread nucleation along the sub-steps should provide a growth rate exceeding the one provided by conventional 2D nucleation at low and high supersaturations.

1. Introduction

Experimental evidence has been reported to support the fact that stacking faults can act as step-generating sources. To mention some of these reports, we may refer to the observations by Bauser and co-workers on solution grown Si crystals [1,2], by Nishizawa et al. on vapor grown Si crystals [3], and by Tsukamoto et al. on aqueous solution grown $Ba(NO_3)_2$ crystals [4]. In the former two cases, electron microscopy, X-ray topography and surface microtopographic methods have been used and in the last case, in-situ observation techniques. A step generation mechanism of stacking faults has been proposed by Bauser and Strunk [2,5], based on a block model of simple cubic crystals.

The aim of this paper is to theoretically analyze this mechanism. Therefore we consider the (111) face of an fcc lattice as an example of structures where the stacking faults can really exist, contrary to the simple cubic lattice.

2. Sub-steps created by stacking faults

The fault planes in fcc crystals are {111} and the fault vectors are $\frac{1}{6}\langle 112\rangle$ and $\frac{1}{3}\langle 111\rangle$. On the (111) growth surface, three stacking faults intersect at 70.53°, whose fault planes are $(1\bar{1}1)$, $(\bar{1}11)$ and $(11\bar{1})$. Their possible fault vectors are shown in table 1.

Table 1
Height of self-perpetuating steps on the (111) growth surface of a crystal

Growth surface	Fault planes	Fault vectors, $\boldsymbol{b}$	Height of sub-steps, $h = \boldsymbol{n}\cdot\boldsymbol{b}$	
(111)	$(1\bar{1}1)$	$\pm\frac{1}{6}[121]$	$0.385a$	$\frac{2}{3}\delta_{(111)}$
		$\pm\frac{1}{6}[\bar{1}12]$, $\pm\frac{1}{6}[21\bar{1}]$	$0.192a$	$\frac{1}{3}\delta_{(111)}$
		$\pm\frac{1}{3}[1\bar{1}1]$	$0.192a$	$\frac{1}{3}\delta_{(111)}$
(111)	$(\bar{1}11)$	$\pm\frac{1}{6}[211]$	$0.385a$	$\frac{2}{3}\delta_{(111)}$
		$\pm\frac{1}{6}[1\bar{1}2]$, $\pm\frac{1}{6}[12\bar{1}]$	$0.192a$	$\frac{1}{3}\delta_{(111)}$
		$\pm\frac{1}{3}[\bar{1}11]$	$0.192a$	$\frac{1}{3}\delta_{(111)}$
(111)	$(11\bar{1})$	$\pm\frac{1}{6}[112]$	$0.385a$	$\frac{2}{3}\delta_{(111)}$
		$\pm\frac{1}{6}[\bar{1}21]$, $\pm\frac{1}{6}[2\bar{1}1]$	$0.192a$	$\frac{1}{3}\delta_{(111)}$
		$\pm\frac{1}{3}[11\bar{1}]$	$0.192a$	$\frac{1}{3}\delta_{(111)}$

a is the lattice parameter, $\delta_{(111)}$ is the thickness of an elementary growth layer on the (111) surface, and $\boldsymbol{n}$ is the unit vector normal to the growth surface.

* On leave from the Department of Physics, Nanjing University, Nanjing, People's Republic of China.

0022-0248/88/$03.50

The height of a step, h, created by a stacking fault, is

$$h = \boldsymbol{n} \cdot \boldsymbol{b},$$

where $\boldsymbol{n}$ is a unit vector normal to a growth surface and $\boldsymbol{b}$ the fault vector. The heights of the sub-steps outcropped on the {111} growth surface are given in table 1. The table shows that there are two types of sub-steps along the emergence lines of a stacking fault on the (111) surface of an fcc crystal, with thicknesses that are $\frac{1}{3}$ and $\frac{2}{3}$ of the thickness of the elementary growth layer, δ, respectively.

3. Step generation mechanism and the resultant surface morphology

If a sub-step with a height of $\frac{1}{3}\delta_{(111)}$ outcrops on a (111) surface of an fcc crystal under given growth conditions (figs. 1a and 2a), two-dimensional nuclei with a thickness of the elementary layer $\delta_{(111)}$ may be formed along the sub-step, which naturally results in the creation of a sub-step with a height of $\frac{2}{3}\delta_{(111)}$ on the opposite side of the original sub-step, as shown in fig. 1b; in this case, the full-step will move and rotate around the end of the sub-step, which is the emergence point of a partial dislocation associated with the stacking fault (fig. 2b). When an atomic island nucleates at the second sub-step, the first type of sub-step will appear again and another full-step is produced (fig. 1c). This process is repeated and thus the stacking fault may operate as a self-perpetuating step source (fig. 1d). It is clear that the growth

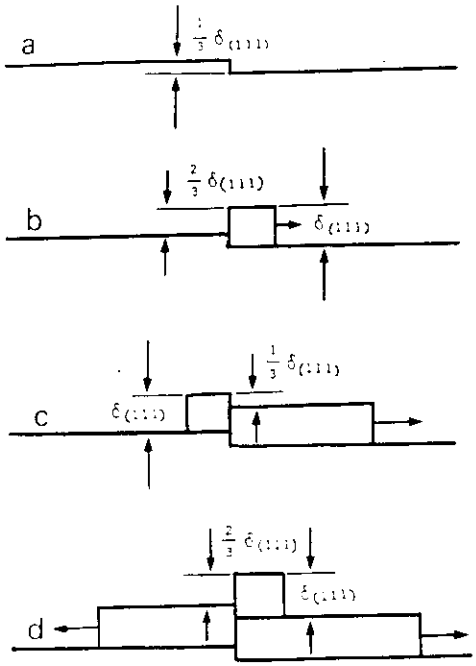

Fig. 1. Step generation mechanism of stacking faults on the (111) growth surface of an fcc crystal: (a) sub-step with height of $\frac{1}{3}\delta_{(111)}$; (b) when a row of atoms is adsorbed along the sub-step, a full-step and a sub-step with height of $\frac{2}{3}\delta_{(111)}$ are created at the same time; (c) after a row of atoms are adsorbed at the sub-step of the second type, a sub-step of the first type and another full-step appear; (d) the event is repeated alternatively and full-step will be produced continuously.

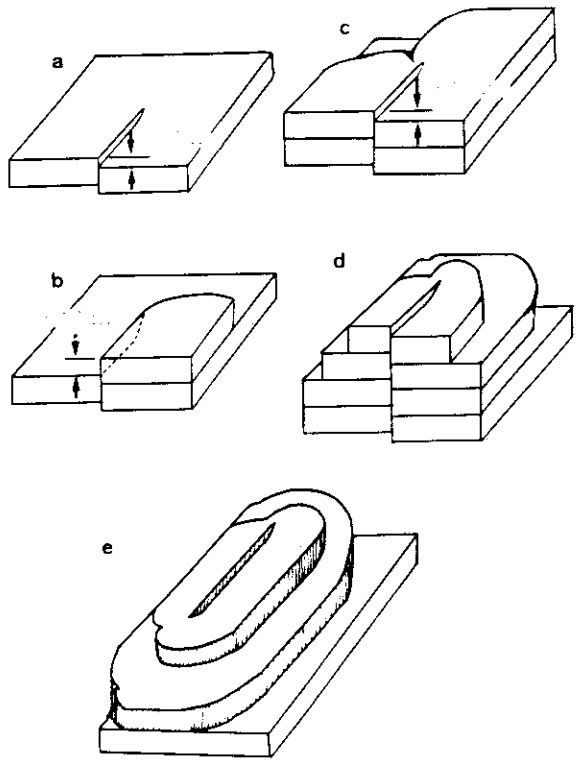

Fig. 2. Surface morphology (step patterns) expected due to the stacking fault growth mechanism: (a) sub-step with height of $\frac{1}{3}\delta_{(111)}$ on a (111) surface; (b) a full-step rotates around the emergence point of a partial dislocation; (c) two full-steps meet each other and a new terrace appears; (d) surface morphology due to the stacking fault growth mechanism; (e) surface morphology expected from the stacking fault growth mechanism of another type.

steps originate alternatively at both sides of a stacking fault. After a couple of full-steps from both sides of a stacking fault meet and annihilate each other, a new terrace appears (fig. 2c). It is worth noting that no spiral pattern appears at the emergence point of the partial dislocation (fig. 2d) and that only a half turn rotation around the emergence point of a partial dislocation is required in order to create a terrace with a unit height, whereas one turn rotation is necessary to grow one layer in the conventional single screw dislocation model.

If a self-perpetuating sub-step due to a stacking fault bounded by two partial dislocations emerges on the (111) growth surface, the resultant surface morphology is similar to that of a dipole of perfect screw dislocations (fig. 2e).

4. Atomic configurations of self-perpetuating sub-steps

The atomic configuration of a self-perpetuating sub-step with a height of $\frac{1}{3}\delta_{(111)}$, corresponding to the schematic step in fig. 1a, is shown in fig. 3a, using a ball model. It is clear that an adsorbed atom at the site of the sub-step of this type (point "a" in fig. 3a) has 4 nearest neighbors. Fig. 3b corresponds to fig. 1b. It can be seen from this figure that after a row of atoms adsorbed on this sub-step, a full-step and a sub-step with a height of $\frac{2}{3}\delta_{(111)}$ appear on the upper and lower sides, respectively. The point "b" in fig. 3b is the site of a sub-step with a height of $\frac{2}{3}\delta_{(111)}$. It is clear that an atom adsorbed at this site also has 4 nearest neighbors. The ball model clearly demonstrates that the numbers of nearest neighbors at the sites of sub-steps of both types are just the same, indicating that there should be no essential difference between the two with respect to the growth-promoting properties, although the heights are different. From fig. 3b we also see that an atom adsorbed at point "c" has 5 nearest neighbors. This position just corresponds to the site at a full-step on a (111) surface of an fcc crystal.

An isolatedly adsorbed atom at the surface site of the (111) face of an fcc crystal has 3 nearest neighbors, whereas the corresponding sites at the sub-steps of the two types have 4 nearest neighbors. This means that the potential well at a sub-step is lower than that on a regular surface site and the difference between the two potential energies is ϕ, the energy of one interatomic bond. Consequently, the density of adatoms per atomic site along the sub-step should be $\exp(\phi/kT)$ times higher than that on a regular surface. For a typical value $\phi/kT = 4$, one gets $\exp(\phi/kT) = 54$, i.e., the preferential nucleation at the sub-step should be very probable.

5. Work of nucleation

It was demonstrated above that the 2D nucleation at a sub-step is a key stage in the activity of the sub-step as a source of the full-height growth steps. To analyze the sub-step activity, let us find the work needed to create a nucleus at a sub-step.

In the first-neighbor approximation, a nucleus on a perfect (111) fcc face should be a regular hexagon. The nuclei of equilibrium shape attached to the sub-step (SS) in fig. 4 should be stretched on being compressed along SS, depending on the relationship between the energy γ_{SS} of a free sub-step, the energy γ_{sf} of a stacking fault and the energy γ of a free normal step. Let the nucleus have M atoms at each edge along SS (fig. 4) and m atoms at each of the other four free edges. The number of atoms in such a nucleus is

$$N = M(2m-1) + (m-1)^2. \tag{1}$$

The change in edge energy accompanying creation of the nucleus is

$$\begin{aligned} F_\gamma &= (M-2)\gamma + 4(m-2)\gamma + (M-2)\gamma' \\ &\quad + 4(3\gamma/2) + 2(\gamma' + \gamma/2) \\ &= M(\gamma + \gamma') + 4m\gamma - 3\gamma. \end{aligned} \tag{2}$$

Here, $\gamma' = \gamma_{sf} - \gamma_{SS}$ is the work (per edge atom) needed to replace a sub-step by a stacking fault strip appearing when an atomic row (or nucleus) is attached to the sub-step. The first term in eq. (2) comes from the regular (not the corner) atoms forming the free edge AB (fig. 4), the second term comes from the regular atoms forming BC, CD,

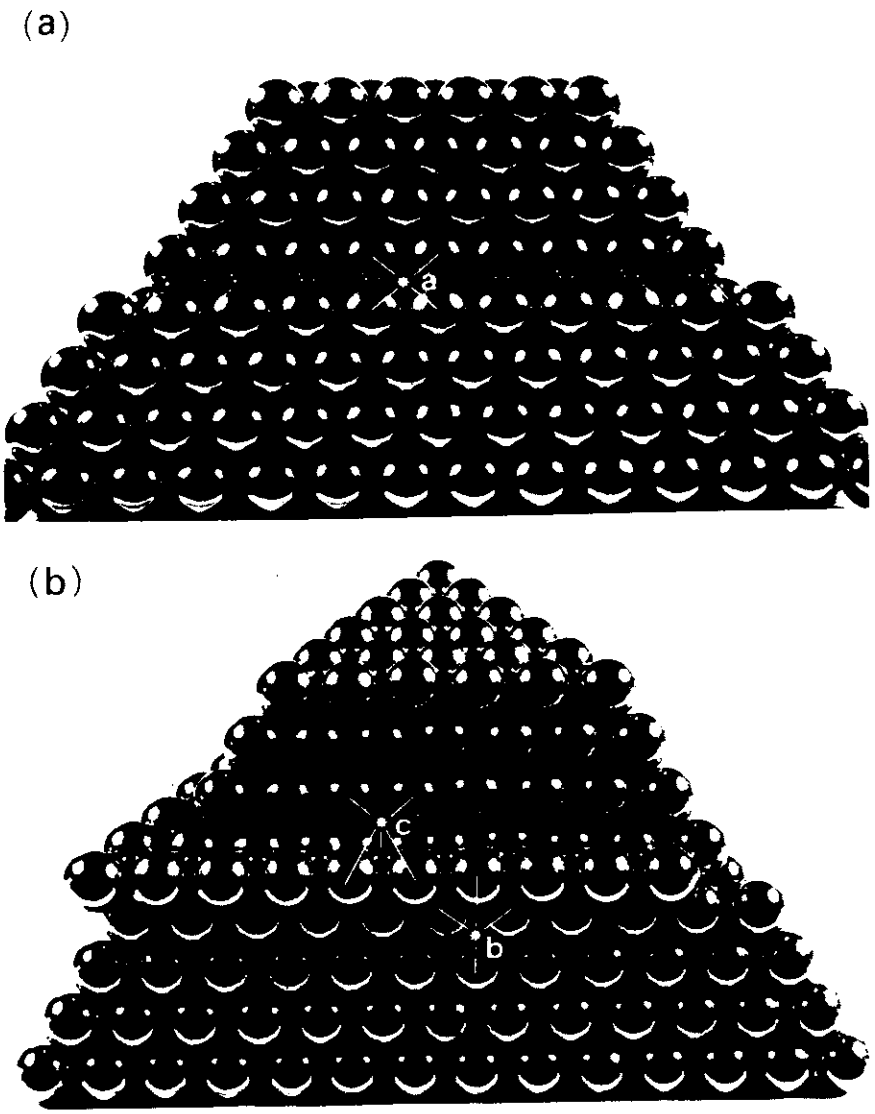

Fig. 3. Atomic configuration of a sub-step: (a) a sub-step with height of $\frac{1}{3}\delta_{(111)}$; (b) a sub-step with height of $\frac{2}{3}\delta_{(111)}$ and a full-step.

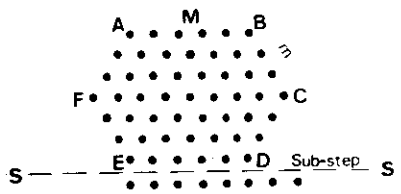

Fig. 4. Two-dimensional heterogeneous nuclei A, B, C, D and E along a sub-step SS formed by the outcrop of a stacking fault on the (111) growth surface of an fcc crystal.

EF and FA, and the third term comes from the regular atoms adjacent to the sub-step. The fourth term gives the contribution of the corner atoms A, B, C and F, and the fifth term that of the corners D and E on the sub-step.

The equilibrium shape of the nuclei, i.e. the relationship between M and m, minimized F_γ under the condition N = constant. This relationship may be easily found making use of the

Lagrange factor λ and of the conventional condition of minimum for $F_\gamma + \lambda N$:

$$\frac{\partial}{\partial M}(F_\gamma + \lambda N) = 0, \quad \frac{\partial}{\partial m}(F_\gamma + \lambda N) = 0. \tag{3}$$

Eqs. (1)–(3) give

$$M = m + (2m - 1)\frac{\Delta\gamma}{\gamma + \gamma'}, \tag{4}$$

where

$$\Delta\gamma \equiv \gamma - \gamma' = \gamma + \gamma_{SS} - \gamma_{sf}.$$

The change G_{het} in the Gibbs potential needed to create an equilibrium shape nucleus of m atoms at its free edge may be found by making use of eq. (4):

$$\begin{aligned} G_{het} &= -N\Delta\mu + F_\gamma \\ &= -\left[m(m-1)(7\gamma - \gamma') + 2\gamma\right]\frac{\Delta\mu}{\gamma + \gamma'} \\ &\quad + m(7\gamma - \gamma') - 4\gamma + \gamma'. \end{aligned} \tag{5}$$

Here, $\Delta\mu$ is the difference between the chemical potentials of the ambient phase and the crystal. The subscripts "het" and "hom" stand for "heterogeneous" and "homogeneous" nucleation, respectively.

Maximizing G_{het} with respect to $m(\partial G_{het}/\partial m = 0)$, one obtains the size m of the critical nucleus:

$$2m = \frac{\gamma + \gamma'}{\Delta\mu} + 1, \tag{6}$$

and the work of its formation:

$$G^*_{het} = \frac{(7\gamma - \gamma')(\gamma + \gamma')}{4\,\Delta\mu} - \frac{\Delta\mu}{4} - \frac{\Delta\gamma}{2}. \tag{7}$$

The nucleation work for a perfect (111) face, i.e., at $\gamma_{SS} = 0$, $\gamma_{sf} = \gamma$, $\gamma' = \gamma$ and $\Delta\gamma = 0$, is

$$G^*_{hom} = \frac{3\gamma^2}{\Delta\mu} - \frac{\Delta\mu}{4}. \tag{8}$$

Thus,

$$G^*_{hom} - G^*_{het} = \frac{\gamma\,\Delta\gamma}{\Delta\mu}\left(1 + \frac{\Delta\gamma}{4\gamma} + \frac{\Delta\gamma}{2}\right). \tag{9}$$

Therefore the heterogeneous nucleation is always easier if $\Delta\gamma > 0$, i.e., if $\gamma + \gamma_{SS} > \gamma_{sf}$, which is natural to expect. The lower $\Delta\gamma/\gamma$ is, the weaker is the growth activity of the sub-step. At low supersaturations, $\Delta\mu/kT$, the role of sub-steps in providing the growth is more important than that at high supersaturations.

For a rough estimate, we may use the conclusion obtained above in section 4 and accept $\gamma = \phi$, $\gamma' = \gamma_{sf} - \gamma_{SS} = \phi/2$. If $\phi/kT = 4$, and $\Delta\mu/kT = 2$, one obtains $G^*_{hom} = 23.5kT$ and $G^*_{het} = 18kT$.

6. Growth rates

Although the work of nucleation at a sub-step is less than that on regular surface sites, the latter are much more numerous on a given face. Thus, generally speaking, the condition $G^*_{hom} - G^*_{het} > 0$ is insufficient for the sub-step control of the growth kinetics. To find more rigorous conditions, we have to compare the growth rates of a given face, R_S and R_L, provided by the conventional (R_S) and the sub-step (R_L) nucleation.

Suppose that nucleation occurs at the rate I_S ($cm^{-2}\ s^{-1}$) on the regular surface and I_L ($cm^{-1}\ s^{-1}$) along the sub-step, respectively. Let us denote by S the area of the growth surface, by L the length of a sub-step and by v the propagation rate of a step. The nucleation period, i.e., the time interval for the appearance of each consecutive nucleus, can be expressed as:

$t_n = 1/I_S S$ for homogeneous nucleation,
$t_n = 1/I_L L$ for heterogeneous nucleation.

The sweeping time, i.e., the time needed for propagation of a step loop from a nucleus over the entire surface, is

$$t_s = S^{1/2}/v.$$

For low supersaturations (low I_S and I_L) and small growth surfaces, we have $t_s < t_n$, or:

$S^{1/2} < (v/I_S)^{1/3}$ for homogeneous nucleation,
$S^{1/2} < v/I_L L$, for heterogenous nucleation. (10a)

In this case, there is enough time for propagation of a step loop from a nucleus over the entire

growth surface, and only one nucleus is needed for one growth layer formed, i.e., a 2D mono-nuclear growth mechanism. The normal growth rates R_S for conventional 2D nucleation and R_L for heterogeneous 2D nucleation at a sub-step can be expressed as:

$$R_S = \delta_{(111)} S I_S, \tag{11}$$

$$R_L = \delta_{(111)} L I_L. \tag{12}$$

For high supersaturations (high I_S and I_L) and large growth surfaces, we have

$$t_s > t_n,$$

or

$$S^{1/2} > (v/I_S)^{1/3} \quad \text{for homogeneous nucleation,}$$
$$S^{1/2} > v/I_L L \quad \text{for heterogeneous nucleation.} \tag{10b}$$

In this case, new nuclei may appear on the growth surface before the proceeding layer completely covers the surface. As an approximation, we only consider that the nucleus appears on the top of the previous one (a spreading step loop) before the proceeding layer completely covers the surface, i.e., the so-called birth-and-spread model, or repeated, or self-consistent nucleation (eqs. (11) and (12)). The normal growth rates are

$$R_S = \delta_{(111)} (v^2 I_S)^{1/3}, \tag{13}$$

$$R_L = \delta_{(111)} (v I_L)^{1/2}. \tag{14}$$

It is to be noted that R_S and R_L are independent of surface size S and sub-step length L, respectively.

The nucleation rates can be expressed [8] as:

$$I_S = B_S \exp(-G^*_{hom}/kT), \tag{15}$$

$$I_L = B_L \exp(-G^*_{het}/kT), \tag{16}$$

and

$$B_S \doteq Z a^{-2} n_s a \theta \nu \exp(-\epsilon/kT), \tag{17}$$

$$B_L \doteq Z a^{-1} n_s a \theta \nu \exp(-\epsilon/kT), \tag{18}$$

where Z is the Zeldovich factor (for our case, $Z \doteq 10^{-1}$ [8,9]), a^{-2} and a^{-1} are the number of atomic sites per unit area on the surface and unit length along the sub-step (a is a typical interatomic spacing) and n_s is the surface concentration of adatoms of which the nucleus is building up. $\theta \doteq (\gamma a/\Delta\mu) \times$ constant is the length of the nucleus perimeter (an item independent of $\Delta\mu$ and γ is omitted), the constant being a factor depending on the shape of the nucleus; for an equilateral hexagon, the constant is 9 and for disc-shaped nuclei, the constant is 2π. Finally, ν is the thermal vibration frequency and ϵ is the activation energy for surface diffusion. All the quantities in (17) and (18), except for a, ν and ϵ, may slightly differ one from another. However, for a rough estimate, we may neglect this discrepancy and conclude that:

$$B_L/B_S = a. \tag{19}$$

For low supersaturations and small growth surfaces, the ratio of R_L to R_S can be expressed from eqs. (11), (12) and (15)–(19) as:

$$\frac{R_L}{R_S} = a\frac{L}{S}\exp\left(\frac{G^*_{hom} - G^*_{het}}{kT}\right), \tag{20}$$

or

$$\ln\left(\frac{R_L}{R_S}\right) = \frac{G^*_{hom} - G^*_{het}}{kT} + \ln\left(\frac{aL}{S}\right), \tag{21}$$

where L/S is the sub-step density, the length of sub-steps per unit surface. It is clear from eq. (20) that the ratio of normal growth rates is directly proportional to the sub-step density on the growth surface.

Substituting (9) into (21), one can conclude that $R_L > R_S$ only if:

$$\frac{\Delta\mu}{kT} < \frac{[\gamma\Delta\gamma/(kT)^2][1 + (\Delta\gamma/4\gamma)]}{\ln(S/aL) - (\Delta\gamma/2kT)}. \tag{22}$$

At $\gamma/kT = 4$, $\Delta\gamma/kT = 2$ and $aL/S = 3 \times 10^{-9}$, we obtain that the sub-step nucleation is more effective than the regular nucleation if $\Delta\mu/kT \lesssim 0.1$. However, if the supersaturation is as low as 10%, neither of the two types of nucleation can provide a noticeable growth rate. The activity of the sub-step nucleation may nevertheless be comparable with that of the regular nucleation at reasonably high supersaturations for a very high

density of sub-steps, i.e., for a very poor crystal quality. Taking the same values of γ/kT and $\Delta\gamma/kT$, we obtain from (22) that $R_L > R_S$ already at $\Delta\mu/kT \lesssim 1$ if $aL/S \simeq 5\times10^{-5}$. The latter quantity is equivalent to $L/S \simeq 2\times10^{3}\ \mathrm{cm}^{-1}$, i.e., 20,000 stacking faults per cm^2 of the surface.

In the more realistic case of higher supersaturations, R_L/R_S can be expressed from (13)–(18) as:

$$\frac{R_L}{R_S} = \left(\frac{a^3 B_S}{v}\right)^{1/6} \exp\left(\frac{G^*_{hom}/3 - G^*_{het}/2}{kT}\right). \quad (23)$$

In order to make numerical estimates, we need to know the average interstep distance λ provided by nucleation, and the process of the birth-and-spread (or repeated or self-consistent) nucleation, as mentioned above, should be considered. In the estimates made above, the interstep distance λ is accepted to be equal to the radius of such an island (the expanding nucleated circular step loop) at which a next nucleus appears on top of the previous one. For the conventional homogeneous 2D nucleation,

$$\lambda = (v/I_S)^{1/3}, \quad (24)$$

and for the 2D nucleation along a sub-step,

$$\lambda = (v/I_L)^{1/2}. \quad (25)$$

In both eq. (24) and (25), the numerical factor close to unity is omitted. This inaccuracy is unimportant, since the key dependences arise anyhow from the exponents with G^*_{hom} and G^*_{het}. Eqs. (24) and (25) are transcendental equations with respect to λ since v, I_S and I_L are functions of λ for conventional and sub-step nucleation.

Supposing that the radius of the background spreading island is equal to the interstep distance λ, the adatom concentration at an arbitrary distance r from its center is given by:

$$n_s(\lambda, r) = \left[F - (F - F_e)\frac{I_0(2r/\lambda_s)}{I_0(2\lambda/\lambda_s)}\right]\tau, \quad (26)$$

where F and F_e are the actual impinging molecular flux and its equilibrium value at the growth temperature, respectively; I_0 is a modified Bessel function,

$$\lambda_s = a\exp[(\epsilon_s - \epsilon)/2kT]$$

is the mean surface diffusion length (ϵ_s being the evaporation energy of an adatom, $\epsilon_s = 3\phi$ on the (111) surface of an fcc crystal, and ϵ being the activation energy of surface diffusion), and $\tau = \tau_0\exp(\epsilon_s/kT)$ is the adatom lifetime on the surface (τ_0 being the period of thermal vibration). Let us accept, further, that nuclei appear in the center of the previous spreading loop where the supersaturation reaches its maximum. Thus, the adatom concentration at $r = 0$ is, from (26):

$$n_s(\lambda, 0) = \frac{F - (F - F_e)}{I_0(2\lambda/\lambda_s)}\tau. \quad (27)$$

According to Fick's first law and eq. (26), the step velocity can be obtained as follows:

$$v \doteq -2a^2 D_s \left.\frac{dn_s}{dr}\right|_{r=a}$$
$$= a^2\lambda_s(F - F_e)\frac{I_1(2\lambda/\lambda_s)}{I_0(2\lambda/\lambda_s)}, \quad (28)$$

where the factor of 2 is based on the supposition of equal feeding of the step from both its sides (for a more accurate expression, see the paper by Burton, Cabrera and Frank [6]).

If $F \gg F_e$, both the cases $\lambda > \lambda_s$ (lower supersaturation, $\Delta\mu/kT$) and $\lambda < \lambda_s$ (higher $\Delta\mu/kT$) may occur. An analysis of these cases shows that in many interesting situations the inequality $\lambda > \lambda_s$ is realized, although under many MBE conditions, the opposite is valid.

For $\lambda > \lambda_s$, we obtain from eqs. (27) and (28):

$$v = a^2\lambda_s F, \quad n_s = F\tau. \quad (29)$$

Starting from the expression for the Zeldovich factor Z [8,9], it may be shown that for a 2D circular nucleus:

$$Z = \frac{(\Delta\mu/kT)^{3/2}}{2\pi(\gamma/kT)}. \quad (30)$$

Substituting eqs. (29) and (30) into eq. (17), we obtain

$$B_s = \left(\frac{\Delta\mu}{kT}\right)^{1/2}\left(\frac{\lambda_s}{a}\right)^2 F \quad (31)$$

and

$$\frac{a^3 B_s}{v} = \left(\frac{\Delta\mu}{kT}\right)^{1/2}\frac{\lambda_s}{a}. \quad (32)$$

Finally, the equation for R_L/R_S can be expressed by substituting eq. (32) into eq. (23) as follows:

$$\frac{R_L}{R_S} = \left(\frac{\lambda_s}{a}\right)^{1/6}\left(\frac{\Delta\mu}{kT}\right)^{1/12} \exp\left(\frac{G^*_{hom}/3 - G^*_{het}/2}{kT}\right). \tag{33}$$

It can be readily obtained from eqs. (7) and (8) that

$$\frac{G^*_{hom}}{2} - \frac{G^*_{het}}{3} = -\frac{\gamma^2}{2\Delta\mu}\left[1 - \frac{\Delta\gamma}{\gamma} + \frac{1}{4}\left(\frac{\Delta\gamma}{\gamma}\right)^2\right] + \frac{\Delta\mu}{24} + \frac{\Delta\gamma}{4}. \tag{34}$$

Eq. (33) is applicable if the face size and the supersaturation are sufficiently high so that among conditions (10a) and (10b), the strongest one is satisfied.

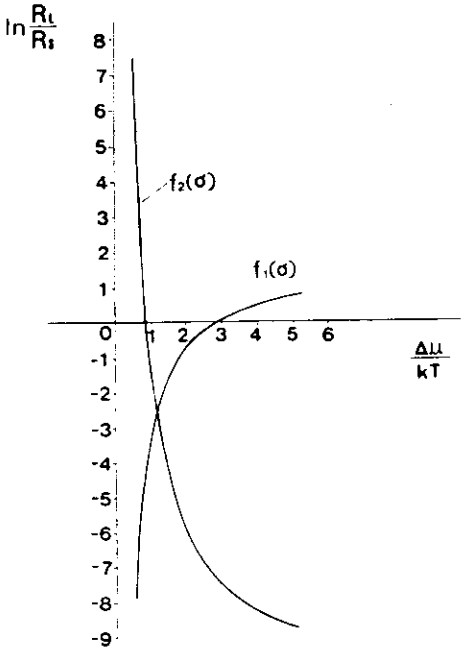

Fig. 5. Plot of $\ln(R_L/R_S)$ versus $\Delta\mu/kT$ for $f_1(\sigma)$, calculated using eqs. (33) and (34), and for $f_2(\sigma)$, calculated using eqs. (20) and (9). The following programs were used for the calculation:

$$\ln\left(\frac{R_L}{R_S}\right) = 1.4583336 - \frac{4.5}{\sigma} + \frac{\sigma}{24} \equiv f_1(\sigma),$$

$$\ln\left(\frac{R_L}{R_S}\right) = -10.512925 + \frac{9}{\sigma} \equiv f_2(\sigma).$$

The ratio $\Delta\gamma/\gamma$ is expected to be noticeably less than unity and thus the ratio R_L/R_S increases together with the supersaturation, as can be seen from curve 1 in fig. 5. This curve is plotted according to eqs. (33) and (34) with $\gamma/kT = \phi/kT = 4$, $\Delta\gamma/\gamma = 1/2$ and $\lambda_s/a = \exp(2\phi/kT) = 2980$ (i.e., it is taken that $\epsilon_s = \phi$ and $\epsilon = 3\phi$). Curve 2 in fig. 5 represents eqs. (20) and (9) with $aL/S = 10^{-5}$ and the same values of $\phi = \gamma$ and $\Delta\gamma = \phi/2$. The relationship between curves 1 and 2 in fig. 5 demonstrates that $R_L > R_S$ (i.e., $\ln(R_L/R_S) > 0$) at low and high supersaturations, and $R_L < R_S$ in the middle range of supersaturations. If the overall density of stacking faults, i.e., the factor aL/S, increases, curve 2 moves up. The supersaturation range where $R_L < R_S$ diminishes. It is worth mentioning that the pre-exponential factor in (33) is practically independent of supersaturation.

Unfortunately, there are no experimental data available to be directly confronted with the theory, although the recent experimental evidence from observations under the electron microscope and in situ observations with the optical microscope has at least qualitatively shown that stacking faults exposed on the (111) surfaces of Si crystals and $Ba(NO_3)_2$ crystals are active as sources for self-perpetuating growth steps [1–4]. The so-called oval defects on MBE grown Si surfaces may be ascribed to the stacking fault activity.

6. Conclusion

Based on the analysis of atomic configurations of sub-steps created on a (111) growth surface be stacking faults with fault vectors $\frac{1}{6}\langle 112\rangle$ and $\frac{1}{3}\langle 111\rangle$, it has been demonstrated that these sub-steps (there are two types of sub-steps, with $\frac{1}{3}\delta_{(111)}$ and $\frac{2}{3}\delta_{(111)}$) can act as self-perpetuating step sources. Comparing the activation energies and the normal growth rates of conventional 2D nucleation and heterogeneous nucleation along the sub-steps, it has been shown that growth steps may be generated by the sub-steps in the manner of mono-nuclear and birth-and-spread nucleation under low and high supersaturations, respectively, before conventional 2D nucleations take place. The sub-step mechanism should be most effective at low and high supersaturations.

Acknowledgements

One of us (N.-B. Ming) wishes to acknowledge a grant given from the Japan Society for Promotion of Science, which made his stay at the Tohoku University possible. We are grateful to Dr. M. Elwenspoek for valuable discussions and to Mr. K. Onuma for technical assistance.

References

[1] D. Kass and H. Strunk, Thin Solid Films 93 (1982) L101.
[2] E. Bauser and H. Strunk, Thin Solid Films 93 (1982) 185.
[3] J. Nishizawa and M. Shimbo, J. Japan. Assoc. Crystal Growth 4 (1977) 23 (in Japanese).
[4] K. Tsukamoto, K. Onuma and I. Sunagawa, unpublished, 1987.
[5] E. Bauser and H. Strunk, J. Crystal Growth 69 (1984) 561.
[6] W.K. Burton, N. Cabrera and F.C. Frank, Phil. Trans. Roy. Soc. London A243 (1951) 299.
[7] A. Ookawa, Kotai-Butsuri (Solid State Phys.) 10 (1975) 113 (in Japanese).
[8] A.A. Chernov, Modern Crystallography III: Crystal Growth (Springer, Berlin, 1984).
[9] S. Toshev, Homogeneous nucleation, in: Crystal Growth: An Introduction, Ed. P. Hartman (North-Holland, Amsterdam, 1973) pp. 1–49.
[10] A.A. Chernov, J. Crystal Growth 42 (1977) 55.
[11] T. Surek, J.P. Hirth and G.M. Pound, J. Crystal Growth 18 (1973) 20.

nen ein. Im Prozeß 5 sollte die Verdünnung micellar gebundenen Alkohols deutlich gemacht werden. Dieser Teileffekt ist jedoch nicht nachweisbar, da er vom Verdünnungseffekt des Alkohols bei Konstanthaltung der Tensidkonzentration überdeckt wird. Der Prozeß 6 zeigt die Verdünnung einer wäßrig-alkoholischen Tensidlösung. Genau wie im Prozeß 3 treten auch hier vier bestimmende Effekte in Erscheinung, jedoch sind mit großer Wahrscheinlichkeit Mischmicellen vorhanden und demzufolge weichen die experimentell ermittelten Verdünnungsenthalpiekurven bei konstantem Alkoholgehalt von denen im Prozeß 3 ab (Abb. 5). Die Zerstörung der Mischmicellen wird von einem endothermen Enthalpieeffekt begleitet.

Die vorgelegten Untersuchungen sollen einerseits die Komplexität des Micellbildungsprozesses unter Einbeziehung eines mittelkettigen Alkohols im Zustandsbereich normaler Micellen verdeutlichen und andererseits die Mikrokalorimetrie als geeignete experimentelle Methode zur Aufklärung der energetischen Verhältnisse des oben genannten Prozesses herausstellen. Die dargestellten Ergebnisse weisen qualitativ auf die Existenz von Mischmicellen hin, womit die cosolubilisierende Wirkung mittelkettiger Alkoholkomponenten in Tensidlösungen begründet ist. Die Untersuchungen dazu werden fortgesetzt.

Schrifttum

[1] Prince, L. M.: Microemulsions, Theory and Practice. New York: Academic Press 1977.
[2] Langevin, D.: Mol. Cryst. Liq. Cryst. **138** (1986) 259.
[3] Goddard, E. D., und G. C. Benson: Trans. Faraday Soc. **52** (1956) 409.
[4] Benjamin, L.: J. Coll. Int. Sci. **22** (1966) 386.
[5] Eatough, D. J., und S. J. Rehfeld: Thermochimica Acta **2** (1971) 443.
[6] Kreshek, G. C., und W. A. Hargraves: J. Coll. Int. Sci. **48** (1974) 481.
[7] Benjamin, L.: J. Phys. Chem. **68** (1964) 3575.
[8] Pitcher, G., M. N. Jones, L. Espada und H. A. Skinner: J. Chem. Thermodyn. **1** (1969) 381.
[9] Leduc, P. A., J. L. Fortier und J. E. Desnoyers: J. Phys. Chem. **78** (1974) 1217.
[10] Berg, R. L., L. A. Nolt und W. D. Good: Chemistry of Oil Recovery, American Chemical Society, ACS Symp. Ser. **91** (1979) 87.
[11] Ueberwirth, I.: unveröffentlicht.
[12] Bittner, C.: Diplomarbeit: Karl-Marx-Universität Leipzig 1985.
[13] Lumry, R., und E. Battistel: Faraday Symp. Chem. Soc. **17** (1982) 93.
[14] Zana, R., S. Yiv, C. Strazielle und P. Lianos: J. Coll. Int. Sci. **80** (1981) 208.
[15] Lara, J., L. Avtdikian, G. Perron und J. E. Desnoyers: J. Solution Chem. **11** (1981) 351.
[16] Desnoyers, J. E., R. DeLisi und G. Perron: Pure Appl. Chem. **52** (1980) 433.
[17] Hauthal, H. G., L. Möhle, R. Pfestorf und K. Quitzsch: VI. International Conference on Surface Active Substances, Bad Stuer 1985, Akademie-Verlag Berlin 1987, S. 63.
[18] Perron, G., und J. E. Desnoyers: J. Chem. Thermodyn. **13** (1981) 1105.

ISSN 0323-4479 · Z. phys. Chemie · Leipzig · **269** (1988) 5 · S. 941–970

Institute of Crystallography, USSR Academy of Sciences, Moscow, USSR

Results and Problems in Crystal Growth Studies[1]

By A. A. Chernov[2]

With 24 Figures

1. Introduction

At present we continue to study, at a new experimental and theoretical level, the atomic-molecular phenomena of crystallization and macroscopic processes of heat and mass transfer. The analysis originated by Gibbs, Curie, Wulff, Volmer, Kossel, Stranski, Kaishev, Frenkel and Zel'dovich was continued in the post-war period by the discovery of the dislocation mechanism of crystal growth, the stability and instability phenomena in growing interface, mechanisms of impurity capture and defect formation during crystallization [1]. Of all crystal growth problems (about 2000 annual publications) I should like to consider here the following:

– structure of interfaces, including the atomic structure of boundary layers in liquids, surface melting and wetting;
– crystal growth from solutions, including the growth kinetics provided by elementary and complex dislocation sources and new nonlinear effects;
– dissipative structures including the consequences of conventional morphological instability for dislocation structure and the formation of dendritic structures;
– Ostwald and nonostwald ripening;
– crystallization under strongly nonequlibrium conditions, including nucleation of crystals and molecular beam epitaxy.

2. Structure of Surfaces and Adjacent Layers

2.1. Atomically Smooth and Rough Surfaces: Lattice and Non-lattice Models of Melts

The analytical theory of thermal fluctuations at the crystal-vapor, crystal-melt, and crystal-solution interfaces [1] takes its origin more than forty years ago [2–8]. It leads to the conclusion that faces along which binding energy ϵ between surface atoms or molecules is much higher than kT cannot be destroyed by thermal fluctuations. Such faces remain atomically smooth and grow layer-by-layer by building up their atomic planes, i.e., by the motion of steps which end these planes [2, 3].

[1] Plenarvortrag, gehalten auf der Hauptjahrestagung im August 1987 der Chemischen Gesellschaft in der Deutschen Demokratischen Republik.

[2] A. A. Chernov, Institute of Crystallography, USSR Academy of Sciences, 117 333 Moscow, Leninsky Prosp. 59, USSR.

The surface with the binding energy-to-temperature ratio $\epsilon/kT \ll 1$ are atomically rough (Fig. 1). Such surfaces during the growth process coincide with the surface where either temperature or concentration has an equilibrium value.

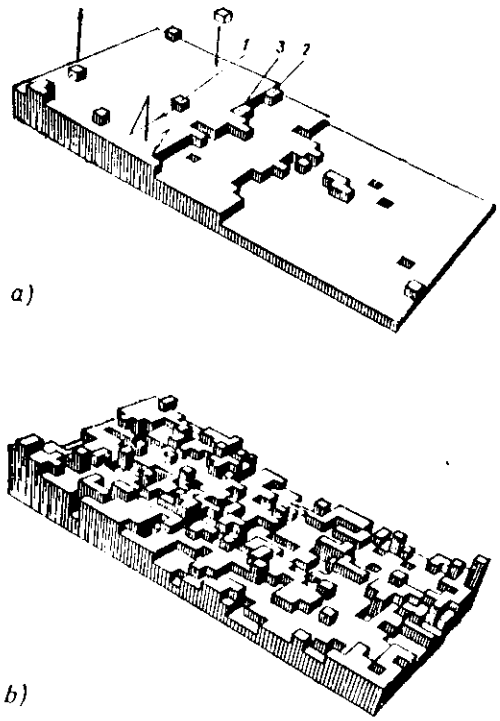

Fig. 1
Atomically flat surface with two steps (*a*) and the same surface above the roughening temperature (*b*). Monte Carlo simulation. (G. H. GILMER and J. D. WEEKS) 1 – an atom adsorbed on a surface, 2 – at a step, 3 – an atom in the kink

Energy ϵ can be expressed in terms of the heat of a phase transition and atomic structure of the surface. Thus the criterion $\epsilon/kT \ll 1$ or $\epsilon/kT \gg 1$ reduces to the conditions imposed on entropy of the transformation [5]. In a system with low melting entropy, e.g., for the interface between a metal crystal and its melt we have

$$\Delta s/k \lessapprox 1 - 2, \tag{1}$$

and the surface of any orientation is rough. For a substance with high transition entropy,

$$\Delta s/k > 5 \tag{2}$$

all close-packed crystallographic faces are expected to be atomically smooth, which was the fact observed experimentally. In cases intermediate between (1) and (2), only the most close-packed faces are atomically smooth. The faces having other orientations are rough. These conclusions are confirmed by numerous data on the Monte-Carlo simulation of surfaces (Fig. 1). Such results are based on the lattice model of the phase which surrounds the crystal and, in particular, of the melt. The lattice model implies

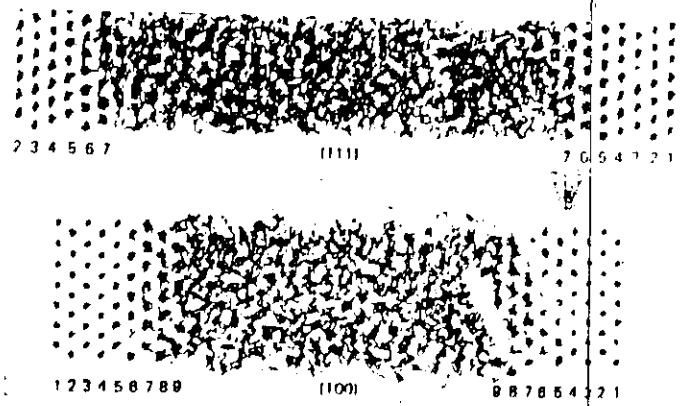

Fig. 2. Molecular dynamic simulation of Lennard-Jones system (J. Q. BROUGHTON, A. BOBIS-SENT, F. F. ABRAHAM): isothermal liquid between two fcc crystalline plates oriented parallel to (111) and (100)

that each atom can be considered either as belonging to the crystal or to the (lattice) liquid. Thus roughness appears only as a result of averaging either over the area or time. But modeling of the interface structure by the method of molecular dynamics [9, 10] yields a different picture – the closer is an atom to the interface, the larger is the amplitude of its vibrations. In the layers intermediate between the crystal and the melt the localized vibrations change, first partly and then completely, to the delocalized motion – diffusion (Fig. 2). The complete absence of localization signifies the transition of an atom into the liquid. Thus we face the problem of an adequate description of the liquid-crystal interface not invoking the lattice model. In other words, such a description should include the real spacial (and temporal) correlation in the liquid and different density values for the crystal and the melt. The solution of this problem is also very important since the transition from binding energy ϵ of surface atoms to the observed transition entropies for the crystal-melt and crystal-solution interfaces is rather ambiguous. The best results are obtained by the renormalization-group roughness criterion in the form [15] first obtained by CHOI and WEEKS

$$T > T_R = (2/\pi k)\, d^2\alpha \tag{3}$$

where T is the system temperature, k is the Boltzmann constant, d is the interplanar distances along the normal to the surface under consideration, α is the free energy of the surface, and T_R is the temperature at which the surface becomes rough.

From (3) it follows that the smaller is the interplanar distance, i.e., the larger are the Miller indices of the face, the lower is the critical temperature T_R at which the surface becomes rough. It should be especially low for vicinal faces (see below, Sect. 2.2).

Concluding this section, it is worth noting that the attractive roughness problem in the lattice model gave rise to a new theoretical direction within the framework of which an important problem on the nature of the transition, correlation function of the interface [11-16] and its temperature dependence was considered. In such studies the

called Gaussian discrete model was widely used in which a crystal was considered as built of closely packed parallel columns ("pencils") of various lengths z_j, where j is the column number. The potential energy of the surface is then proportional to $\sum_j (z_j - z_{j+1})^2$, i.e., to the sum of squared "open" side surface of each column. This model was shown to be equivalent to $2D$ Coulomb gas or a system of parallel vortices. Consequently, the roughening transition undergone by the surface belongs to the same universality class as the $2D$ Kosterlitz-Thouless transition and not the Ising model transition.

Another approach uses the renormalization-group analysis of the continuous (not atomically discrete) interface model which is very similar to the data of the molecular-dynamics simulation (Fig. 2). The latter approach leads to the same conclusion on the type of the roughening transition – it is of infinite order.

Nonlattice theory of the crystal-melt interface structure which correctly describes the atomic structure of the boundary layer between the crystal and the melt can also be applied to the structure of a liquid in the vicinity of a foreign solid wall (see Sects. 2.4 and 2.5).

2.2. Roughness of Vicinal Faces

As has already been noted in connection with formula (3), the larger are the Miller indices of the face under consideration, the lower is its temperature of roughening transition, T_R. A vicinal face slightly deviated from the close-packed one has, e.g., the indices of the $(11n)$, $(1nn)$, $(10n)$ type where integers $m, n \gg 1$. A vicinal is built by steps. If steps are ordered, i.e., are equidistant, it is a smooth vicinal. And vice versa, disordered steps suggest that the vicinal is in the rough state. The interaction between the steps is the weaker, the larger is the distance between them. Therefore the temperature of the transition to the rough state is the lower, the larger are the Miller indices of the vicinal. The transition to the rough state was observed on the $(11n)$ Cu (from intensity measurements of X-ray grazing reflection) and also on the $(11n)$ Ni [17] and $(11n)$ Pb [18]. The evaluation of the transition temperature by eq. (3) for copper ($\alpha = 1300$ erg/cm^2, the melt – vacuum interface) yields $T_R = 980$ K. The experiment gives $T_R \approx 600$ K. The time autocorrelation function of the emission current permits one to measure the self-diffusion coefficient on the faces of the (011) (112) W zone. The peak of the temperature curve of the self-diffusion coefficient ($T = 950$ K) can be interpreted as the roughening transition [21].

2.3. Surface Melting: Problem and Experiment

In the vicinity of a solid wall or free surface, the structure of a liquid should be different from the bulk one, i.e., should be partly ordered. Therefore the liquid in the film with the thickness of the order of the bulk correlation length may have a chemical potential which differs from that of the bulk liquid. Thus a crystalline layer of such a thickness adjacent to the interface should melt (due to thermodynamical reasons) at a temperature

lower than that for the crystal bulk. It is the so-called surface melting. The contributions to this effect come from both VAN DER WAALS, i.e. electromagnetic, [22] and acoustic [23] correlations to the free energy of the thin film.

The above defined surface melting differs from surface roughening [22, 24]. Indeed, the crystal-film interface may be either atomically smooth or atomically rough – similar to the case of two states of interfaces between the crystal and the bulk melt. In other words, the atomically smooth crystal-medium interface (Fig. 3a) can acquire one of three states shown in Fig. 3b, c, d. Which of the transformations indicated in Fig. 3 does really occur with the approach to the melting point?

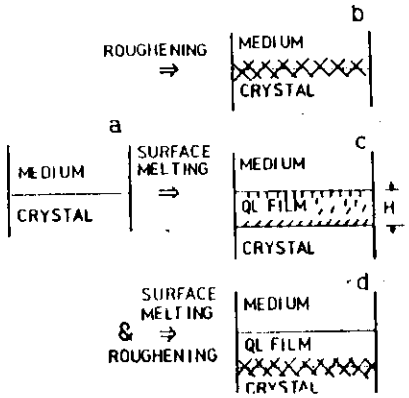

Fig. 3
Possible transitions of a crystal-medium interface (a): roughening (b), creation of melt film with the atomically smooth (c) and rough (d) crystal-film interface

Biphenyl. We studied ellipsometrically [24–26] the biphenyl boundary which was in the optical contact with a glass. It turned out that at temperature ≈ 0.5 K lower than the melting point, i.e., at a supercooling of $\Delta T = T_m - T \approx 0.5$ K, the thickness of the liquid layer reaches ≈ 100 Å on the most densely packed (001) basal face (Fig. 4) ≈ 300 Å on the least dense packed (010) face. It is and known from independent experiments that the basal face which is in the contact with the melt remains atomically smooth since it grows by deposition of subsequent layers as is shown in Fig. 1a. The (010) face is rough, being in the contact with the melt. Therefore, in this case we seem to observe the a → c transition (Fig. 3) for the (001) face and the a → d transition for the (010) face. We use here the word "seem" because the crystal-film interface may slightly differ from the interface between the crystal and the bulk melt.

Under supercooling $\Delta T < 0.5$ K, incoherent light scattering by the specimen becomes stronger: an ellipsometric signal cannot be nulled by any rotations of the analyzer or polarizer [26]. If $\Delta T = 0.30$ K for (001) or $\Delta T = 0.45$ K for (010), the intensity of such scattering reaches its maximum (up to 40 times higher than the background value) (Fig. 5). With the further approach to the melting point, i.e. for $\Delta T \to 0$ (the accuracy of T and ΔT measurements was better than 10^{-2} K) scattering becomes weaker and drops down to the values corresponding to large supercooling, as is seen from Fig. 5. This means that the surface melt film experiences a certain transition. This is also confirmed

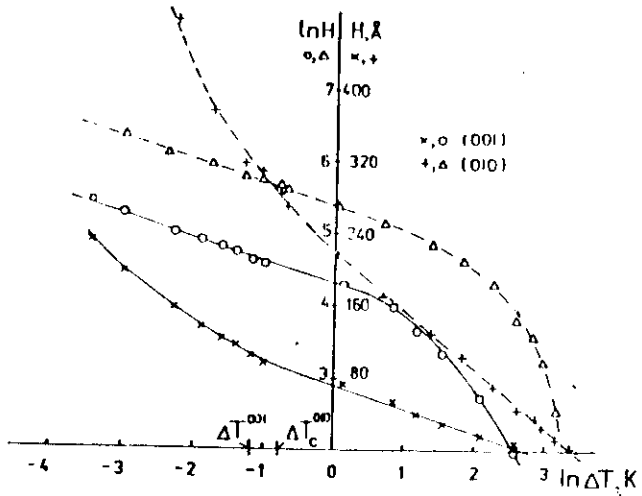

Fig. 4. Thickness H of the melt film appearing on the (001) and the (010) biphenyl faces contacting with the glass at a supercooling ΔT below the melting point. The same data are plotted in ln H vs ΔT and H vs ΔT coordinates demonstrating that $H(\Delta T)$ dependence changes from $H \sim \ln \Delta T$ to $H \sim (\Delta T)^{1/n}$ at $\Delta T = \Delta T_c$

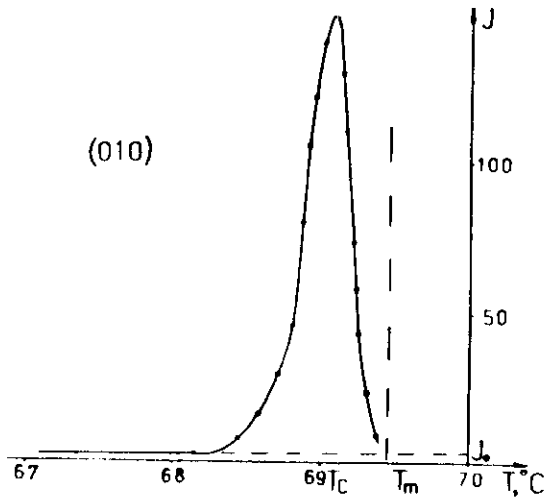

Fig. 5. Intensity J (arbitrary units) of light scattered by the surface film on the (010) biphenyl face. The peak corresponds to the supercooling ΔT_c at which the $H(\Delta T)$ dependence changes (see Fig. 4)

by the changes in the law of the thickness increase for large supercooling. Namely, for $\Delta T \geqq 0.3$ and $\Delta T \geqq 0.45$ we have

$$H_{001}(\text{Å}) = 73 - 28 \ln \Delta T(\text{K})$$
$$H_{010}(\text{Å}) = 220 - 65 \ln \Delta T(\text{K}) \quad (4)$$

and for $\Delta T \leqq 0.3$ K or 0.45 K (Fig. 4) we have

$$H = 1/(\Delta T)^{1/n} \qquad 2.5 < n < 3.5. \quad (5)$$

Therefore we suggest that for $\Delta T > 0.3$ or > 0.45 K the films at both interfaces have partly ordered liquid-crystalline structure. In the close vicinity of the melting point, where the film is rather thick, it has, in its largest part, a disordered structure of the bulk liquid [26]. It is important that the biphenyl melt and thin biphenyl films on glass have, according to our and the literature data, no liquid-crystalline structure, although they consist of elongated molecules which include two benzene rings (the latter being parallel to one another in the crystal and form an angle of 23° in the melt). Thus ordering is due to the crystal surface.

Lead [27, 28]. The asymmetric shape of molecules cannot be responsible for the subsurface order in lead where surface disorder was qualitatively observed by the extinction of structure reflections on high-energy electron diffraction patterns (Fig. 6) and quantitatively by the intensities of back scattered protons (Fig. 7).

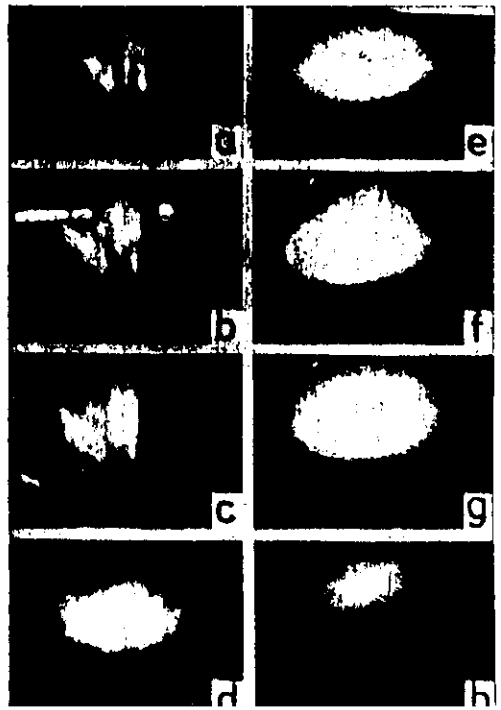

Fig. 6
RHEED pattern from (100) Pb surface at different temperatures: a: 295 K, b: 370 K, c: 475 K, d: 532 K, e: 554 K, f: 558 K, g: 565 K, h: just below T_m
(I. Ebnesajjad, Thesis 1986)

Other Materials. The first studies of surface melting were performed as far back as 1859 by M. FARADAY who observed under a microscope the water meniscus in ice at temperatures below 0°C. The same effect was observed later on ice [30], and a film was shot. There are known numerous investigations of surface melting of ice made by other methods [31–36]. The liquid phase was observed in the form of droplets on the surface of p-toluidine crystals grown from vapor. If the temperature of crystals growing from vapor approaches the melting temperature, the growth rate becomes zero despite the fact that there is a finite not too low vapor supersaturation with respect to the crystal [37, 22]. Therefore it may be concluded that the crystal (or, more precisely, steps on its surface) grows not directly from vapor but from a thin melt film the chemical potential of which approaches the potential of the crystal if $T \to T_m$. The effect of surface melting and the lowering of the melting point of thin ($\leqq$ 100 Å) films were observed (by different methods) also on gallium [38], sodium [39], lead [27, 28, 40, 41], copper [42, 43], gold [44], argon [45], neon [46], and oxygen [47].

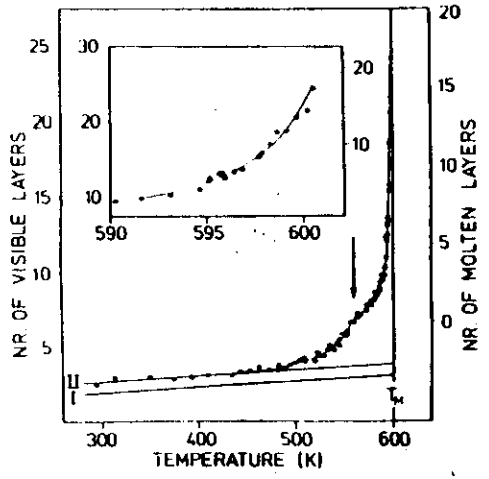

Fig. 7
Number of molten layers on the (100) Pb surface depending on temperature below the melting point T_m = 600 K (VAN DER VEEN and J. FRENKEN)

More than 100 K below the melting point of germanium (1210 K), the (111) Ge face seems to be covered with a liquid film which is indicated by the disappearance of the (00) and (01) reflections on LEED patterns [48].

The references to other investigations can be found in [1, 49] and the above cited articles.

Modeling. Disordering of one-three surface layers was also revealed in numerous computational experiments carried out by the methods of molecular dynamics [50–53].

2.4. Structure of Layers Adjacent to Surface in Simple Dense Liquids (Theory)

Consider a dense liquid built by spheres and contacting a structureless wall. Then the first layer of spheres is ordered in the plane parallel to the wall just because it is in the

contact with this wall. The second layer partly inherits the order of the first one, the third layer inherits that of the second, etc. Let the fraction of an inherited order be proportional to the ratio of spacing d in the lattice of spheres to a certain correlation length ξ. The n the density $n(z)$ of the liquid, averaged along the plane parallel to the wall and being at a distance of z from it, experiences attenuating oscillations and tends to a constant value of n_0 in the melt bulk

$$n = n_0 + (n_s - n_0) \exp\left[-(z - d/2)/\xi\right] \tag{6}$$

where n_s is the spatial density of the sphere centers in the first layer adjacent to the surface.

The above described "relay race" mechanism of order succession in the depth of the melt is, of course, heuristic. The consistent analysis can be carried out [55] by studying the free energy of a liquid represented as a functional of the density deviation Δn from its mean value n_0: $\Delta n(\boldsymbol{r}) = n(\boldsymbol{r}) - n_0$. It can be shown that the free energy of the liquid reaches the minimum if $\Delta n(\boldsymbol{r})$ is the superposition of the density waves of the type

$$n(z) = \sum_j n_{0j} \exp\left(i\boldsymbol{k}_j \cdot \boldsymbol{r} - z/\xi_j\right). \tag{7}$$

Here the wave vector $\boldsymbol{k}_j$ is such that its module k_j is an abscissa of the jth maximum of the structure amplitude of the liquid, $S(k_j)$ ($j = 1, 2, \ldots$), readily obtainable from the experiment. Constants n_{0j} turned out to be (see below) close to the density of the liquid, which provides the importance of the effects under consideration.

The two-dimensional structure of the crystal surface (but not of a smooth structureless wall) is determined by the set $\boldsymbol{g}$ of the reciprocal lattice vectors projected onto this surface. Therefore the surface excites in the liquid the density waves such that the projections of their wave vectors $\boldsymbol{k}_j$ onto the surface plane coincide with one of projections $\boldsymbol{g}$ (Fig. 8a). Thus from the whole diversity of the density waves whose superposition makes the bulk liquid, the surfaces "selects" only those which are symmetrically compatible with it. The layers whose density amplitudes weakly attenuate with z are smectic layers corresponding to the main maximum of the structure amplitude at $k = k_1$ which are oriented parallel to the surface, i.e., $\boldsymbol{k}_1 \parallel z$ and $\boldsymbol{g} = 0$ (Fig. 8b). For such layers $\xi \approx 1.5\,a$, which seems to imply that the ordered layer is very thin. However the estimate of the

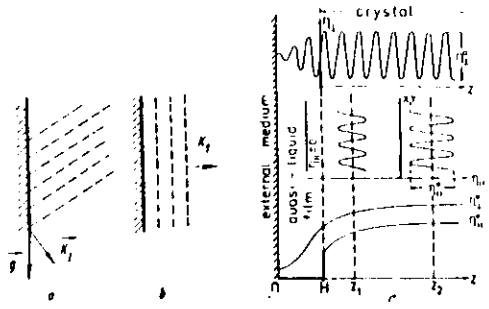

Fig. 8a, b
Smectic layers (dash-lines) of simple liquid in the vicinity of solid interface (solid line); $\boldsymbol{g}$ is the wave vector of the 2D – reciprocal lattice of the solid surface, $\boldsymbol{k}_j$, k_1 – wave vectors of the bulk liquid; c. density distribution normal to the interface, $\eta_{\perp}(z)$, and parallel to the interface, $\eta_{\parallel}(x, y)$; the two lower curves, $\eta^0_{\perp}(z)$ and $\eta^0_{\parallel}(z)$, illustrate the change of density wave amplitudes (the order parameters) with distance z to the interface.

wave amplitude with the use of the Ornshtein-Zernike equations and the Perkus-Yevik solid rigid sphere approximation yields the conclusion that the amplitude of waves near the surface is rather large, $\approx 0.8 n_0$ [55]. The diffusion coefficients in the crystal and in the melt differ by five-seven orders of magnitude. Therefore if the ordering amplitude at the surface is large (~ 1), the absolute value of the kinetic parameters of the liquid may notably differ from the bulk values for layers far from the surface, not to mention the first layers adjacent to the surface. Therefore, ordering may essentially change the kinetic properties of the interface. In particular, the delocalization of the crystal-melt interface can increase its kinetic coefficient in crystallization similar to the case where delocalization of the dislocation core results in a decrease of the Peierls potential barrier for its motion, thus increasing the dislocation mobility.

2.5. Elements of the Theory of Surface Melting

The violation of the translation symmetry of a crystal at its boundary, the loosening of a surface bonding of atoms and an enhancement of their thermal vibrations result in disorder of the layer adjacent to the surface and therefore in higher entropy and lower chemical potential of this layer. The analysis of these phenomena was performed [25, 26] with the use of the Ginzburg-Landau functional for the free energy, the density of which includes a function of the order parameter η and the squared gradient $(d\eta/dz)^2$ along the surface normal z. This local form of the functional can be obtained from the general (nonlocal) density functional by introducing complex order parameters having the sense of amplitudes of the density waves propagating in different directions (Chernov and Mikheev, in print) which take account of the atomic structure.

The simplest order parameters are transverse $\eta_\perp$ and longitudinal $\eta_\parallel$ ones; they describe the density waves along the surface normal ($\eta_\perp$) and along x and y in the surface itself ($\eta_\parallel$). The pictorial representation of $\eta_\perp$ and $\eta_\parallel$ is given in Fig. 8c. Below, the parameters η are equal to the amplitudes of the corresponding density waves. Generally speaking, $\eta_\parallel$ consists of a set of parameters $\eta_{G_{jk}}$, where the wave vector of the density wave $G_{jk} = g_j$, and $k_j^2 - g_k^2$ is related to the jth maximum of the structure amplitude of the liquid and the kth vector g_k of the plane reciprocal lattice. For highly symmetric densely packed plane faces it is possible to restrict oneself to only one set of vectors $\pm g$. Thus for the (111) face of a fcc crystal it is the {111} family. The expansion of the free energy U of the crystal in the order parameters should be translationally invariant and, hence, contain only the combinations of $\eta_{G_{jk}}$ such that $\sum G_{jk} = 0$. Therefore in the case of the (111) face of fcc crystals, the linear terms of the free energy expansion are absent, i.e.

$$U = U_0(\eta_\perp) + U_2(\eta_\perp)\eta_\parallel^2 + U_3(\eta_\perp)\eta_\parallel^3 + \ldots \tag{8}$$

The latter expression has the form of the Landau expansion from the theory of phase transitions, the role of temperature being played by the transverse order parameter $\eta_\perp$. Coefficients U_1, U_2, and U_3 may be expressed in terms of the parameters of $S(k)$ maxima. If one moves from the crystal bulk to its surface, a decrease in $\eta_\perp$ provides the minimum of free energy (in the form of the gradient-quadratic functional). In turn, the decrease in $\eta_\perp$ results in a sudden disappearance of $\eta_\parallel$ if $\eta_\perp$ are such that $U_2(\eta_\perp) = 0$.

The disappearance of the longitudinal order in the layer of a finite thickness, H, and the retaining of a certain degree of the layer order along the face normal marks the appearance of a liquid crystalline phase. Such surface melting may readily be understood. Indeed, $\eta_\parallel$ describes the order within the atomic planes in the directions x and y normal to z. It arises because a notable fraction of atoms leave the lattice planes. The atoms which have obtained much more freedom of motion along the planes start disordering in the (x, y) planes upon reaching a certain degree of order $\eta_\perp(H) = \eta_{\perp c}$.

The estimation of the thickness H of the melt film as a function of supercooling ΔT is based on the correction to the chemical potential of the film compared to the potential of the bulk melt. The Van der Waals attraction forces between the liquid and crystal yield

$$\Delta\mu = -A(d/H)^3 \tag{9}$$

where $A \approx 10^{-13}$ erg cm^3, d^3 is the atomic (molecular) volume of the liquid. If the crystal-film system is supercooled below the melting (triple) point by ΔT, then $\Delta s\, \Delta T = \Delta\mu$. Therefore the equilibrium film thickness [22] is

$$H/d = (A/\Delta s\, \Delta T)^{1/3}. \tag{10}$$

Acoustic repulsion [23] gives also universal $\Delta\mu$ analogous to (9) with A of the opposite sign. Both estimates do not take into account the order of the liquid discussed earlier.

The simplest allowance for ordering consists in the minimization of the free energy functional in which only one order parameter η is used which indicates, e.g., the mean orientation of nonspherical molecules, which is of great importance for the experiments with biphenyl. The limitation to the free energy expansion in η^2 and $(\partial\eta/\partial z)^2$ results in the exponential dependence of the size-dependent correction to the chemical potential

$$\Delta\mu \sim \exp(-H/\xi). \tag{11}$$

Therefore

$$H \sim -\xi \ln \Delta T \tag{12}$$

where ξ is the correlation length which depends on the coefficients before η^2 and $(d\eta/dz)^2$ in the free energy functional. These coefficients may be estimated in terms of the temperature and surface energy [25]. Recently, an attempt has been made to analyze microscopically and more consistently these coefficients with due regard for the renormalization of the correlation lengths ξ and the fluctuations (capillary waves) at a free boundary [57].

3. Crystal Growth from Solutions

The microscopic aspect of these phenomena includes the molecularionic structure of solutions, their stability to supercooling, the structure of interface layers of solutions and the effect of thermodynamic variables onto these quantities. The atomic structure of solutions and interface layers determines the kinetics of crystallization processes on steps. The latter together with the processes of the step generation by dislocations and

nuclei (which are also dependent on the atomic structure) determine the crystallization rate and crystal composition.

If to take into account the hydrodynamic processes at the growing surface and the phenomena of the morphological stability (the appearance of the so-called dissipative structures), we arrive at the complete set of factors determining the defect structure of the crystal.

Below we consider only the kinetics of the layer growth, the dissipative structures, and also the phenomenology of coarsening processes in the multicrystal systems.

3.1. Kinetics of Layer Growth

3.1.1. Dislocation Activity

If a dislocation crossing the surface has a nonzero Burgers vector component normal to this surface, i.e., $b \neq 0$, then it generates on this surface a step which is terminated at the dislocation outcrop. If the solution on the surface is supersaturated, then the step starts moving and twisting into a spiral around the dislocation outcrop [3]. Recently it was noted [58, 59] that the growth layers (i.e. the steps) are generated not only by screw but also by edge dislocations, or, more exactly, by dislocations with $b = 0$. Indeed, NaCl deposition from molecular beams under large supersaturations has shown that upon some time the spiral growth steps on the surface are replaced by concentric ones [90] (Fig. 9). A series of indirect data indicate that nucleation of such concentric centers occurs at points where edge dislocations cross the crystal surface [58]. In ionic crystals nucleation seems to be facilitated by electric charges at dislocations [61]. However such an explanation is hardly applicable to GaAs crystals growing from their solution in molten gallium. Nevertheless, using the decoration and X-ray topography, it is possible to observe growth hillocks on the (111) GaAs produced by dislocations with $b = 0$ [59].

We carried out experiments on $NH_4H_2PO_4$ (ADP) crystals growing from aqueous solutions with the simultaneous in-situ X-ray topographic check ups [62]. Thus we managed to observe both crystal growth and the defect formation in their lattices. Edge dislocations turned out to be inactive—the bipyramidal face crossed by such dislocations in the supersaturated solution ($\sigma = 2$–3%)[1] did not grow (at least with an observable rate $R > 10^{-7}$ cm/s). To the contrary, screw dislocations provided notable growth rate. The disapperance of screw dislocations from the face halted face growth.

One more interesting phenomenon should be mentioned. Let dislocation D_1 (Fig. 10a) outcrop to the bipyramidal (011) face growing notably faster than the (001) prismatic face. Upon some time, it will reach edge E. This occurs simply due to the displacement of the (011) face since the dislocation is immobile with respect to the crystal lattice. If D_1 is the only dislocation providing growth of the (011) face, then the outcome of

[1] We mean here relative supersaturation, $\sigma = (C - C_e)/C_e$, where C and C_e are the true and equilibrium concentrations of the solution, respectively.

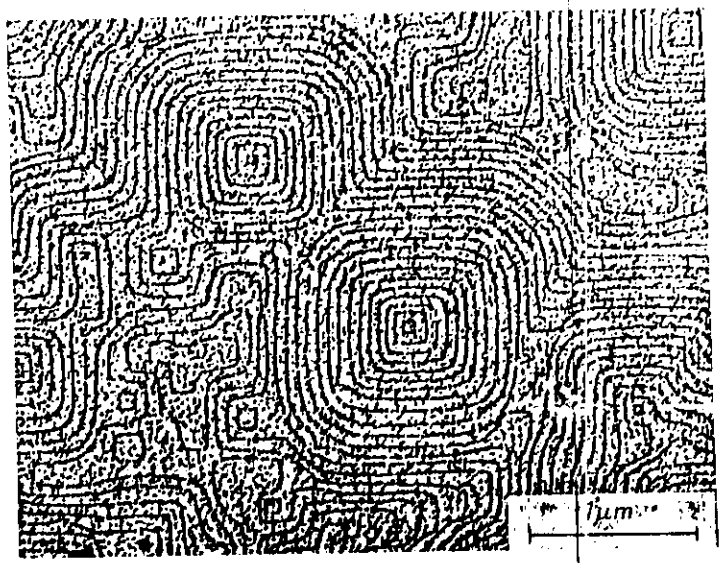

Fig. 9. Concentric growth steps appeared on the (100) NaCl surface during its growth from NaCl molecular beam

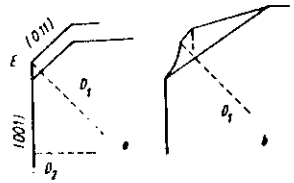

Fig. 10. Effect of dislocations on growth of neighbouring faces: a: the (011) face is growing if the screw dislocation D_1 provides layers on it, i.e. till the moment when D_1 reaches the edge E between the (011) and (001) faces; later, the face (011) can grow only if the face (001) moves due to another dislocation D_2, the dislocation D_1 remains on the edge E. b: the dislocation D_1 crossing an edge does not generate a step on the face

D_1 to edge E should stop the face growth. Indeed, a dislocation coming out to the edge does not generate any step unlike a dislocation outcoming to the face (Fig. 10b). If nevertheless the (001) prismatic face (Fig. 10a) continue to grow (e.g., because of the activity of another dislocation, D_2) then the (011) face also grows at a rate such that the dislocation D_1 will remain at the edge E. Thus the growth rate of the bipyramidal face is entirely determined by the growth rate of the neighboring prismatic face, the angle between these faces and the orientation of the "connecting" dislocation D_1. Such a growth explains the mutual dependence of the growth rates observed for the neighboring faces.

The Burgers vector of a dislocation equal to one lattice parameter is rarely observed. More often we encounter larger values and X-ray topographs show either only one or several dislocation lines. Different power of dislocation sources generating steps is clearly seen if we compare the curves which describe the growth rates R of prismatic faces as functions of relative supersaturation σ (Fig. 11, Fig. 12) [63]. Both studied prismatic faces grew from one solution, the temperature, accidity, and supersaturation being equal as well. Nevertheless, for $\sigma = 3\%$, the normal growth rate R of one prismatic face (Fig. 12) turned out to be four times higher than that of the other face (Fig. 11). Figures 11 and 12 also show the curves of the tangential growth rates $v(\sigma)$ of the steps on these faces and slopes $p(\sigma)$ of the vicinal spiral growth hillocks formed around the dislocation on this face as functions of supersaturation. It is just this growth hillock which provides the face growth at the rate R.

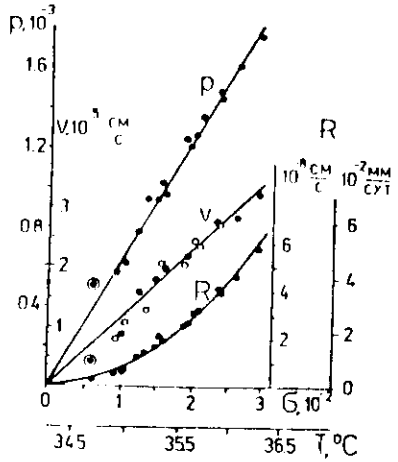

Fig. 11
Average step velocity v, dislocation hillock slope p and normal growth rate R provided by this dislocation hillock as functions of relative supersaturation σ. The hillock is formed around elementary screw dislocation

Figure 11 illustrates the growth kinetics on a dislocation with the unit Burgers vector. According to the theory [3], for such a dislocation we have

$$p = hkT\sigma/19\omega\alpha \tag{13}$$

where h is the step height (corresponding to the lattice parameter) T is the temperature, ω is the specific molecular volume of the crystal, and α is the specific surface free energy of a step riser. The comparison of p calculated by (13) and the experimental $p(\sigma)$ dependence shown in Fig. 12 permits one to obtain the value of $\alpha \approx 20$ erg/cm^2 (we do not go here into a finer effect of anisotropy in α).

The total normal component $b = mh$ of the Burgers vector for a nonelementary dislocation is larger than the lattice parameter h (the integer $m > 1$). The core perimeter of such a dislocation may be $2L$, which largely exceeds the interatomic distance. Thus the slope of the growth hillock formed around such a dislocation is

$$p = mhkT\sigma/(19\omega\alpha + 2LkT\sigma). \tag{14}$$

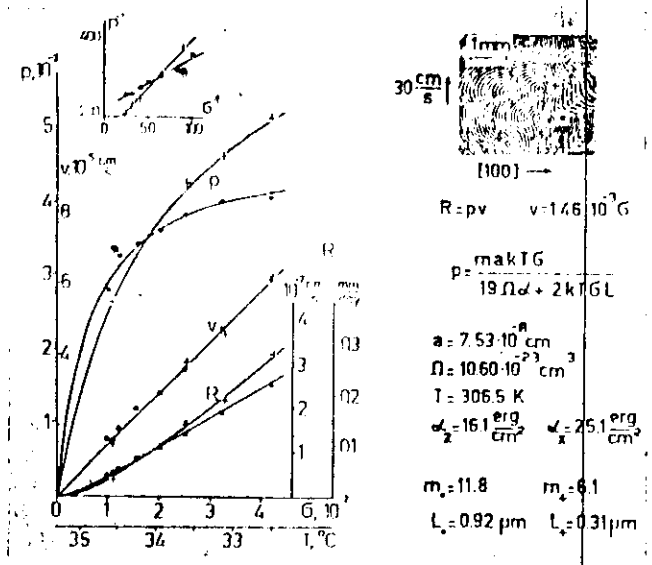

Fig. 12. Average step velocity v, dislocation hillock slope p and normal growth rate R provided by this complex dislocation step sources, denoted by · and + on the upper right insert presenting MICHAELSON interference fringes of the growing face. The Burgers vectors, m_0 and m_+, and another parameters of the sources are indicated. The upper left insert presents the same data in the p^{-1} vs σ^{-1} coordinates

It is seen from (14) that p^{-1} linearly depends on σ^{-1}, which was in fact confirmed experimentally (see the insert in Fig. 12). Two straight lines on this insert are related to two dislocation growth hillocks marked with a cross and a circle in Fig. 12. The positions and slopes of these two straight lines yield the values: $m_0 = 12$, $m_+ = 6$, $L_0 = 0.92\,\mu$m, $L_+ = 0.31\,\mu$m. Thus not only the presence of a dislocation source as small as $\sim 1\,\mu$m in diameter but also its structure may effect the growth rate of a macroscopic face of the crystal changing it by a considerable factor.

3.1.2. What Does Limit Growth Rate?

Figures 11 and 12 help one to solve one more problem already discussed for many years – how important is surface diffusion in crystal growth from solutions.

In crystal growth from vapor, molecular beams, and, to a lesser degree, from the gas phase with the participation of chemical reactions, surface diffusion plays an important part. The point is that the density of a crystallizing substance in the gas phase is much lower (up to a factor of 10^6) than the density of the same substance adsorbed at the atomically smooth terraces between the steps. If the temperature is not too low, then admolecules (adatoms) may diffuse over the surface. In this case, they provide a larger inflow of the crystallizing substance to a step than the atoms arrived directly from the gas phase.

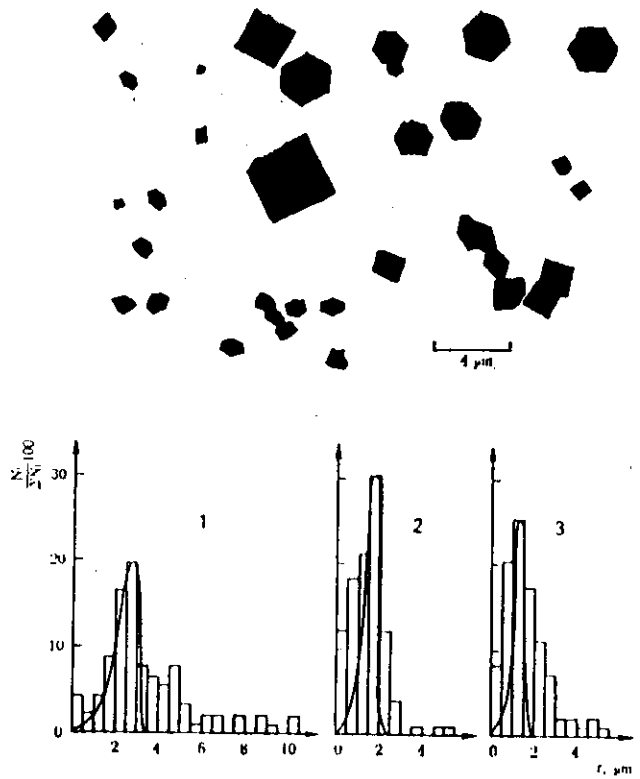

Fig. 13. Above – electron microphotographs of Ca oxalate crystals in human urine of an ill person. For healthy persons, the crystals are tens of percent smaller and possess the same shape. Below – the size distribution of crystals in human urine: 1 – total histogram reflecting data of all patients, 2, 3 – typical histogram for ill persons. Solid line gives size distribution expected for Ostwald ripening. It does not fit the data demonstrating that the size distribution is controlled by growth kinetics and inhibition [91]

At temperatures exceeding a surface energy per atomic site each step strongly fluctuate, i.e., it has a lot of kinks (Fig. 1a). Therefore its velocity v should linearly increase with the supersaturation attained in the immediate proximity of the step. At the same time, each step is the linear sink for a crystallizing substance and therefore is surrounded with a diffusion field. If the decisive role in step feeding is played by diffusion in the bulk solution, then the symmetry of the concentration diffusion cloud around the step should be cylindrical. If diffusion proceeds only on the terraces between the rectangular steps, then the diffusion field is one-dimensional and depends only on the coordinate perpendicular to the step normal. The overlap of the diffusion fields of neighboring (and more distant) steps is the measure of "competition" for the crystallizing substance. The stronger the diffusion field overlap, the lower the supersaturation in the immediate

vicinity of each step and the lower is its velocity v, the supersaturation in the solution bulk being the same. In the experiments illustrated by Figs. 11 and 12 an increase in supersaturation results in steeper dislocation hills or in an approach of steps to one another. Therefore if the diffusion fields of the steps overlap, then the velocity v of a steps forming the vicinal hillock should increase with σ at a lower rate than it is required by the linear law. In fact, Figs. 11 and 12 show that $v(\sigma)$ is a linear function. Hence the steps do not "compete" for their feeding by overlapping their diffusion fields, and the supersaturation at each step equals to that in the solution bulk. Therefore, the observed step velocity and therefore the growth rate of the face are completely determined by the process of ion building into the lattice directly on the steps (Of course, the face growth rate strongly depends also on the rate of step generation). The process of ion building into the steps is characterized by the kinetic coefficients β_t relating the step velocity v and supersaturation σ on it:

$$v = \omega C_e \beta_t. \tag{15}$$

The kinetic coefficient β_t is anisotropic. For the prismatic face this coefficient along the optical axis is $\beta_t \approx 4 \times 10^{-3}$ cm/s [63], whereas in the normal direction it is by a factor of 1.5 smaller. On the bipyramidal face the value of β_t is much higher, for three different step orientations on this face it is $\beta_t \approx 0.8$, 0.6, and 0.4 cm/s, respectively [64]. The linear energies of steps for the prismatic and bipyramidal faces determined in our experiments were almost the same. Being recalculated into the surface energy of a step riser, it is 20 erg/cm^2. Thus the large difference observed in the growth rates of prismatic and bipyramidal faces under low supersaturations is determined by the kinetics of the step motion alone.

It is worth noting that the kinetic coefficients of face growth for garnets in high-temperature solutions determined by another technique are $3 \times (10^{-3} - 10^{-4})$ cm/s [65].

The kinetics of the ion (molecule) incorporation into the lattice at the steps determines not only the growth rate of the face and its morphology but also the capture of impurities, the density of point defects in crystals, morphological stability of the face.

3.1.3. Impurities and Strongly Nonlinear Growth Kinetics

The types of functions $p(\sigma)$, $v(\sigma)$, and $R(\sigma)$ shown in Figs. 11 and 12 are in good agreement with the classical theory of growth on dislocations. This, however, is not true for the functions shown in Fig. 14 [66, 67]. Here the kinetic coefficient of layer propagation sharply increases if the supersaturation exceeds a certain critical value $\sigma = \sigma_* = 3$–4%. The variation in the slope of the dislocation growth hillock $p(\sigma)$ turns out to be nonmonotonic: with the rise in supersaturation $p(\sigma)$ first increases (for small σ), then decreases (for moderate σ), and finally increases again (for large σ). For $\sigma > \sigma_*$ the growth processes on the face proceed at a much higher rate.

The strongly nonlinear dependence $v(\sigma)$ seems to be due to impurities adsorbed on the growing face but hardly entering the crystal. The molecules (ions, complexes) of such impurities together with their solvate shells thus become stoppers for step motion. If the distance between such stoppers, $(C_{at})^{-1/2}$, is smaller than the diameter $\omega\alpha/kT\sigma$

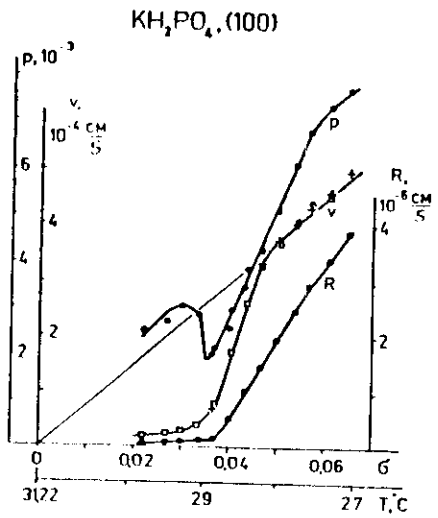

Fig. 14
Average step velocity v non-linearly depends on supersaturation σ due to impurities providing the non-monotonous variation of the hillock slope, p, and about 10 times increase in kinetic coefficient for the face growth rate, R. The impurities are believed to hinder the step propagation at $\sigma < \sigma_* \cong 3$–$4\%$ and do not influence the kinetics at higher supersaturations

of a two-dimensional critical nucleus for the given supersaturation, then steps cannot overcome the impurity "fence" and their motion is halted (N. Cabrera and D. Vermilyea). Here ω is the specific molecular volume of the crystal, and C_{st} is the surface stopper concentration related to bulk impurity concentration by one of the conventinal adsorption formulae. Thus each surface impurity concentration C_{st} determines the threshold supersaturation $\sigma_* \approx \omega\alpha\sqrt{C_{st}}/kT$ below which the steps and therefore the face stop growing. Our $v(\sigma)$ and $R(\sigma)$ curves (Fig. 14) are similar to such threshold functions. The important difference however lies in that no complete halt of growth for $\sigma < \sigma_*$ occurs. We believe that stoppers in the adsorbed state live for a finite time. Being desorbed, they provide step motion even under low supersaturations. The velocity of such a motion is determined by both supersaturation and stopper lifetime. This situation is analogous to dislocation motion in crystals with impurities. The analytical solution of such problems has not been known as yet.

If the step velocity varies nonlinearly with supersaturation, then the classical theory of the layer-spiral growth is not applicable, since it is based on the linear relationship (15). The adequate analytical theory for the piecewise linear dependence $v(\sigma)$ which describes approximately the nonlinear $v(\sigma)$ curve in Fig. 14, was recently developed in [66]. In [67], numerical calculations for an arbitrary $v(\sigma)$ have been performed. The main effect of nonmonotonic $p(\sigma)$ dependence is explained, within the ideology developed in [66], as follows. Consider a step which ends at point D of the screw dislocation outcrop (Fig. 15). Since the step center D is immobile, the curvature radius of the step at D should be equal to the curvature radius of a two-dimensional critical nucleus. Indeed, the supersaturation with respect to such a curved step is zero and $v = 0$. The farer from the center D is a point on the step under consideration, the smaller is the step curvature at this point. Thus the closer to σ in the bulk the supersaturation which

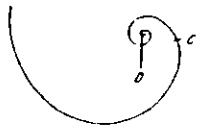

Fig. 15. Growth sprial around point D where an elementary screw dislocation crosses the interface. Within the central part DC of the spiral an effective supersaturation (Gibbs-Thomson effect included) $\sigma < \sigma_* \cong 3$–$4\%$ (see Fig. 14). At larger distance from D, i.e. beyond C, the acting supersaturation equals the one in solution. Therefore the interstep distance within DC is much less than beyond C

really "moves" the step (with due regard for its curvature). Therefore there should exist a segment DC of the step close to its center D where the "driving" supersaturation is lower than the thereshold value, $\sigma < \sigma_*$. The step growth here is determined by the slow kinetics. At a distance from the center exceeding DC, the motion and the shape of the step are determined by the fast kinetics ($\sigma > \sigma_*$, Fig. 14). In the steady-state mode the step flow pv and therefore the rate R of the face growth are the same at any face point, i.e., $R = pv = \text{const}$. At the step periphery the kinetic coefficient β_i and therefore the velocity v are by an order of magnitude larger than at the spiral center where the "driving" supersaturation is lower than the threshold value σ_*. Therefore the slope p at the step periphery is smaller (by the same factor) as that in the center D. If the supersaturation in the solution bulk is lower than the threshold value, $\sigma < \sigma_*$, then the whole spiral (from its center to the periphery) is characterized by the slow, or, roughly speaking, linear kinetics (Figs. 11, 12). For the linear kinetics, the slope p is governed by expressions (13) or (14), being independent of the kinetic step coefficient. Thus, if supersaturation increases up to values exceeding σ_*, the slope of the observed peripheral part decreases by the same factor as the kinetic coefficient of the fast kinetics (for $\sigma \gg \sigma_*$ in Fig. 14) exeeds the coefficient of the slow kinetics ($\sigma < \sigma_*$ in Fig. 14). With a further increase of supersaturation, the slowly growing central part of the spiral becomes smaller, whereas the slope of the hillock reapproaches the value determined by expression (14).

The normal growth rate $R = pv$ in the model under consideration is described by the experimental curve in Fig. 14. It is clear from the above said that the steep linear rise of $R(\sigma)$ for $\sigma > \sigma_*$ has nothing to do with the normal growth and high step density on the surface and the threshold supersaturation has nothing to do with the critical value for the formation of two-dimensional nuclei. Both features are thus explained by the presence of impurities.

4. Dissipative Structures

4.1. Morphological Instability in Normal Growth and Dislocation Structures

If a face is atomically rough (Fig. 1b), then new particles may be attached to the crystal almost at any point. It is the so-called normal face growth (see Sect. 2.1). In dissi-

from layer growth, normal growth is characterized by high rates of face motion, since in this case there is no problem of step generation. Moreover, normal growth is almost isotropic whereas singular faces give rise to the corresponding sharp minima on the dependence of the surface growth rate on surface orientation. Therefore in solutions (and melts with high impurity concentration) macroscopic wavy perturbations on the crystallization front do not disappear, on the contrary they become even more pronounced. As a result the planar growing surface becomes corrugated, the so-called morphological instability [1]. Its development makes the growth front cellular or pavement-like (Fig. 16). Dome-like cells of the front are connected by grooves whose tracks in the crystal bulk form the boundaries of the so-called pencil structure [1].

Fig. 16. Basal interface of quartz crystal, as grown in hydrothermal solution, revealing cellular ("cobble") structure. The small pits have appeared as a result of point-growth etching and mark outcrop points of dislocations. The pits are preferentially located in the boundaries between cells

A typical example of the cellular structure obtained in growth from solutions is the pinacoidal face of quartz (Fig. 16). It results either from normal growth or feebly marked layer growth.

Here the question may arise how do dislocations behave if they outcome to the cellular growth front.

It should be reminded that a dislocation outcoming to the planar growth front orients in such a way that the dislocation energy is minimal. The specific linear energy of a dislocation is anisotropic and therefore the most favorable orientation not necessarily coincides with the surface normal [1]. The cellular surface whose profiles at

sequential instants of time 1, 2, 3, 4 are shown in Fig. 17, has the wedge-like grooves denoted by letter E in Fig. 17. As a rule, inclusions appear on the seed surface S which form, upon closure, dislocations. With the growth front displacement, the emergence point of each dislocation moves along the surface and sooner or later reaches the groove bottom. It has been established (Dimitrov and Chernov) that this position of the outcrop point is stable for a certain range of spatial orientations of dislocations, their Burgers vectors, and the orientations of the groove traces in the crystal bulk, i.e., for the cell boundaries. As a result, dislocations are trapped by grooves and with further growth of the crystal they appear within the groove traces in the crystal bulk. Gradually dislocations form piles at cell boundaries; such dislocations are not parallel to one another. Being elongated during the surface growth displacement, they intersect one another, which results either in dislocation annihilation or, vice versa, their piling and formation of cracks. About 75% of the dislocation etch pits in Fig. 16 are located along the grooves, thus confirming our conclusion about trapping of dislocations by the

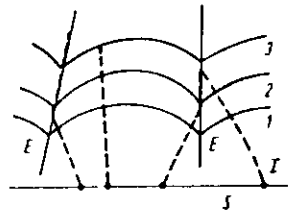

Fig. 17. Subsequent positions (1, 2, 3) of the growing interface possessing cellular structure. The dislocations—the dashed lines—are trapped by the edges E of the cellular growing interface

Fig. 18. Quartz plate cutted parallel to the basal plane (see Fig. 17) and etched. Accumulation of etch pits in the boundaries between neighbouring cells is clearly seen

grooves. The same phenomenon is also seen on the photograph of a plate cut out from the crystal bulk in the orientation parallel to the same pinacoidal face and then etched (Fig. 18). Preferential etching occurs along the cell boundaries.

4.2. Hydrodynamic-Kinetic Instability [68]

The above described morphological instability (Fig. 16) is due to the existence of the diffusion field over the normally growing face. In layer growth, instability manifests itself in the formation of the macrosteps from elementary ones on vicinal faces, e.g., at the slope of a growth hillock. The risers of such macrosteps may also loose stability. As a result, the mother liquid may be included into the crystal bulk, which may be very dangerous, e.g., in crystals used for doubling the frequency of strong laser radiation since it causes crystal cracking beginning at inclusions. The stresses due to micro-inclusions or inhomogeneous distribution of captured impurities seem to be responsible for anomalous birefrigence. Therefore the formation of macrosteps should be eliminated by refinement of the solution, by its thorough mixing or by any other method.

Studying growth of ADP ($NH_4H_2PO_4$) crystals from aqueous solution we observed a new type of instability giving rise to the formation of macrosteps. Figure 19 shows the morphology of the growth hillock around a dislocation whose outcrop is indicated by filled arrows. Open arrows indicate the direction of the mother liquid flow along the face. It is seen that the surface wrinkles up, i.e., macrosteps are always formed at the hillock slope where the direction of the elementary step motion during growth coicides with that of the mother liquid. Macrostep smoothening at one slope of the hillock and their formation at the opposite slope upon the change of the direction of the solution flow (this corresponds to the passage from Fig. 19a to Fig. 19b) takes one-two minutes. The above described instability is observed in the purely kinetic growth mode, when the velocity of solution flow ($\geq$ 25 cm/s) is so high that its further increase does not intensify the growth any more.

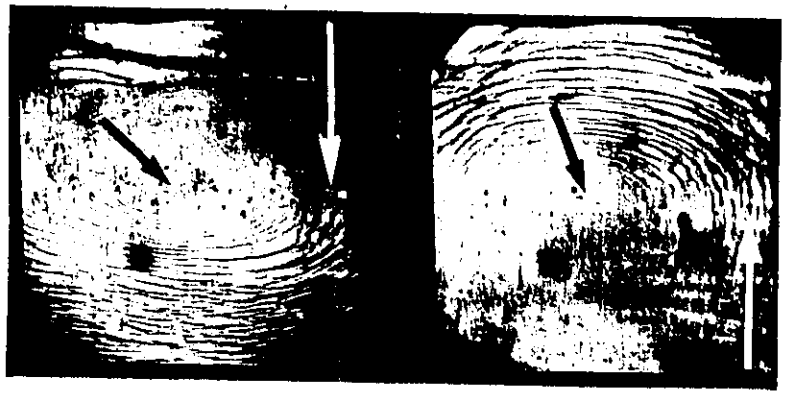

Fig. 19. Creation of macrosteps – hydrodynamic-dissipative structures – on the vicinal slopes of growth hillock formed around the dislocation indicated by black arrow. The white arrow indicates the solution flow direction

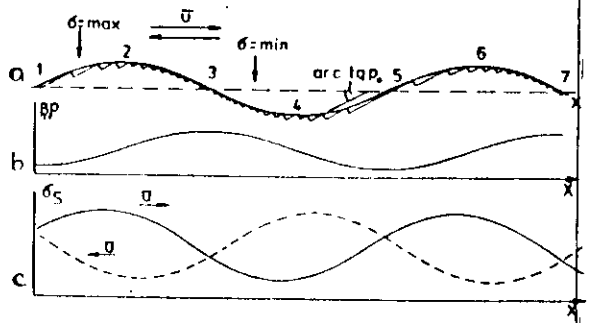

Fig. 20. To an explanation of dissipative step structure. a: periodically perturbed vicinal stepped surface, b: kinetic coefficient $\beta_{st}p$ of the perturbed surface, c: supersaturation σ_s immediately above the growing surface at different solution flow rates u

The cause of the phenomenon may be understood from Fig. 20, showing a stepped profile of a corrugated surface with the periodically varying step density. Figure 20b represents the plot of the product of the step density p and the constant kinetic coefficient of steps, β_{st}. In the vicinity of the surface regions 1, 5, etc. the step density (and hence the absorption power of the surface with respect to crystallizing substance) are minimal. Regions 2,6 lie at the deepest position in the supersaturated solution and therefore are best fed. Therefore the supersaturation at the surface is maximal at 1–2 and 5–6 segments indicated by arrows in Fig. 20a. In the immobile solution such a distribution gives rise to an even higher amplitude of a goffer, i.e., to instability.

The solution moving to the right in Fig. 20 is transferred from the regions of high supersaturation towards the bulges 2,6 on the goffered surface. Thus the bulges are better fed, their growth rate increases, and instability becomes more pronounced. If the solution flows to the left, i.e., in the direction reversed to that of step motion, the enriched solution is transferred to valleys indicated by 4 (Fig. 20a). The valleys grow faster and under sufficiently strong removal of the substance they are healed, or, in other words, the plane surface becomes stable.

4.3. Dendrites

The well known dendritic and eutectic structures forming during fast solidification of one-, two-, and multicomponent melts are studied both theoretically and experimentally [69–79] as representatives of self-organizing synergetic systems. The essence and the difficulty of the problem consist in the following. A dendritic crystal or a crystal of a more simple almost parabolic shape grows in the thermal (and/or concentration) field created by the crystal itself. The crystal shape is then described by an eigen function of the nonlinear problem of heat conduction (and diffusion). The analysis of such a problem for a one-component system has shown that, firstly, a dendrite of a certain shape and symmetry and not fractal structure can grow only if there is at least feebly marked anisotropy of the surface energy or, as has been recently shown by Brener, Mel'nikov and Temkin, nonzero kinetic coefficient. This statement is also true for the

initial stage of the transformation of a spherical crystal into a skeletal one via, first, the development of bulges on this sphere and then intense growth of one of these bulges, the top of which can be approximated by a slightly distorted paraboloid. In the latter case, the solution of the simplest thermal problem provides only the condition which should be imposed onto the product of the paraboloid top velocity by the radius of its curvature. In order to determine these quantities one more condition is necessary which can be obtained from the stability conditions in the neighborhood of the top. It yields the whole spectrum of eigen values for the paraboloid velocity and radius.

In the eutectic structure the platelets of the alloys of different compositions may alternate. Then the problem reduces to the establishment of the relation between the platelet size and the repetition period of the structure as a function of the solidification rate. Recently fresh attention was focussed on this direction.

5. Ostwald and Non-Ostwald Ripening

A multitude of small ($\leq 1\,\mu m$) crystals which exist in the solution at the constant equilibrium temperature are, in fact, not in the complete equlibrium. Smaller crystals are being dissolved, whereas the large ones are growing at their expense [1]. Such Ostwald ripening occurs since the system strives to lower its surface energy. It is well known that growth of large particles at the expense of small ones proceeds also in the systems of particles up to several millimeters in size [1, 80, 81]. The observed growth rates are by several orders of magnitudes larger than those which could be expected, if the driving force of ripening in such coarse disperse systems is the obersved decrease in the surface energy. Such non-Ostwald ripening is explained by the kinetics—the "asymmetry" between growth and dissolution under the conditions of oscillating temperature.

Namely, easier generation of dissolution steps by crystal edge and defects of its structure in comparison with growth steps results in the fact that the dissolution rate is usually several times higher than the growth rate. If the amplitude and the oscillation period about the equilibrium concentration of the solution (or, generally speaking, about vapor pressure or the melt temperature) are chosen appropriately, then the atomic layers on the faces of sufficiently small crystals have enough time to dissolve completely during the dissolution half-periods. To the contrary, most layers on large crystal faces, which are dissolved layer-by-layer, are preserved. During growth half-periods such layers are built up whereas the generation of new layers proceeds at lower rates. Indeed, experimentally determined growth rates in systems of large ($> 100\,\mu m$) particles are dependent on the period and the amplitude of temperature oscillations. Such a process may be called "kinetic ripening".

6. Crystallization Under Strongly Nonequilibrium Conditions

6.1. Nucleation and the Ostwald Rule

It is an important independent topic. I should like to mention here only one its aspect—the atomic structure of nuclei seems to be strongly different from that of the bulk phase. In particular, in recent years the clusters containing any number of atoms (from one up to 5000 and more [94]) have been obtained in vacuum. This closed the gap between molecular beams and microparticles (up to 100 Å in diameter) consisting of tens of thousands of atoms. Clusters are obtained either by the evaporation of the substance under question in the atmosphere of cold helium (10 mbar) or by adiabatic cooling of gas entering vacuum from a nozzle under high pressure. The experiments with lead and xenon have shown that there exist clearly pronounced "magic numbers", $N_m = 7, 10, 13, 17, 19, \ldots$ of atoms in clusters. The fraction of clusters consisting of such magic number of atoms is maximal in comparison with the fraction of cluster consisting of $N_m \pm 1$ atoms. Some of magic numbers (7, 13, 19) correspond to completed coordination spheres of the pentagonal packing of spheres forbidden for stable macroscopic crystals.

Gallium droplets several μm in diameter may be supercooled down to 150 K, half the value of the melting point. Being crystallized, they show, in addition to stable tetragonal phase, also four modifications metastable at room temperature.

Finally, nuclei having the metastable structure were also observed during devitrfiication in a high-resolution electron microscope.

It has not been clear as yet whether nuclei with the structure not observed in macrophases are stable under the conditions of their formation. Nevertheless it is obvious that all the above mentioned phenomena confirm once again the validity of the Ostwald rule.

6.2. Molecular-Beam Epitaxy

Molecular-beam epitaxy (MBE) is being studied at least at 30 world known laboratories. Impressive advances in this technique have been demonstrated at the International Conference on molecular beam epitaxy [82].

MBE requires high supersaturations—the vapor pressure in the source of the molecular beam exceeds the equilibrium pressure over the growing film by a factor of 10^3–10^8. And yet, the MBE technique yields single crystalline films of high perfection, since atoms incident onto the growing surface (e.g. Si atoms in the case of silicon film growth) do not enter the lattice immediately—they first form a movable adsorption layer. When atoms start "showering" the surface, the supersaturation in this layer drastically increases and, upon the attainment of the cirtical value of the surface concentration, two-dimensional nuclei of new lattice planes are formed and grow. A step ending each nucleus is a linear sink for atoms diffusing along the surface. Therefore the appearance of nuclei decreases the supersaturation in the adlayer. As a result, the supersaturation at any surface point may only slightly exceed the critical value. Such self-regulation provides relatively "tender" conditions for atoms which are built into the lattice at the steps.

And what about dislocations? The experiments with NaCl deposition [60] have shown that at the very beginning of growth, dislocations work hard and the surface is being covered with spiral steps. But soon afterwards they are replaced by the systems of concentric steps one interplanar distance high (2.82 Å for (100) NaCl) (Fig. 9) or by islands randomly scattered over the surface (Fig. 21). Indeed, as is known, the growth rate due

to layer generation by dislocations (Fig. 22, curve D) is much higher than the growth rate due to two-dimensional nulceation (Fig. 22, curve N) if the system slightly deviates from the equilibrium ($\Delta\mu/kT \ll 1$). To the contrary, two-dimensional nuclei provide a high rate of normal growth of the face. The threshold value of $\Delta\mu/kT$ at which the cross-over occurs is strongly dependent on the specific energy of steps and surface imperfections.

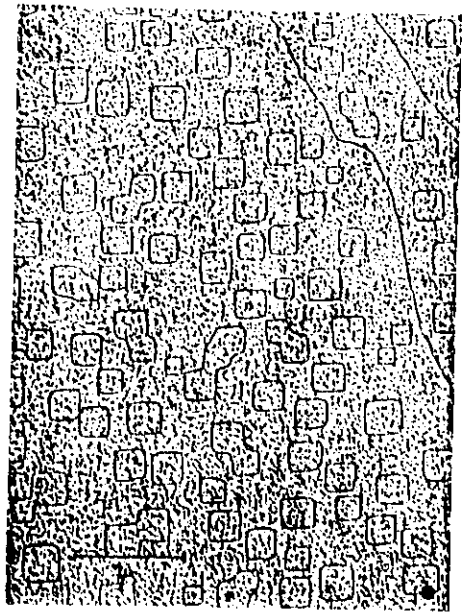

Fig. 21
Concentric steps on the (100)NaCl face randomly nucleated and spread during molecular beam expitary, like the one in Fig. 9. (H. J. Meyer and B. J. Stein)

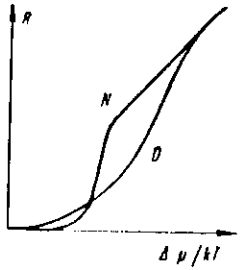

Fig. 22

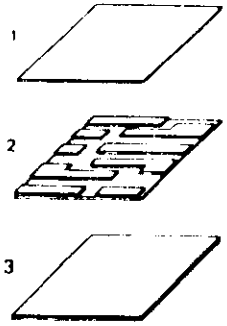

Fig. 23

Fig. 22. Face growth rate R provided by $2D$-nucleation (N) and by dislocations (D)—as functions of crystallization driving force, $\Delta\mu/kT$

Fig. 23. Subsequent stages of molecular beam epitaxy by $2D$-nucleation – 1: initial atomically flat surface, 2: steps have appeared, grow and annihilate, 3: all the steps have annihilated and the new atomic plane is completed

Now consider an atomically smooth surface (Fig. 23a) bombarded with a highly supersaturated molecular beam. On such a surface two-dimensional nuclei appear and grow. Their size increases (Fig. 23b), the steps of opposite signs encounter, annihilate (Fig. 23) and finally disappear, thus completing the formation of a new atomic plane of the lattice. Then the process restarts. The total perimeter of steps (per unit surface) is periodically varying from zero up to a certain maximum value. The absorption of incident molecules by the surface also varies periodically. Hence, the fraction of incident molecules which leave the surface should oscillate. Several (three-four) such oscillations of the intensity of the beam of molecules leaving the surface were recorded for (100) KCl. In this case it is possible to observe not islands of new planes but the holes in the already existing planes. Oscillations in the intensity of the reflected molecular beam were also observed for growth of (100) KCl [83-85].

Now let a beam of high-energy electrons be incident on the growing surface at a grazing angle. The larger is the step density, the larger the fraction of such electrons which are scattered incoherently thus decreasing the intensity of the elastically reflected beam. Therefore the step density oscillations in the procees illustrated by Fig. 23 will be reflected in the oscillation intensities of RHEED spots. This phenomenon was first observed in the molecular-beam epitaxy on the (100) GaAs [86]. Later on the phenomenon was repeatedly confirmed by observations on AlGaAs, InGaAs, Ge, Si, and ZnS [82, 88]. A decrease of the oscillation amplitude with time was different in different experiments. The maximum number of recorded oscillations exceeds 400 [90]. The oscillation attenuation is associated with the fact that the events of the nucleus formation are random. Therefore at different points of the surface "showered" with electrons the moments of new layer nucleation and the moments of the disappearance of already existing ones do not coicide. Such "desynchronization" results in a certain mean step density showing no oscillations.

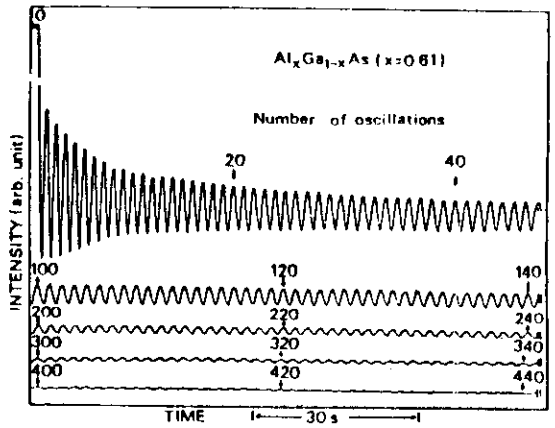

Fig. 24. RHEED spot intensity oscillations in time. Each period corresponds to deposition of one atomic layer 88

It also turned out that the oscillation amplitude of the RHEED signal decreases with the temperature rise. For vicimals related to the (100) GaAs oscillations disappear at a substrate temperature exceeding 590°C, when surface diffusivity becomes so high that all the admolecules manage to join the already existing steps [82].

The phenomenon of periodic nucleation and annihilation of steps finds practical application in the MBE technique. Namely, the RHEED signal is used to control the shuts of molecular guns, in particular, of various dopants [89]. Terminating the process at the stage of the minimum step perimeter, one may attain very sharp transitions and boundaries of the modulated structures.

7. Conclusion

The sixties and seventies saw the great interest to the phenomenological study of crystal growth. In the eighties, we witness the application of sophisticated techniques opening new vistas for investigating growth phenomena at almost atomic level. These are nuclei of several atoms, interatomic layers and individual dislocations. High-resolution electron microscopy studies of the profiles of moving columns consisting of four-five atoms and clusters on substrates will provide direct observation of atomic processes and the measurement of their quantitative characteristics. Crystal growth and physical chemistry of surfaces enrich one another.

On the other hand, with the development of synergetics, an interest is renewed to the problems of morphological stability of the growth forms of crystals and to hydrodynamics and heat- and mass-transfer in melts.

The efforts made by scientists studying micro- and macroscopic aspects of the above phenomena have already found their practical application in the development of new technologies and creation of new materials.

References

[1] Chernov, A. A.: Modern Crystallography III. Crystal Growth. Springer Ser Sol. St., Vol. 36. Berlin/New York: Springer 1984.
[2] Frenkel, Ya. I.: ZhExpTeorFiz (in Russ.) 16 (1946) N1, 39.
[3] Burton, W. K., N. Cabrera and F. C. Frank: Phil. Trans. A243 (1951) 299.
[4] Temkin, D. E. in: N. N. Sirota (Ed.) Mekhanism i kinetika kristallizatsii, Nauka i Technika, Minsk 1964, p. 86.
[5] Jackson, K. A. in: R. H. Doremus, B. W. Roberts and D. Turnbull: Growth and Perfection of Crystals. New York, Wiley 1958.
[6] Voronkov, V. V., and A. A. Chernov: J. Phys. Chem. Sol., Suppl. 1 (1967) 593; Sov. Phys. Cryst. 11 (1967) 571.
[7] Kerr, H. W., and W. C. Winegard: ibid, p. 179.
[8] Chernov, A. A., and D. E. Temkin: Comm. Department Chem. Bulg. Ac. Sci. XI (1978) N3–4, 643.
[9] Bonissent, A.: in Crystals. Growth, Properties and Applications, Vol. 9, Modern Theory of Crystal Growth, A. A. Chernov, H. Muller-Krumbhaar (Eds.). Berlin/New York: Springer 1983, p. 1.
[10] Broughton, J. Q., A. Bonissent, and F. F. Abraham: J. Chem. Phys. 74 (1981) 4029.
[11] Nozier, P., and F. Gallet: J. Physique 48 (1987) 353.
[12] Harrowell, P. H., and D. W. Oxtoby: Phys. Rev. B 33 (1986) N9, 6283.
[13] Rys, F. S.: Surf. Sci. 178 (1986) N1–3, 419.

[14] Rys, F. S.: Phys. Rev. Lett. 56 (1986) 624.
[15] Ohta, T., and K. Kawasaki: Progr. Theor. Phys. 60 (1978) N2, 365.
[16] Rottman, C., and M. Wortis: Phys. Rep. 103 (1984) 59.
[17] Villan, J., D. R. Grempel and J. Lapojou-Lade: J. Physics F15 (1985) 809.
[18] Mochrie, S. G. J.: Phys. Rev. Lett. 59 (1987) N3.
[19] Conrad, E. H., R. A. Aten, D. S. Kaufman, L. R. Allen, T. Engel, M. den Nija and E. K. Riedel: J. Chem. Phys. 84 (1986) 1015; 85 (1986) 4756.
[20] Rottman, C., M. Wortis, J. C. Heyrand and J. J. Metois: Phys. Rev. Lett. 52 (1984) 1009.
[21] Gong, Y. M., and R. Gomer: preprint, submitted to J. Chem. Phys., 1987.
[22] Chernov, A. A.: J. Cryst. Gr. 42 (1977) 55.
[23] Chernov, A. A., and L. V. Mikheev: Dokl. AN SSSR (in Russ.) 297 (1987) 349.
[24] Chernov, A. A., and V. A. Yakovlev: Langmuir 3 (1987) 635.
[25] Chernov, A. A., and V. A. Yakovlev: Poverchnost (in Russ.) (1986) 5 (2) 39.
[26] Chernov, A. A., and V. A. Yakovlev: ZhETF Letters 45 (1987) 130.
[27] van der Veen, J. F., and J. W. M. Frenken: Surf. Sci. 178 (1986) 382.
[28] Frenken, J. W. M., M. J. Maree and J. E. van der Veen: Phys. Rev. B 34 (1986) 7506.
[29] Faraday, M.: Phil. Mag. (4th Ser) 17 (1859) 126.
[30] Kliya, M. O.: Kristallografiya (in Russ.) 4 (1959) 263.
[31] Nason, D., and N. H. Fletcher: J. Chem. Phys. 62 (1975) 4444.
[32] Caranti, J. M., and A. J. Illingworth: J. Chem. Phys. 87 (1983) 407.
[33] Golecky, I., and C. Jaccard: Phys. Lett. 63A (1977) 374; J. Phys. C 11 (1978) 4229.
[34] Beaglehole, D., and D. Nason: Surf. Sci. 96 (1980) 357.
[35] Kvlividze, V. I., V. F. Kiselev, A. B. Kurzaev and L. A. Uschakova: Surf. Sci. 44 (1974) 60.
[36] Mantovani, S., S. Valeri, A. Loria and U. del Pennino: J. Chem. Phys. 72 (1980) 289.
[37] Lemmlein, G. G., D. E. Dukova and A. A. Chernov: Kristallografiya (in Russ.) 5 (1960) 662.
[38] Frisch, G., and E. Lüscher: Phil. Mag. A48 (1983) 21; Cheyssac, P., R. Kofman and R. Garrigos: Soc. St. Comm. 44 (1982) 1583.
[39] Frisch, G., H. Diletti and E. Lüscher: Phil. Mag. A50 (1984) 545.
[40] Willens, R. H., A. Kornblit, L. R. Testard and S. Nakahara: Phys Rev. B 25 (1982) 290.
[41] Devand, G., and R. H. Willens: Phys. Rev. Lett. 57 (1986) 2683.
[42] Stock, K. D., and E. Menzel: J. Cryst. Gr. 43 (1978) 135.
[43] Stock, K. D.: Surf. Sci. 91 (1980) 655.
[44] Stock, K. D., and B. Grosser: J. Cryst. Gr. 50 (1980) 485.
[45] Zhu, Da-Ming, and J. G. Dash: Phys. Rev. Lett. 57 (1986) 2599.
[46] Migone, A. D., J. G. Dash, M. Schick and O. E. Vilches: Phys. Rev. B 34 (1980) 6322.
[47] Krim, J., J. P. Coulomb and J. Bouzidi: Phys. Rev. Lett. 58 (1987) 583.
[48] McRae, E. G., and R. A. Malic: Phys. Rev. Lett. 58 (1987) 1437.
[49] Nenov, D.: Progr. Cryst. Gr. Charact. 9 (1981) 185.
[50] Schomeers, W.: Phys. Rev. B 32 (1985) 6845.
[51] Rosato, V., G. Giceotti and V. Pontikis: Phys. Rev. B 33 (1986) 1860.
[52] Nguen, Tue, P. S. Ho, T. Kwok, C. Nitta and S. Yip: Phys. Rev. Lett. 57 (1986) 1919.
[53] Broughton, J. Q., and G. H. Gilmer: Phys. Rev. Lett. 56 (1986).
[54] Abraham, F. F.: Phys. Rev. B 29 (1984) 2606.
[55] Mikheev, L. V., and A. A. Chernov: ZhETF (in Russ.) 92 (1987) 1732; Sov. Phys. JETP 65 (5) (1987) 971.
[56] Lipowsky, R., and W. Speth: Phys. Rev. 28 (1983) 3983.
[57] Chernov, A. A., and L. V. Mikheev: in preparation.
[58] Keller, K. W.: J. Cryst. Gr. 74 (1986) 161, 469.
[59] Bauser, E., and H. Strunk: J. Cryst. Gr. 51 (1981) 362.
[60] Chernov, A. A., and G. F. Kopylova: Kristallografiya 22 (1977) 1247. (Sov. Phys. Crystallogr. 22 (1977) 709).

[61] Trusov, L. I., and A. A. Chernov: Kristallografiya 24 (1979) 11.
[62] Chernov, A. A., I. L. Smol'sky, V. F. Parvov, Yu. G. Kuznetsov and V. N. Rozhansky: Kristallografiya 25 (1980) 821.
[63] Chernov, A. A., L. N. Rashkovich and A. A. Mkrtchan: J. Cryst. Gr. 74 (1986) 101.
[64] Kuznetsov, Yu. G., A. A. Chernov, P. G. Vekilov and I. L. Smol'sky: Kristallografiya 32 (1987).
[65] Görnert, P., and F. Voigt: High Temperature Solution Growth of Garnets: Theoretical Models and Experimentae Results, in: E. Kaldis (Ed.) Current Topics in Materials Sci. N. H. Amsterdam/Tokyo, 1984, p. 1–149.
[66] Chernov, A. A., L. N. Rashkovich and A. A. Mkrtchan: Kristallografiya 32 (1987) 737; Chernov, A. A., and L. N. Rashkovich: J. Cryst. Gr. in print.
[67] Mikhailov, A. A., L. N. Rashkovich, V. V. Rzhevsky and A. A. Chernov: Kristallografiya in print.
[68] Chernov, A. A., Yu. G. Kuznetsov, I. L. Smol'sky and V. N. Rozhansky: Kristallografiya 31 (1986) 1193.
[69] Langer, J. S.: Rev. Mod. Phys. 52 (1980) 1.
[70] Langer, J. S., and H. Müller-Krumbhaar: Acta Met. 26 (1978) 1689.
[71] Bensimon, D., L. P. Kadanoff, S. Liang, B. Shraiman and C. Tang: Rev. Mod. Phys. 58 (1986) 977.
[72] Kessler, D., and H. Levine: Phys. Rev. 33 (1986) 7867.
[73] Kessler, D., J. Koplik and H. Levine: Phys. Rev. A 34 (1986) 4980.
[74] Brener, E. A., C. E. Esipov and V. I. Mel'nikov: ZhEFF Letters (in Russ.) 45 (1987) 595.
[75] Dorsey, A., and M. Oliver: Phys. Rev. A 35 (1987) 3989.
[76] Caroli, B., C. Caroli, C. Misbah and B. Roulet: J. Phisique 48 (1987) 547.
[77] Saito, Y., G. Goldbeck-Wood and H. Müller-Krumbhaar: Phys. Rev. Lett. 58 (1987) 1541.
[78] Glicksmann, M. E.: Mat. Sci. Eng. 65 (1984) 45.
[79] Honjo, H., S. Ohta and Y. Sawada: Phys. Rev. Lett. 55 (1985) 841.
[80] Gordeeva, N. V., and A. V. Shubnikov: Kristallografiya 12 (1967) 186. (Sov. Phys. Crystallogr. 12 (1967) 154).
[81] Bazhal, I. G.: Kristallografiya 14 (1969) 1106. (Sov. Phys. Crystallogr. 14 (1970) 127).
[82] Molecular Beam Epitaxy 1986, J. Cryst. Gr. 81 (1987).
[83] Dabringhaus, H., and H. J. Meyer: J. Cryst. Gr. 16 (1972) 17, 31; 61 (1983) 86, 91, 95.
[84] Meyer, H. J., H. Dabringhaus, A. Maas and B. J. Stein: J. Cryst. Gr. 30 (1975) 225.
[85] Laaser, W., H. Dabringhaus and H. J. Meyer: J. Cryst. Gr. 62 (1983) 284.
[86] Neave, J. H., B. A. Joyce, P. J. Dobson and N. Norton: Appl. Phys. A31 (1983) 1.
[87] Dobson, P. J., B. A. Joyce, J. H. Neave and J. Zhang: Ref. 83, p. 1; Appl. Phys. Lett. 47 (1985) 400.
[88] Sakamoto, T., I. Kawamura, S. Nago, G. Hashiguchi, K. Sakamoto and K. Kuniyoshi: Ref. 82, p. 59.
[89] Sakamoto, T., H. Funabashi, K. Ohta, T. Nakagawa, N. J. Kawai and Kojima: Japan. J. Appl. Phys. 23 (1984) L 657.
[90] Joyce, B. A., P. J. Dobson, J. H. Neave, K. Woodbridge, J. Zhang, P. K. Larsen and B. Bölger: Surf. Sci. 168 (1986) 423.
[91] Atanasova, S., I. Gutsov and G. Budevsky: Communications of the Department of Chemistry, Bulgarian Academy of Sciences 17 (1984) N 3, 312.

ISSN 0323-4479 · Z. phys. Chemie · Leipzig · 269 (1988) 5 · S. 971–976

Departamento de Electroquímica, Facultad de Ciencias, Universidad Autonoma de Madrid, Carretera de Colmenar Viejo (Spain)

The Application of Digital Simulation to the Study of Spatial Distribution of the Oxidized and Reduced Forms of a System Excited by Alternate Current

By P. Cañas, R. Duo, M. S. Lorenzo and A. Aldaz[1]

With 3 Figures (Received 14th November 1986)

Abstract

A study of the spatial distribution of the concentrations of the oxidized and reduced forms of a simple electrochemical system excited by an a.c. perturbation has been done. This system has been analyzed by digital simulation using the explicit method. It is important to point out that no type of linearization of the system has been carried out.

Introduction

The methods of digital simulation have been applied to many electrochemical problems, even though these methods have only recently been used in studies of systems excited by an alternate current [1, 2].

In this work, the distribution of the oxidized and reduced forms of an electrochemical system submitted to an a.c. perturbation has been analyzed [3].

It is important to point out that in this study, no type of linearization of the system has been carried out, thus differing from the theoretical studies that have been done to date.

Theory

The simple electrodic process $O + e \rightleftarrows R$ has been analyzed. Taking into consideration semi-infinite plane geometry, the equations that rule over this process are the following:

$$\frac{\partial_O C(x,t)}{\partial t} = D_O \frac{\partial C_O(x,t)}{\partial x^2}, \tag{1}$$

$$\frac{\partial C_R(x,t)}{\partial t} = D_R \frac{\partial C_R(x,t)}{\partial x^2}, \tag{2}$$

$$j(t) = k_0[C_O(0,t)\exp[-\alpha\phi(t)] - C_R(0,t)\exp[(1-\alpha)\phi(t)]] + \frac{C_{dl}}{F}\frac{dV(t)}{dt}. \tag{3}$$

[1] P. Cañas, R. Duo, M. S. Lorenzo and A. Aldaz, Departamento de Electroquímica, Facultad de Ciencias, Universidad Autónoma de Madrid, Carretera de Colmenar Viejo, 28049 Madrid (Spain)